UNIVERSITI TEKNOLOGI MARA

ENHANCED CORROSION RESISTANCE AND MECHANICAL PERFORMANCE OF REINFORCED CONCRETE USING RHIZOPUS-DERIVED PHOSPHOLIPID BIOSURFACTANT

OLIVIA ANAK RAYEG

PhD

March 2026

UNIVERSITI TEKNOLOGI MARA

ENHANCED CORROSION RESISTANCE AND MECHANICAL PERFORMANCE OF REINFORCED CONCRETE USING RHIZOPUS-DERIVED PHOSPHOLIPID BIOSURFACTANT

OLIVIA ANAK RAYEG

Thesis submitted in fulfilment
of the requirements for the degree of
Doctor of Philosophy
(Civil Engineering)

Faculty of Civil Engineering

March 2026

CONFIRMATION BY PANEL OF EXAMINERS

I certify that a Panel of Examiners has met on 4 November 2025 to conduct the final examination of Olivia Anak Rayeg on her Doctor of Philosophy thesis entitled "Enhanced Corrosion Resistance and Mechanical Performance of Reinforced Concrete Using Rhizopus-Derived Phospholipid Biosurfactant" in accordance with Universiti Teknologi MARA Act 1976 (Akta 173). The Panel of Examiners recommend that the student be awarded the relevant degree. The Panel of Examiners was as follows:

Jezan Md Diah, PhD
Associate Professor
Faculty of Civil Engineering
Universiti Teknologi MARA
(Chairman)

Kay Dora Abd Ghani, PhD
Associate Professor
Faculty of Civil Engineering
Universiti Teknologi MARA
(Internal Examiner)

Norzila Othman, PhD
Professor
Faculty of Civil Engineering and Built Environment
Universiti Tun Hussein Onn Malaysia
(External Examiner)

PROFESSOR DR HJH ZURAEDA IBRAHIM
Dean
Institute of Postgraduates Studies
Universiti Teknologi MARA

Date: 27 March 2026

AUTHOR'S DECLARATION

I declare that the work in this thesis was carried out in accordance with the regulations of Universiti Teknologi MARA. It is original and is the results of my own work, unless otherwise indicated or acknowledged as referenced work. This thesis has not been submitted to any other academic institution or non-academic institution for any degree or qualification.

I, hereby, acknowledge that I have been supplied with the Academic Rules and Regulations for Post Graduate, Universiti Teknologi MARA, regulating the conduct of my study and research.

Name of Student	:	Olivia Anak Rayeg
Student ID. No.	:	2021549835
Programme	:	Doctor of Philosophy (Civil Engineering) – EC950
Faculty	:	Civil Engineering
Thesis Title	:	Enhanced Corrosion Resistance and Mechanical Performance of Reinforced Concrete Using Rhizopus-Derived Phospholipid Biosurfactant
Signature of Student	:	
Date	:	March 2026

ABSTRACT

The corrosion of steel reinforcement remains a critical challenge affecting the durability and service life of reinforced concrete structures, particularly under aggressive environmental conditions. Although conventional chemical corrosion inhibitors are widely applied, their associated environmental and health risks necessitate the development of sustainable alternatives. This study investigates the potential of fungal-derived biosurfactants as eco-friendly corrosion inhibitors and multifunctional admixtures for reinforced concrete. Indigenous biosurfactant-producing fungi were isolated from contaminated soils, among which *Rhizopus sp.* demonstrated the highest corrosion inhibition efficiency. The biosurfactant produced via submerged-batch fermentation using WFO as sole carbon source was characterised as phospholipid. The corrosion inhibition performance of the biosurfactant on mild steel reinforcement was evaluated using the migrating corrosion method, supported by weight loss measurements, electrical resistivity testing, and electrochemical impedance spectroscopy. Surface morphology and elemental composition of treated steel specimens were examined using scanning electron microscopy coupled with energy-dispersive X-ray spectroscopy, while tensile tests assessed mechanical performance retention of the steel bars. Results indicate that the phospholipid biosurfactant exhibited superior corrosion inhibition performance compared to the commercial surfactant Tween 80, achieving a maximum inhibition efficiency of 72.08% at a concentration of 20% (v/v) and reducing the corrosion rate to 0.0227 mm/year. When incorporated into fresh concrete as a water-replacement admixture, the biosurfactant significantly enhanced workability. Optimal performance was observed at a 10% (w/w) replacement level, resulting in increases of 13.8% in compressive strength (f_c) and 8.7% in flexural strength (f_s). Furthermore, pull-out testing confirmed a 9% improvement in steel–concrete bond strength after 120 days of curing. The findings demonstrate that the amphiphilic phospholipid biosurfactant derived from *Rhizopus sp.* functions as a mixed anodic–cathodic corrosion inhibitor by forming a protective barrier on steel surfaces, while simultaneously improving the mechanical and interfacial properties of reinforced concrete. Overall, this study provides new scientific insight into the dual-function role of *Rhizopus*-derived phospholipid biosurfactants and establishes their practical potential as sustainable green admixtures for corrosion mitigation and performance enhancement in reinforced concrete, contributing to the advancement of durable and environmentally responsible construction materials.

ACKNOWLEDGEMENT

The journey towards the completion of this doctoral study has been both humbling and transformative. It has taught me to embrace the present, release the past, and trust the promise of the future. First and foremost, I am deeply grateful to God Almighty for granting me the strength, knowledge, and perseverance to embark upon and complete this PhD journey. His unwavering grace and infinite love have sustained me through every challenge and triumph.

I wish to express my heartfelt appreciation to my supervisor, Associate Professor Ts. Dr. Clotilda Binti Peterus, whose guidance has been instrumental throughout this journey. Her exemplary mentorship, profound knowledge, patience, and motivation have been a continuous source of inspiration. I am sincerely thankful for her dedication and for instilling in me a spirit of academic excellence.

My deepest gratitude also extends to my co-supervisors, Dr. Ang Chung Huap, Dr. Caroline Marajan, and Dr. Rudy Tawie. To Dr. Ang, thank you for introducing me to the fascinating realm of biotechnology and for your steadfast guidance throughout my research. To Dr. Caroline, I am especially thankful for your invaluable advice, consistent encouragement, and support during the various phases of my doctoral journey.

With deepest love and appreciation, I thank my husband, Arnel Reanturco Ascotia, and our daughters, Lavinia Clarissa Ascotia and Chelsea Arianna Ascotia. Your enduring love, understanding, and emotional strength have been the foundation upon which this academic pursuit has stood. Thank you for your unwavering belief in me and for walking beside me every step of the way. To my beloved parents, I extend my heartfelt thanks for your unconditional love, prayers, and constant encouragement.

I gratefully acknowledge the financial support provided by the Government of Malaysia through the Jabatan Perkhidmatan Awam Malaysia (JPA) under the Hadiah Latihan Persekutuan Scholarship. This support has been vital in enabling the successful completion of this study.

I would also like to extend my sincere thanks to Puan Edah Binti Kassim and the laboratory technicians of the Faculty of Applied Sciences for their technical assistance and support during the experimental phases of this research.

To all who have journeyed with me, directly or indirectly, in the realization of this work, Thank you.

TABLE OF CONTENTS

		Page
CONFIRMATION BY PANEL OF EXAMINERS		**ii**
AUTHOR'S DECLARATION		**iii**
ABSTRACT		**iv**
ACKNOWLEDGEMENT		**v**
TABLE OF CONTENTS		**vi**
LIST OF TABLES		**xii**
LIST OF FIGURES		**xvii**
LIST OF SYMBOLS		**xxvii**
LIST OF ABBREVIATIONS		**xxix**
CHAPTER 1 INTRODUCTION		**1**
1.1	Research Background	1
1.2	Motivation for the Study	4
1.3	Problem Statement	5
1.4	Research Objectives	6
1.5	Research Questions	7
1.6	Significance of the Study	8
1.7	Limitations of Study	9
1.8	Scope of Study	10
1.9	Thesis Outline	11
CHAPTER 2 LITERATURE REVIEW		**13**
2.1	Introduction	13
2.2	Reinforced Concrete Structures	14
	2.2.1 Materials Used in RC	15
2.3	Corrosion in RC Structures	28
	2.3.1 Types of Corrosion	30
	2.3.2 Mechanisms of Corrosion in Reinforced Concrete	33

2.3.3 Factors Influencing Corrosion 38
2.3.4 Impacts of Corrosion on Structural Integrity and Service Life of RC 43
2.4 Protection Against Corrosion in RC Structures 45
2.4.1 Enhancement of Concrete Quality 46
2.4.2 Optimising the Thickness and Quality of Concrete Cover 48
2.4.3 Application of Surface Protective Coatings 49
2.4.4 Application of Corrosion Inhibitors 50
2.5 Surfactants 56
2.5.1 Biosurfactants 57
2.5.2 Fungal Biosurfactants 62
2.5.3 Properties of Biosurfactant 65
2.6 Production of Biosurfactants from Renewable Substrates 67
2.6.1 Factors Influencing the Productions of Biosurfactants 73
2.6.2 WFO as Substrate in Biosurfactant Production 81
2.6.3 Strategies for Increasing Yield and Productivity of Fungal-Based Biosurfactants 83
2.7 Applications of Biosurfactants 85
2.7.1 Biosurfactants as Corrosion Inhibitor 86
2.7.2 Biosurfactant as Concrete Admixture 90
2.8 *Rhizopus sp.* as a Biosurfactant Producer 94
2.9 Phospholipids -Based Biosurfactants 99
2.9.1 Classification of Phospholipids 99
2.9.2 Amphiphilic Properties and Self-Assembly 102
2.9.3 Sources and Composition of Phospholipids 106
2.9.4 Functional Properties and Applications of Phospholipids 106
2.9.5 Application of Phospholipids in Corrosion Inhibition 107
2.10 Biocorrosion 109
2.10.1 Biosurfactant in Biocorrosion Mitigation 111
2.11 Corrosion Monitoring Techniques 112
2.11.1 Electrochemical Impedance Spectroscopy (EIS) 113
2.11.2 Electrical Resistivity Testing 113
2.11.3 Weight Loss Measurement 114
2.11.4 SEM-EDX for Surface Morphology and Elemental Analysis 114

2.12 Strength and Durability Testing of Concrete 115
2.12.1 Slump Flow and Vertical Slump Tests for Fresh Concrete 116
2.12.2 Compressive Strength 117
2.12.3 Flexural Strength 119
2.12.4 Pull-out Test 120
2.13 Concluding Remarks 122

CHAPTER 3 RESEARCH METHODOLOGY 124
3.1 Introduction 124
3.2 Isolation of Biosurfactant-Producing Fungi 128
3.2.1 Environmental Screening for Biosurfactant-Producing Fungi from Contaminated Soils 130
3.2.2 Isolation of Soil Fungi from Contaminated Environments 132
3.2.3 Cultivation of Potential Biosurfactant Producers 135
3.3 Extraction and quantification of Biosurfactant 138
3.3.1 Centrifugation and Filtration 139
3.3.2 Liquid-to-Liquid Extraction 140
3.3.3 Growth Measurement with DCW and OD 143
3.4 Screening Tests for Biosurfactant Production 143
3.4.1 Drop Collapse Test 144
3.4.2 Oil Displacement Test 145
3.4.3 Emulsification Index (E_{24}) Test 146
3.5 Identification of Fungi and Biosurfactant Characterization 148
3.5.1 Macroscopic and Microscopic Identification of Fungal Strains 148
3.5.2 Biosurfactant Identification and Characterisation 149
3.6 Stability Studies of the Biosurfactant 151
3.6.1 Effect of Temperature on Biosurfactant Properties 151
3.6.2 Time-Based Assessment of Biosurfactant Activity and Fungal Growth Impact 152
3.6.3 Effect of High Salinity on Emulsification Properties 152
3.7 Toxicity Screening 152
3.7.1 Toxicity Screening Using Zebrafish 154
3.7.2 Toxicity Screening with Monstera adansonii and Syngonium podophyllum 154

3.8 Corrosion Inhibition Study 155
3.8.1 Preparation of Materials and Inhibitor Solutions 156
3.8.2 Weight Loss Measurements 159
3.8.3 Surface Morphology and Physical Characteristic Observations 161
3.8.4 Electrical Resistivity Test 162
3.8.5 Electrochemical Impedance Spectroscopy (EIS) 163
3.8.6 SEM and EDX 166
3.8.7 R_m Test of Biosurfactant-Coated Reinforcement Bars 167
3.9 Mechanical Performance Evaluation of RC with Biosurfactant as Admixture 169
3.9.1 Selection of Concrete Materials 170
3.9.2 Concrete Trial Mixes 174
3.9.3 Proportion of Concrete Materials for Flowability & Strength Studies 178
3.9.4 Fresh Concrete Workability Test 181
3.9.5 Hardened Concrete Strength Assessment 183

CHAPTER 4 RESULT AND DISCUSSION 197
4.1 Introduction 197
4.2 Isolation of Biosurfactant-Producing Fungi 198
4.2.1 Screening of Fungi from Contaminated Soils 198
4.2.2 Isolation of Soil Fungi 200
4.2.3 Fermentation and Enrichment of Potential Biosurfactant Producers 202
4.2.4 Screening Test for Biosurfactant Production 205
4.2.5 Growth Measurement and Quantification of Biosurfactant 209
4.3 Identification of Biosurfactant Producing Fungi 211
4.4 Biosurfactant Characterization Using LC-QTOF-MS Analysis 215
4.4.1 Positive Ion Mode 215
4.4.2 Negative Ion Mode 223
4.5 Stability Studies of the Biosurfactant 228
4.5.1 Effect of Temperature 228
4.5.2 Time-Based Assessment on Fungal Growth and Biosurfactant Activity 229

4.5.3 Effect of High Salinity on Biosurfactant Activity 230
4.6 Toxicity Analysis of the Biosurfactant 230
4.7 Corrosion Inhibition Analysis 232
4.7.1 Weight Loss Measurement 233
4.7.2 Surface Morphology and Physical Characteristics of Inhibitor Solutions 242
4.7.3 Electrical Resistivity Test 247
4.7.4 Electrochemical Impedance Spectroscopy (EIS) 250
4.7.5 Scanning Electron Microscope (SEM) and Energy Dispersive X-ray Spectroscopy (EDX) 255
4.7.6 R_m of Plain Mild Steel in 0.9% NaCl Solution with Corrosion Inhibitors 263
4.8 Fresh Concrete Flowability Tests 267
4.8.1 Effect of Admixture Dosage on Vertical Slump and Slump Flow 268
4.8.2 Effect of Admixture Dosage on T500 (Flow Time) 269
4.8.3 Results Analysis of Flowability Tests 269
4.9 Mechanical Properties of RC 273
4.9.1 f_c and Density of Concrete with Admixtures 273
4.9.2 f_s of Non-RC Beams 281
4.9.3 f_s Test of Single RC Beams 285
4.9.4 Pull-out Test of Reinforcement Bars Embedded in Concrete 289

CHAPTER 5 CONCLUSION AND RECOMMENDATIONS 292
5.1 Introduction 292
5.2 Summary of Major Findings 292
5.2.1 Biosurfactant Production, Characterisation and Analysis of Stability 292
5.2.2 Efficiency of Phospholipid-Based Biosurfactants as a Green Corrosion Inhibitor 294
5.2.3 Phospholipid-Based Biosurfactants as Bio-Admixtures for Corrosion Inhibition in RC 296
5.3 Conclusion 298
5.4 Future Recommendations 299

REFERENCES **301**

APPENDICES **322**

AUTHOR'S PROFILE **334**

LIST OF TABLES

Tables	Title	Page
Table 2.1	Chemical Composition Summary Of Mild Steel Bars (R10 Grade 250) According To MS144:2014	20
Table 2.2	Different Types Of Admixtures Commonly Used In Concrete Manufacturing	24
Table 2.3	Summary Of The Major Chemical Constituent Of OPC Following Malaysian Standard (MS) 197-1:2014	26
Table 2.4	Bogue Compounds Of Ordinary Portland Cement	27
Table 2.5	Summary Of The Composition And Percentage For Compounds Concerning Normal, Rapid Hardening And Low-Heat Portland Cement	27
Table 2.6	Summary Of The Major Biosurfactant Classes And Their Producer Microorganism	58
Table 2.7	Classification Summary Of Biosurfactants	61
Table 2.8	Summary Of Biosurfactants Applications And Their Microbial Producers	61
Table 2.9	Types Of Biosurfactants Or Bioemulsifiers Produced By Filamentous Fungi	64
Table 2.10	Comparison Summary Of Biosurfactants And Chemical Surfactants Regarding Their CMC And Surface Tension Values	66
Table 2.11	Biosurfactants Production From Renewable Substrates	70
Table 2.12	Summary Of Essential Parameters Influencing Microbial Biosurfactant Production	74
Table 2.13	Parameters Influencing Fungal Biosurfactant Production	76
Table 2.14	Summary Of Biosurfactant Production Using WCO As A Substrate	82
Table 2.15	Summary Of Previous Studies On Biosurfactants As Corrosion Inhibitors In Metals	89
Table 2.16	Production Of Secondary Metabolites By *Rhizopus Sp.*	98

Table 2.17	Summary Of The Typical f_c Development Over Time	118
Table 3.1	Summary Of The Sampling Locations And The Characteristics Of The Soil Samples Collected	131
Table 3.2	Summary Of The Initial Variables In The Fermentation Enrichment Process For Biosurfactant Production	136
Table 3.3	The Qualitative And Quantitative Method To Detect Biosurfactant Production By Soil Fungi	144
Table 3.4	Summary Of Experimental Methods For Corrosion Inhibition Analysis	155
Table 3.5	Chemical Composition Of Mild Steel Bar (MS144:2014) Grade 250	157
Table 3.6	Summary Of The Biosurfactant Concentrations Used In Corrosion Inhibition Analysis	160
Table 3.7	Summary Of The Physical Properties Of The OPC 42.5N Used In This Study According To MS 197-1:2014	171
Table 3.8	Summary Of The Major Chemical Constituent Of The OPC Based On MS 197-1:2014	171
Table 3.9	Summary Of The Physical Properties Of The Aggregates Used In Concrete Mixing	173
Table 3.10	Summary Of The Nominal Design Requirement	174
Table 3.11	Summary Of The Mix Design For Concrete Grade 30 (kg/m^3)	174
Table 3.12	Fresh And Hardened Concrete Properties For Trial Mix Designs	177
Table 3.13	The Design Mix Proportions For Every 1 M^3 Of Concrete G30	180
Table 3.14	Summary Of The Specimen Details And Composition Of Materials For 1 m^3 Concrete Grade 30 Used In The f_s Test	187
Table 3.15	Summary Of The Mix Design And Corrosion Inhibitor Treatment For Single-RC Beams	192
Table 3.16	Mix Proportion Of Concrete Grade 30 For Test Specimens	194
Table 4.1	Physicochemical Characteristic Summary Of Soil Samples And Fungal Growth Assessment On MEA	199
Table 4.2	Summary Of The Variables Affecting Biosurfactant Production	202

Table 4.3	Visual Characteristic Summary Of The Metabolites Produced By Each Fungal Isolate Observed In The Fermentation Broths As Presented In Figure 4.5	204
Table 4.4	Summary Of The Drop Collapse Test Results	205
Table 4.5	Summary Of The Oil Displacement Areas By Biosurfactants, Distilled Water, And A Synthetic Surfactant (Tween 80)	207
Table 4.6	Summary Of The E_{24} Results For Biosurfactant Production	208
Table 4.7	Summary Of The ODs For The Crude Biosurfactants Taken On Days 10 And 14 Of The Fermentation Process	210
Table 4.8	Summary Of The DCW Values Of The Crystallised Biosurfactants	210
Table 4.9	Summary Of The Macroscopic Morphological Characteristics Of Biosurfactant-Producing Fungi	212
Table 4.10	Summary Of The Identified Compounds Obtained Via The Positive Mode Of LC-QTOF-MS Analysis.	220
Table 4.11	Summary Of The Identified Compounds Obtained Via The Negative Mode Of LC-QTOF-MS	226
Table 4.12	Summary Of The Relationship Between Shelf Life And Emulsification Activity Of The Crude Biosurfactant	229
Table 4.13	Summary Of The Relationship Between Salinity And Emulsification Activity Of The Crude Biosurfactant	230
Table 4.14	Summary Of The Physiological And Behavioural Responses In Fish Exposed To Biosurfactant Solution For 14 Days	231
Table 4.15	Observations Summary Of Plant Health And Water Quality Over 14 Days	232
Table 4.16	Corrosion Inhibition Studies Assessing The Corrosion Inhibition Efficiency Of Biosurfactants Produced By The Four Fungal Isolates	232
Table 4.17	Summary Of The Weight Loss Measurement Test Results For Tween 80	234
Table 4.18	Summary Of The Weight Loss Measurement Test Results For *Fusarium Sp.*-Derived Biosurfactant	235
Table 4.19	Summary Of The Weight Loss Measurement Test Results For *Rhizopus Sp.*- Derived Biosurfactant	236

Table 4.20	Summary Of The Weight Loss Measurement Test Results For *Trichoderma Sp.*-Derived Biosurfactant	237
Table 4.21	Summary Of The Weight Loss Measurement Test Results For *Penicillium Sp*-Derived Biosurfactant	238
Table 4.22	Effect Of Biosurfatants Concentration On Corrosion Inhibition Of Mild Steel Specimens After 100 Days Of Exposure In 0.9% NaCl Solutions	239
Table 4.23	Summary Of The ER Values For Mild Steel Specimens Exposed To Tween 80 And Fungal-Based Biosurfactants In 0.9% NaCl Solution At Varying Inhibitor Concentrations	249
Table 4.24	Electrochemical Impedance Parameters Of Mild Steel Samples In 0.9%NaCl Solution In The Absence And Presence Of Inhibitors At 303K (29.85^{o}C)	252
Table 4.25	Summary Of The Elemental Composition (Weight And Atomic Percentages) Of Mild Steel Specimens Obtained Through The EDX Analysis	263
Table 4.26	Summary Of The Mechanical Properties Of Plain Mild Steel After Immersion In 0.9%NaCl Solution With Various Inhibitors Concentrations For 28 Days	266
Table 4.27	Summary Of The Slump Variation (Vertical and Horizontal) With Different Inhibitor Concentrations	267
Table 4.28	Summary Of The Tabulated Results According To EFNARC And JKR Standards	272
Table 4.29	Summary Of f_c For Concrete Cubes After 7 And 28 Days Of Curing	275
Table 4.30	Summary Of The f_s Of Non-RC Beams Tested On Day 7 With Biosurfactant And Tween 80 As Water Replacement Admixtures	283
Table 4.31	Summary Of The f_s Of Non-RC Beams Tested On Day 28 With Biosurfactant And Tween 80 As Water Replacement Admixtures	284
Table 4.32	Summary Of f_s And Physical Properties Of Single RC Beams With Varying Admixture Percentages	286

Table 4.33 Comparison Summary Of The Corrosion Resistance And Mechanical Performance Between The Control And Biosurfactant-Treated Groups 291

LIST OF FIGURES

Figures	Title	Page
Figure 1.1	Biosurfactant Production And Its Applications	3
Figure 2.1	The Steel Stress-Strain Diagram	19
Figure 2.2	Property Summary Of Mild Steel Bars Commonly Used In Malaysia As Provided By The Southern Steel Sdn. Bhd.	20
Figure 2.3	The Factors Contributing To The Degradation Of RC	30
Figure 2.4	The Classification Of Major Corrosion Types	33
Figure 2.5	The Corrosion Sequences On Reinforcements And Consequences	35
Figure 2.6	The Effect Of Reinforcement Corrosion On The Mechanical Properties Of RC Structures	36
Figure 2.7	Detrimental Effects Of Reinforcement Corrosion On The Performance And Durability of RC Structures	44
Figure 2.8	Comparison Of Normalized Bond Strength At Different Corrosion Levels	45
Figure 2.9	The Classification Of Corrosion Inhibitors And Application Methods In RC Systems	52
Figure 2.10	Number Of Published Papers On OCI-related Articles Vs. Publication Year	55
Figure 2.11	The Schematic Illustration Of A Surfactant	57
Figure 2.12	The Relationship Between Biosurfactant Concentration, Surface Tension And Formation Of Micelles	67
Figure 2.13	The Factor Influencing Microbial Biosurfactant Production	73
Figure 2.14	The Various Modes Of Submerged Fermentation	79
Figure 2.15	The Morphology Of *Rhizopus Oryzae*	95
Figure 2.16	The Morphological Characteristics Of *Rhizopus Sp* (a) Colony Observed On Malt Extract Agar (MEA) Following Three Days Of Cultivation At 30°C. (b) Intact And Germinating Sporangiospores Are Presented, With Arrows Denoting Spores Of Varying Sizes (Scale Bar = 10 Mm). (c) Zygospores	

	Exhibiting Unequal Suspensors (Scale Bar = 10 Mm). (d) *S*porangiospore Release And Columella (Scale Bar = 10 Mm). (f) Sporangiophore, Rhizoids, And Pigmented Hyphae Of *Rhizopus Oryzae* (Scale Bar = 10 Mm). (g) Stolons (Scale Bar = 50 Mm). (h) Empty Sporangiophore (Scale Bar = 50 Mm)	96
Figure 2.17	The Lipid Family Tree	102
Figure 2.18	The Lipids Aggregates Based On Their Shapes	103
Figure 2.19	The Amphiphilic Molecules Of Phospholipids With Hydrophilic Heads And Hydrophobic Tails Of A Phospholipid Molecule	103
Figure 2.20	The Configuration Of Lipid Micelles And Phospholipids Bilayers Molecule	105
Figure 2.21	The Molecular Structure Of Phospholipid	105
Figure 2.22	The Correlation Between Corrosion Level And Ultimate Bond Strength (τ) Of Reinforcement	121
Figure 3.1	Flowchart Of Research Methodology	126
Figure 3.2	Summary Of Research Activities	128
Figure 3.3	The Biosurfactant Production Stages For This Study	130
Figure 3.4	The Soil Collected From 10 Different Contaminated Sites At Kuching And Kota Samarahan	132
Figure 3.5	The Dilution Process Ranging From 10^{-1} To 10^{-10}	133
Figure 3.6	The Diluted Samples Poured On Sterilised Malt Extract Agar (MEA)	133
Figure 3.7	The Fungi Growth Observed On Agar Plates After 7 Days. (a) Fungi Isolated From Aeroville Municipals Waste- *Rhizopus Sp.* (b) Fungi Isolated From ILP Car Garage- *Pennicilium Sp.* (c) Fungi Isolated From KBS Municipal Waste -*Tricoderma Sp.* (d) Fungi Isolated From Riveria Car Garage - *Fusarium Sp.*	134
Figure 3.8	The Repeated Plating On MEA To Obtain A Pure Culture. This Sub-Culture Process Is Repeated At Least Twice For Every Strain	135

Figure 3.9	The Working Stocks That Are Cut From Agar Plates And Kept In Sealed Glass Bottles. These Strains Are The Biosurfactant-Producing Fungi	135
Figure 3.10	(a) The Fungi Mycelia Fermented In MSM Broth Supplemented With 5% WFO (v/v) In Erlenmeyer Flasks On Day 1 And (b) Fermentation Broth On Day 4 Of Batch Fermentation	138
Figure 3.11	The Centrifugation Process To Separate The Supernatant From Pellet -Containing Cells And Unutilised Substrates	139
Figure 3.12	Further Extraction By Filtration Of Supernatant From Cell-Free Broth. This Process Was Performed After Centrifugation	140
Figure 3.13	The Crude Biosurfactant Collected After Filtration	140
Figure 3.14	The Liquid-Liquid Extraction With N-Hexane	142
Figure 3.15	The Extracted Cell-Free Biosurfactant	142
Figure 3.16	The Crystalized Biosurfactant After Evaporation	142
Figure 3.17	The Biosurfactant (Left) And Saline Solution (Right) For OD Measurement	143
Figure 3.18	The Designated 96-Well Microplate And Its Component	145
Figure 3.19	The Initial Surface Tension Of Motor Oil And (b) Reduction After 2 Mins With A Phospholipids-Based Biosurfactant	146
Figure 3.20	The Emulsification Test Involving (a) An Initial Biosurfactant-Motor Oil Mixture And (b) A Stable Emulsified Layer Based On Phospholipid-Based Biosurfactants After 24 H	147
Figure 3.21	The Acid Fuchsin Used In Staining For Strain Identification	149
Figure 3.22	The Complex Structure Of *Rhizopus Sp.* (a) Illustration Adapted From Literature For Reference (b) Microscopic Image Captured At 400× Magnification Showing Hyphal And Sporangial Features Of The Isolated Strain	149
Figure 3.23	The Toxicity Studies On (a) Green Zebra Danio Fishes And (b) *Monstera Adansonii* With *Syngonium Podophyllum*	155
Figure 3.24	The Mill Certificate Of The Mild Steel Bars Used In The Corrosion Inhibition Analysis	157
Figure 3.25	Mild Steel Bars Used For The Corrosion Inhibition Studies	157
Figure 3.26	(a) The Cleaned Mild Steel Bars And (b) Dimension Of The Specimens	160

Figure 3.27	The Soldered Mild Steel Before EIS Analysis	164
Figure 3.28	Mild Steel Bar After EIS Analysis With (a) 10% Tween 80 (b) 10% Biosurfactant	164
Figure 3.29	The 10% Tween 80, 5% Biosurfactant, And 10% Biosurfactant In 0.9 % NaCl Solution	165
Figure 3.30	The Randle's Constant Phase Angle Element (CPE) Equivalent Circuit For Blank Mild Steel (Control)	165
Figure 3.31	The Proposed Equivalent Circuit To Fit Nyquist Plot Of EIS Data For The Mild Steels In The Presence Of Biosurfactant Displaying Warburg Impedance	166
Figure 3.32	(a – b). The Conditioning Of Steel Bars With Different Biosurfactant Concentrations	168
Figure 3.33	The Tensile Test On The Reinforcement (a) Before And (b) After Applied Force	169
Figure 3.34	The OPC Is Manufactured By CMS Cement Industries Sdn. Bhd. In Sarawak	171
Figure 3.35	The Crushed Granite Obtained From A Quarry At Jangkang, Sebuyau	173
Figure 3.36	The Concrete Ingredients Mixed Within A Concrete Mixer In Batches According To Their Admixture Compositions	175
Figure 3.37	The Slump Test For Design Mix 1 Involves A Vertical Slump Of 70 Mm, Which Is Below The Required Slump For G30. The Low Slump Value Indicates A Dense Mix With High Aggregate Content, Making It Unsuitable As A Control Mix	176
Figure 3.38	The Measurement Of Slump Flow And The Duration Needed For The Flow To Reach A 500 mm Diameter Marking	183
Figure 3.39	The 150 mm × 150 mm × 150 mm Cube Mould Used In This Study	184
Figure 3.40	The Preparation Of Concrete Cubes (a) After Casting (b) Demoulding After 24 H (c), And In The Curing Tank For 7 And 28 Days	184
Figure 3.41	The Measurement Setup Of The Concrete Cube f_c	186
Figure 3.42	The f_c Test For Concrete Cubes (a) Before And (b) After The Test	186

Figure 3.43	The Beam Mould (500 mm × 100 mm × 100 mm) Used For Specimen Preparation	189
Figure 3.44	(a-b) The Grade 30 Concrete Beam Specimens Prepared For The f_s Test	189
Figure 3.45	The Specimens in the Curing Tank At 25 ± 2°C For 28 Days	190
Figure 3.46	The Experimental Setup With A Central Point Flexural Loading Test Using A UTM	190
Figure 3.47	The Measurement Of The Distance Of a = Line of Fracture To The Nearest Support	191
Figure 3.48	The Treatment Of Reinforcing Bars In Inhibitor Solution	193
Figure 3.49	The Flexural Failure Of The Concrete Beam Under The Three-Point Bending Test (a) Before Testing And (b) After Failure	193
Figure 3.50	The τ Details Of The Test Specimen	196
Figure 4.1	The Morphological Features Of (a) S1 (*Rhizopus sp.*), (b) S2 (*Pennicilium Sp.*), (c) S3 (*Tricoderma Sp.*), and (d) S4 (*Fusarium Sp.*) Observed On PDA Plates After Seven Days Of Isolation At A Controlled Temperature Of 30°C	201
Figure 4.2	(a) The *Rhizopus Sp.* Growth On The MEA After 14 Days Of Isolation At A Controlled Temperature Of 30°C And (b) Three-dimensional Mycelial Of *Rhizopus Sp.*	201
Figure 4.3	(a-b) The *Rhizopus Sp.* Growth On The MEA After 60 Days Of Isolation At Room Temperature (~25°C)	202
Figure 4.4	The Culture Broths At The Beginning Of The Fermentation Process (a) The MSM Broth Is Supplemented With 5% WFO (b) The Shake Flask Fermentation Setup Used For Biosurfactant Production	203
Figure 4.5	The Emulsified MSM Broth Containing Metabolites Secreted By (a) *Rhizopus Sp.* (b) *Penicillium Sp.* (c) *Trichoderma Sp.*, And (d) *Fusarium Sp.*, After 14 Days Of Cultivation In Erlenmeyer Flasks Under Anaerobic And Agitated Conditions	204
Figure 4.6	The Drop Collapse Assays. Negative And Positive Results Are Characterised By The Presence Of Beaded Droplets Of Culture Supernatant On The Oil Surface Or The Absence Of Beaded Droplets (Drops Appearing Collapsed). (a) *Rhizopus* Sp., (b)	

Penicillium Sp., (c) *Trichoderma Sp.*, and (d) *Fusarium Sp.* Indicates Collapsed Droplets. (e) Distilled Water (Negative Control) Suggests Beaded Droplets. (f) Tween 80 (Positive Control) Presents Collapsed Droplets 206

Figure 4.7 The ODAs In Petri Dishes Containing Used Motor Oil Involving (a) *Rhizopus Sp.* (b) *Penicillium Sp.* (c) *Tricoderma Sp.* (d) *Fusarium Sp.* (e) Tween 80 And, (f) Distilled Water 207

Figure 4.8 The E_{24} Of A Phospholipids-Based Biosurfactant Produced By *Rhizopus Sp.* (a) Initial Mixture Of Biosurfactant And Used Motor Oil (b) A Stable Emulsified Layer Of Biosurfactant After 24 H 208

Figure 4.9 Macroscopic And Micromorphological Characteristics Of *Rhizopus Sp.* Following 14 Days Of Incubation on PDA At 30 °C: (a) Macroscopic Morphology On PDA Plate, (b) Micromorphological Features Showing Hyphae, Rhizoids, Sporangiophore, and Sporangium Observed Under Light Microscope At 400×, And (c) Microscopic View Illustrating Sporangial Structures And Hyphal Network Observed Under Light Microscope At 40× Magnification. 213

Figure 4.10 Macroscopic And Micromorphological Characteristics Of *Penicillium Sp.* Following 14 Days Of Incubation On Potato Dextrose Agar (PDA) At 30 °C. (a) Macroscopic Colony Morphology On PDA Plate And (b) Micromorphological Features Showing Conidiophores And Conidia Under Light Microscopy At 400× Magnification. 213

Figure 4.11 Macroscopic And Micromorphological Characteristics Of *Trichoderma Sp.* Following 14 Days Of Incubation On PDA At 30 °C. (a) Macroscopic Colony Morphology Exhibiting A Dense Green Conidial Surface With A Distinct White Marginal Zone, Characteristic Of *Trichoderma Sp.* And (b) Micromorphological Features Showing Branched Conidiophores Bearing Phialides. 214

Figure 4.12 Macroscopic And Micromorphological Characteristics Of *Fusarium Sp.* Following 14 Days Of Incubation On PDA At 30

	°C. (a) Macroscopic Colony Morphology Showing Abundant White, Cottony Aerial Mycelium; And (b) Micromorphological Features Illustrating Septate Hyphae With Characteristic Macroconidia, Microconidia, And Chlamydospores.	214
Figure 4.13	The *Rhizopus Sp.* Morphology. (a) The Colony On MEA Following 14 Days Of Cultivation At 30°C. (b) Sporangiophore, Rhizoids, and Pigmented Hyphae of *Rhizopus Sp.* (c) Stolons, (d) Empty Sporangiophore, (e) Sporangiophore With Columella, And (f) Intact With Germinating Sporangiospores	215
Figure 4.14	The Photodiode Array Chromatograms Comparing A Blank Sample (ACN) With A Biosurfactant Sample Analysed In The Positive Ion Mode. The Absorbance Was Recorded Over A Wavelength Range Of 190–500 nm	216
Figure 4.15	The Identified Compounds In The Biosurfactant Sample Obtained Via The Positive Mode Of LC-QTOF-MS Analysis	218
Figure 4.16	The Photodiode Array Chromatograms Comparing a Blank Sample (ACN) With A Biosurfactant Sample Analysed In The Negative Ion Mode. The Absorbance Was Recorded Between 190 nm and 500 nm	223
Figure 4.17	The Identified Compounds In The Biosurfactant Sample Via The Negative Mode Of LC-QTOF-MS	225
Figure 4.18	The Emulsified Layer Of Biosurfactant In Cooking Oil After Heating At 60°C	228
Figure 4.19	(a-b) The *Rhizopus Sp.* Growth On MEA Following 60 Days Of Isolation In Room Temperature (~ 25°C)	229
Figure 4.20	The Corrosion Inhibition Efficiency Of Biosurfactants and Tween 80 At Various Concentrations	233
Figure 4.21	The Corrosion IE of *Rhizopus Sp.* Phospholipid-Based Biosurfactant At Concentrations From 5% To 20% After 100 Days Of Mild Steel Specimen Immersion In The Inhibitor Solution	242
Figure 4.22	The Mild Steel Specimens In A 0.9% NaCl Solution Without Corrosion Inhibitors (a) Before Cleaning, Showing The	

	Formation Of Thick Brownish-Orange Corrosion Products (b) After Cleaning With A Fine Brush And A Microfibre Cloth, Revealing A Black-Coloured Surface	243
Figure 4.23	The Mild Steel Specimens In A 0.9% NaCl Solution With 20% Tween 80 (a) Surface Condition Of Mild Steel Specimens Before Cleaning, Exhibiting Black Rust Formation With Orange Traces (b) Cleaned Steel Surfaces Showing Sign Of Localised Corrosion	244
Figure 4.24	The Mild Steel Specimens In A 0.9% NaCl Solution With 20% Phospholipid-Based Biosurfactant. (a) Images Before And (b) Specimens After Cleaning, Exhibiting Minimal Corrosion Features And Uniform Surfaces	244
Figure 4.25	The Physical Observation Of The Solutions Involving (a) Positive Control (Tween 80), (b) Negative Control (Distilled Water), and (c) Phospholipid-Based Biosurfactant	246
Figure 4.26	The 0.9% NaCl (Negative Control) Solution After Immersion Of Mild Steel Bars Coupons For 100 Days	246
Figure 4.27	The Tween 80 Solutions After Immersion Of Mild Steel Bars Coupons For 100 Days (Positive Control)	246
Figure 4.28	The Clear Appearance Of The 0.9% NaCl Solutions Containing Phospholipid-Based Biosurfactants 100 Days Of Immersion Of Mild Steel Bar Coupons	247
Figure 4.29	The Relationship Between ER And Inhibitor Concentration For Tween 80 And Fungal-Based Biosurfactants (*Fusarium Sp., Rhizopus Sp., Trichoderma Sp.*, And *Penicillium Sp.*). The ER Consistently Decreased With Increasing Inhibitor Concentration, Indicating Improved Corrosion Inhibition	250
Figure 4.30	The Correlation Between Resistivity And IE Of *Rhizopus Sp.* - Based Biosurfactant At Varying Concentrations	250
Figure 4.31	The Nyquist Plot Of Mild Steel (Referred As BK_1 and BK_2) in 0.9 % NaCl Solution (As Negative Control) At 303 K	252
Figure 4.32	The Nyquist Plot Of Mild Steel In The Presence Of 10% Tween 80 And A Blank Control (BK_2) In A 0.9 % NaCl Solution At 303 K	253

Figure 4.33	The Nyquist Plot Represents The Electrochemical Impedance Behavior Of Mild Steel In The Presence Of 5% Phospholipids-Based Biosurfactant (BS_1 And BS_2) And Blank Control (BK_2) In A 0.9% NaCl Solution At 303 K.	253
Figure 4.34	The Nyquist Plot Represents The Electrochemical Impedance Behavior Of Mild Steel In The Presence Of 10 % Phospholipids-Based Biosurfactant (BS_1 and BS_2) And Blank Control In A 0.9% NaCl Solution At 303 K.	254
Figure 4.35	The SEM Images (a) Fresh Mild Steel, (b) Specimen Without Corrosion Inhibitor, (c) Specimen Treated With 10% Tween 80, (d) Specimen Treated With 5% Biosurfactant, (e) Specimen Treated With 10% Biosurfactant, And (f) Specimen Treated With 15% Biosurfactant.	258
Figure 4.36	The EDX Spectrum Of Fresh Mild Steel	260
Figure 4.37	The EDX Spectrum Of Mild Steel Immersed In 0.9%NaCl Without An Inhibitor	260
Figure 4.38	The EDX Spectrum Of Mild Steel Immersed In 0.9%NaCl With 10% Tween 80	260
Figure 4.39	The EDX Spectrum Of Mild Steel Immersed In 0.9%NaCl With 5% Phospholipids-Based Biosurfactant	261
Figure 4.40	The EDX Spectrum Of Mild Steel Immersed In 0.9%NaCl With 10% Phospholipids-Based Biosurfactant	261
Figure 4.41	The EDX Spectrum Of Mild Steel Immersed In 0.9%NaCl With 15% Phospholipids-Based Biosurfactant	261
Figure 4.42	The Impact Of Inhibitors Concentration On Mechanical Properties Of Steel Reinforcement	266
Figure 4.43	The Vertical And Horizontal Slump Flow Values Of Fresh Concretes With T500 Time Analysis	268
Figure 4.44	The Effect Of Admixture On The f_c Of Concrete	274
Figure 4.45	Post-Compression Failure Patterns Of Concrete Cube Specimens (a) Control Specimen Without Admixture And Specimens With Biosurfactant Dosages Of (b) 5%, (c) 7.5%, (d) 10%, (e) 12.5%, (f) 15%, (g) 17.5%, And (h) 20%	277

Figure 4.46	Explosive Failure Of Concrete Cubes Specimens Containing 10% Tween 80 Due To Brittle Behaviour	279
Figure 4.47	The Effect Of Water Absorption On The f_c of Concrete Specimens	280
Figure 4.48	The Relationship Of Phospholipid Biosurfactant And Tween 80 Dosage With f_s Of Concrete Over Time	282
Figure 4.49	The f_s Of RC Beam Specimens With Biosurfactant As Admixture After 28 Days Of Curing	285
Figure 4.50	Biosurfactant Flexural Failure Pattern Of Singly Reinforced Concrete Beams With 10% Biosurfactant.	288
Figure 4.51	The Flexural Failure Modes Of (a) Control Specimen And (b) Beam Incorporating 10% Biosurfactant As A Corrosion Inhibitor And As An Admixture (10% Water Replacement By Weight)	289
Figure 4.52	The Relationship Of CR And the τ of Control Specimens And Specimens Incorporating 10% Biosurfactant As A Corrosion Inhibitor And Water Replacement Admixture	291

LIST OF SYMBOLS

Symbols

τ	Bonding strength
CaCO3	Calcium carbonate
$CaCl_2 \cdot 6H_2O$	Calcium chloride dihydrate
Ca(OH)2	Calcium hydroxide
CO2	Carbon dioxide
R_{ct}	Charge Transfer Resistance
Cl	Chloride
f_c	Compressive strength
K_2HPO_4	Dipotassium hydrogen phosphate
CPE_{dl}	Double-layer Capacitance
Ω	Electrical Resistance (Ohm)
Fe^{2+}	Ferrous iron
f_s	Flexural strength
H^+	Hydrogen ions
Fe	Iron
Fe_2O_3	Iron oxide
$Fe(OH)_2$	Iron (II) hydroxide
$MgSO_4$	Magnesium sulfate

μL	microliter = 10^{-6} liters = 0.001 milliliters
O_2	Oxygen
R_p	Polarisation Resistance
KOH	Potassium hydroxide
R_s	Solution Resistance
NaCl	Sodium Chloride
NaOH	Sodium hydroxide
$NaNO_3$	Sodium nitrate
S	Sulphate
n	Surface Heterogeneity Factor
R_m	Tensile strength
H_2O	Water
Re	Yield strength

LIST OF ABBREVIATIONS

Abbreviations

AC	Alternating Current
CAN	Acetonitrile
CMC	Critical Micelle Concentration
DCW	Dry Cell Weight
DMPA	Di-myristoyl Phosphatidic Acid
DO	Dissolved Oxygen
EDX	Energy Dispersive X-ray
EIS	Electrochemical Impedance Spectroscopy
IE	Inhibition Efficiency
LC-QTOF-MS	Liquid Chromatography-Quadrupole Time-of-Flight Mass Spectrometry
LPC	Lysophosphatidylcholine (1-Linoleoyl-sn-glycero-3-phosphocholine)
LPE	Lysophosphatidylethanolamines
MEA	Malt Extract Agar
MICI	Microbially Influenced Corrosion Inhibition
MoR	Modulus of Rupture
MSM	Minimal Salt Medium
NAC	Natural Aggregate Concrete
OD	Optical Density

OPC	Ordinary Portland Cement
PDA	Photodiode Array
PDA	Potato Dextrose Agar
PE	Glycerophosphoethanolamines
pH	Potential of Hydrogen
PI	Glycerophosphoinositols
POPE	Palmitoyl-2-oleoyl-sn-glycero-3-phosphoethanolamine
PS	Glycerophosphoserines
RC	Reinforced Concrete
RCA	Recycled Concrete Aggregate
RT	Retention Times
SCC	Self-compacting Concrete
SEM	Scanning Electron Microscopy
SRB	Sulphate-reducing Bacteria
W/C	Water to Cement Ratio

CHAPTER 1
INTRODUCTION

1.1 Research Background

Corrosion of steel reinforcement is widely recognised as the most critical deterioration mechanism affecting the durability and serviceability of reinforced concrete (RC) structures. The NACE International IMPACT study estimates that corrosion imposes an annual global cost of approximately US$2.5 trillion, equivalent to 3–4% of the world's GDP, underscoring the magnitude of the problem (Koch et al., 2016). In RC systems, premature deterioration is predominantly driven by the depassivation of embedded steel, particularly under chloride ingress and carbonation exposure, which accelerates the electrochemical corrosion process (Bastidas-Arteaga, 2015). This deterioration mechanism leads to cracking, spalling, loss of bond, and reductions in structural capacity, ultimately increasing safety risks and maintenance demands (Sosdean et al., 2015; Anthony et al., 2016).

Life-cycle cost analyses consistently show that corrosion significantly elevates long-term maintenance and rehabilitation expenditure, often becoming the dominant component of the total life-cycle cost of RC structures, especially in aggressive environments (Alexander & Beushausen, 2019). Although conventional corrosion inhibitors such as inorganic and synthetic organic compounds are widely used, their application has raised concerns due to issues of toxicity, carcinogenicity, and environmental persistence. (Rivetti et al., 2018),

These environmental limitations have intensified interest in eco-friendly corrosion mitigation approaches, including biosurfactant-based organic inhibitors. Such green alternatives offer the potential for effective corrosion protection while reducing ecological and human-health risks, providing a strong scientific basis for investigating biosurfactants as sustainable corrosion inhibitors for RC infrastructure. These corrosion inhibitors can be classified into two categories: (i) organic and (ii) inorganic. Organic inhibitors are commonly known as bio-based surfactants or biosurfactants, which are compounds synthesised by microorganisms (bacteria, fungi, and yeasts). These microorganisms produce biosurfactants that emulsify hydrocarbon substrates in their growth media.

Kapadia and Yagnik (2013) classified biosurfactants into two categories based on molecular weight: (i) low and (ii) high molecular-weight compounds. Low-molecular-weight biosurfactants encompass lipopeptides, glycolipids (rhamnolipids, sophorolipids, and trehalolipids), glycopeptides, fatty acids, phospholipids, and proteins. Conversely, high-molecular-weight biosurfactants comprise complex polyanionic heteropolysaccharides (polysaccharides, proteins, lipoproteins, and entire cells) (Vanavil et al., 2013). These compounds exhibit amphipathic characteristics and possess significant emulsifying and surface-active properties (Marchant & Banat, 2012).

The benefits of biosurfactants compared to synthetic surfactants are extensively reported. Their critical attributes include high biodegradability, low toxicity, functional stability across a wide range of pH, salinity, and temperature conditions, and the ability to be produced from renewable and cost-effective substrates such as agro-industrial by-products and domestic waste (Marchant & Banat, 2012; George & Jayachandran, 2013; Ramírez et al., 2015). While substantial research has focused on biosurfactant production by bacterial strains, fungal-derived biosurfactants remain comparatively underexplored. Notably, several studies have shown that filamentous fungi can synthesise biosurfactants using low-value raw materials, including industrial and household waste oils (Bhardwaj, 2013).

Beyond their well-established roles in emulsification, wetting, and corrosion inhibition in solution, biosurfactants have also demonstrated significant potential as eco-friendly coating materials. Their amphiphilic molecular structure enables strong adsorption onto solid surfaces, allowing the formation of thin, protective films that act as physical and chemical barriers against moisture, chloride penetration, and other corrosive agents. This film-forming capability positions biosurfactants as promising candidates for green surface-coating formulations, particularly for metallic substrates such as reinforcing steel in concrete. The use of biosurfactants as surface-applied coatings introduces an additional functional pathway, beyond admixture application, offering potential to enhance durability by imparting hydrophobicity, reducing permeability, and improving resistance to electrochemical corrosion. Figure 1.1 illustrates the general process of biosurfactant production and the range of its emerging applications, including its potential role as a sustainable coating agent.

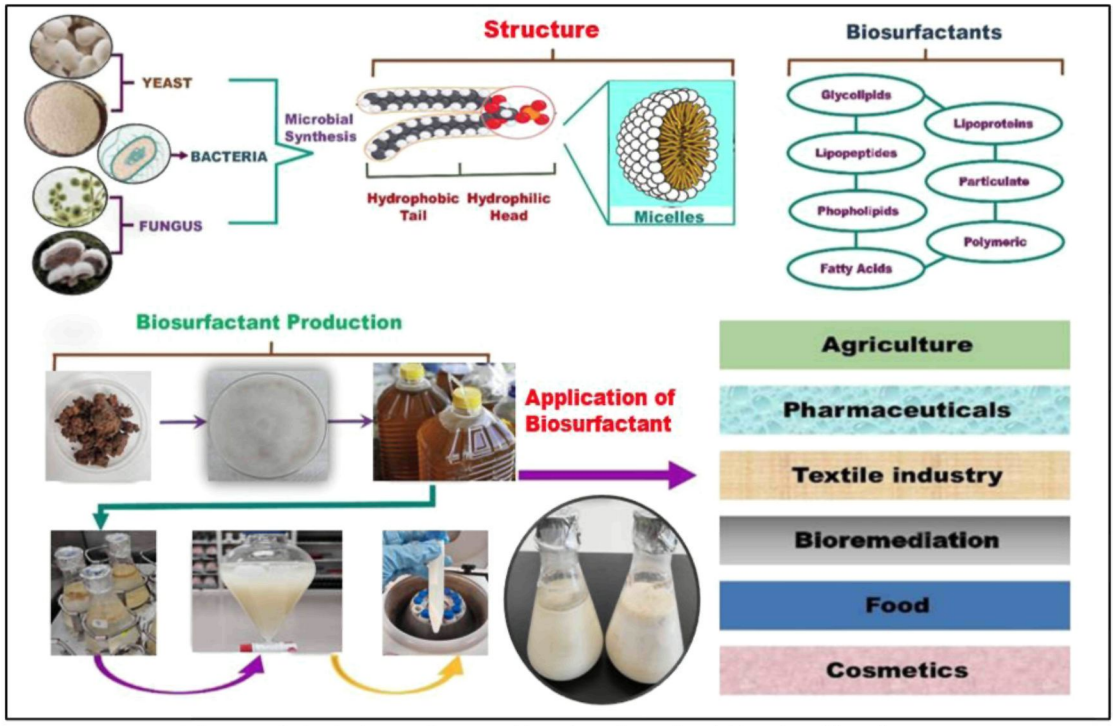

Figure 1.1 Biosurfactant Production And Its Applications

This study investigated the potential application of renewable and economical OCIs sourced from soil fungi. The fungi were obtained from municipal waste disposal sites and automobile garages in Kota Samarahan and Kuching, Sarawak. Consequently, this study presented a value-added strategy for waste management by employing waste frying oil (WFO) as the carbon (C) source for biosurfactant production through fermentation in reducing and mitigating the environmental impact linked to this waste material. WFO was selected as the carbon source in this study due to its chemical composition, biodegradability, availability, and proven suitability for microbial biosurfactant production. WFO contains elevated levels of free fatty acids (FFAs), triglycerides, and partially oxidised lipid compounds, which serve as excellent hydrophobic substrates for fungal metabolism and biosurfactant synthesis (Nurul Fatihah Khairudin, 2016).

From a sustainability standpoint, WFO is an abundant, low-cost, and renewable agro-industrial waste, making it an economically viable substrate that reduces the overall production cost while contributing to waste valorisation. Its reuse aligns with circular-economy principles and mitigates the environmental impacts associated with improper disposal (Cheah et al., 2021). Several studies have demonstrated that WFO enhances biosurfactant yield in fungi and bacteria due to its rich lipid profile, making it

a favourable substrate for industrial-scale bioprocesses (George & Jayachandran, 2013; Nur Afini Binti Wan Adlin et al., 2020; Liepins et al., 2021).

The outcomes of this study also implied a promising and economically viable research area that required in-depth investigation through sustained and comprehensive studies. These data could then enhance the existing knowledge on biosurfactants and aid in the advancement of environmentally sustainable construction materials.

1.2 Motivation for the Study

Corrosion of reinforced concrete remains a persistent and costly challenge in Malaysia, particularly in humid and chloride-rich environments where premature deterioration significantly reduces service life and elevates maintenance expenditure. While synthetic corrosion inhibitors are widely used, their toxicity, carcinogenic risks, and environmental persistence highlight the need for a safer and sustainable solutions.

Malaysia simultaneously generates large volumes of WFO much of which is improperly discarded, contributing to soil and water pollution. Despite its abundance and high lipid content, limited studies have been conducted on its potential as a substrate for biosurfactant production particularly for corrosion mitigation. No studies have examined fungal-derived biosurfactants from indigenous Sarawak strains as the existing local research focuses mainly on bacterial biosurfactants, leaving a notable gap in leveraging local fungal biodiversity for green engineering applications.

This study is motivated by the opportunity to transform a locally generated waste into a high-value, environmentally friendly product that can mitigate corrosion in reinforced concrete. By linking waste valorisation with green bioprocessing and corrosion mitigation, the study contributes to two key ambitions:

i. reducing reliance on toxic synthetic inhibitors by introducing a safer, sustainable alternative, and
ii. supporting local bioindustry development by demonstrating the feasibility of producing fungal biosurfactants from Sarawak's indigenous microbial resources.

Ultimately, the motivation behind this research is to promote a circular, environmentally conscious approach to corrosion protection that benefits both infrastructure durability and environmental sustainability.

1.3 Problem Statement

Reinforced concrete (RC) structures in Malaysia are increasingly affected by premature corrosion of embedded steel, a problem that is especially pronounced in regions with high humidity, frequent rainfall, and chloride-laden environments. Sarawak's equatorial climate, characterised by consistently high temperatures ranging between 26–34 °C, relative humidity often exceeding 80%, and prolonged wet seasons creates an environment highly conducive to corrosion initiation and acceleration. Coastal districts such as Kuching, Mukah, Bintulu and Miri are further exposed to airborne chlorides from the South China Sea, intensifying the risk of steel depassivation even in relatively new RC structures. These harsh environmental conditions result in rapid deterioration, reduced structural service life, and increased maintenance and repair costs for public infrastructure, buildings, and transportation systems across the state. Despite these persistent challenges, corrosion mitigation strategies suitable for Sarawak's unique climatic conditions remain limited and heavily dependent on synthetic chemical inhibitors.

Despite the growing global interest in eco-friendly corrosion inhibitors, Malaysia still lacks a sustainable, locally produced alternative suitable for reinforced concrete applications. Current practice continues to rely heavily on synthetic chemical inhibitors, which pose health and environmental risks and are increasingly incompatible with long-term sustainability goals.

Although biosurfactants offer a promising green alternative, their application in corrosion protection remains limited due to high production costs, inconsistent availability, and a lack of locally sourced raw materials. In Malaysia, research has focused mainly on bacterial biosurfactants, leaving indigenous fungal-derived biosurfactants unexplored. This gap persists despite their potential advantages in film formation, surface activity, and biodegradability (da Silva et al., 2021).

In addition, while biosurfactants have been studied as corrosion inhibitors in liquid media, their performance as protective coatings on steel reinforcement and as admixtures or surface treatments in reinforced concrete remains unknown. There is

limited understanding of their film uniformity, stability, and potential interaction with concrete matrices. The possibility of microbiologically influenced corrosion (MIC) under certain conditions further underscores the need for comprehensive evaluation before such biosurfactants can be confidently applied in structural applications. The lack of empirical data on these locally sourced fungal biosurfactants creates a significant knowledge gap in both material performance and practical feasibility for reinforced concrete protection.

Therefore, this research is needed to generate the first systematic evidence on the production, characterisation, and corrosion-mitigating behaviour of *Rhizopus*-derived biosurfactants for sustainable reinforced concrete applications in Malaysia. A clear framework for the research direction and anticipated outcomes of this study is then outlined within the research objectives in the following section

1.4 Research Objectives

This study investigates the potential of Rhizopus *sp.*–derived phospholipid biosurfactants, produced WFO as the sole carbon source, as a sustainable corrosion inhibitor for RC. To achieve this aim, the following specific objectives were formulated:

i) To isolate, identify, and screen indigenous fungal strains from contaminated environments for their ability to produce biosurfactants, and to optimise growth conditions to maximise biosurfactant yield

ii) To characterise the compounds, functional groups, and biosurfactant class of the most efficient fungal strain, and to quantify its inhibitory performance against mild steel corrosion.

iii) To determine the corrosion inhibition efficiency of the characterised biosurfactant on mild steel reinforcing bars using the migrating inhibitor approach, and to establish the relationship between inhibitor dosage and electrochemical performance.

iv) To analyse the effect of biosurfactant incorporation as a concrete admixture on the mechanical properties of fresh and hardened concrete.

v) To develop a corrosion protection strategy for reinforced concrete that integrates both admixed and migrating applications of Rhizopus-derived phospholipid biosurfactants.

1.5 Research Questions

This study establishes a clear scientific novel contribution by demonstrating that phospholipid-based biosurfactants derived from *Rhizopus sp.* function as dual-purpose agents, serving both as migrating corrosion inhibitors for steel reinforcement and as admixtures that influence the behaviour of fresh and hardened concrete. This dual-function application has not been previously reported in the literature. The research questions were therefore formulated to investigate this contribution and to align with the study's objectives.

i) Which indigenous fungal strains can be isolated, identified, and screened from municipal dumpsites and automotive workshop soils, and under what optimised growth conditions do these strains produce the highest yield of biosurfactants?

ii) What are the chemical compounds, functional groups, and biosurfactant class of the most efficient fungal-derived biosurfactant, and how does its molecular composition relate to its inhibitory performance against mild steel corrosion?

iii) What is the corrosion inhibition efficiency of the phospholipid biosurfactant when applied to mild steel reinforcement using the migrating inhibitor technique, and how does variation in inhibitor dosage influence its electrochemical performance?

iv) How does the incorporation of the biosurfactant as an admixture affect the mechanical behaviour of concrete, specifically in terms of workability, compressive strength (f_c), flexural strength (f_s), and bond strength (τ) under standard curing conditions?

v) How can a corrosion protection strategy for reinforced concrete be developed through the integration of both admixed and migrating applications of *Rhizopus*-derived phospholipid biosurfactants?

1.6 Significance of the Study

The findings of this study enhanced environmental sustainability in accordance with the Malaysian government initiative detailed in the 12th Malaysian Plan 2021–2025 (12th Plan). This plan was announced by the 9th Prime Minister of Malaysia, Dato' Sri Ismail Sabri Yaakob, on 27th September 2021 as a medium-term strategy designed to realise 'A Prosperous, Inclusive, Sustainable Malaysia'. Thus, the plan signals the onset of a new phase in the Malaysian development journey [Shared Prosperity Vision 2030 (WKB 2030)]. The government is also dedicated to executing transformative and radical initiatives to achieve the goals of prosperity, inclusivity, and sustainability during the 12th Plan. This plan focuses on economic reset, enhancement of security, promotion of well-being and inclusivity, and advancement of sustainability. Generally, the 12th Plan is underpinned by three themes and four catalytic policy enablers aimed at cultivating future talent, promoting technology adoption with innovation, improving connectivity with transportation infrastructure, and reinforcing public service capabilities. These essential enablers constitute the fundamental components of Malaysian development for the next five years and beyond.

Theme 3 is devoted to advancing green growth, enhancing energy sustainability, and reforming the water sector. This theme aims for a significant transition to sustainable economic practices and lifestyles that emphasise the importance of natural resources and environmental health. Therefore, this paradigm shift can tackle climate change, unsustainable consumption with production patterns, biodiversity loss, policy incoherence, and inefficient water resource management. The 12th Plan also enhances green growth to obtain sustainability and resilience. This process involves a collective responsibility to advance a low-carbon nation, fostering equitable benefit distribution from natural resource utilisation while managing energy in a holistic and sustainable manner. The implementation of policies and strategies under Theme 3 can then facilitate sustainable and resilient growth and support the attainment of the 2030 Agenda.

This study presented the use of biosurfactants derived from indigenous fungi as corrosion inhibitors for steel reinforcement in concrete. Biosurfactants often possess

characteristics akin to those of chemical surfactants, which are anticipated to demonstrate equivalent or superior effectiveness in mitigating corrosion within steel rebars. This approach can substantially enhance methods for mitigating corrosion in the construction sector by offering a non-harmful technique for corrosion inhibition regarding steel concrete reinforcement. Consequently, the corrosion inhibition formulation in this study presented a cost-effective solution for the prevention and maintenance of corrosion in civil infrastructure. The generation of WFO in significant amounts during food preparation also exhibits disposal challenges, contributing to environmental pollution. Hence, utilising WFO as a substrate for biosurfactant production is beneficial owing to WFO serving as a low-cost carbon source. This study could then support the initiatives of the government to improve environmental sustainability. Moreover, this study could facilitate opportunities for further research by presenting novel concepts, innovations, and environmentally safe corrosion inhibitors

1.7 Limitations of Study

This study aimed to fulfil its primary core objectives. Nevertheless, several limitations were identified that could affect the scope and depth of the outcomes. The extent of biosurfactant screening and characterisation was constrained by limitations in fungal strain diversity, restricted laboratory access during the COVID-19 Movement Control Order (MCO), and the elevated costs of advanced analytical instrumentation. The use of crude biosurfactants instead of purified ones was also required due to practical volume needs. Nonetheless, this necessity was consistent with the objective of this study for real-world application. Hence, these acknowledged limitations offered context for result interpretation and informed future research directions. The specific details of these limitations are as follows:

i) Scope of fungal strain diversity

The range of fungal strains assessed in this study was shaped by the availability of indigenous isolates collected from municipal dumpsites and automotive waste sites. This deliberate focus ensured relevance to real contaminated environments. While only four isolates demonstrated biosurfactant-producing potential, this targeted diversity provides a foundation for future studies to expand strain screening across broader ecological niches or to employ

molecular identification techniques for deeper taxonomic resolution.

ii) Selective chemical characterisation of biosurfactants

Only the biosurfactant exhibiting the highest yield and inhibition efficiency was subjected to detailed LC–QTOF–MS characterisation. This prioritisation was adopted to optimise resources given the high cost of advanced analytical instrumentation.

iii) Laboratory accessibility and screening approach during MCO

The screening of potential biosurfactant-producing fungal strains was limited by restricted access to laboratory facilities and equipment, requiring the implementation of rapid detection methods. These limitations primarily resulted from the screening stage being conducted during the COVID-19 pandemic under the Malaysian MCO enforced from 2020 to 2022. Therefore, this study employed qualitative and rapid screening assays to adapt to limited laboratory operations while maintaining the continuity of experimental activities in accordance with public health protocols. Conversely, the tests performed were widely utilised in previous studies for initial biosurfactant screening under time and equipment limitations.

iv) Use of crude rather than purified biosurfactant

Crude biosurfactant was employed for corrosion and concrete testing due to the substantial volumes required for both migrating and admixed applications. This choice was intentionally aligned with the study's aim of assessing practical scalability. Nevertheless, future studies could isolate and purify specific Phospholipids compounds to evaluate their individual inhibition performance. Comparative evaluations also utilised a commercial synthetic surfactant [Tween 80 (product code: P8074)] for performance benchmarking

1.8 Scope of Study

This study focuses on the development and evaluation of a fungal-derived biosurfactant for corrosion inhibition in RC. The scope encompasses:

1. The collection of contaminated soil samples from selected sites in Kuching and Kota Samarahan, Sarawak, for the isolation of indigenous fungi with biosurfactant-producing potential.
2. The identification of the most promising fungal strain and the biosurfactant it produces.
3. The assessment of the biosurfactant's feasibility as a corrosion inhibitor for steel reinforcement in concrete.
4. The evaluation of the mechanical performance of concrete incorporating the selected biosurfactant through two application approaches: admixed and migrating.

This study includes corrosion inhibition testing, mechanical strength assessment, and comparison with a commercial reference biosurfactant (Tween 80). Toxicity screening was also included to ensure the environmental safety of the selected biosurfactant.

1.9 Thesis Outline

This thesis comprises five chapters, each systematically addressing distinct components of the research as follows:

i) Chapter 1 presents the research background, objectives, problem statement, research questions, and the significance of the study. The information established the context and relevance of this study for both academic research and practical engineering applications.

ii) Chapter 2 provides a comprehensive examination of the academic literature related to RC structures, corrosion protection methods for RC, the production of biosurfactants by soil fungi, and phospholipid-based biosurfactants. This chapter also examines previous studies regarding the application of biosurfactants as eco-friendly corrosion inhibitors.

iii) Chapter 3 details the research design and methodological approach utilised in this study. The methodology involved the isolation and identification of soil

fungi capable of producing biosurfactants, characterisation of the obtained biosurfactants, and evaluation in corrosion inhibition studies. This chapter also discusses the integration of biosurfactants as admixtures in concrete. Furthermore, comprehensive accounts of materials, equipment, and experimental methodologies were presented.

iv) Chapter 4 outlines the experimental results derived from this study, along with a critical analysis and interpretation. Comparative assessments were performed, and results were analysed in relation to existing studies, emphasising both consistencies and deviations.

v) Chapter 5 presents the findings and conclusions derived from this study. This chapter also offers recommendations for future research and examines the potential of phospholipid biosurfactants in reducing corrosion in RC systems for advancing sustainable construction practices.

CHAPTER 2
LITERATURE REVIEW

2.1 Introduction

This chapter critically reviews existing research on the application of fungal-derived biosurfactants as corrosion inhibitors in RC and positions the literature to demonstrate how scientific knowledge has evolved and where substantive gaps remain. The first section synthesises foundational studies on RC corrosion mechanisms and current prevention strategies, highlighting established principles as well as unresolved limitations in corrosion science. The subsequent section evaluates the feasibility of fungal-based biosurfactants for corrosion mitigation, with emphasis on empirical evidence, methodological constraints, and the technological challenges that restrict their broader implementation. The final section examines the state of knowledge regarding concrete rheology, mechanical strength, and durability when incorporating surface-active agents. Due to the scarcity of studies on phospholipid biosurfactants in RC systems, relevant findings from conventional surfactants and biobased admixtures are critically assessed to enable meaningful comparison.

Despite the expanding body of research on green corrosion inhibitors and bio-based admixtures, several critical gaps persist. First, there is a limited understanding of the corrosion inhibition mechanisms of phospholipid-based fungal biosurfactants, particularly their interfacial interactions with steel embedded in RC and their performance under tropical environmental conditions characteristic of regions such as Sarawak. Existing studies predominantly focus on bacterial and fungal-derived glycolipid biosurfactants, leaving a significant knowledge deficit concerning fungal-derived phospholipids and their electrochemical behaviour in RC systems. Second, empirical evidence on the dual functionality of fungal biosurfactants as both corrosion inhibitors and concrete admixtures remains sparse. Specifically, their influence on fresh-state properties, strength development, steel–concrete bond performance, and long-term durability has not been systematically established, resulting in fragmented insights that limit practical implementation. Third, there is a lack of integrated, multidisciplinary investigations that combine microbiological characterisation, material performance testing, and mechanistic corrosion analyses. Current literature typically

isolates these dimensions, preventing the development of a coherent scientific framework for safely and effectively incorporating biosurfactants into RC technology.

These gaps highlight the need for a comprehensive evaluation of phospholipid fungal biosurfactants from both microbiological and structural engineering perspectives, thereby informing the direction and significance of the study.

2.2 Reinforced Concrete Structures

Reinforced concrete (RC) remains the principal structural material in modern infrastructure due to its favourable balance of compressive strength, constructability, and cost-effectiveness. Its performance is governed by the composite interaction between concrete, which bears compressive forces, and embedded steel reinforcement that provides resistance against tensile stresses. When functioning synergistically, this composite system offers significant mechanical reliability and long-term structural stability. However, the durability of RC is not solely dependent on mechanical properties; it is critically influenced by physicochemical processes at the steel–concrete interface and by environmental exposure conditions (Shunmuga et al., 2023).

Recent studies highlight that RC deterioration is increasingly associated with progressive mechanisms such as carbonation, chloride penetration, moisture cycling, and temperature fluctuations—factors that accelerate depassivation and corrosion initiation (Kopiika et al., 2025). Life-cycle cost analyses demonstrate that corrosion-induced degradation constitutes one of the most substantial long-term financial burdens for RC infrastructure, often exceeding initial construction costs due to maintenance, repair, and premature replacement (Yadav et al., 2024). These findings underscore the need for innovative, sustainable corrosion mitigation strategies that reduce long-term deterioration and operational costs.

Understanding the fundamental behaviour of RC is especially important when evaluating the suitability of biosurfactants for corrosion inhibition. Biosurfactant efficiency is influenced by the alkalinity of the concrete pore solution, ionic composition, moisture dynamics, and the transport behaviour of molecules within the cementitious matrix. Therefore, an appreciation of RC's microstructural evolution, pore connectivity, and electrochemical environment is essential for predicting how biosurfactant compounds may migrate, adsorb, or form protective films on reinforcement surfaces. Without grounding the study in RC fundamentals, the

interpretation of biosurfactant performance as migrating inhibitors or as admixtures would remain incomplete and potentially inaccurate.

Thus, this section establishes the structural and durability context necessary to justify the application and evaluation of phospholipid-based fungal biosurfactants within RC systems.

2.2.1 Materials Used in RC

Reinforced concrete (RC) performance is fundamentally governed by the characteristics and interactions of its constituent materials. These include coarse and fine aggregates, cementitious binders, water, admixtures, reinforcement bars, and other additives that collectively determine the structural, mechanical, and durability properties of the composite system. The selection and quality of these materials are therefore critical, as they directly influence key concrete attributes such as f_c, workability, permeability, long-term durability, and the overall corrosion resistance of embedded steel reinforcement (Amin et al., 2022; Surahyo, 2019). The contribution of each component differs in magnitude and function, yet their combined behaviour forms a composite material that is widely regarded for its versatility in meeting both functional and architectural construction demands.

In tropical regions such as Malaysia, and particularly in Sarawak, the performance of RC materials exhibits pronounced variability due to persistent climatic stressors. Elevated humidity, high annual rainfall, chloride-laden marine winds, and temperature-driven microstructural changes collectively intensify material degradation processes. These environmental influences extend beyond the intrinsic properties of the constituent materials, necessitating a critical evaluation of how tropical exposure conditions accelerate deterioration mechanisms and ultimately affect the long-term durability of RC structures.

2.2.1.1 Reinforcement Bars

Sarawak's geography characterised by extensive coastlines, estuarine zones, and high atmospheric chloride concentrations creates corrosion challenges. Reinforcing steel in RC is frequently exposed to airborne salts transported inland by monsoon winds, as well as contaminated groundwater in low-lying construction areas. Studies from

coastal Malaysia have reported chloride deposition rates up to *four times higher* than inland regions, accelerating pitting corrosion and reducing service life by 30–50% without adequate mitigation (Binyehmed, F. 2018). Such exposure conditions directly influence the selection of reinforcement type, protective coatings, and the need for corrosion-inhibiting admixtures.

The high f_c of concrete facilitates the construction of skyscrapers, large bridges, and complex underground structures. Even though this feature addresses the dynamic requirements of urban development, plain concrete demonstrates low R_m, limited ductility, and a tendency to crack (in response to temperature variations and shrinkage). Therefore, engineers have addressed these concerns by integrating steel reinforcement (rebars) into the concrete matrix. This process results in RC capable of withstanding both tension and compression. The coefficient of thermal expansion of steel reinforcement and concrete are also almost comparable, as both materials exhibit similar expansion behaviours in response to temperature variations. This property guarantees that the concrete experiences minimal stress during temperature fluctuations.

Steel reinforcing bars consist of high-strength steel and are crucial for providing R_m to offset the inherent tensile weaknesses of concrete. These bars enhance bonding with concrete through specific characteristics (ribs, ridges, and indentations) and are available in various shapes and sizes (round, square, and deformed profiles). Consequently, improved load transfer and lower slippage can be observed between the materials through this interaction. Several advantages are also indicated through the strategic placement of rebars in concrete elements (beams, columns, and foundations). These benefits include increased overall structural performance, enhanced load distribution, and less cracking. Nonetheless, achieving the long-term stability and safety of the constructed structure can be significantly impacted by multiple factors. Critical examples are pre-installation treatment, regular inspection, material selection, and precise installation of reinforcing bars.

Specific structural requirements are necessary for different reinforcement bar types. Several examples are denoted as follows:

i) Hot-rolled deformed bars possess enhanced τ with concrete, rendering them suitable for RC. These bars are usually manufactured by heating steel billets to high temperatures exceeding their recrystallisation point and rolling them into

the specified shape. Improved τ with concrete is presented through deformation, which involves surface ribs or lugs along the length of these bars. Grading typically occurs according to yield strength (R_e) (Grades 40 or 60). The specified grades denote the minimum R_e of the bars, which is usually designated as high tensile steel (T = for 460 N/mm^2 or Y = for 410 N/mm^2).

ii) Cold-worked steel bars are created through the processes of stretching and drawing steel bars at ambient temperature. The enhanced strength of cold-worked renders them appropriate for secondary reinforcement or structures with elevated R_m without high elongation. In contrast, the diminished ductility makes them less suitable for seismic-prone areas, in which increased energy absorption and elongation are critical to avert catastrophic failure. These materials are also typically manufactured in smaller diameters, rendering them appropriate for secondary reinforcement in structures that demand high R_m with minimal elongation. One notable example is lighter constructions or secondary reinforcements (stirrups and ties).

iii) Mild steel plain bars contain mild steels from low-carbon steel, which are commonly utilised in smaller-scale or cost-effective projects. The plain-surfaced reinforcement bars lack surface ribs, leading to reduced τ with concrete. Although mild steel bars exhibit lower τ, they demonstrate superior ductility and elongation. These features render them appropriate for applications requiring flexibility and the capacity to absorb bending stresses. The use of plain (non-deformed) mild steel bars is typically restricted to non-primary reinforcement elements (ties and stirrups) owing to their inferior R_m and bond capacity relative to deformed bars. The tensile R_e of these bars is also 40,000 psi (275.79 N/mm^2). Notably, mild tensile steel is identified as R for 250N/mm^2.

iv) Prestressing steel bars are utilised in prestressed concrete, which are composed of high-carbon steel and are engineered to withstand significant tensile stresses. These bars are generally composed of high-strength steel wires or strands that are pre-tensioned prior to the application of load on the concrete. The process can enhance the load-bearing capacity of the concrete during service. Prestressing steel bars exhibit an R_m ranging between 250,000 and 270,000 psi,

which are predominantly utilised in bridges, long-span beams, and high-performance concrete-based structures. Prestressing steel is also employed to reduce cracks and deflections in concrete when subjected to service loads.

Comprehending the mechanical properties of mild steel-based reinforcing bars necessitates gaining information regarding the effects of R_m, R_e, and elongation on these bars. The capacity to resist stress, undergo deformation, and sustain loads without failure of a material can be demonstrated by analysing these characteristics. Specifically, several factors can affect these relationships, including composition, microstructure, and processing treatments. The maximum stress a material can endure when subjected to tension before failure occurs is known as the R_m (ultimate strength). This indicator is useful to denote the resistance of a material to fracture when subjected to tensile stress, which usually occurs subsequent to yielding and prior to rupture. The maximum stress that steel can withstand prior to failure is also denoted through this indicator. This value indicates the ultimate load-bearing capacity of the steel, which the R_e is lower than this value.

The maximum load that steel can withstand without experiencing permanent deformation is denoted as R_e. A material undergoes permanent deformation and fails to revert to its initial shape upon removal of the load once the yield point is surpassed. Thus, establishing the safe limits of the structural application of a material is significantly influenced by this parameter. Elastic deformation criteria in structural design also necessitate obtaining this value. Meanwhile, the steel bars that can endure the loads imposed by the concrete and the overall structure without premature failure are indicated by this indicator for RC. The ductility of a material can also be evaluated using the ratio between R_m and R_e. A ductile material that undergoes substantial elongation prior to failure is signified by a notable difference. On the contrary, a more brittle material that may fracture abruptly is denoted by a minimal difference. Overall, the R_e and R_m of mild steel bars are critical factors influencing the overall strength and stability of RC structures. The R_e of steel reinforcement guarantees sufficient support under typical service loads, whereas R_m offers a safety margin for extreme conditions, such as earthquakes and heavy traffic (Morales, 1998).

Elongation measures the ductility of a material and its ability to experience plastic deformation prior to failure. Increased elongation indicates enhanced ductility and toughness, enabling the material to absorb greater energy before failure. Figure 2.1

depicts the stress-strain diagram of the steel bar regarding the main mechanical properties (elastic limit, yield point, ultimate R_m, and breaking stress). This diagram provides a framework for assessing the R_m, ductility, and R_e of the material under examination.

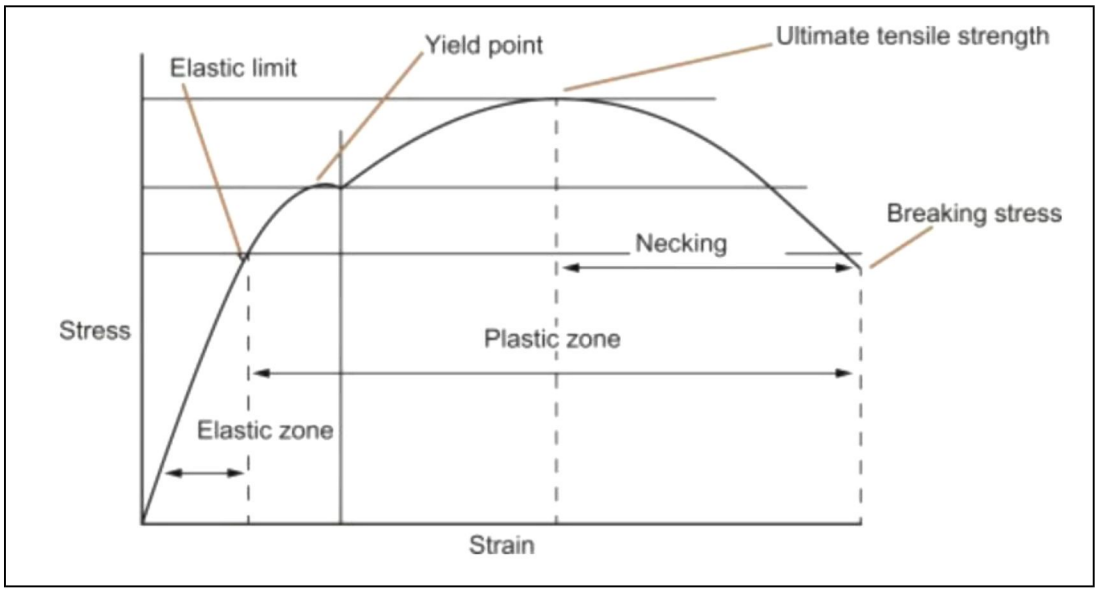

Figure 2.1 The Steel Stress-Strain Diagram

Figure 2.2 outlines the chemical composition and mechanical properties of Grade 250 mild steel bars in accordance with Malaysian Standard, MS144:2014 Steel wire for the reinforcement of concrete products. This material was provided by Southern Steel Sdn. Bhd., which is a prominent supplier of mild steel reinforcing bars in Malaysia. The compositions are representative of the mild steel bars frequently utilised in the nation. Table 2.1 summarises the chemical composition of R10 Grade 250 mild steel bars, which is consistent with MS144:2014. This material was designated for use as reinforcement in this study.

Southern Steel

HOT ROLLED STEEL BARS SPECIFICATIONS (DEFORMED/RIBBED)

Standard	Grade	Size (mm)	C	P	S	Cu	N	CE	YS (MPa)	Ratio*	AGT (%)	Certified By
MS 146 : 2014	B500B	10,12,16,20,25,32,40	0.22 max	0.050 max	0.050 max	0.80 max	0.012 max	0.50 max	500 min	1.08 min	5.0 min	SIRIM QAS
	B500C									≥1.15, <1.35	7.5 min	
BS 4449:2005 +A3 :2016	B500B	10,12,16,20,25,32,40	0.22 max	0.050 max	0.050 max	0.80 max	0.012 max	0.50 max	500 min	1.08 min	5.0 min	SIRIM QAS & CARES
	B500C									≥1.15, <1.35	7.5 min	
CS2 : 2012	B500B	10,12,16,20,25,32,40	0.22 max	0.050 max	0.050 max	0.80 max	0.012 max	0.50 max	500 min	1.08 min	5.0 min	SIRIM QAS & CARES
	B500C									≥1.15, <1.35	7.5 min	
SS 560 : 2016	B500B	10,12,13,16,20,25,32,40	0.22 max	0.050 max	0.050 max	0.80 max	0.012 max	0.50 max	500 min	1.08 min	5.0 min	SIRIM QAS & CARES
		10 - 40										
AS/NZS 4671 : 2019	500N	10,12,16,20,24,25,32,40	0.22 max	0.050 max	0.050 max	-	-	0.44 max	500 min	1.08 min	5.0 min	ACRS

HOT ROLLED STEEL BARS SPECIFICATIONS (ROUND/PLAIN)

Standard	Grade	Size (mm)	C	P	S	Cu	N	CE	YS (MPa)	Ratio*	AGT (%)	Certified By
MS 144:2014	G250	6,8,10	0.22 max	0.050 max	0.050 max	0.80 max	0.012 max	0.42 max	250 min	1.15 min	5.0 min	SIRIM QAS
MS 146:2006	G250	16,20	0.25 max	0.060 max	0.060 max	-	0.012 max	0.42 max	250 min	-	22** min	SIRIM QAS
BS 4449:1997	G250	16,20	0.25 max	0.060 max	0.060 max	-	0.012 max	0.42 max	250 min	-	22** min	SIRIM QAS
AS/NZS 4671 : 2019	250N	10,12,16	0.22 max	0.050 max	0.050 max	-	-	0.43 max	250 min	1.08 min	5.0 min	ACRS

Note : * Ratio = Tensile strength / Yield Strength ; **Elongation at fracture

Figure 2.2 Property Summary Of Mild Steel Bars Commonly Used In Malaysia As Provided By The Southern Steel Sdn. Bhd.

Table 2.1
Chemical Composition Summary Of Mild Steel Bars (R10 Grade 250) According To MS144:2014

Chemical Composition (%)	C	Si	Mn	P	S	V	Cu	Ni	Cr	Mo	Nb	C_{eq}
	X100			X1000			X100				X10000	X100
	19	17	66	21	18	3	19	6	12	1	50	34

2.2.1.2 Coarse and Fine Aggregates

In Malaysia, aggregates are often sourced from granite, limestone, or river deposits, each with distinct mineralogical compositions that influence alkali–silica reactivity, absorption capacity, and mechanical behaviour. For example, crushed limestone commonly used in Sarawak demonstrates lower density and higher water absorption than granite aggregates, contributing to an increased risk of chloride diffusivity under coastal exposure (Ismail et al., 2021).

Aggregate selection is a crucial determinant in enhancing concrete performance. The mechanical characteristics of concrete (strength and durability) are related to the aggregate properties (size distribution, shape, porosity, and specific gravity) (Amin et

al., 2022). Generally, the main categories consist of crushed stone, natural sand, granite aggregates, and recycled concrete aggregates (RCAs) as follows:

i) Crushed stone aggregates used in these studies are primarily obtained from quarries. This material is extensively utilised owing to its availability and mechanical properties. Osouli et al. (2019) discovered that these aggregates significantly enhanced the load-bearing capacity of concrete, leading to their frequent use in structural applications. Enhanced packing density was also observed by the gradation of particle sizes in crushed stones. This process could improve overall f_c and reduce void content in the concrete matrix.

ii) Exceptional strength and durability are observed for granites. (Murlidhar et al., 2016) documented improved f_c and long-term durability of concrete structures. This outcome was attributed to the mineralogical composition and coarse surface texture of granite aggregates.

iii) Growing sustainability concerns have rendered the use of RCAs. Given that the bond between concrete and steel bars is a key factor influencing the structural integrity of RC, a thorough assessment of its interaction with steel reinforcement is pivotal. Numerous studies have examined the bond performance of RCA relative to natural aggregate concrete (NAC). Choi and Kang (2008) and Ayob et al. (2016) published that at replacement ratios of up to 50%, the bond stress-slip behaviour of RCA was comparable to NAC. This outcome suggested insignificant degradation in bond characteristics. Kim et al. (2012) revealed through pull-out testing that RCA demonstrated approximately 18% lower τ than NAC. This finding implied possible limitations in adhesion at elevated replacement levels. Zuhud (2008) recorded a larger τ between deformed steel bars and concrete with a higher proportion of recycled aggregate. Therefore, all these variations underscore the impact of multiple parameters (aggregate quality, surface texture, and mix design) on the bond behaviour of RCA. This confusion necessitates further investigation for a comprehensive understanding.

iv) An essential fine aggregate in concrete mixtures that are primarily sourced from riverbeds is natural sand. This material is well recognised for increasing workability and mix consistency. Prasad et al. (2019) asserted that an enhanced hydration process and decreased bleeding in concrete could be accomplished through the fineness modulus and clean grain texture of natural sand.

The workability and strength of concrete are significantly influenced by several components in aggregates. Primarily, this relationship is impacted by particle size distribution, absorption, shape with surface texture, specific gravity, mineral composition, and porosity. Hence, several benefits are observed by a balanced distribution of coarse and fine particles within well-graded aggregates. These advantages include enhanced cohesion, f_c, and packing density, alongside lower void content in the concrete. Additionally, the interlocking ability and τ with the cement paste is highly dependent on the morphology of aggregate particles. Compared to rounded and smooth-surfaced particles, enhanced mechanical interlocks are indicated with angular aggregates with rough surface textures. This process can increase the load-bearing capacity through superior stress transfer in the concrete induced by the interlock. Chemical stability and resistance to degradation, when exposed to environmental conditions, are impacted by specific minerals within the structure. Workability and strength development are also two elements affected by the water content in aggregates during mixing. The bond between cement and aggregate can be compromised by excess moisture that disrupts the water-to-cement (w/c) ratio. Conversely, adequate water available for cement hydration is impaired by excessively dry aggregates that absorb mixing water. Therefore, optimised concrete mix design and structural performance require an in-depth understanding of these parameters.

2.2.1.3 Admixture and Additives

The incorporation of admixtures and additives plays a critical role in modifying the fresh and hardened properties of concrete. These materials enhance workability, reduce permeability, and improve long-term durability; however, their performance is strongly influenced by curing conditions and moisture retention, which fluctuate significantly in Sarawak's equatorial climate.

Compared to the standard components of concrete, the proportions of admixtures are generally minimal. This component can act either chemically or physically, with typical proportions ranging from 0.02% to 0.5% within the concrete (Gandage, 2023). Air-entraining admixtures also enhance the durability of concrete concerning its resistance to freeze-thaw cycles and its performance against de-icing salts. These admixtures generate and stabilise microscopic air bubbles within the concrete matrix, aiding in the absorption and distribution of stresses induced by freezing and thawing cycles. Therefore, surface scaling and deterioration can be mitigated through this process (Faqe et al., 2020).

Water-reducing admixtures serve to decrease the water-cement ratio, improving concrete strength or attaining a greater slump without increasing the water content. This process can preserve workability. These water reducers reduce water content by 5% to 10%, which results in a direct improvement in the concrete's 28-day strength by 10% to 25% compared to concrete without admixtures. Research by Binns (2003) indicates that mid-range water reducers can significantly improve concrete workability, particularly within slump ranges of 125 mm to 200 mm(Binns, 2003).

Likewise, accelerator-based admixtures are incorporated to reduce the initial setting time, improving early strength for cold weather concreting and expedited construction projects. These materials enable the prompt removal of formworks and opening of concrete pavements to vehicular traffic. Typically, chloride-based (calcium chloride) or non-chloride-based compounds (triethanolamine, sodium thiocyanate, calcium formate, calcium nitrite, or calcium nitrate) are utilised in non-reinforced structures or reinforced and prestressed concrete, respectively. Despite that these admixtures are effective in accelerating setting times, it is important to exercise caution to prevent overdosing. This outcome can result in drying shrinkage, reinforcement corrosion, and a reduction in strength at later ages (Myrdal, 2007).

A retarder is incorporated into concrete to decelerate the cement hydration process, prolonging its workability and postponing the initial setting time. This characteristic is beneficial in high temperatures, substantial applications, or when prolonged workability is required. Consequently, workability is preserved while lowering slump loss, rendering it suitable for mass concreting applications (pier foundations and oil well cementation). These retarders extend the setting time of concrete, allowing for improved placement and finishing without compromising the strength of the concrete (Costa et al., 2023).

Meanwhile, superplasticisers enhance the workability of concrete, facilitating a decrease in water content while maintaining the consistency of the mix. This reduction in w/c ratio results in a denser and more compact concrete matrix, which enhances f_c and durability. Overall, plasticisers or superplasticisers admixtures can notably reduce the water requirements of concrete. Nevertheless, these materials can introduce finishing, significant retardation, and slump loss-related issues (Chen et al., 2023).

Various concrete admixtures (organic and inorganic) have been proposed as targeted inhibitors of steel corrosion. Corrosion inhibitors are generally employed as admixtures in concrete for new construction. These inhibitors can also be applied in repair processes by being mixed with concrete for patches, sprayed onto the concrete surface, or utilised through saturation treatment. In contrast, certain admixtures may delay the setting time of cement or have adverse effects at later stages. Other corrosion inhibitors can also produce adverse side effects. High dosage may delay the setting time of cement and decrease concrete strength due to incompatibility or chemical reactions with cement compounds. Furthermore, various additional admixtures are employed to alter the properties of concrete in both its fresh and hardened states, including accelerators, retarders, and various specialised additives. Table 2.2 lists these additional admixtures that enhance the performance of concrete in specific applications. Thus, the choice of the suitable admixture type is essential for attaining the desired characteristics in fresh and hardened states of concrete when considering environmental conditions and project specifications.

Table 2.2
Different Types Of Admixtures Commonly Used In Concrete Manufacturing

Type of Admixture	**Application in Concrete**
Air entraining	Introduce and stabilize microscopic air bubbles, improving resistance to surface scaling.
Water reducing	Lower water-cement ratio, increase strength, or achieve higher slump without adding water. Improve 28-day strength by 10% to 25%.
Retarders	Delay setting time, useful for hot weather concreting and mass concreting works. Extend workability and reduce slump loss.
Accelerators	Speeds up the rate of strength development at early ages, crucial for rapid construction processes.

Type of Admixture	Application in Concrete
High range water reducing (Superplasticizers)	Lead to 12% to 30% water reduction, increasing early age strength, reducing chloride ion penetration, and ultimate compressive strength. Enhance flowability. May cause finishing difficulties, significant retardation, and slump loss.
Hydration control	Comprises a two-part chemical system; Stabilizer or retarder that stops the hydration of cementitious material and activator that re-establishes normal hydration and setting. Commonly adopted for ready-mix concrete operations.
Corrosion inhibitors	Protect reinforcement steel from corrosion, extending the lifespan of reinforced concrete structures.
Shrinkage reducing	Adopted for concrete in bridge decks, floor slabs to minimize formation of cracks preventing adverse environmental influence.
Colouring admixtures	Natural and synthetic materials to colour concrete for aesthetic and safety applications. To prevent adverse effects of pigments on concrete properties, the dosage is limited to 6%.
Pumpability and Penetration	Improve concrete pumpability for high-rise construction projects. Increases the ease with which concrete can be pumped and placed in difficult-to-reach areas, ensuring consistent compaction and strength.
Damp proofing	Soap, stearate, and petroleum-based admixtures added to concrete mixes with low cement content and high-water cement ratio to improve their water impermeability.
Bonding admixtures	Rubber, polyvinyl chloride, polyvinyl acetate, acrylic, styrene butadiene-based admixtures. Enhances the bond between old and new concrete surfaces and between steel reinforcement and concrete, critical for structural integrity in repairs and retrofits.
Other special Properties Production	Produces concrete with specific properties, such as colored, cellular, fungicidal, germicidal, or insecticidal characteristics.

2.2.1.4 Cement and its Role in Concrete Technology

Cement is a fundamental component of RC that exerts a profound influence on the structural performance and long-term durability of concrete composites. Its role spans a wide spectrum of applications including buildings, pavements, runways, bridges, sidewalks, and hydraulic structures such as dams (H. Kim et al., 2020). In Malaysia, Ordinary Portland Cement (OPC) remains the predominant cementitious binder in reinforced concrete (RC). However, its hydration kinetics and pore structure evolution are highly sensitive to moisture fluctuations characteristic of equatorial climates. In regions such as Sarawak, where relative humidity frequently exceeds 80%,

elevated moisture levels can accelerate early hydration yet simultaneously increase long-term permeability when curing conditions are suboptimal. This increased permeability heightens vulnerability to chloride ingress and carbonation, both of which are critical precursors to reinforcement corrosion (Alexander & Beushausen, 2019). Moreover, inconsistency in water content during field mixing further contributes to pore refinement variability, exacerbating porosity and diminishing the protective capacity of the concrete cover against corrosion-induced deterioration.

The performance of OPC is determined largely by its chemical composition, which governs its hydration behaviour, setting characteristics, and strength development. Ali et al. (2008) described the principal raw materials such as limestone, clay, and iron ore as sources of calcium oxide (CaO), silicon dioxide (SiO_2), aluminium oxide (Al_2O_3), and iron oxide (Fe_2O_3), which together form the major oxide constituents of OPC. Table 2.3 outlines the typical oxide compositions of OPC (Anon et al., 2020).

During clinker production, calcium reacts with these oxides to form the four principal Bogue compounds which collectively account for roughly 90% of the cement mass (see Table 2.4) (Mitchell, 2010). Variations in the proportions of these compounds, as summarised in Table 2.5 for normal, rapid-hardening, and low-heat OPCs, directly influence early strength gain, heat generation during hydration, and long-term durability. Higher C_3S content, for example, promotes rapid strength development, whereas increased C_2S contributes to improved long-term performance and reduced heat of hydration.

Table 2.3
Summary Of The Major Chemical Constituent Of OPC Following Malaysian Standard (MS) 197-1:2014

Chemical Component	**Percentage Composition**
Lime / Calcium oxide (CaO)	60-67%
Silica (SiO_2)	17-25%
Aluminum oxide (Al_2O_3)	3-8%
Chemical Component	**Percentage Composition**
Iron oxide (Fe_2O_3)	0.5-6%
Magnesium oxide (MgO)	1-4%
Sulfur trioxide (SO_3)	1-3%
Loss on Ignition (LOI)	0.5%-4%

Table 2.4
Bogue Compounds Of Ordinary Portland Cement

Compound	Chemical formula	Functional Roles
Tricalcium silicate (C_3S)	$3CaO \cdot SiO_2$	Rapidly hydrates to provide early-age strength, especially within the first seven days of curing. Its hydration releases substantial heat, beneficial for cold weather concreting but potentially problematic in mass pours due to thermal stress.
Dicalcium silicate (C_2S)	$2CaO \cdot SiO_2$	Contributes to strength development over a longer period, particularly beyond 28 days. It generates less heat during hydration, making it ideal for use in low-heat and large-scale concrete applications.
Tricalcium aluminate (C_3A)	$3CaO \cdot Al2O_3$	Reacts quickly with water and contributes to the early setting of cement. However, its high heat release and poor sulphate resistance can negatively impact concrete durability, especially in aggressive environments
Tetracalcium aluminoferrite (C_4AF)	$4CaO \cdot Al_2O_3 \cdot Fe_2O_3$	Has limited impact on mechanical properties but contributes to the color and hydration dynamics of cement. Its slower reaction and lower heat evolution offer minor benefits in thermal control.

Table 2.5
Summary Of The Composition And Percentage For Compounds Concerning Normal, Rapid Hardening And Low-Heat Portland Cement

Portland Cement	Normal	Rapid hardening	Low heat
(a) Composition: Percent			
Lime	63.1	64.5	60
Silica	20.6	20.7	22.5
Alumina	6.3	5.2	5.2
Iron Oxide	3.6	2.9	4.6
(b) Compound: Percent			
Tricalcium silicate (C_3S)	40	50	25
Dicalcium silicate (C_2S)	30	21	35
Tricalcium aluminate (C_3A)	11	9	6
Tetracalcium aluminoferrite (C_4AF)	12	9	14

The previous literatures on the constituent materials of reinforced concrete highlights how their performance is strongly influenced by the environmental and climatic conditions typical of Sarawak's tropical, high-humidity, and chloride-rich setting. Variations in cement hydration, aggregate moisture sensitivity, admixture effectiveness, and steel–concrete interfacial behaviour collectively heighten the vulnerability of RC structures to premature deterioration, particularly through corrosion of embedded reinforcement. These material-specific challenges underscore the limitations of conventional RC systems when exposed to aggressive tropical environments and reinforce the need for innovative, locally adaptable corrosion-mitigation strategies. Accordingly, the present study investigates the potential of a *Rhizopus*-derived biosurfactant as an eco-friendly admixture and corrosion inhibitor, positioning it as a targeted solution to enhance durability and extend the service life of RC structures in tropical marine climates.

2.3 Corrosion in RC Structures

Globally, corrosion imposes a substantial economic burden on infrastructure systems. The International Measures of Prevention, Application and Economics of Corrosion Technologies (IMPACT) study by NACE International reports that corrosion-related damage costs approximately US$2.5 trillion annually, equivalent to about 3–4% of the global GDP (NACE International, 2016). For RC structures in particular, premature deterioration of bridges, ports, and marine facilities accounts for a significant portion of global expenditure. In tropical and coastal environments, high humidity, persistent rainfall, and chloride-laden winds intensify the transport of aggressive ions into concrete, thereby increasing corrosion risk and maintenance frequency compared with temperate climates (Rincon et al., 2024).

Figure 2.3 illustrates the principal factors contributing to the degradation of RC and highlights the interconnected mechanisms that govern both concrete deterioration and reinforcement corrosion. The diagram categorises the causes into mechanical, physical, structural, chemical, biological, and corrosion-related processes, each comprising specific deterioration pathways such as abrasion, freeze–thaw damage, overloading, alkali–aggregate reactions, sulphate attack, fouling, carbonation, chloride ingress, and stray electrical currents. These mechanisms act either independently or synergistically to compromise the integrity of the concrete matrix and weaken the

protective environment surrounding embedded steel. Ultimately, the cumulative effects of these processes accelerate both concrete degradation and reinforcement corrosion, thereby reducing the service life and structural reliability of RC systems.

The corrosion of embedded steel in reinforced concrete is governed by an electrochemical mechanism involving two coupled reactions: (i) oxidation at the anodic site, where iron loses electrons and forms corrosion products, and (ii) reduction at the cathodic site, where oxygen or water gains electrons. This natural process progresses when moisture and oxygen reach the reinforcement, a condition often facilitated by deficiencies in the concrete cover such as high permeability, excessive porosity, or cracking. Multiple factors accelerate corrosion, including poor mix design, high water–cement ratios, shrinkage, inadequate curing, chloride and sulphate ingress, and carbonation-induced loss of alkalinity (Ayop & Cairns, 2013). Additional influences arise from heterogeneities in the steel–concrete interface, reduced pore-water pH, stray electrical currents, and galvanic coupling between dissimilar metals (Angst et al., 2009).

Under normal conditions, the high alkalinity of concrete (pH 12–13) promotes the formation of a passive film that protects reinforcement from corrosion. However, this protection deteriorates when aggressive agents penetrate the concrete matrix. Chloride ingress, particularly in marine environments, disrupts the passive film and initiates localised pitting, while carbonation reduces alkalinity to approximately pH 9 through the formation of calcium carbonate, leaving the steel vulnerable. Ageing and cracking further increase penetrability, enabling rust formation, bond deterioration, and spalling. These effects are most severe in prestressed systems, where even minor reductions in steel cross-sectional area can lead to tendon failure (Rivetti et al., 2018).

The severity of corrosion is closely linked to the quality of design and construction, particularly with respect to parameters such as concrete cover thickness, reinforcement detailing, compaction and curing practices, and the incorporation of protective measures such as coatings or corrosion inhibitors. Deficiencies in these aspects, when compounded by environmental factors such as high moisture levels, salt-laden winds, and fluctuating service conditions, significantly accelerate the onset of corrosion. This observation aligns with the findings of Angst et al. (2009) and Bertolini et al. (2013), who concluded that premature deterioration in RC structures is primarily driven by shortcomings in design and construction practices rather than intrinsic material deficiencies.

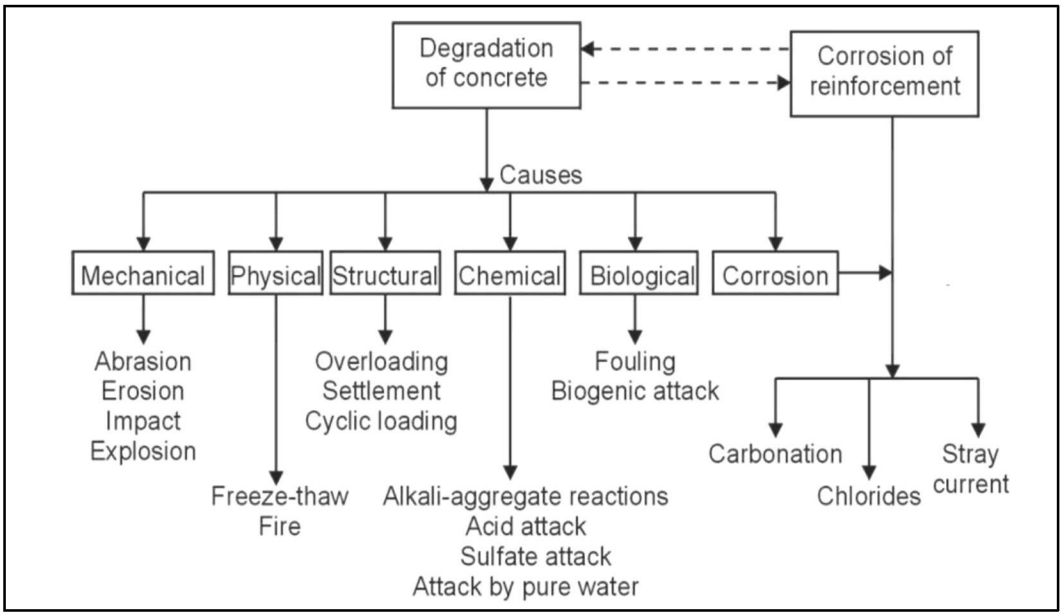

Figure 2.3 The Factors Contributing To The Degradation Of RC

2.3.1 Types of Corrosion

The 12 commonly recognised types of corrosion are uniform corrosion, pitting corrosion, crevice corrosion, galvanic corrosion, intergranular corrosion, selective leaching, erosion corrosion, cavitation corrosion, fretting corrosion, stress corrosion cracking, fatigue corrosion, and thermogalvanic corrosion. In RC systems, chloride-induced pitting, carbonation-related uniform corrosion, and crevice conditions around embedded reinforcement are the most critical, as they directly compromise structural integrity and shorten service life. The following subsections critically evaluate the corrosion forms most relevant to RC durability, with particular emphasis on those prevalent in tropical, chloride-rich environments such as Sarawak. Figure 2.4 provides an illustration of the corrosion forms discussed.

2.3.1.1 Uniform (General) Corrosion

Uniform corrosion represents the most prevalent corrosion type based on uniform material loss over the exposed surface (Cicek, 2017). This process yields a consistent reduction in thickness, rendering it predictable and manageable. The phenomenon generally takes place in aqueous environments, wherein the entire metal surface functions as a reaction site. Although uniform corrosion is easily detectable and

predictable, it constitutes the primary source of material degradation in industrial systems. The predictability also facilitates effective control via protective coatings, corrosion inhibitors, and deliberate material selection.

2.3.1.2 Pitting Corrosion

Among the various corrosion forms identified in the literature, chloride-induced pitting corrosion is widely regarded as the most severe and structurally detrimental mechanism in reinforced concrete (RC). It is characterised by highly localised attack that produces deep, narrow cavities on the steel surface once chloride ions (Cl^-) penetrate the concrete and destabilise the passive film protecting the reinforcement (Cicek, 2017). Following initiation, pit propagation progresses rapidly, even when the overall corrosion rate appears low, making this mechanism responsible for many cases of sudden and severe structural degradation in coastal and marine environments.

In contrast to uniform corrosion, which develops gradually and predictably, pitting corrosion advances in a concentrated and often undetectable manner during early stages, yet it can lead to significant loss of steel cross-sectional area and tensile capacity. This phenomenon is especially prevalent in tropical regions such as Sarawak, where chloride deposition, high humidity, and persistent wetting cycles accelerate chloride ingress and amplify the risk of pitting.

Given its dominance in chloride-rich environments, pitting corrosion is directly relevant to the present study. The NaCl-based experimental design employed here specifically replicates chloride-driven pitting conditions, enabling a targeted evaluation of the inhibitory effectiveness of the *Rhizopus*-derived biosurfactant.

2.3.1.3 Crevice Corrosion

Crevice corrosion represents a localised corrosion type that occurs within narrow gaps, including those present in joints, seams, gaskets, and fasteners. The micro-environment within the crevice often becomes stagnant, resulting in O_2 depletion. This O_2 differential creates an electrochemical cell, causing the metal within the crevice to act anodically compared to the surrounding surface. Eventually, the process accelerates localised corrosion (Roberge, 1977). Crevice corrosion is frequently exacerbated in chloride-rich or acidic environments and is commonly observed in marine and industrial

settings where stagnant moisture accumulates. In RC structures, inadequate compaction, honeycombing, or construction defects around reinforcement can create crevice-like microenvironments that promote oxygen depletion and significantly elevate corrosion risk, particularly under chloride exposure.

2.3.1.4 Galvanic (Two-Metal) Corrosion

Galvanic corrosion results from the electrochemical interaction of different metals in electrical contact within an electrolyte. The metal exhibiting a lower electrode potential function as the anode and undergoes preferential corrosion. In contrast, the more noble metal serves as the cathode and receives protection. This corrosion type is concerning in RC structures, in which steel reinforcements may contact stainless steel fasteners. The moist, ion-dense conditions of concrete also promote electron movement, hastening the deterioration of the anodic metal element.

2.3.1.5 Intergranular Corrosion

Intergranular corrosion manifests at the grain boundaries of metallic materials while the grains themselves remain predominantly unaltered. This corrosion type is primarily influenced by variations in electrochemical reactivity between grain interiors and boundaries, frequently resulting from inadequate heat treatment or welding regarding steels and copper (Cu) alloys. The presence of precipitates (such as chromium carbides) at grain boundaries leads to localised depletion of corrosion-resistant elements, making these areas more vulnerable to attacks. Microstructural heterogeneity also undermines material integrity in the absence of visible surface damage, rendering intergranular corrosion challenging to identify until structural failure manifests.

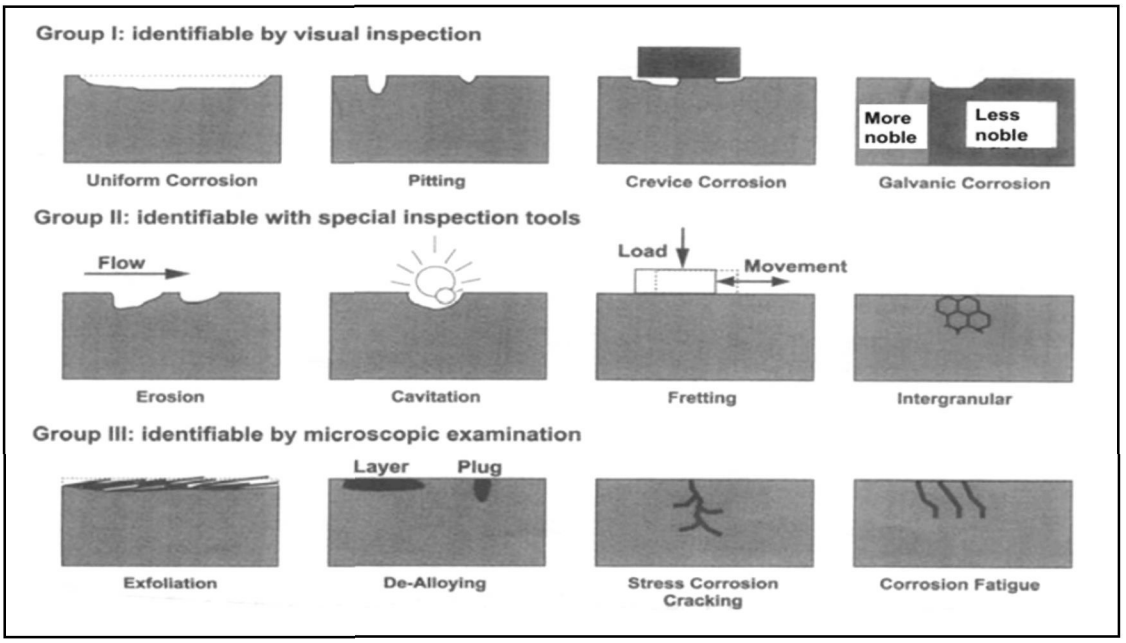

Figure 2.4 The Classification Of Major Corrosion Types

Adopted from Roberge, P.R., *Handbook of Corrosion Engineering*, McGraw-Hill, New York, 1977

2.3.2 Mechanisms of Corrosion in Reinforced Concrete

Various factors affect the rate and extent of corrosion in RC. These factors include environmental parameters (temperature, relative humidity, and exposure to aggressive chemicals) and concrete-related properties (water-to-cement ratio, permeability, pH, cement type, concrete cover, and workmanship quality. Under optimal conditions, concrete sustains a highly alkaline environment (pH 12–13), facilitating the development of a thin, stable, and adherent passive oxide film on the surface of reinforcing steel. This passive layer is primarily composed of ferric oxides and hydroxides, acting as a barrier against aggressive ions while effectively inhibiting the electrochemical reactions responsible for corrosion (Bertolini et al., 2013). Nonetheless, this protective layer remains stable only as long as high pH levels are maintained. The deterioration of the passive film and the initiation of active corrosion can still occur when chlorides or other aggressive species reduce the pH to a critical threshold of 10. Consequently, increased repair costs and safety issues are denoted due to the weakening strength, durability, and safety of RC structures (Amin et al., 2022).

The formation of carbonic acid is observed when CO_2 penetrates porous concrete and reacts with calcium hydroxide, $Ca(OH)_2$. Hence, this process is known as

carbonation corrosion, which destabilises the passive layer and exposes the reinforcement to corrosion through a gradual decrease in pH (Menna Barreto et al., 2021). The progression of corrosion also entails the oxidation of iron to form iron oxides, Fe_2O_3 and iron hydroxide (FeH_2O_2), which occupy a greater volume than the original metallic iron. Corrosion products can then expand between three and six times the volume of the original steel, creating internal tensile stresses within the concrete matrix. This expansion results in cracking, spalling, and delamination of the concrete cover, which accelerates deterioration and compromises structural integrity (Asri et al., 2017).

Alternatively, the concrete serves as a physical barrier due to its strength and resistance to fluid penetration, limiting access to aggressive agents and harmful compounds. A well-designed RC structure should experience minimal issues with steel corrosion throughout its intended service life. Nevertheless, steel reinforcement is the primary cause of RC deterioration, potentially leading to catastrophic failures. One notable is the collapse of the Berlin Congress Hall and parking garage in Minnesota, causing injuries and deaths (Abosrra, 2010).

The primary cause of failure in concrete structures is internal reinforcement. Corrosion of reinforcement steel leads to deformation and a loss of bonds with the concrete. This loss of bonding results from deformity and lower effective area on a cross-sectional plane, leading to detachment between the two primary components (steel and concrete). This detachment compromises the overall integrity of the structure, undermining its intended performance. Despite the effect is not immediate, it can be fatal if the condition persists without intervention over an extended period.

Spalling of concrete covers resulting from surface cracking also accelerates corrosion rates (CRs). Defects in the concrete arise when the original reinforcement material is compromised by corrosion, leading to an increase in volume that generates stresses on the steel. This effect is then transferred to the concrete. Eventually, the process deteriorates, resulting in a cross-section reduction of the steel due to the decline in its mechanical properties. Figure 2.5 illustrates the consequences of the corrosion mechanism.

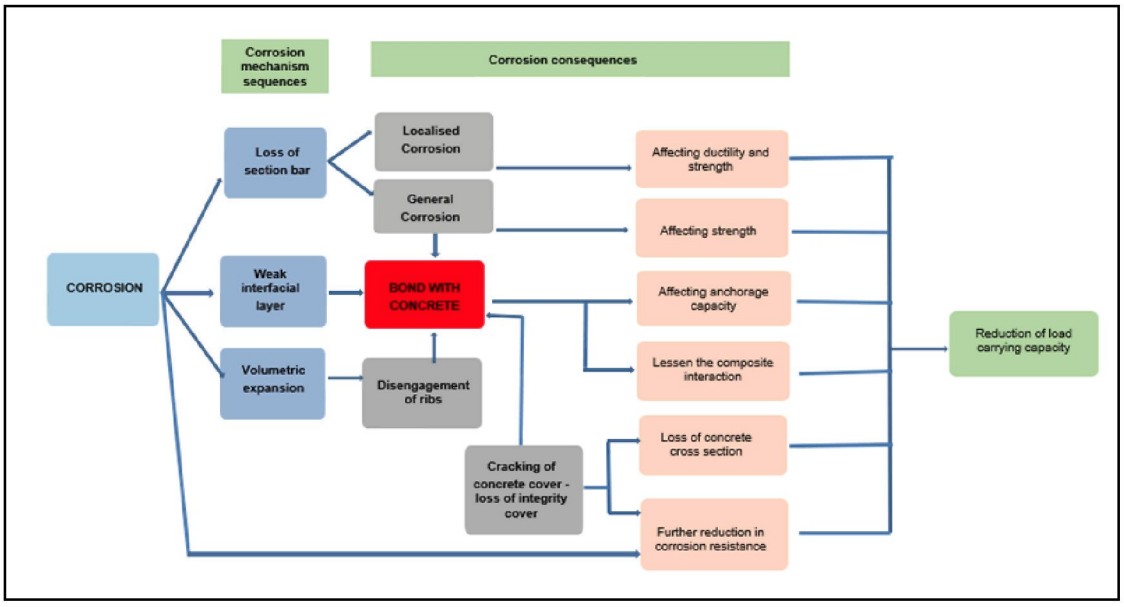

Figure 2.5 The Corrosion Sequences On Reinforcements And Consequences

Source: Cairns et al. (1999)

The primary characteristic of RC is its load-bearing capacity. Particularly, the maintenance of this property relies significantly on the performance of the concrete and reinforcement as an integrated unit to manage stresses from various planes. Considering that a reduction of this property can adversely affect the integrity of the structure, both components must consistently be maintained in optimal condition. Steel reinforcements also exhibit increased vulnerability to damage owing to their natural protective properties being more sensitive to external forces. If not addressed, corrosion of reinforcing steel bars can produce a loss of strength due to a lower effective area of the steel within the concrete. The concrete structural properties (such as stiffness) can then decrease, compromising the shear and moment capacities of the structure.

The critical factor in reinforcement survivability is the degree of exposure or its absence. Therefore, the initial component of the structure (concrete) must offer sufficient protection. Leakage from this concrete cover can expose the reinforcement, lowering the confinement that is crucial for the interaction and directly related to the anchorage capacity of the structural components. Concrete cracking or spalling affecting mechanical properties are also localised phenomena that directly influence the optimal condition maintenance of the reinforcement.

Meanwhile, cracked concrete around corroded reinforcements and stirrups affects the anchorage and shear capacity of a beam. In this region, when the concrete

experiences cracking due to corrosion, it attains its maximum strength. Consequently, any extra loading on the structure activates environmental factors. This condition can eventually compromise bonding, diminishing the shear and loading capacities of the structure (Tahershamsi M, 2016). The orientation of the cracks can also influence the stiffness of the structure, affecting the internal force distribution. Figure 2.6 portrays the correlation between the mechanical properties of RC and the corrosion of steel reinforcement.

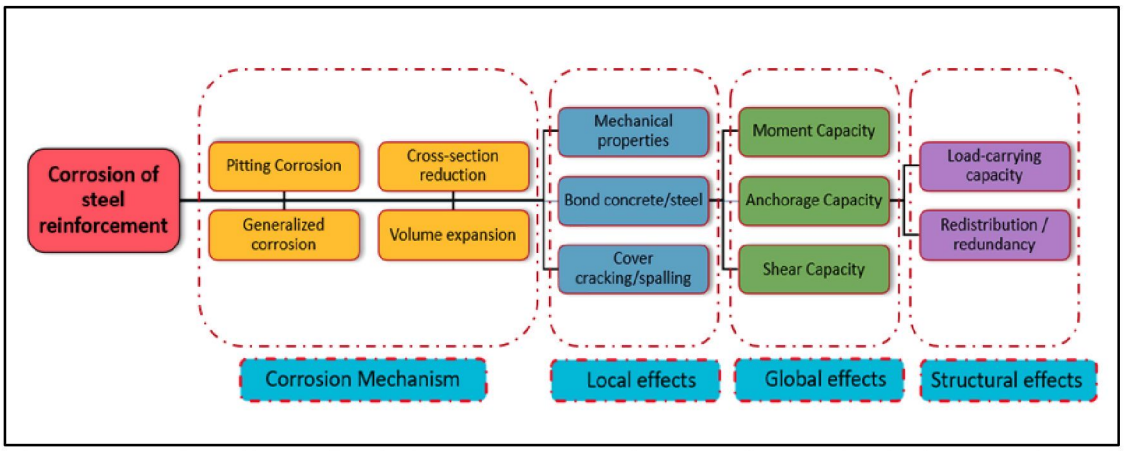

Figure 2.6 The Effect Of Reinforcement Corrosion On The Mechanical Properties Of RC Structures

2.3.2.1 Electrochemical Reactions in Steel Reinforcement

The electrochemical reactions resulting from the penetration of chloride ions (Cl-) in RC are essential for the initiation and propagation of corrosion in steel reinforcement. This Cl- compromises the passive oxide film that protects the steel, resulting in localised corrosion. The electrochemical corrosion process encompasses anodic and cathodic reactions as follows:

i) The anodic reaction occurs at locations where the protective layer on the steel is compromised, initiating the corrosion process of the steel. Fe undergoes oxidation in this process, resulting in the formation of Fe ions (Fe^{2+}) that subsequently dissolve in the concrete. This process results in the release of electrons that traverse the steel as follows:

$$Fe \rightarrow Fe^{2+} + 2e^{-} \quad (2.1)$$

ii) The cathodic reaction occurs in O_2-rich areas where electrons released from the corroding area (anode) flow through the steel to another area (the cathode). At the cathode, these electrons react with water and O_2 to produce hydroxide ions (OH^-), sustaining the alkaline environment surrounding the cathode. This reaction generally takes place in areas where chloride ions (Cl^-) is absent at the concrete surface distant from the anode. The cathodic reaction is expressed as follows:

$$O_2 + 2H_2O + 4e^{-} \rightarrow 4OH^{-} \quad (2.2)$$

iii) The formation of iron hydroxide [$Fe(OH)_2$] occurs when Ferrous iron (Fe^{2+}) generated at the corroding steel surface (anode) interacts with OH^- produced in the O_2-rich region (cathode). This combination results in the formation of a solid substance known as $Fe(OH)_2$ as follows:

$$Fe^{2+} + 2OH^{-} \rightarrow Fe(OH)_2 \quad (2.3)$$

2.3.2.2 Protective Mechanism of Biosurfactants in RC Corrosion Inhibition

The electrochemical mechanisms described above demonstrate that corrosion in RC progresses once the passive film on steel is disrupted by chloride ions, carbonation, or increased permeability allowing oxygen and moisture ingress. To effectively suppress these reactions, a corrosion inhibitor must either (i) prevent chloride interaction with the steel surface, (ii) restore or stabilise the passive layer, or (iii) form an adsorbed protective film that impedes electron transfer at both anodic and cathodic sites. This mode of interference aligns with the expected behaviour of biosurfactants.

Biosurfactants, including the *Rhizopus*-derived phospholipid biosurfactant evaluated in this study, possess amphiphilic molecular structures that enable them to adsorb strongly onto steel surfaces, forming a compact, hydrophobic barrier. This adsorbed layer can inhibit corrosion through several mechanisms:

i) Physical film formation - reducing the accessibility of aggressive ions (e.g., Cl^-) and limiting metal–electrolyte interaction.
ii) Anodic and cathodic site blocking - decreasing electron exchange and slowing both oxidation and reduction reactions.
iii) Stabilisation of passive layer - enhancing the uniformity of the protective oxide film and reducing its susceptibility to chloride-induced breakdown.
iv) Reduction of concrete permeability (when admixed) - modifying pore structure and reducing transport of moisture and ionic species toward reinforcement.

Through these mechanisms, biosurfactants act as multifunctional inhibitors capable of interrupting the electrochemical processes responsible for corrosion initiation and propagation. Therefore, the inclusion of the biosurfactant directly targets the key corrosion mechanisms operating in chloride-exposed RC, aligning with the theoretical framework presented in this subsection.

2.3.3 Factors Influencing Corrosion

Corrosion of embedded steel in reinforced concrete is governed by a complex interaction of environmental, material, and structural parameters. While the underlying electrochemical mechanisms are globally consistent, the severity and rate of corrosion are markedly intensified under tropical climatic conditions, particularly in Malaysia and Sarawak. Sarawak consistently experiences relative humidity above 80% and annual rainfall exceeding 3,500–4,000 mm, resulting in prolonged saturation of concrete pore networks. This promotes sustained ionic mobility, continuous electrochemical activity, and intense wet–dry cycling that accelerates chloride accumulation at the steel surface. Additionally, elevated ambient temperatures of 28–35°C accelerate diffusion and reaction kinetics, increasing the corrosion rate relative to temperate environments (Sa'adi et al., 2017).

Sarawak's extensive coastal exposure further compounds deterioration risk. Marine aerosols and salt-laden winds in areas such as Kuching, Kota Samarahan, Bintulu, and Miri contribute to chloride deposition levels reported to be up to four times higher than inland regions (Binyehmed, F. 2018). These conditions make chloride-induced pitting corrosion the dominant form of degradation in Sarawak's RC infrastructure. Frequent rainfall, fluctuating groundwater, and rapid drying cycles

intensify chloride ingress through capillary action and repeatedly destabilise the passive film on steel.

Collectively, the combination of high humidity, heavy rainfall, elevated temperatures, and substantial chloride exposure create an environment highly conducive to corrosion, reinforcing the need for protective systems specifically adapted to Sarawak's climatic and exposure conditions. A clear understanding of these influences is essential for accurately predicting corrosion behaviour and designing durable RC systems for tropical regions.

Corrosion in RC is governed by a wide range of interconnected physicochemical and electrochemical factors. These include the properties of the concrete and steel, the characteristics of the steel–concrete interface, and the environmental conditions affecting ion transport and electrochemical reactions. Key aspects influencing corrosion behaviour include:

i) The steel-concrete interface characteristics act as conduits for aggressive agents, such as microcracks, air voids, and interfacial transition zones.
ii) The concentration of hydroxide ion (OH^-) in the pore solution regulates pH and directly influences the stability of the passive oxide layer on steel surfaces.
iii) The electrochemical potential of steel determines the thermodynamic probability of corrosion initiation.
iv) The binder type influences the composition and buffering capacity of the pore solution.
v) The surface condition and roughness of steel reinforcement influence the formation and integrity of the passive film.
vi) The moisture content and degree of saturation in the concrete manage ionic mobility and O_2 transport.
vii) The O_2 availability at the steel surface is pivotal for the cathodic reaction in the corrosion process.
viii) Water-to-binder (w/b) ratio, which affects the porosity, permeability, and overall durability of concrete.
ix) The electrical resistivity of concrete affects the magnitude of electrochemical currents that contribute to corrosion.
x) The extent of cement hydration influences the microstructural evolution and

chemical stability of the matrix.

xi) The chemical composition of steel concerns the inclusion of alloying elements, which improve corrosion resistance.

xii) The exposure temperature influences chloride (Cl^-) diffusion rates and the kinetics of corrosion reactions.

xiii) The mechanism of chloride ingress occurs through initial mixing or subsequent penetration in hardened concrete.

xiv) The type of accompanying cations (Na^+, Ca^{2+}, and K^+) influencing Cl^- binding and solubility.

xv) Additional chemical species in mitigating or accelerating corrosion, such as corrosion inhibitors or aggressive ions.

Numerous studies have reported the steel-concrete interface, pH of the pore solution, and electrochemical potential of the embedded steel as the primary factors influencing corrosion initiation (Angst et al., 2009; Rodrigues et al., 2021; Sohail et al., 2023). Given that localised chloride buildup and physical disturbances in the passive barrier are correlated with this steel-concrete interface, this factor remains the most significant aspect. Therefore, improved passivation of steel and service life of RC structures necessitates maintaining a robust and enduring steel-concrete interface.

2.3.3.1 pH of Concrete Pore Solution

The pH of the concrete pore solution is crucial for the corrosion resistance of embedded steel reinforcement. Historically, the pH scale was established by a Danish biochemist (Søren Peter Lauritz Sørensen) in 1909. This scale quantifies the acidity or alkalinity of a solution as the negative logarithm of hydrogen ion (H^+) concentration. The term "pH" derives from the German word *potenz*, meaning power. This term is utilised to indicate the strength or concentration of H^+ in aqueous solutions. The pH scale typically extends from 0 to 14, with values under or over 7 denoting acidity or alkalinity, respectively. A change of one pH unit results in a tenfold variation in H^+ concentration (Roberge, 2015). Thus, the pore solution of fresh Portland cement-based concrete generally presents a highly alkaline environment, presenting pH values between 12.5 and 13.5. This elevated alkalinity results from the dissolution of alkali hydroxides (NaOH and KOH) during the hydration of cement. The increased pH

promotes the development of a stable passive oxide layer on the surface of steel reinforcement, serving as a protective barrier against corrosion (Angst et al., 2009).

The durability of this passive layer is significantly affected by variations in pH. When pH decreases below a critical threshold (~11.5), the passive film may destabilise and degrade. This process can leave the steel vulnerable to corrosion. Generally, the reduction in alkalinity results from carbonation, wherein atmospheric CO_2 infiltrates the concrete and reacts with $Ca(OH)_2$ to yield $CaCO_3$. The carbonation process reduces the pore solution pH to approximately 9, which undermines the corrosion resistance of steel reinforcement (Polder, 2001). In addition, the introduction of low-pH solutions significantly enhances CRs in acidic water-based environments, such as those impacted by industrial discharge or mine drainage. These acidic environments supply H^+ to the electrochemical corrosion process, increasing the anodic metal dissolution rate. Dissolved CO_2 (even at mildly acidic conditions) can also substantially elevate the depassivation risk and trigger corrosion processes in the concrete matrix. Overall, maintaining a high and stable pH within the concrete pore solution is crucial for preserving the passive state of embedded steel. Factors that diminish alkalinity can significantly threaten the long-term durability of RC structures, including carbonation, chloride ingress, and environmental acidification.

2.3.3.2 Role of Chloride Ingress and Carbonation

The primary factor in the corrosion of steel reinforcement within concrete structures is chloride. Cicek (2017) stated that the initiation and acceleration of corrosion processes could be observed when the durability of RC was significantly compromised by chlorides. Several routes are often demonstrated that cause these Cl^- penetrations. Particularly, this phenomenon can be caused internally (contaminated raw materials, mixing water, and specific chemical admixtures) and externally (environmental exposure). Marine aerosols, direct contact with seawater, and de-icing salts are typical examples of external causes (Bertolini et al., 2013). Both these processes occur via diffusion, capillary suction, and hydraulic pressure mechanisms when chlorides are introduced. The passive ferric oxide film that usually develops in the highly alkaline environment of concrete (pH > 12.5) is disrupted by chlorides at the steel surface. Consequently, a notably aggressive and subtle form of deterioration that advances swiftly and frequently remains unnoticed (localised pitting corrosion) can then

occur (Tahershamsi, 2016). Several components also demonstrated significant correlations with the rate and extent of chloride ingress, particularly in relation to ion transport and moisture movement. These components are saturation level, degree of saturation, concrete permeability, porosity, and cracks or microcracks (Sohail et al., 2023).

Marine or chloride-rich environments require examining a critical factor in the design of durable RC structures, which is the resistance of concrete. Therefore, several techniques have been developed for addressing chloride-induced corrosion. Notable examples include corrosion inhibitors for passivity preservation of embedded steel, low w/c ratios, and pozzolanic for microstructure densification. In carbonation or chloride-induced corrosion cases, the pH adjacent to the steel surface is reduced by chlorides. Corrosion then takes place when the depassivation of the steel reinforcement occurs at a pH below 9.0. Even though chloride themselves do not directly change the pH of the concrete, their presence can initiate reactions that result in a localised drop in pH (facilitating corrosion) (Andrade & Alonso, 2001).

2.3.3.3 Design and Construction Practices

The design and construction practices of concrete structures significantly influence the probability and CR in steel reinforcement. Thus, the thickness of the concrete cover is a crucial parameter. A proper cover can safeguard the steel from external corrosive factors. In contrast, inadequate cover or improperly compacted concrete elevates the corrosion risk by facilitating pathways for moisture and chlorides to access the steel. Water and chlorides can infiltrate and access the reinforcing steel through direct pathways caused by concrete-based cracks. These cracks can form due to shrinkage, thermal movements, or structural loads. Subsequently, more aggressive agents can infiltrate the concrete, facilitating the corrosion process. This phenomenon necessitates reducing the likelihood of corrosion through effective structural design to enhance the longevity of RC structures. Specific methods involve crack control measures, suitable concrete mix proportions, and adequate concrete cover.

An evaluation of the service environment and potential exposure to corrosive elements can also help address this issue. Likewise, protective measures can aid in mitigating this challenge. Examples of commonly utilised protective measures are cathodic protection, surface coatings, and corrosion-resistant materials. Specifically, an

extra barrier to moisture and chloride penetration is made possible through epoxy or polyurethane as surface coatings.

2.3.4 Impacts of Corrosion on Structural Integrity and Service Life of RC

Corrosion of steel reinforcement poses a major threat to RC structures, as the formation of corrosion products (rust) arising from chloride ingress or carbonation expands the volume of steel by up to four times its original size (Almusallam et al., 1996; Hassan et al., 2000). This expansive pressure induces internal tensile stresses that manifest as surface staining, cracking, spalling, and delamination. Once cracks propagate, the reinforcement becomes more directly exposed to moisture, oxygen, and aggressive ions, and this condition accelerates the corrosion process (Shunmuga Vembu & Ammasi, 2023). As corrosion progresses, structural integrity, performance, and long-term durability are compromised.

The bond between steel and concrete is essential for composite action. This bond is generated through several mechanisms, including mechanical interlocking of bar deformations, friction, cohesion, and adhesion at the steel–concrete interface. Although early-stage corrosion may slightly increase surface roughness, continued rust expansion significantly reduces the bond stress (τ), which weakens the load-transfer mechanism between concrete and reinforcement (Abosrra, 2010). This deterioration is particularly critical in beams and slabs because their structural performance relies heavily on adequate tensile reinforcement (Lin et al., 2019).

In advanced corrosion phases, extensive spalling of the concrete cover exposes the reinforcement directly to environmental conditions. This exposure further intensifies deterioration. The loss of the protective concrete layer reduces structural stiffness and decreases the load-bearing capacity of RC members. In severe deterioration levels, load restrictions may be necessary to prevent structural failure (Shunmuga Vembu & Ammasi, 2023). Cracking and spalling therefore serve as visible indicators of underlying structural damage and weakening (Bertolini et al., 2013).

The long-term effects of corrosion include a reduction in the cross-sectional area of steel and progressive degradation of the concrete–rebar system. These cumulative impacts lead to substantial reductions in serviceability and shorten the functional lifespan of RC structures. Consequently, improving durability and ensuring timely

corrosion prevention are essential for maintaining long-term structural performance (H. Lin et al., 2019).

Evidence from Malaysian coastal infrastructure demonstrates the severity of chloride-induced deterioration. Case studies reveal premature degradation of RC jetties, seawalls, and bridge components occurring approximately 20 to 25 years earlier than expected due to chloride-induced corrosion (Ismail et al., 2019). The same study reported that steel reinforcement corrosion associated with chloride penetration constituted between 45 and 78 percent of all deterioration cases across five marine structures. Sulfate attack contributed between 14 and 55 percent, while factors such as marine biological activity and workmanship-related issues accounted for between 14 and 22 percent of deterioration. These findings clearly indicate that chloride-induced corrosion is the most significant durability threat to RC structures in marine environments.

Figure 2.7 illustrates the primary effects of corrosion on RC, including reduced bond strength, cracking, delamination, and overall structural degradation. Figure 2.8 further demonstrates how increasing corrosion levels correspond to decreasing bond stress (τ), highlighting the direct relationship between corrosion progression, declining serviceability, and reduced service life (Shunmuga Vembu & Ammasi, 2023).

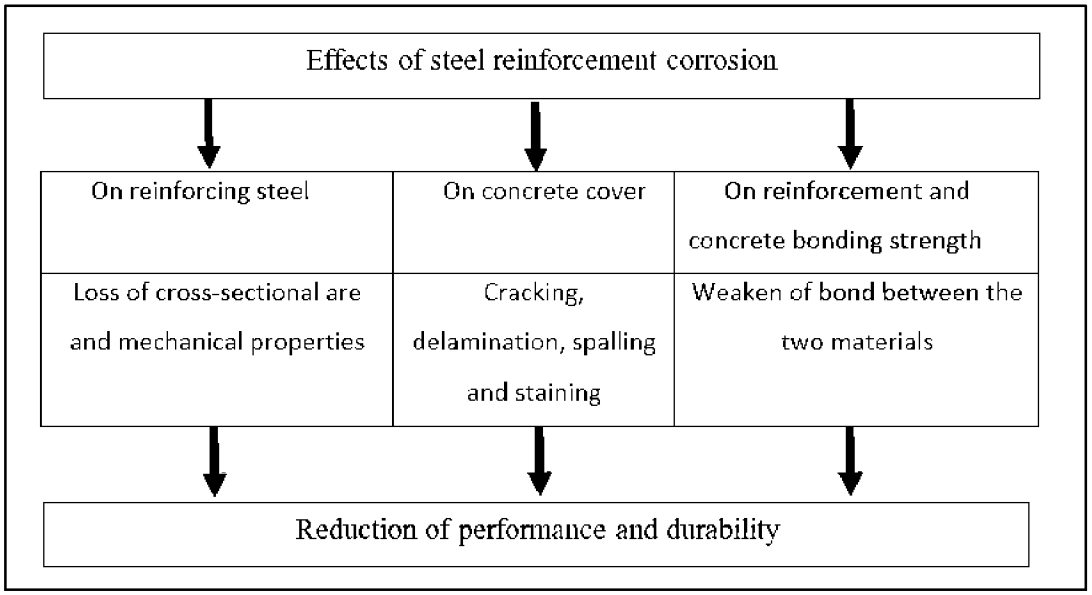

Figure 2.7 Detrimental Effects Of Reinforcement Corrosion On The Performance And Durability of RC Structures

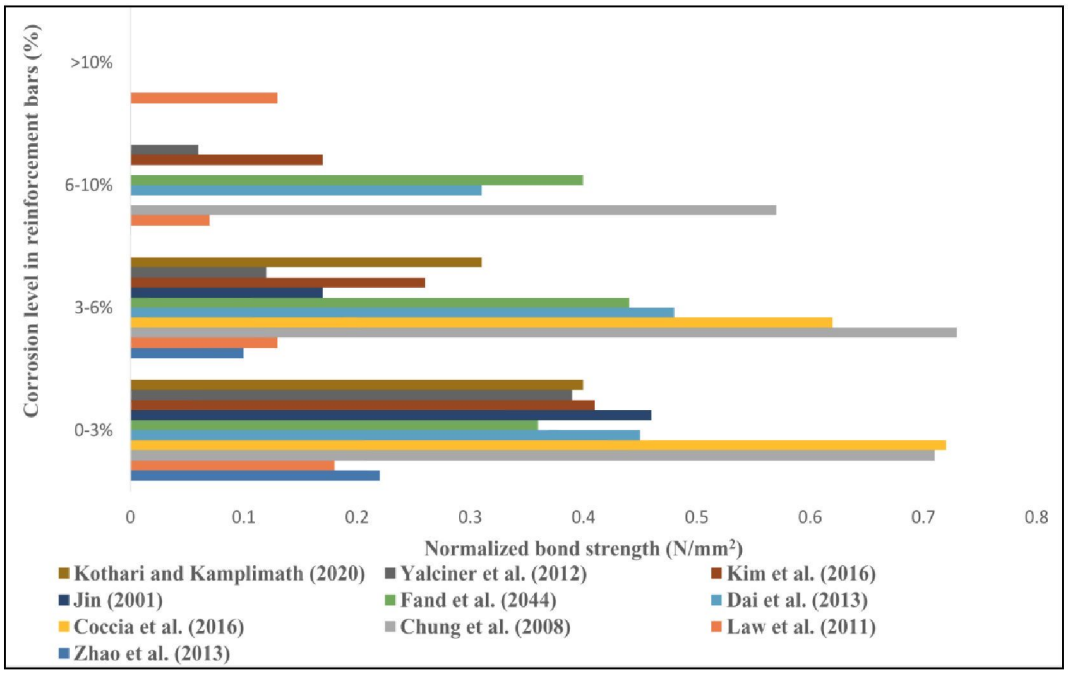

Figure 2.8 Comparison Of Normalized Bond Strength At Different Corrosion Levels

Source: Shunmuga Vembu & Ammasi (2023)

2.4 Protection Against Corrosion in RC Structures

Conventional corrosion protection strategies for RC structures such as epoxy-coated reinforcement, surface sealers, cathodic protection, chemical corrosion inhibitors, and low-permeability high-performance concrete have demonstrated varying degrees of effectiveness. However, each approach presents notable limitations that restrict long-term performance, cost efficiency, or environmental compatibility.

Epoxy-coated or galvanized reinforcement provides an initial physical barrier, but these systems are susceptible to coating damage during transport or construction, which can create localised corrosion hotspots. Their installation costs remain considerably higher than standard reinforcement, making them less feasible for large-scale infrastructure applications. Similarly, surface coatings and sealers rely heavily on maintenance cycles. Many polymer-based coatings degrade under ultraviolet radiation, abrasion, and aggressive marine conditions, leading to declining performance and frequent reapplication requirements. This creates significant long-term maintenance burdens, particularly for coastal regions such as Sarawak.

Conventional chemical corrosion inhibitors, including inorganic nitrites and synthetic organic compounds, can effectively delay corrosion initiation but also present

concerns related to toxicity, safety, and environmental persistence. Some inhibitors have been associated with carcinogenicity or harmful leaching into surrounding soils and waterways. Furthermore, their performance may vary depending on dosage, concrete composition, pH conditions, and the presence of competing ions. Several inhibitors demonstrate declining effectiveness over time due to chemical breakdown or reduced adsorption efficiency, leading to shorter durability and inconsistent long-term protection.

In contrast, biosurfactants offer several promising advantages that address these shortcomings. Biosurfactants are naturally derived amphiphilic molecules produced by microorganisms, and they exhibit strong surface activity with significantly lower toxicity compared to synthetic inhibitors. Their biodegradability and environmental compatibility make them attractive candidates for sustainable corrosion protection systems. Importantly, biosurfactants possess a high affinity for metal surfaces, enabling them to adsorb onto reinforcement and form protective hydrophobic films that hinder chloride ingress, reduce electron transfer, and stabilise the passive layer. This mechanism directly interrupts the corrosion processes most relevant to chloride-induced deterioration in tropical marine environments.

Additionally, biosurfactant production can be achieved using renewable, low-cost substrates, including waste frying oil, which enhances economic feasibility and reduces environmental burden. Their multifunctional behaviour such as wetting reduction, dispersion, and pore modification may further improve concrete microstructural quality when used as an admixture, thereby enhancing resistance to moisture transport and ion penetration. These combined attributes suggest that biosurfactants can outperform traditional inhibitors in terms of sustainability, cost-effectiveness, and adaptability to aggressive environments.

Given the high chloride exposure, intense rainfall, and elevated temperatures characteristic of Sarawak, biosurfactants represent a promising alternative capable of providing durable, environmentally responsible corrosion mitigation tailored to tropical RC infrastructure.

2.4.1 Enhancement of Concrete Quality

The corrosion of embedded steel reinforcement can be tackled via high-quality concrete due to its effective protection feature, which enhanced concrete quality is often

produced through a lower w/c ratio. This process involves addressing the significant factors in the corrosion process by inhibiting the diffusion rates of ions. Examples of these factors include chlorides, CO_2, and O_2. The service life of the structure can also be prolonged through high-strength concrete. This concrete type can postpone the initiation of corrosion-induced cracking by demonstrating smaller pore volume and permeability. Therefore, increased long-term durability can be achieved by improving the resistance of the concrete to external chemical attacks.

Numerous aspects can significantly affect the permeability properties of concrete, including cement type and supplementary cementitious materials with admixtures. Studies have recorded that refined pore structure and decreased overall porosity can increase the microstructural density of concrete. This outcome is usually attained by adding additives, such as fly ash, silica fume, and ground granulated blast furnace slag (GGBS), which are commonly used to improve the microstructural density of concrete by refining its pore structure and reducing overall porosity. Consequently, increased resistance to chloride penetration and mechanical performance can be accomplished through these enhancements (Cicek, 2017). Nonetheless, chemical incompatibility with other concrete components can occur if admixtures are not selected carefully. This observation then leads to studies examining compatible, cost-effective, and environmentally sustainable organic-based admixtures.

In the Malaysian construction industry, several types of chemical admixtures are widely incorporated to enhance concrete quality and durability. Water-reducing and superplasticising admixtures, particularly polycarboxylate ether (PCE)-based formulations, are extensively used to achieve lower water-to-binder ratios while retaining adequate workability (Ban et al., 2020). Set-controlling admixtures, including accelerators and retarders, are frequently utilised to manage setting behaviour under Malaysia's high-temperature conditions, which can significantly influence construction scheduling and early-age performance (Amin et al., 2022). Supplementary cementitious materials, particularly pulverised fuel ash (PFA), palm oil fuel as (POFA), ground granulated blast-furnace slag (GGBS), and silica fume, are increasingly adopted in major infrastructure and urban development projects to reduce concrete permeability, enhance long-term compressive strength, and improve resistance to chloride ingress (Rosseli et al., 2019). These admixtures and mineral additives have therefore become an integral component of Malaysia's concrete practice, reflecting proven performance under the nation's tropical climatic conditions.

2.4.2 Optimising the Thickness and Quality of Concrete Cover

Corrosion protection for embedded reinforcing steel is strongly influenced by the thickness and integrity of the concrete cover. A sufficiently thick cover delays the onset of corrosion by extending the diffusion path of aggressive agents, particularly chloride ions. Numerous studies have demonstrated that increasing the cover depth enhances the durability of reinforced concrete (RC) structures by restricting chloride ingress when supported by appropriate structural design and environmental exposure considerations (Basheer et al., 2001; Diab et al., 2014; Lin et al., 2019; Song & Saraswathy, 2007). Additionally, physical adsorption and chemical binding within the cementitious matrix regulate the mobility of chlorides, thereby reducing the concentration of free Cl^- capable of initiating corrosion at the steel surface (Angst et al., 2009; Eloget et al., 2021). When combined with a low-permeability mix design, an adequate concrete cover therefore plays a crucial role in slowing chloride penetration and postponing corrosion initiation.

Despite its importance, real-life construction conditions often compromise the effectiveness of concrete cover. Poor workmanship such as inadequate compaction, misplacement of reinforcement, and inconsistent cover depth can significantly reduce the intended protective capacity of the cover layer. Cracking, whether caused by plastic shrinkage, drying shrinkage, thermal gradients, or structural loading, further accelerates chloride ingress by providing preferential pathways that bypass the diffusion resistance of intact concrete (H. Lin et al., 2019). These practical issues underscore that compliance with cover standards alone does not guarantee long-term durability, particularly in aggressive marine and tropical climates.

A properly engineered concrete cover comprising low-permeability concrete remains an essential defence mechanism by forming a resilient barrier against chloride ingress. However, relying solely on increasing cover thickness is not considered an optimal approach. Excessively thick cover may conflict with architectural and structural constraints, affecting member dimensions, constructability, and even the structural performance efficiency. Moreover, larger cover depth can increase construction costs without proportionate gains in corrosion resistance (Menna Barreto et al., 2021). Therefore, while optimising cover thickness is fundamental to corrosion control, it must be complemented by additional protective strategies such as corrosion inhibitors,

surface treatments, supplementary cementitious materials, and stringent construction quality control to ensure enhanced and reliable durability of RC structures in practice.

2.4.3 Application of Surface Protective Coatings

Steel reinforcement is protected against corrosion through surface coatings, which are categorised into two types: (i) sacrificial and (ii) noble (non-sacrificial) coatings. Sacrificial coatings [zinc (Zn) and cadmium (Cd)] provide protection to steel by undergoing corrosion prior to the substrate material. This coating functions as the anode when it is compromised, maintaining security for the underlying steel via a galvanic mechanism (Ye et al., 2020). Likewise, noble coatings [Copper (Cu) and nickel (Ni]) provide protection to steel only while the coating remains intact. The exposed steel assumes an anodic state when the coating fails, increasing its vulnerability to corrosion. Currently, Zn-coated (galvanised) bars are the most prevalent type of sacrificial coating.

Long-term field studies concerning marine environments and areas subjected to de-icing salts have reported that galvanised steel can postpone the onset of cracking and spalling, although it cannot eliminate these issues (Ahmad, 2003; Ye et al., 2020). Thus, it is essential that all reinforcement and metallic elements within a structure are uniformly coated with Zn to prevent galvanic corrosion between coated and uncoated steel components to ensure optimal performance,

Fusion-bonded epoxy coating is another commonly utilised protective method. This coating protects the steel reinforcement from O_2, moisture, and chlorides, which are critical factors in the corrosion process. The application of the coating involves spraying epoxy powder onto steel bars that have been cleaned and heated (Poursaee, 2016). Conversely, a significant issue is preserving the integrity of the coating throughout transportation and installation. Therefore, minimisation of damage to the epoxy layer can be achieved with padded bundling bands, non-metallic slings, and coated tie wires during handling.

Studies have also contended that minor imperfections (small nicks and scratches in the epoxy coating) do not promptly result in substantial corrosion (Poursaee, 2016). This observation implies that in aggressive environments with high chloride levels, it is advisable to coat all steel reinforcement with epoxy to enhance the service life of the structure. Nevertheless, it is essential to prevent electrical coupling between coated and extensive uncoated steel areas to avoid localised galvanic corrosion. Despite the

corrosion mitigation can be achieved through sacrificial and noble surface coatings, they are not infallible. The success of corrosion mitigation is contingent upon appropriate application, comprehensive coverage, and meticulous handling throughout the construction process.

2.4.4 Application of Corrosion Inhibitors

A well-recognised method for preventing and mitigating the corrosion and degradation of mild steel reinforcement in RC structures is using corrosion inhibitors. Several determinants can be utilised to categorise these inhibitors, such as chemical composition (organic and inorganic), application methods, and mechanisms of action. The corrosion process is also hindered by these inhibitors through two primary types: (i) cathodic (enhanced polarity and diminished corrosion potential) and anodic inhibitors (creation of protective layer). Interestingly, both protective mechanisms can be integrated as dual-action inhibitors (Rivetti et al., 2018). Specific information regarding these inhibitors is then explained as follows:

i) Anodic inhibitors create a protective layer on the metal surface, preventing further oxidation or corrosion. The interaction between metal and corrosive agents (water or O_2) is minimised by this layer serving as a barrier. A significant association is also observed between the effectiveness of anodic inhibitors and the maintenance of optimal concentrations. Therefore, underdosing or overdosing can expedite localised damage (pitting) or influence the setting and mechanical characteristics of concrete, respectively. This observation suggests that dosage should be precisely adjusted based on the chloride concentration in the concrete pore solution (Song & Saraswathy, 2006).

ii) Cathodic inhibitors enhance the surface polarity of the metal and decrease its corrosion potential. This outcome is often achieved by interfering with the cathodic reaction (where reduction of electrons occurs), slowing or halting the progression of corrosion. These inhibitors operate by obstructing the cathodic half-cell reactions, which are typically via the formation of insoluble precipitates [Ca, magnesium (Mg), and Zn salts)] on cathodic sites. The

compounds function as cathodic precipitation inhibitors by creating protective films that impede the diffusion of aggressive species (O_2 and Cl^-). Even though these inhibitors demonstrate notable efficacy in mitigating localised pitting, their effectiveness in combating uniform corrosion is inferior to that of anodic inhibitors (Teng, 2001).

iii) Dual-action inhibitors (or mixed-type inhibitors) integrate both protective mechanisms. This process creates a uniform and hydrophobic film that adheres to the steel surface, diminishing anodic dissolution and cathodic reduction reactions. The synergistic action also enhances corrosion resistance across various environmental exposures (Kondratova et al., 2003).

Corrosion inhibitors exist in both liquid and powder forms. When introduced into a corrosive environment at appropriate concentrations, these inhibitors significantly reduce, delay, or mitigate the corrosion of embedded steel reinforcement. The efficacy of these inhibitors is also determined by various factors, such as their interaction with electrochemical processes, appropriate dosage, and compatibility with the concrete matrix (Rezaierod et al., 2014). Moreover, application techniques differ based on the particular function and site conditions as follows:

i) As an inhibitor in the mixing water during the concrete batching process. The choice of admixture is essential to prevent adverse effects on the properties of cement paste.

ii) As surface or immersion treatments for steel bars before casting (Soylev & Richardson, 2008).

iii) As migrating corrosion inhibitors (MCIs) post-construction. These inhibitors involve their application to the surface of hardened concrete, allowing penetration through capillary action to access the embedded steel reinforcement. This method is suitable for existing structures that already show signs of corrosion. The effectiveness is also contingent upon the capacity of the inhibitor to permeate the concrete matrix and attain sufficient concentrations at the steel

surface to impede or reduce the corrosion process (Goyal et al., 2018).

The effectiveness of corrosion inhibitors is significantly influenced by concentration. Chemical inhibitors also pose concerns about their long-term environmental effects, while organic inhibitors (particularly biosurfactants) offer a sustainable alternative due to their low cost, practical synthesis and high efficacy in corrosion prevention. Conversely, inorganic inhibitors are frequently expensive and may exhibit inherent toxicity in specific environments. These concerns have led to increased interest in ecologically friendly, cost-effective, and sustainable alternatives to conventional inorganic inhibitors (Okafor et al., 2012). Hence, there is a pressing necessity to substitute traditional inhibitors with other options that are effective, non-toxic, and environmentally sustainable. Furthermore, multiple factors must be considered when selecting a suitable corrosion inhibitor. These factors include environmental impact, ease of application, availability, compatibility, and cost-effectiveness. Unlike conventional inhibitors that serve a single corrosion-mitigation function, biosurfactant-based inhibitors provide combined corrosion protection and concrete performance enhancement, potentially reducing the need for multiple admixtures in reinforced concrete systems. Figure 2.9 portrays the classification of corrosion inhibitors and their application methods in RC (Hosseinalipour et al., 2010).

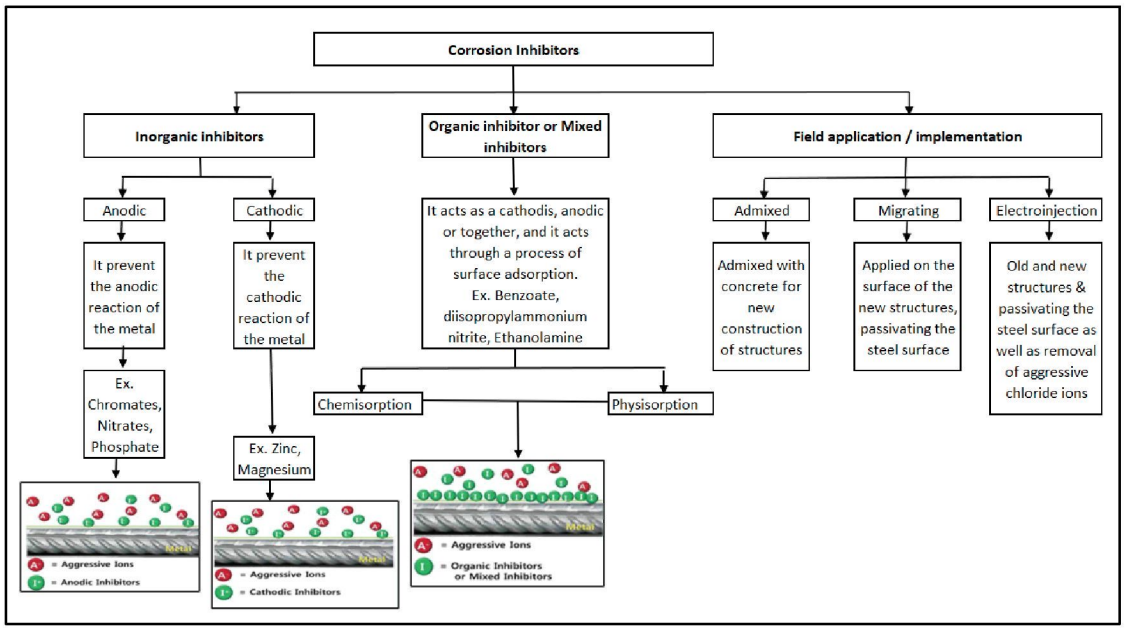

Figure 2.9 The Classification Of Corrosion Inhibitors And Application Methods In RC Systems

2.4.4.1 Organic Corrosion Inhibitors (OCIs)

Numerous benefits render the broad industrial utilisation of OCIs. These advantages are favourable solubility, compatibility with protected materials, high efficiency across varying temperatures, and low toxicity (Meng Y. et al., 2017). Generally, a protective layer that inhibits direct contact between the metal and the corrosive medium is created owing to the adsorption of inhibitor molecules onto the metal surface by OCIs. Multiple mechanisms can cause this adsorption process, including physical, chemical, or a combination of both routes. Electrostatic interactions between charged inhibitor molecules and the metal surface primarily cause physical adsorption. On the contrary, the formation of bonds between the inhibitor and metal atoms [nitrogen (N), O, and S)] is observed in chemical adsorption. Consequently, the CR-related electrochemical reactions are diminished through both these processes via a compact and stable protective layer (El-Sayed et al., 2010). Numerous components are significantly correlated to the effectiveness of OCIs. Primarily, examples include metal surface characteristics, environmental conditions (pH and temperature), chemical structure of the inhibitor, and corrosive environment type.

The OCIs are favoured as a more sustainable alternative to achieve equivalent outcomes. This selection is attributed to the substantial link between industrial corrosion inhibitors and environmental impact when disposing of them. The OCIs can also be synthesised in synthetic and natural forms. Targeted protection against corrosion is provided by synthetic OCIs (amines, fatty acids, and their derivatives). Corrosion within harsh environments (acidic and saline solutions) is effectively mitigated by these inhibitors when they are designed for particular uses. Alternatively, renewable sources are fundamental in creating natural organic inhibitors. Examples of these sources are plant extracts, microbial by-products, and biosurfactants. Effective corrosion inhibition characteristics are also demonstrated by plant-based inhibitors that are obtained from fruit peels, leaves, and seeds. This observation is likely caused by the natural organic compounds (flavonoids, tannins, and alkaloids) within these sources. Additionally, good biodegradability and low toxicity are presented by microbial-derived inhibitors. One notable example is bacteria, fungi, and yeast-based biosurfactants. Hence, these inhibitors are ecologically friendly alternatives to synthetic chemicals (Rani & Basu, 2012).

Various sectors have employed OCIs in their operations and designs. Among these industries, steel reinforcement has frequently applied OCIs in RC structures within the construction sector. In addition, a significant potential is indicated by organic inhibitors for coastal and industrial environments to enhance the durability and longevity of RC. These settings typically demonstrate chloride-induced corrosion as a substantial issue. Aggressive substances-based corrosion (seawater and hydrogen sulphide) can also produce corrosion in pipelines, storage tanks, and offshore structures. Therefore, the oil and gas sector has utilised OCIs to address this concern. Saltwater exposure-based corrosion is another issue encountered in the marine industry. Ships and offshore platforms employ OCIs to safeguard their metal surfaces. Likewise, environmental stressors (road salts, humidity, and atmospheric conditions) can negatively impact coatings, lubricants, and protective films in the automotive and aerospace sectors. Hence, OCIs can be utilised to prevent corrosion of the metal components (Bahr & Murphey, 2014).

Several relationships are observed between performance and several factors for OCIs. These factors include protected metal type, chemical structure, and specific environmental conditions of the exposed metal. Moreover, two characteristics (stability and adsorption efficiency) of the protective film formed on the metal surface are highly dependent on the heteroatoms in the inhibitor molecule. One prominent example is the formation of a stable, protective barrier owing to the strong interactions between nitrogen-containing compounds (amines) and metal surfaces. The development of a strong protective film can also be accomplished through significant adsorption capacity in sulphur-containing compounds. Specifically, several elements can affect the adsorption process that is correlated to corrosion inhibition performance. These elements are temperature, pH of the environment, and concentration of aggressive ions (Cl^-) (Zhang et al., 2015).

Biodegradable OCIs sourced from natural materials are examined in numerous studies. Compared to synthetic chemicals that present environmental and health risks, these green inhibitors are increasingly recognised as viable alternatives. Naturally occurring amphiphilic molecules (biosurfactants) that adsorb onto metal surfaces are also gaining popularity. These biosurfactants are a viable choice for sectors aiming to minimise their environmental impact by being biodegradable and non-toxic while offering corrosion protection. In addition, notable corrosion inhibition properties

attributed to active organic compounds (flavonoids and tannins) are demonstrated by plant-based inhibitors (neem, turmeric, and hibiscus) (Nabil & Al-Sabagh, 2013).

The effectiveness of OCIs is well-documented. Figure 2.10 indicates that the growing number of publications on the topic represents the rising popularity of OCIs (Bogumił Eugeniusz Brycki & Adrianna Szulc, 2018). Nonetheless, large-scale applications have encountered performance optimisation-related issues regarding OCIs. Primarily, natural inhibitors require high production costs, which tend to be more costly to extract and process than synthetic alternatives. In extreme environmental conditions (high temperatures or aggressive acidic solutions, constrained applicability in specific industries is also frequently observed in organic inhibitors. This outcome is attributed to the reduced stability of the inhibitors. Overall, protective layers on metal surfaces are established by OCIs via adsorption mechanisms. This process can reduce corrosion in RC, ensuring protection under diverse environmental conditions. Nevertheless, several factors must be addressed to ensure their full applicability, including elevated production costs, stability issues, and low suitability in extreme environmental conditions.

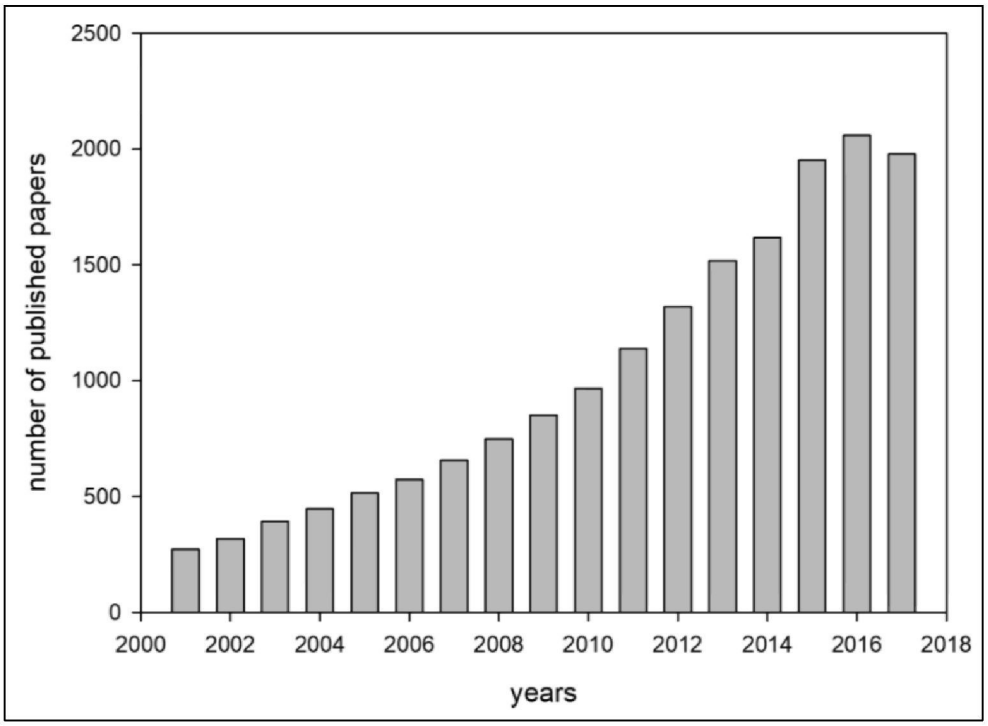

Figure 2.10 Number Of Published Papers On OCI-related Articles Vs. Publication Year

Source: Adopted from Bogumil et al. (2018)

2.5 Surfactants

Surfactants are amphiphilic compounds characterised by the presence of both hydrophilic and hydrophobic functional groups, enabling them to reduce interfacial tension between different phases such as solid–liquid, liquid–liquid, or liquid–gas systems (Mulligan, 2005). Their ability to self-assemble into micelles, bilayers, and other supramolecular structures plays a critical role in modifying interfacial behaviour across diverse environments (Banat et al., 2010). In the context of RC, the molecular behaviour of surfactants is particularly relevant because many CI function through adsorption on the steel surface and the formation of protective interfacial layers.

A strong connection exists between surfactant chemistry and corrosion protection mechanisms. Surfactants can act as corrosion inhibitors by adsorbing onto active anodic and cathodic sites on the steel surface, forming a compact, adherent film that reduces access of corrosive agents such as O_2, moisture, and chloride ions. The hydrophobic portion of the surfactant molecule typically orients outward, creating a barrier that limits charge transfer and ion diffusion at the steel–concrete interface (Abd-El-Nabey et al., 2017). This molecular arrangement can also reduce the wettability of the steel surface, thereby decreasing its susceptibility to electrolyte penetration and corrosion initiation.

Micelle formation further enhances inhibitor efficiency, particularly for biosurfactants. At concentrations exceeding the CMC, surfactants aggregate into micelles that can encapsulate chloride ions or interact with corrosion intermediates, reducing their availability for electrochemical reactions. In highly alkaline environments typical of concrete pore solutions, micelle stability contributes to the sustained release and distribution of inhibitory molecules, reinforcing the protective barrier formed on the steel substrate (Zhu et al., 2017).

Understanding surfactant behaviour is therefore essential within the corrosion context, as biosurfactants operate primarily through micelle formation and surface adsorption on steel. Their amphiphilic structure enables them to assemble into protective films, improving inhibition efficiency by both blocking active corrosion sites and altering interfacial chemistry at the steel–concrete boundary.

Figure 2.11 reveals that amphiphilic compounds that possess a hydrophilic (polar) head group and a hydrophobic (non-polar) tail of surfactants (Marchant and Banat, 2012).

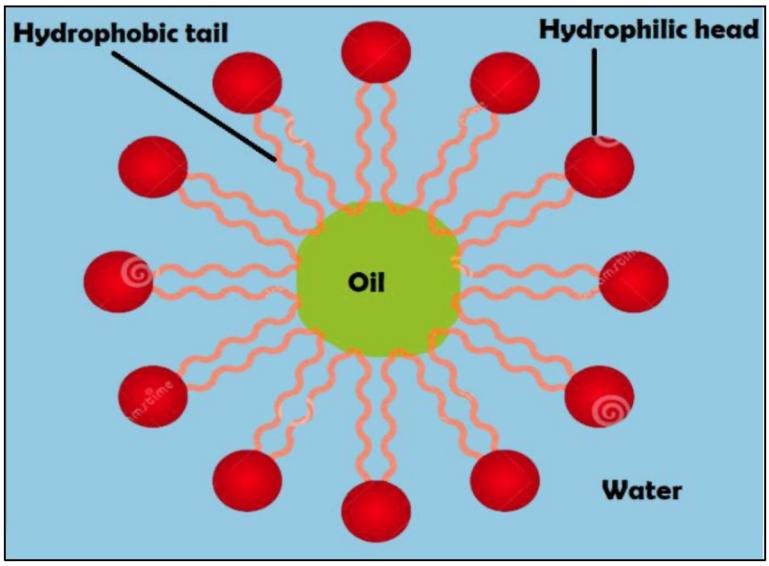

Figure 2.11 The Schematic Illustration Of A Surfactant

2.5.1 Biosurfactants

Biosurfactants are a structurally diverse group of amphiphilic compounds produced by microorganisms. A specific strain of bacteria, yeasts and fungi generates metabolic products or membrane components that exhibit properties akin to surfactants when cultivated on water-insoluble substrates (Bordoloi & Konwar, 2009; Cameotra & Makkar, 2020). These microorganisms produce biosurfactants as secondary metabolites, which may either adhere to the cell surface or be secreted extracellularly (Liepins et al., 2021). The material also exhibits amphipathic properties and demonstrates significant emulsifying and surface activities (Ji et al., 2016). These compounds contain hydrophilic and hydrophobic moieties, which facilitate the reduction of surface tension and improve the solubility of hydrophobic compounds in water-based environments. Meanwhile, biosurfactants serve as a sustainable alternative to synthetic counterparts, being producible from renewable substrates and naturally synthesised by biological systems of microorganisms. This procedure results in reduced toxicity and improved degradability (Geetha SJ et al., 2018). The material also presents enhanced environmental compatibility and retains activity under extreme conditions (temperatures, salinity, and pH) (Kapadia and Yagnik, 2013; Santos et al., 2013; Silva et al., 2014). Thus, biosurfactants possess characteristics that render them suitable for various applications, including environmental remediation, antimicrobial agents, food industry, oil recovery processes, and medical use (Ramírez et al., 2015).

The type of biosurfactant generated depends on the producer microorganism and substrates. Conversely, fermentation time, ion concentration, pH, temperature, and O_2 levels are parameters that affect both the quantity and the quality of the biosurfactant. Based on their structures, biosurfactants are divided into lipopeptides, glycolipids, phospholipids, neutral lipids, and polymeric compounds (Liu et al., 2015). Biosurfactants are also classified into five primary categories based on their structures: (i) lipopeptides, (ii) glycolipids, (iii) polymeric compounds, (iv) phospholipids, (v) and neutral lipids. Table 2.6 summarises the significant classes of biosurfactants and their respective producer microorganisms (Sobrinho et al., 2014).

Table 2.6
Summary Of The Major Biosurfactant Classes And Their Producer Microorganism

Class / Type of Biosurfactant	**Microorganism**
Glycolipids	
Rhamnolipids	Pseudomonas aeruginosa
Sophorolipids	Torulopsis bombicola, T. apicola
Trehalose lipids	Rhodococcus erythropolis, Mycobacterium sp
Mannosylerythritol lipids	Candida antartica
Lipopeptides and lipoproteins	
Peptide-lipid	Bacillus licheniformis
Viscosin	Pseudomonas fluorescens
Serrawettin	Serratia marcescens
Surfactin /iturin/fengycin/subtilisin	Bacillus subtilis
Gramicidin	Bacillus brevis
Polymyxin	Bacillus polymyxia
Fatty acids, neutral lipids and phospholipids	
Fatty acids	Corynebacterium lepus
Neutral lipids	Nocardia erythropolis
Phospholipids	Thiobacillus thiooxidans
Polymeric surfactants	
Emulsan / biodispersan	Acinetobacter calcoaceticus
Liposan	Candida lipolytica
Carbohydrate-lipid-protein	Pseudomonas fluorescens
Mannan-lipid-protein	Candida tropicalis
Particulate surfactant	
Vesicles	Acinetobacter calcoaceticus
Cells	Various bacteria

Biosurfactants are classified according to their molecular weight: (i) low and (ii) high molecular weight biosurfactants. The physicochemical properties and functional applications of biosurfactants are fundamentally influenced by their molecular mass and structural complexity. Typically, significant reduction capacity of the surface with interfacial tensions and straightforward molecular structures are observed in low molecular weight biosurfactants. The cohesive forces among water molecules are lowered owing to the rapid orientation at interfaces. This process is caused by the amphiphilic characteristics and diminutive size of low molecular weight biosurfactants.

Consequently, specific applications requiring surface activity can benefit from this material concerning micelle formation, wettability control, and corrosion inhibition. On the contrary, structural complexity is denoted in high molecular weight biosurfactants. This material mainly comprises heteropolysaccharides, lipopolysaccharides, or glycoproteins. The material can also function as bioemulsifiers (emulsan, liposan, and alasan) in stabilising emulsion rather than substantially reducing surface tension. Particularly, enhanced kinetic stability of oil-water mixtures and steric hindrance promotion is observed owing to the increased molecular size. This observation suggests that specific applications necessitating long-term emulsion stability can benefit from this material. Examples of these applications include environmental remediation, bioremediation of hydrocarbons, and cosmetics with pharmaceutical formulations (Uzoigwe et al., 2015).

The evolution of microbial biosurfactant production can be explained through multiple theories as follows:

i) The initial theory explains that a microenvironment conducive to microbial growth and production is based on the emulsification and solubilisation of hydrophobic substrates (Van Hamme et al., 2006).

ii) The second theory posits that biosurfactants play a role in the adhesion and release of cells from surfaces. This process is accomplished by searching for nutrient-rich habitats, regulating cell surface features, facilitating detachment from unfavourable environments, and improving membrane permeability (Cameotra et al., 2010).

iii) The third theory reveals that a defensive strategy against substrate competitors by biosurfactants involves antibiotic activity (Bogaert et al., 2007).

iv) The fourth theory indicates that biosurfactants participate in the catabolic process under conditions of nutrient limitation by functioning as an energy reserve (Mimee et al., 2009).

v) The final theory denotes that high osmotic pressure, ionic imbalances, and freeze or thaw cycles can be mitigated by biosurfactants on microorganisms (Selbmann et al., 2002).

Generally, the rigid cell walls of fungi cause greater quantities of biosurfactants when renewable substrates are employed. Reports have indicated that various Carbon sources (tallow fatty acid residues, animal fat, glycerol, and oleic acid) produce larger fungal surfactant yields (Bhardwaj, 2013). Therefore, biochemical composition and molecular weight directly influence the diversity of chemical structures in fungal-based biosurfactants, in which the macromolecules possess physicochemical and biological properties relevant to biotechnology. Molar masses from 0.5 kDa to 1.5 kDa are also often observed for low molecular weight biosurfactants (Mulligan, 2005). In contrast, bioemulsifiers [high molecular weight or exopolysaccharides (EPS)] can attain molar masses of up to 500 kDa (Uzoigwe et al., 2015).

Table 2.7 delineates the primary differences between low and high-molecular-weight biosurfactants involving their variations in molecular mass, functional properties, structural complexity, and representative examples. Therefore, this classification can facilitate the precise selection of biosurfactants for specific engineering and biotechnological applications in which performance attributes (surface activity, emulsification potential, and biofilm disruption) are pivotal. Table 2.8 further illustrates these practical applications by aligning biosurfactant types with their optimal use cases.

Table 2.7
Classification Summary Of Biosurfactants

Parameter	Low Molecular Weight	High Molecular Weight (Bioemulsifier)
Molecular Weight	< 1,000 Da	> 10,000 Da (can exceed 1,000 kDa)
Main Function	Reduce surface and interfacial tension	Stabilize emulsions (bioemulsifiers)
Surface Activity	High	Low
Structural Complexity	Simple (lipids, peptides)	Complex (polysaccharide-protein complexes)
Examples	Surfactin, Rhamnolipid, Sophorolipid	Emulsan, Liposan, Alasan

Table 2.8
Summary Of Biosurfactants Applications And Their Microbial Producers

Molecular weight	Microbial origin	Biosurfactant	Application	Reference
Low	Pseudomonas aeruginosa	Rhamnolipids	Enhanced oil recovery, bioremediation, cosmetics	Radzuan (2018)
	Bacillus subtilis	Lipopeptides	Anti-cancer, laundry detergent	Zhao et al. (2018) Mukherjee (2007)
	Candida bombicola	Sophorolipids	Soil Bioremediation, Detergent, personal care product	Minucelli et al. (2017), (Sundaram et al., 2024)
	Rhodococcus erythropolis	Trehalolipids	Microbially enhanced oil recovery	Franzetti et al., (2010)
	Pseudozyma antarctica	Mannosylerythritol lipids	Degradation control of degradable polymer	Fukuoka et al., (2016)
	Corynebacterium insidiosum	Phospholipids	Environmental remediation	(Randhawa & Rahman, 2014)

Molecular weight	Microbial origin	Biosurfactant	Application	Reference
High (Bioemulsifier)	Paenibacillus macerans	Exopolysaccharides	Cosmetics, for removal of oil contamination, and as antimicrobial agents	Liang et al., (2014)
	Bacillus subtilis	Lipoprotein	Remediation of Heavy Metals	Saranya et al., (2014)

2.5.2 Fungal Biosurfactants

Most research on biosurfactants for corrosion inhibition has primarily focused on bacterial-derived compounds, while the potential of fungal biosurfactants remains significantly underexplored. Bacterial biosurfactants (glycolipids, glycoproteins, lipopeptides) are produced by different strains mainly Pseudomonas and Bacillus strains, leading the largest volume of data and scientific output. Fungal biosurfactants, in comparison, represent only 19% out of the total (12% from ascomycetes and 7% from basidiomycetes), while having the widest chemical structural variant of biosurfactants, some of these are produced exclusively by fungi, like sophorolipids, mannosylerythritol lipids, cellobiose lipids, xylolipids, lipid polyols and hydrophobins. Fungi, with their rigid cell walls, tend to produce larger quantities of biosurfactants compared to bacteria. Among fungi, species such as *Candida bombicola*, *Candida lipolytica*, *Candida ishiwadae*, *Candida batistae*, *Aspergillus ustus*, *Ustilago maydis*, and *Trichosporon ashii* have been extensively studied (Bhardwaj, 2013).

The versatility of the chemical structures of fungal biosurfactants is directly correlated to their biochemical composition and molecular weight, these macromolecules carryout physicochemical and biological properties of biotechnological interest. Low molecular weight biosurfactants have their molar mass ranging between 0.5 and 1.5 kDa, while bioemulsifiers (high molecular weight) can reach up to 500 kDa (da Silva et al., 2021).

The environments where fungi thrive play a significant role in determining the types of biosurfactants produced. Understanding the natural origin of these fungi is essential for the selection of suitable growth conditions and production of specific biosurfactant classes, helping to achieve the desired yield and functionality. Fungal

strains capable of biosurfactant production have been isolated from a diverse range of natural environments. These include petroleum-contaminated soils (Yalçın et al., 2018), as well as various plant structures such as roots (Eldin et al., 2019), stems, leaves (Silva et al., 2019), cones (Adnan et al., 2018), flowers (Kim et al., 2015), and fruits (Derguine et al., 2018). Additionally, fungi with biosurfactant-producing capabilities have been isolated from animal-associated environments, such as marine sponges (Kiran et al., 2009) and arthropods (Mousavi et al., 2015).

The widespread presence of fungi across different environments reflects their strong ability to adapt and survive under various conditions. This adaptability is closely linked to their ability to produce a wide range of biologically active compounds, including biosurfactants. Understanding the ecological roles of fungi helps researchers identify promising environments for isolating new biosurfactant-producing strains, which can then be used for industrial or environmental applications.

Fungi produce biosurfactants for various ecological and survival-related purposes. These include:

i) Emulsification and Solubilization: Fungi can use biosurfactants to emulsify and solubilize hydrophobic substrates, creating microenvironments that facilitate their growth and the production of secondary metabolites (Marchant & Banat, 2012; Van Hamme et al., 2006).

ii) Surface Interaction and Adhesion: Some biosurfactants aid in the adhesion and release of fungal cells from surfaces, allowing them to regulate cell surface properties and improve membrane permeability. This enables fungi to detach from unfavorable environments or seek out new habitats with better nutrient availability (Cameotra et al., 2010).

iii) Defense Mechanism: Certain biosurfactants exhibit antimicrobial properties, serving as a defense mechanism against competitors for nutrients and substrates (Bogaert et al., 2007).

iv) Energy Reserve: Biosurfactants can function as energy reserves, enabling fungi to enter catabolic processes when nutrients are limited (Mimee et al., 2009).

v) Protection Against Environmental Stress: Biosurfactants help fungi survive in harsh conditions by protecting them from osmotic pressure, desiccation, ionic imbalances, and freeze-thaw cycles, thereby enhancing their resilience to extreme environmental stresses (Selbmann et al., 2002).

Filamentous fungi (Table 2.9) are less exploited than bacteria, due to their slower growth. However, they are excellent producers of biosurfactant and bioemulsifier, with stable emulsions, and have an excellent capacity to reduce surface tension. Moreover, they promote the dispersion of hydrophobic compounds, which enables them to be applied in different sectors(da Silva et al., 2021) (Sena et al., 2018).

Table 2.9
Types Of Biosurfactants Or Bioemulsifiers Produced By Filamentous Fungi

Fungal Genus / Species	**Identified Biosurfactant**	**Reference**
Aspergillus niger	Glycolipid	Kannahi & Sherley (2012)
Penicillium chrysogenum SNP5	Lipopeptide	Gautam et al. (2014)
Cunninghamella echinulata	Mixed macromolecules (lipid/protein/carbohydrate)	Silva et al. (2014)
Aspergillus fumigatus	Unspecified biosurfactant	Castiglioni et al. (2009)
Penicillium, *Fusarium*, *Trichoderma*	Not clearly defined (potential emulsifiers)	Castillo-Méndez et al. (2017)
Aspergillus spp.	Not clearly defined	Cavalcanti et al. (2017)
Fusarium sp.	Not identified	Qazi et al. (2014)
Rhizopus arrhizus	Not identified	Pele et al. (2018)
Rhizopus oryzae	Glycolipid	Kashef et al., 2018

Although certain fungal species produce biosurfactants, such as glycolipids and lipopeptides, with physicochemical properties favorable for corrosion inhibition, their application in protecting materials like reinforced concrete and mild steel has not been extensively studied. Existing literature on fungal biosurfactants has largely emphasized their roles in bioremediation and emulsification, rather than corrosion control.

Fungal genera such as *Aspergillus*, *Penicillium*, and *Trichoderma* are known to synthesize structurally diverse biosurfactants (Rodrigues et al., 2006), which have demonstrated efficacy in environmental applications. The efficacy of fungal bioremediation is demonstrated in its ability to degrade persistent organic pollutants

such as polycyclic aromatic hydrocarbons (PAHs), polychlorinated biphenyls (PCBs), and petroleum hydrocarbons, as well as to immobilize and transform heavy metals through biosorption and bioaccumulation. However, their potential in mitigating corrosion of reinforced concrete has not been explored.

The amphiphilic nature of fungal biosurfactants enables interactions with both hydrophobic and hydrophilic surfaces, potentially facilitating the formation of protective films on metal substrates and thereby impeding corrosion processes. Compounds such as mannosylerythritol lipids (MELs) and sophorolipids, produced by certain fungal species, have been reported to possess antimicrobial and environmentally friendly properties, indicating their promise as green corrosion inhibitors (Schneemann et al., 2020).

Despite these promising characteristics, studies specifically evaluating the corrosion-inhibiting effects of fungal biosurfactants in reinforced concrete and mild steel systems remain scarce.

2.5.3 Properties of Biosurfactant

Biosurfactants exhibit notable surface activity, which includes their ability to reduce surface and interfacial tensions across different phases (liquid-air, liquid-liquid, and liquid-solid interfaces). These substances demonstrate a low critical micelle concentration (CMC) and possess the capacity to form stable emulsions. Biosurfactants are also defined by their effectiveness in lowering the surface tension of a liquid. This surface tension quantifies the interfacial free energy per unit area at the boundary between the liquid and the overlying air (Rosen & Kunjappu, 2012). The reduction of surface and interfacial tensions occurs through the adsorption of biosurfactant onto various phases, enhancing interaction and mixing between dissimilar phases. A surfactant can lower the surface tension of water from 72 mN/m to 35 mN/m and the interfacial tension between water and hexadecane from 40 mN/m to 1 mN/m (Mulligan, 2005). Meanwhile, the minimum surface tension in water and micelle formation can be achieved based on CMC, which is the lowest concentration of biosurfactant needed and represents the efficiency of biosurfactants. This value is established by assessing the decrease in surface tension resulting from the serial dilution of the solution. At this concentration, hydrophobic tails are shielded by hydrophilic heads when biosurfactant molecules aggregate to produce micelles. Thus, the minimum concentration necessary

for the effective reduction of surface and interfacial tensions is denoted by the CMC (Uzoigwe et al., 2015).

Compared to synthetic surfactants, the unique molecular structure and amphiphilic characteristics of biosurfactants correspond to lower CMC values. Thus, improved efficacy in certain applications is presented when these properties facilitate self-assembly into micelles at reduced concentrations. These applications included oil recovery, soil remediation, and food processing. Considering that optimal surface tension reduction can be accomplished through low CMC of biosurfactants, environmental compatibility can be effectively enhanced. This process can minimise potential ecological impacts. The CMC of biosurfactants also generally varies between 1 mg/L and 2000 mg/L, with average surface and interfacial tension values of 30 mN/m and 1 mN/m, respectively. Specifically, biosurfactants are more economically feasible their CMCfor industrial use when their CMC is smaller, indicating enhanced surfactant efficacy (Kapadia & Yagnik, 2013). Table 2.10 compares biosurfactants and other chemical surfactants concerning their CMC values and surface properties. Comparison summary of biosurfactants and chemical surfactants regarding their CMC and surface tension values

Table 2.10
Comparison Summary Of Biosurfactants And Chemical Surfactants Regarding Their CMC And Surface Tension Values

Surfactant	Producer	CMC (mg/L)	Surface Tension (mN/m)	References
Biosurfactant				
Rhamnolipids	*Pseudomonas aeruginosa*	50-200	29.0	Liu et al., 2018
Sophorolipids	*Candida bombicola*	82	33.0	Chandran & Das, 2012
Surfactin	*Bacillus subtilis*	23	27.0	Saimmai et al., 2012
Lipopeptides	*Bacillus subtilis*	11	27.0	(Srivastava et al., 2023)
Phospholipids	*Rhizopus Oryzae*	NA	28.8	(Pele et al., 2019)
Chemical surfactant				
Tween 80		600	30.0	Wang et al., 2018
Sodium dodecyl sulphate (SDS)		2120	37.0	Louvado et al., 2012
Triton X-100		189	33.0	Reddy et al., 2018

Figure 2.12 depicts the correlation between biosurfactant concentration and surface tension. Biosurfactants are amphiphilic molecules that consist of hydrophilic (water-attracting) and hydrophobic (water-repelling) regions. This material adsorbs at the air-water or oil-water interface when introduced into an aqueous medium at low concentrations, positioning its hydrophobic tails away from the aqueous phase and its hydrophilic heads towards it. The alignment then interferes with the cohesive forces among water molecules at the interface, diminishing and reducing surface tension. Moreover, an increase in biosurfactant concentration leads to a gradual decrease in surface tension. Hence, the CMC represents a threshold point at which the surface becomes saturated with biosurfactant molecules, resulting in no significant reduction in surface tension with further addition of biosurfactants.

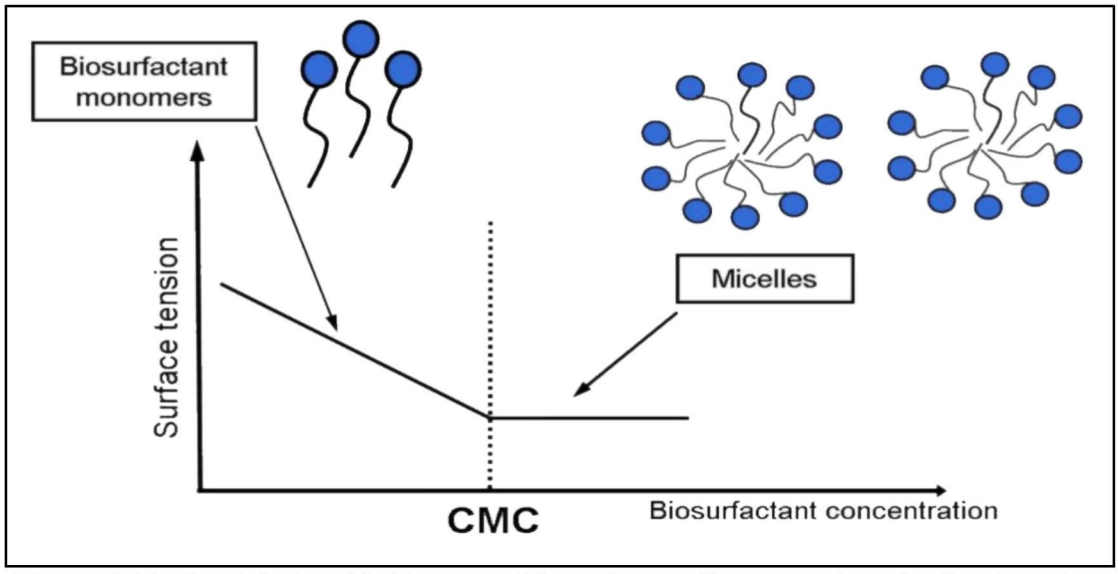

Figure 2.12 The Relationship Between Biosurfactant Concentration, Surface Tension And Formation Of Micelles

2.6 Production of Biosurfactants from Renewable Substrates

The main obstacle to the widespread adoption of biosurfactants lies in their unfavourable economic viability in comparison to petrochemical surfactants. Raw material costs (generally comprising 10–30%) of total production expenses, the availability of cost-effective production with recovery techniques, and the yield with productivity of the producing microorganism significantly influence the elevated market cost of biosurfactants (Wadekar et al., 2012). Therefore, the transition toward sustainable practices in technology seeks to establish a more environmentally

sustainable future. This cost barriers linked to biosurfactant production are often addressed through two global primary strategies in improving cost-effectiveness: (i) using low-cost and waste substrates for formulating fermentation media (lower initial raw material expenses) and (ii) creating efficient with optimised bioprocesses. These bioprocesses can then enhance biosurfactant production and retrieval through the optimisation of culture conditions and cost-effective recovery methods.

The biosurfactant production sector has recently examined substrate fabrication based on cost-effective materials. Numerous studies have reported using suitable substrates in fermentation bioprocesses through renewable and economically viable industrial and domestic waste. Commonly utilised waste includes WFO, fruit peels, seeds, leaves, rice straw, sugarcane bagasse, corncobs, banana stalks, corn husks, and cassava wastewater. Consequently, these studies have verified that the growth of various microbial amphiphilic molecules is effectively facilitated by these substrates (Marchant & Banat, 2012). These substrates can aid in the effective management of rising environmental waste production while providing cost-efficient solutions. Nonetheless, the process should still consider several other aspects, such as pH, thermal with salt stabilities, substrate form, and required quantity concerning feedstock selection for biosurfactant production.

Numerous studies have validated the feasibility of renewable substrates for biosurfactant production. For instance, Kaur et al. (2019) demonstrated the efficient synthesis of sophorolipids using food waste–based media. Andrade et al. (2017) utilised cassava leaves to produce mannosylerythritol lipids, whereas Ni'matuzahroh et al. (2020) highlighted the potential of lignocellulosic residues such as rice straw and corn cobs as economical feedstocks. Das and Kumar (2018) reported the successful conversion of potato peels into biosurfactants via *Bacillus licheniformis*. Similar trends were observed by Paraszkiewicz et al. (2018) using molasses and apple peels. For fungi, several studies have highlighted the suitability of fruit-based wastes for lipid-derived biosurfactants, including the use of pineapple peels by *Rhizopus arrhizus* (Vieira et al., 2021) and mixtures of pineapple peels with sunflower oil by *Rhizopus oryzae* (Al-Kashef et al., 2018).

Among the various substrates investigated, WFO emerges as one of the most viable and strategically advantageous feedstocks. Its high lipid content provides an efficient carbon source for oleaginous microorganisms, particularly *Rhizopus* species, facilitating the synthesis of glycolipid and phospholipid biosurfactants with

comparatively higher yields. Economically, WFO is inexpensive, readily available in large volumes, and requires minimal pre-treatment, reducing overall production costs. Importantly, in the context of Sarawak, WFO is a locally abundant waste generated by extensive household, food-service, and commercial frying activities, making it an accessible and sustainable substrate that aligns with regional waste-valorisation priorities.

Overall, the literature strongly supports the utilisation of renewable and waste-based substrates for cost-effective biosurfactant production. Given its lipid richness, low cost, and strong local availability, WFO represents the most viable substrate for large-scale biosurfactant production in Sarawak. Its valorisation contributes simultaneously to waste management, environmental protection, and the economic feasibility of biosurfactant-based solutions. Table 2.11 presents an overview of biosurfactant production utilising renewable substrates.

Table 2.11
Biosurfactants Production From Renewable Substrates

Substrates	Microbial origin	Production conditions	Biosurfactant type	Application	References
Rice straw	Serratia nematodiphila	Addition of minimal salts and xylose-rich substrate hydrolysate with 1 mL seed culture (OD600 = 1). Incubation at 37 ◦C for 7 days at 150rev/min	Glycolipids	Emulsifying and antimicrobial applications	(Panjiar et al., 2020)
Exploded sugarcane bagasse	Co-culturing Pseudomonas aeruginosa and Saccharomyces cerevisiae	Hydrolysis-fermentations simultaneous experiments using 250 g/L exploded sugarcane bagasse, 2 g/L P. aeruginosa and 30 g/L S. cerevisiae at 30 ◦C and 120 rpm	Rhamnolipids	Biorefinery	(Lopes et al., 2017)
Sugarcane bagasse	Cutaneotrichosporon mucoides	200 mL of xylose and detoxified hydrolysate media were prepared. Fermentative production was carried out using a rotary shaker (30 ◦C and 200 rev/min for 144 h)	Sophorolipids	Food, cosmetic, and pharmaceutical industries	(Marcelino et al., 2019)
Rice straw and corncobs	Achromobacter sp.	Bacterial culture (2%, v/v) was added to synthetic mineral water. Culture was incubated at 30 ◦C for 7 days at 120 rev/min	Biosurfactant (Not determined)	Biorefinery and emulsifying applications	(Ni'matuzahroh et al., 2020)
Palm oil mill effluent	Nevskia ramos	5% inocula added to MSM (v/w) and supplemented with POME (20%, v/v) in a rotary shaker, incubated at 30 hrs at 30°C and 200 rpm	Biosurfactant (Not determined)	Microbial enhanced oil recovery and emulsifying agent in food	(Chooklin et al., 2013)

Substrates	Microbial origin	Production conditions	Biosurfactant type	Application	References
Corncob liquor	Bacillus subtillis	Nutrient solution (95 mL) was added with 5 mL of fresh inoculum. Varying concentration of hemicellulosic corncob liquor was added and adjusted to pH 6.85 and incubated for 72 hours	Surfactin	Environmental bioremediation applications	(Prado et al., 2019)
Cassava wastewater	Pseudozyma tsukubaensis	Cassava wastewater containing culture media was added to the bioreactor (aeration rate of 0.4 vessel volume per minute) and 100 rev/min) and kept under 150 rev/min, 0.8 vv/m from 24 to 84 hours	Mannosylerythritol lipids	Cosmetic and skincare product formulations	(C. J. de Andrade et al., 2017)
Banana stalks	Aspergillus niger	SSF of banana stalk (5 g) moistened with 5 mL of fungal growth media was added with 2 mL of spore suspension, and incubated at 37◦C for 6 to 8 days	Biosurfactant (Not determined)	Emulsifying applications	(Asgher et al., 2020)
Pineapple peels	Bacillus subtillis	Culture media containing concentrated pineapple peel juice was inoculated, adjusted to pH 6.8, and incubated for 72 h, at 30 ◦C and 120 rev/min	Biosurfactant (Not determined)	Emulsifying applications	(Vieira et al., 2021)
Beet molasses and apple peel extract	Bacillus subtillis	Luria-Bertani broth and Cooper's broth were added with two different brewery wastewaters, 2% beet molasses and apple peels extract were added with 0.25% of peptone or yeast extract and carrot peels extract.	Lipopeptides (surfactin and iturin)	Industrial applications	(Paraszkiewicz et al., 2018)

Substrates	Microbial origin	Production conditions	Biosurfactant type	Application	References
Orange peels	Bacillus licheniformis	50 mL minimal salt media was added with 2% (v/v) inoculum using 250 mL flask. Dried orange peel powder was added with 2% (w/v) concentration, and placed at 30 ◦C for 120 h	Lipopeptides	Biodegradation of hydrocarbons	(Kumar et al., 2016)
Beet peels	Bacillus subtillis	Aeration and agitation combination was investigated in a bench-bioreactor using beet peel and glycerol from a biodiesel production as substrate. Optimization study suggested agitation. 200 rpm and aeration 0.5 vvm, producing 1931.2 mg/L of biosurfactant yield	Biosurfactant (Not determined)	Oil spreading and emulsification applications	(dos Santos et al., 2018)
Leftover food waste	Starmerella bombicola	Flasks containing feedstock hydrolysate or oil waste were added with 10% inoculum from pre-culture, and incubated in an orbital shaker at 200 rev/min and 30 ◦C for 5 days	Sophorolipids	Enhanced oil recovery, cosmetic, detergents, lubricants, and antimicrobial applications	(Kaur et al., 2019)
Potato peel powder	Bacillus licheniformis	MSM added with potato peels powder and incubated on rotary shaker at 150 rev/min for 72 hours	Biosurfactant (Not determined)	Bioremediation of petroleum-contaminated	(Das & Kumar, 2018)
Waste cooking oil	Penicillium citrinum	MSM broth was added with waste cooking oil at 5% (v/v), incubated at 30°C for 14 days	Biosurfactant (Not determined)	Corrosion inhibitor	(Olivia et al., 2023)

2.6.1 Factors Influencing the Productions of Biosurfactants

The production of microbial biosurfactants is affected by various factors, including the selection of C sources and nutrient compositions [nitrogen-to-phosphate (N/P) ratio], presence of micronutrients, pH, temperature, agitation, humidity, and aeration (Pirollo, 2006; Fontes et al., 2008; Banat et al., 2010). Other critical factors include the selection of microorganisms, downstream processing of the biosurfactant, and genetic engineering of the production. The cost and environmental implications of biosurfactant production are also influenced by these factors (Liepins et al., 2021).

The factors influencing biosurfactant production are illustrated in Figure 2.14 and comprehensively described in Table 2.12. These factors are essential for optimising microbial biosurfactant synthesis.

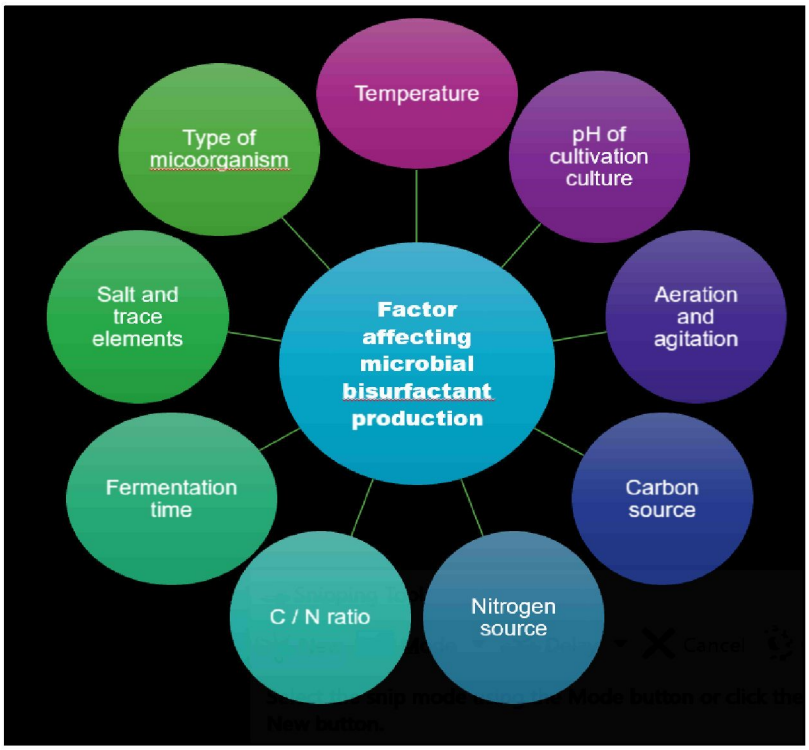

Figure 2.13 The Factor Influencing Microbial Biosurfactant Production

Table 2.12
Summary Of Essential Parameters Influencing Microbial Biosurfactant Production

Factor	Details	Microbial Specificity
Carbon Source	Diesel, crude oil, glucose, sucrose, and glycerol. Affects biosurfactant synthesis, but chain length of substrate does not impact fatty acid chain length in glycolipids.	Substrate effects vary by microbial strain (e.g., *Pseudomonas sp.*)
Nitrogen Source	Yeast extract, ammonium sulfate, ammonium nitrate, sodium nitrate, meat extract, malt extract, and urea. Biosurfactant often produced during nitrogen limitation phase.	*P. aeruginosa* prefers nitrate sources; *Arthrobacter paraffineus* favors ammonium salts and urea
C:N Ratio	Influences microbial metabolism and product yield. Optimal ratios are organism- and medium-specific.	Strain-dependent
Temperature	Optimal range generally 25–30°C. Deviations may alter biosurfactant composition.	*Pseudomonas sp.* DSM-2874 affected by temperature shifts
pH	Influences biosurfactant synthesis; optimal pH reported between 6.0–8.0 depending on strain.	pH 8.0 for *Y. lipolytica*; pH 6–6.5 optimal for *Pseudomonas sp.*
Aeration & Agitation	Enhance oxygen transfer and nutrient availability. High aeration and 50% dissolved oxygen saturation improve yields.	Required for most aerobic strains
Salinity	Salinity affects yield variably; some strains tolerate up to 10% w/v without major effect on critical micelle concentration (CMC).	Strain-specific tolerance
Culture Phase	Biosurfactants often produced during the stationary phase, particularly when nutrients become limiting.	Common among biosurfactant-producing microbes

2.6.1.1 Substrates

Microbial growth and metabolic functions necessitate selecting suitable carbon and nitrogen sources (Bhardwaj et al., 2013). The yield and efficiency of biosurfactant production are also influenced by the type and concentration of carbon source (Cooper and Paddock, 1984; Kim et al., 1997). Furthermore, the total product cost contributed by these carbon and nitrogen sources comprises between 10% and 30% (da Silva et al., 2021). Nevertheless, the surface-active properties and applications of biosurfactants are affected by the relationship between the carbon source and molecular structure. One

substantial example involves enhanced microbial growth and biosurfactant production due to the readily metabolisable sugars, such as glucose. Another example is the lower production costs and improved sustainability generated by more complex substrates (agricultural and industrial wastes). The carbon-to-nitrogen (C/N) ratio is also critical, facilitating the required metabolic pathways in microorganisms when the optimal balance is achieved. Likewise, the carbon sources supplied and utilised in the culture medium notably affect the biosurfactant production-related metabolic pathways. Particularly, combining energy sources (carbohydrates and lipids) is frequently documented. Culture media can also use various carbon sources, such as glucose, sucrose, xylose, inulin, cassava wastewater, cane with soy molasses, glycerol, and hydrolysates derived from restaurant food waste. Additionally, lipid sources (refined vegetable oils, residual food frying oils, wastewater from the oil industry, motor oil, and animal fat) have been utilised.

Various sources of inorganic and organic nitrogen can affect the synthesis of biosurfactants. Commonly utilised organic sources include corn-steep liquor, yeast extract, and urea. Conversely, familiar inorganic sources are nitrate and ammonium salts. Thus, it is advisable to ensure an ample supply of both carbon and nitrogen at the onset of cell growth. The nitrogen level should then be decreased after a specific period. The C/N ratio also significantly influences biosurfactant production, with a recommended high C/N ratio typically ranging between 16:1 and 18:1 (Jahan et al., 2020). Therefore, the physicochemical properties of biosurfactants can be altered by varying the carbon and nitrogen sources. For example, the yield of biosurfactants produced by *Torulopsis bombicola* increased significantly (up to 70 g/L) when cultivated in a medium containing glucose and vegetable oil (Cooper and Paddock, 1984). Kim et al. (1997) reported optimising the biosurfactant yield concerning SLs produced by *Torulopsis bombicola*. This outcome was attained by integrating glucose (concentration between 40 g/L and 80 g/L) and soybean oil.

Fungi tend to yield higher amounts of biosurfactants using renewable substrates compared to bacteria due to their rigid cell walls. Higher yields of 120 g/L and 40 g/L of fungal surfactants have been reported using carbon sources like tallow fatty acid residues, animal fat, glycerol, and oleic acid (Bhardwaj, 2013). Fungal biosurfactants production parameters found in the literatures are presented in Table 2.13.

Table 2.13
Parameters Influencing Fungal Biosurfactant Production

Producer Microorganism	Substrates (C/N)	Working Volume (L)	Mixing (rpm)	Aeration (vvm)	pH/Temperature (°C)	Volumetric Productivity ($g \cdot L^{-1} \cdot h^{-1}$)	Maximum Yield ($g \cdot L^{-1}$)	Surface Tension ($mN \cdot m^{-1}$)	References
Candida lipolytica	Animal fat (5%) and corn-steep liquor (2.5%)	50	200	ND	5.3/28	0.3	40	25	Santos et al., 2017
Candida tropicalis UCP0996	Frying oil (2.5%), corn liquor (2.5%) and cane molasses (2.5%)	25	200	1	5.5/28	0.06	7.36	27.48	Almeida et al., 2017
Candida sphaerica	Groundnut oil refinery residue (9%) and corn-steep liquor (9%)	20	150	ND	5.3/27	0.15	21	27	Ye et al., 2016
Candida antarctica	Soybean oil (80 $g \cdot L^{-1}$) and yeast extract (1 $g \cdot L^{-1}$)	2	200	1	ND/19	0.19	28	35	Adamczak et al., 2000
Starmerella bombicola	Glucose (10%), sunflower acid oil (10%), yeast extract (4 $g \cdot L^{-1}$), and urea (4 $g \cdot L^{-1}$)	2	550	1	3.5/30	0.27	51.5	35.5	Jadhav et., 2019
Starmerella bombicola	Glucose (100 $g \cdot L^{-1}$) and corn-steep liquor (10 $g \cdot L^{-1}$)	2.5	800	1	3.9/25	1.55	342	ND	Liu et al., 2019
Pseudomonas tsukubensis	Cassava wastewater	3	100/150	0.4 and 0.8	ND	0.02	1.26	26	CJ Andrade et al., 2017

Producer Microorganism	Substrates (C/N)	Working Volume (L)	Mixing (rpm)	Aeration (vvm)	pH/Temperature (°C)	Volumetric Productivity ($g \cdot L^{-1} \cdot h^{-1}$)	Maximum Yield ($g \cdot L^{-1}$)	Surface Tension ($mN \cdot m^{-1}$)	References
Rhodotorula paludigena	Glucose (150 $g \cdot L^{-1}$) and yeast extract	4	ND	1	6.5/27	0.12	20.9	ND	Garey et al., 2017
Aureobasidium pullulans	Sucrose (50 $g \cdot L^{-1}$), peptone (0.6 $g \cdot L^{-1}$) and yeast extract (0.4 $g \cdot L^{-1}$)	0.7	300–1200	0.5	6.5–3.5/30	0.09	15	ND	KM Saur et al., 2019
Rhizopus oryzae	Crude glycerol (3%) and corn-steep liquor (5%)	ND	150	ND	5.5/28	0.02	1.74	28.8	Pele et al., 2019
Fusarium sp.	Sucrose (40 $g \cdot L^{-1}$) and yeast extract (0.8 $g \cdot L^{-1}$)	ND	150	ND	7.0/30	0.01	2.43	ND	Qazi et al., 2014
Mucor hiemalis	Soybean oil waste (5%) and sodium glutamate (1%)	150	ND	ND	ND/28	0.08	7.73	32	Ferreira et al., 2020
Aspergillus niger	Banana stalk powder (5.75 g), yeast extract (1 $g \cdot L^{-1}$), and peptone (3 $g \cdot L^{-1}$)	ND	ND	ND	7.0/35	0.03	5.5	ND	M. Asgher et al., 2017
Cunninghamella echinulata	Soybean oil waste (2%) and corn-steep liquor (8%)	150	ND	ND	5.5/28	0.04	5.18	31.7	Souza et al., 2018

2.6.1.2 Fermentation

Fermentation serves as a crucial metabolic process in biosurfactant production, significantly affecting the yield and quality of the resultant metabolites. The fermentation process involves the utilisation of microorganisms to convert substrates into products (Soetaert and Vandamme, 2010). This process also comprises enzyme-catalysed reactions within a specific cellular system, with the response contingent upon the chemical and physical conditions in the environment (Smith 2009). Moreover, the process may be conducted under solid-state or submerged fermentation conditions. Each condition presents unique advantages based on the intended application (Soetaert and Vandamme, 2010). Submerged fermentation is deemed more appropriate for large-scale industrial applications due to its shorter production time (1–2 weeks). Alternatively, solid-state fermentation often necessitates several months (X. Y. Zhang et al., 2022).

Solid-state fermentation entails the proliferation of microorganisms on solid material substrates with minimal or no free water present. Nonetheless, solid materials must contain adequate moisture within them. Hence, the submerged fermentation process employs a liquid or solid substrate dissolved in water, creating a medium that supports microbial growth (Soetaert and Vandamme, 2010). In most cases, fungal-based biosurfactants generate a medium that promotes microbial growth cultures conducted in shaking flasks or bioreactors (Adamczak & Bednarski, 2000; Cola ML et al., 2010). Solid-state production also demonstrates potential (Banat et al., 2021). Banat et al. (2021) illustrated that 39% of published biosurfactant production-related articles regarding solid cultivation were fungal, with SLs and hydrophobins accounting for 14% and 2% of the types produced, respectively. Vigueras et al. (2014) explained that solid-state cultivation enhanced the production of hydrophobins by *Purpureocillium lilacinum* (34.8 mN m^{-1} and 1.3 mg of protein g^{-1}), which was not observed in submerged culture. Kulkarni et al. (2020) denoted that a 107% increase in yield was observed in solid culture utilising a complex substrate (sesame oil cake) compared to submerged culture. This finding was based on a yeast-malt-glucose medium for the production of hydrophobins from *Pleurotus ostreatus*. Intriguingly, one infrequently addressed factor that can affect microbial activity and the stability of the production process concerning solid-state fermentation systems is humidity.

The fermentation process is categorised into anaerobic fermentation (absence of O_2) and aerobic process (requires O_2). Anaerobic fermentation is utilised for biohydrogen in biofuels, whereas aerobic fermentation is employed for vinegar production in the food industry (Bakonyi et al., 2014; Gullo et al., 2014). Figure 2.13 depicts that the fermentation process consists of three modes: (i) batch, (ii) fed-batch, and (iii) continuous process. Batch fermentation involves the initial placement of all necessary components into the vessel at the start of fermentation, with no subsequent addition or removal of materials during the fermentation period. Meanwhile, fed-batch fermentation uses an additional substrate that is introduced later in the process. Continuous fermentation also requires an open system in which the solution is continuously in the vessel. A portion of the converted solution is extracted at specified intervals (Chen et al., 2020).

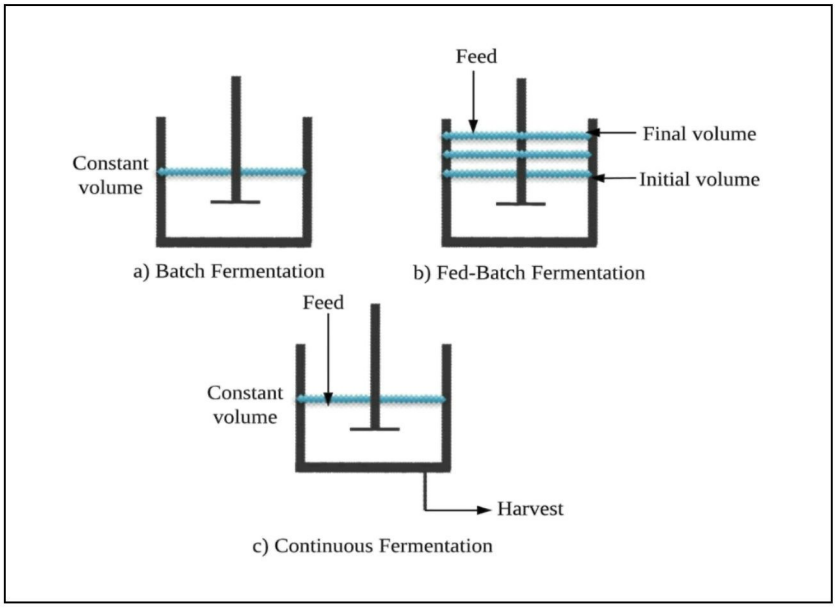

Figure 2.14 The Various Modes Of Submerged Fermentation

2.6.1.3 pH and Temperature

Environmental conditions (specifically pH and temperature) significantly affect the growth, metabolism, and biosurfactant production of microbial strains. These parameters not only influence microbial cell physiology but notably impact the yield, stability, and surface activity of the produced biosurfactants. Biosurfactant-producing microbes predominantly flourish within a neutral to slightly alkaline pH range (6.5–

8.5). Thus, the pH influences the enzyme activity and protein function critical for biosurfactant synthesis, the ionic state of biosurfactant molecules (solubility, emulsification, and adsorption behaviour on surfaces), and the availability of nutrients with trace elements in the medium. Suboptimal pH levels can result in decreased microbial growth rates, enzyme denaturation, and impaired biosurfactant production. In extreme conditions, both acidic and highly alkaline conditions environments can entirely prevent the synthesis of biosurfactants (Marajan et al., 2018).

Given that most biosurfactant-producing bacteria and fungi thrive in a mesophilic range (25–37°C), temperature can influence microbial metabolism and the physicochemical properties of biosurfactants. Thus, efficient enzymatic activity can enhance microbial growth and biosurfactant production at optimal temperatures. Conversely, low or high temperatures can inhibit metabolic processes or cause thermal denaturation of biosynthetic enzymes while compromising the integrity of biosurfactants, respectively. Several essential performance indicators of biosurfactants in practical applications also demonstrate a significant correlation with temperature. These indicators include surface tension, CMC, and emulsifying capacity. Consequently, maximised biosurfactant yield and good functional stability with effectiveness necessitate maintaining optimal pH and temperature conditions. Consistent and efficient biosurfactant production can only be attained through careful control of these environmental indicators in laboratory and industrial-scale fermentation processes.

2.6.1.4 Agitation and Aeration

The aerobic metabolic processes associated with biosurfactant production are highly dependent on sufficient O_2 transfer and nutrient distribution. These features can be facilitated by agitation and aeration. Fungal biosurfactant production processes are typically aerobic, requiring high rates of aeration and mixing during submerged cultivation. In submerged cultures, mixing helps maintain a uniform medium and improves substrate availability. However, in solid-state cultivation, its use is limited due to the risk of damaging filamentous fungi from high shear stress. Although the effect of mixing speed on biosurfactant production is not well studied, intermittent agitation in *Starmerella bombicola* solid cultures has been shown to increase substrate availability and improve yield, likely by enhancing mass and heat transfer.

2.6.2 WFO as Substrate in Biosurfactant Production

Recent years have seen an increasing focus on determining inexpensive materials for substrates in biosurfactant production. The utilisation of renewable and economically feasible industrial and household wastes is recommended due to their capacity to substitute expensive synthetic materials in the synthesis of biosurfactants. Waste lipids (fats, oils, and grease) from catering service providers and households also constitute a substantial category of biogenic waste in urban environments. Specifically, Malaysian WCO from deep-fat fryers represents the primary type of waste lipids. These sources of Malaysian waste lipids are varied, encompassing plant-based oils (palm, soybean, and sunflower oils) and animal-based fats (butter and lard). This nation also exhibits a significant per capita consumption of oils and fats. A report by DPO International indicated that the volume was projected to reach approximately 151.9 million kg by 2027, with a growth rate of 4.5% in 2023 (DPO International, 2022). This value translated to an average per-person consumption of 3.7 kg in 2022.

In Malaysia, the production of waste lipids is affected by population growth and changing consumption patterns. Currently, the Malaysian population in 2024 is 34.7 million, exhibiting a growth of 1.9%. This increase notably influences the demand for oils and fats. The demographic trend, rising urbanisation, and evolving dietary habits also lead to an increase in waste lipid generation (https://www.dosm.gov.my). Furthermore, the WCO derived from deep fat fryers represents the predominant category of lipids. This WCO composition is affected by several factors, including the origin of the oil, number of frying cycles, frying duration, equipment utilised, and type of food processed. During frying, oil is subjected to air and light at elevated temperatures between 160°C and 200°C extended periods. This process results in chemical alterations in the oil, such as oxidation, peroxidation, hydrolysis, and polymerisation. The reactions then modify the fatty acid composition of the oil and generate various compounds (peroxides, hydrocarbons, aldehydes, and ketones). Most of these compounds exhibit volatility. Nevertheless, certain byproducts can impede microbial growth and metabolic processes.

The types and compounds of oils can vary based on the duration of the frying process. This frying oil can absorb traces of metals from the frying equipment and other substances (salt, water, and organic molecules) from the food being fried. Therefore, the disposal and utilisation of waste lipids present significant concerns. Hanisah et al.

(2013) conducted a study in Teluk Bahang, Penang. The study indicated that 17% of participants disposed of used cooking oil in the trash, 6% discarded it on the ground, and 60% poured it into drainage systems. Only 16% were collected for reuse or sale. This inadequate amount could produce various environmental issues, including drain obstructions and pollution. Cheah et al. (2021) argued that the high fat intake of the Malaysian diet (66 g daily) possessed public health implications. This observation was based on the increase in obesity rate from 27.2% (20110 to 30.6% (2015).

The recycling rate of waste lipids in Malaysia is currently inadequate. Even though initiatives like the program by Buddhist Tzu Chi Dialysis Centre for collecting used cooking oil to mitigate pollution are in place, the overall infrastructure for collection and recycling is still inadequately developed. This observed underutilisation highlights the necessity for improved collection systems and increased public awareness to facilitate the recycling of waste lipids into valuable products. Implementing efficient waste lipid management practices is also consistent with sustainable development objectives while promoting a circular bioeconomy.

Overall, WFO in biosurfactant production can decrease production costs and lessen the ecological impact consequences linked to the improper disposal of WFO. This issue attracted considerable significant attention from researchers. Nevertheless, insufficient studies on this topic within Malaysia involving fungi-based biosurfactant production have been denoted. Table 2.14 lists the recent studies on biosurfactant production utilising WFO as a carbon source. The results indicate that *Rhizopus* sp. can utilise WFO for biosurfactant production, potentially providing a sustainable approach for waste management and biosurfactant synthesis.

Table 2.14
Summary Of Biosurfactant Production Using WCO As A Substrate

Strain	**Nitrogen Source**	**Carbon Source**	**Biosurfactant Class**	**References**
Bacillus subtilis	MSM	Fresh cooking oil, WCO	Lipopeptide	(Yañez-Ocampo et al., 2017)
Bacillus subtilis	MSM	WCO	Lipopeptide	(Nur Afini Binti Wan Adlin et al., 2020)
Yeast (Starmerella bombicola)	Urea	WCO	Glycolipid	(Liepins et al., 2021)

Strain	Nitrogen Source	Carbon Source	Biosurfactant Class	References
Pseudomonas aeruginosa	Not mentioned	WCO (with activated earth treatment)	Rhamnolipid	(Wadekar et al., 2012)
Anoxybacillus sp	MSM	WFO	Lipopeptide	(Nurul Fatihah Khairudin, 2016)
Pseudomonas aeruginosa	MSM	Waste frying coconut oil	Rhamnolipid	(George & Jayachandran, 2013)
Bacillus licheniformis	Sodium nitrate	WFO + glucose	Lipopeptide	(Patania et al., 2021)
Rhizopus arrhizus	Sodium glutamate	Soybean waste frying oil	Not mentioned	(Pele et al. 2018)
Rhizopus oryzae	MSM	Sunflower oil cake and pineapple waste mixture	Glycolipid	(Pele et al. 2019)
Mucor circinelloides	Yeast extract	WFO	Not mentioned	(Hasanizadeh et al., 2017)
Cunninghamella bertholetiae	Corn steep liquor	Waste soy oil	Not mentioned	(Souza PM et al., 2017)
Penicillium chrysogenum	MSM with glucose and glycerol	Grease waste	Lipopeptide	(Gautam et al., 2014)
Candida glabrata	Yeast mold broth	Vegetable fat waste	carbohydrate–protein–lipid complexes	(De Gusmao et al., 2010)

2.6.3 Strategies for Increasing Yield and Productivity of Fungal-Based Biosurfactants

The production of biosurfactants is influenced by several factors (cell ageing, nutrient depletion, and the accumulation of products or by-products), which may impede cellular activity and decrease the production rate. Likewise, the yield and chemical characteristics of biosurfactants are influenced by various factors, such as substrate type, producing strain, and cultivation system employed (batch, fed-batch, or semi-continuous). One prominent example is the volume of inoculum and agitation influencing the emulsifying properties, surface activity, and yield of the product in the case of *Mucor hiemalis*. Typically, biosurfactant productivity must surpass 2.0 g/L/h to

be deemed commercially viable. Certain strains (such as *S. bombicola*) exhibit greater productivity in comparison to other species. Filamentous fungi (such as *Mucor* spp.) also often necessitate extended durations for optimal production and produce lower yields relative to yeasts. Nonetheless, high yields are frequently attained through fed-batch bioreactor cultivation, with meticulous regulation of parameters (O_2 concentration, pH, and temperature). Bhardwaj (2013) reported that feeding biodiesel and glucose in pulses enhanced productivity from 0.40 g/L/h to 1.55 g/L/h for *S. bombicola*. The study indicated higher yields of 120 and 40 g/L regarding fungal-based biosurfactants utilising C source (tallow fatty acid residues, animal fat, glycerol, and oleic acid).

Biosurfactant production generally involves the use of pure cultures, with inoculum size influencing the lag phase and biomass growth in bioreactors. Pre-treatments, such as the application of electric fields to *Aspergillus brasiliensis* spores, can improve biosurfactant production. The pH of the culture medium is another critical factor, with an optimal range of slightly acidic pH (5–7) for production. Thus, lower pH during fermentation stimulates biosurfactant synthesis and inhibits microbial contamination. Biosurfactant production also necessitates aerobic conditions, with elevated aeration rates essential for effective O_2 transfer. Conversely, recovery and yield can be diminished when foam formation occurs due to excessive aeration. An optimal moisture content range between 45 and 75% (depending on substrate and strain characteristics) is also pivotal for microbial growth and process yield in solid-state cultivation.

Despite these optimisation strategies, significant scale-up challenges persist, particularly when moving from laboratory to industrial bioreactors. Large-scale fermentation systems often struggle to replicate uniform oxygen transfer, mixing efficiency, and nutrient distribution achieved at smaller volumes. The viscosity of biosurfactant-rich broths further impedes mass transfer, increases agitation energy demands, and complicates process control. Additionally, downstream recovery becomes increasingly cost-intensive at industrial scale, especially when crude biosurfactants are produced from heterogeneous waste substrates. These operational and economic constraints collectively limit the commercial competitiveness of biosurfactants, underscoring the need for integrated bioprocess optimisation and more cost-effective, scalable purification technologies (Chen & Liu, 2021).

2.7 Applications of Biosurfactants

Various sectors have increasingly employed biosurfactants owing to their versatility and biodegradability, including environmental remediation and pharmaceuticals. The cleanup of oil spills and the treatment of industrial effluents in environmental remediation usually utilise this material. This material can improve solubility and bioavailability through efficient degradation of hydrophobic pollutants based on its emulsifying characteristic. Marajan (2020) contended that the bioremediation of contaminated environments benefitted from increased microbial degradation activity of hydrocarbons via biosurfactants. The study explained that environmental cleanup efforts and the breakdown of pollutants were more effective when biosurfactants lowered the interfacial tension between hydrocarbons and water.

Biosurfactants are appropriate for diverse drug delivery systems within pharmaceuticals and cosmetics owing to their low toxicity and antimicrobial properties. Examples of these systems usually involve topical, oral, nasal, ocular, and intravenous applications. Cosmetic formulations also use this material due to their emulsifying capabilities. Another example is the enhanced fat metabolism and detoxification processes caused by Kordel's Lecithin (phospholipid-based biosurfactants). Rivardo et al. (2019) propounded that the inhibition of the colonisation or aggregation of microorganisms could be accomplished through biosurfactants on the wound surface prior to medication administration. The study noted that the adhesion of microorganisms at wound infection sites was regulated by this material. Çelik et al. (2021) stated the significant correlations between phosphatidylcholine (a principal constituent of biosurfactants), brain function, and cholesterol levels.

The antimicrobial properties of biosurfactants within the food industry render them popular for emulsification, stabilisation of food products, and functioning as natural preservatives. Particularly, this material is a vital component in food processing in improving emulsion stability for multiple products (salad dressings, sauces, and dairy products) (Abdallah et al., 2014). This material can also increase oil extraction from reservoirs for the oil sector by decreasing the interfacial tension between oil and water (Sarma et al., 2019). Consequently, wastewater treatment can benefit from this process, as biosurfactants facilitate coagulation and flocculation mechanisms that enhance the removal of fine particles. This procedure then improves water quality (G & Yagnik, 2013).

While these broad applications illustrate the versatility of biosurfactants, recent advancements have increasingly positioned them as promising agents for corrosion inhibition, particularly for steel in reinforced concrete systems. Their amphiphilic structure enables adsorption onto metallic surfaces, forming protective molecular films that hinder electrochemical reactions. Numerous studies have reported that biosurfactants such as glycolipids, lipopeptides, and phospholipids suppress anodic and/or cathodic processes by blocking active corrosion sites and reducing chloride ingress (Lan et al., 2017; Mansour & Elshafei, 2016; Mohammed et al., 2020; Pal & Lavanya, 2022). Plaza & Achal (2020) also highlighted the ability of biosurfactants to disrupt microbial adhesion, a mechanism relevant for mitigating microbiologically influenced corrosion (MIC).

In the context of reinforced concrete, biosurfactants offer additional advantages. Their surface-active properties can modify pore solution characteristics, enhance hydrophobicity, and delay moisture-driven corrosion initiation. Robuschi et al. (2021) further emphasised that phosphatidylcholine-based biosurfactants exhibit strong molecular affinity for metal–oxide interfaces, suggesting their potential to stabilise passive films on steel reinforcement. Moreover, their biodegradability and low environmental impact present a compelling alternative to commercial inhibitors that are often limited by toxicity, regulatory constraints, and high cost. Emerging studies have also demonstrated that certain biosurfactants can simultaneously improve concrete workability and interfacial transition zone (ITZ) characteristics, offering dual functionality as both an eco-friendly admixture and a corrosion inhibitor.

Collectively, the growing body of corrosion-specific research indicates that biosurfactants hold substantial potential for application in reinforced concrete durability enhancement. Their capacity for adsorption-driven film formation, microbial inhibition, and surface hydrophobisation aligns directly with the mechanisms required to mitigate corrosion in steel-reinforced concrete environments.

2.7.1 Biosurfactants as Corrosion Inhibitor

Both efficacy and constraints in biosurfactant-related corrosion inhibitors have been demonstrated in numerous studies. Typically, substantial relationships are indicated between corrosion protection efficiency for metals, biosurfactant type, specific metal being protected, and various environmental aspects. Parthipan et al.

(2018) examined the effects of a glycolipid biosurfactant on microbial corrosion inhibition against bacterial strains. The examined strains included *Streptomyces parvus* B7, *B. subtilis* A1, *Acinetobacter baumannii* MN3, and *Pseudomonas stutzeri* NA3 on carbon steel. A biosurfactant based on glycolipids was then synthesised from *Pseudomonas mosselii* F01. The CRs were also assessed via weight loss and electrochemical analyses. Subsequently, several outcomes were observed, including weight loss measurements, diminished corrosion current with potential, and improved resistance capacity. These findings corresponded to an 87% reduction in corrosion, with the most significant corrosion inhibition linked to the robust interaction energy between the glycolipid and the carbon steel surface. The study also verified the dual roles of glycolipid-based biosurfactants as corrosion inhibitors and biocides. This outcome was attributed to the antibacterial properties of biosurfactants. Biological reactions were obstructed when bacterial cells were attached to the active microbes in the biosurfactant. Notably, improved corrosion inhibition was presented for the adsorption of biosurfactant molecules on the metal surface compared to the interaction between water molecules and the metal surface.

Khan et al. (2020) examined the corrosion behaviour of X80 pipeline steel in marine environments using the marine bacterium *Marinobacter salsuginis*. The study assessed the corrosion process based on EIS and polarisation analysis. Consequently, several benefits were indicated when the pipeline steel contained a biofilm. These advantages were improved polarisation and charge transfer resistance alongside lower corrosion current density. Örnek et al. (2002) introduced EIS as a method to produce pitting corrosion inhibitors based on *Bacillus subtilis* and *Bacillus licheniformis* for aluminium (Al) 2024. The study noticed a lowered CR of the Al alloy due to the secretion of 20 amino acids at pH 6.5. Furthermore, the uninhibited and inhibited media demonstrated multiple uniform pits and fewer pits, respectively. This outcome was attributed to the formation of a biofilm, and the capacitive nature of the impedance spectra was confirmed through electron microscopy. Polyaspartate and γ-polyglutamate produced by *B. licheniformis* within the carboxylic acid groups also reduced the CRs.

Little et al. (2020) employed *Bacillus*-based biosurfactants to address the microbial corrosion of carbon steel ST37 by *Pseudomonas* spp. The study calculated corrosion through weight loss and minimum inhibitory with biofilm inhibitory concentrations through broth microdilution, and. Anodic sites were then established when O_2 was consumed owing to the biofilm produced by *Pseudomonas*. Subsequently,

only a few bacterial cells adhered to the carbon steel surface when the biosurfactant was introduced. This outcome indicated that the microbial corrosion of the carbon steel and biofilm was mitigated by using the biosurfactant. Gana et al. (2011) demonstrated that the corrosion issue in the oil sector could be lowered using biosurfactants from *Bacillus* spp. (Gana et al., 2011). Lesik et al. (2021) inhibit corrosion on carbon steel in 15% hydrochloric acid (HCl) by utilising vegetable oil waste-based phospholipids. Several chemical surfactants were incorporated into the phospholipids as additives, including C12-C14 alkyltrimethylammonium chloride (acetone C.70), C16-C18 alkyldimethylbenzylammonium chloride (catapav), tertiary amine oxides (oxypav), non-ionic surfactant (CP-20)), and oleylamidopropyldimethylamine (a mixture of zwitterionic surfactants). The study computed the CRs based on weight loss and electrochemical analyses. Consequently, an IE of 86.5% was attained by the phospholipids achieved 86.5% IE. A synergistic effect was also indicated based on the increased corrosion IE increased to 95% when combined with surfactants.

Al-Kashef et al. (2018) examined the association between corrosion IE and glycolipid biosurfactants produced by *Rhizopus oryzae* and *Fusarium oxysporum*. The study fermented sunflower cake oil and pineapple peel as carbon sources in a modified mineral salt (MSM) solution. Compared to *Fusarium oxysporum*-based biosurfactants, *Rhizopus oryzae*-based biosurfactants demonstrated greater IE of carbon steel corrosion. Płaza and Achal (2020) stated that biocorrosion corrosion could be substantially lowered using numerous microbial species, such as *Pseudomonas aeruginosa*, *Bacillus subtilis*, *Candida albicans*, and *Acinetobacter calcoaceticus*. Corrosion processes were effectively mitigated by these biosurfactants via protective layers on metal surfaces. Nevertheless, Rao and Mulky (2023) discovered that corrosion was promoted by certain microorganisms (*Lactobacillus* sp., *Acetobacter* sp., *Azospirillum* sp., and *Azotobacter* sp.) by producing organic and inorganic acids.

Compared with synthetic corrosion inhibitors, biosurfactants typically exhibit moderate to high inhibition efficiencies, although their performance may not always match the protection often achieved by optimised chemical formulations under controlled laboratory conditions. Nevertheless, synthetic inhibitors are increasingly constrained by issues of environmental persistence, regulatory limitations, toxicity, and escalating operational costs associated with large-scale application. Previous studies indicate that biosurfactants offer a viable and sustainable alternative, demonstrating competitive inhibition efficiencies when fermentation yields, molecular adsorption

characteristics, and delivery conditions are appropriately optimised. Their biodegradability, low ecotoxicity, and dual functionality in both corrosion mitigation and microbial control further strengthen their relevance for durable and environmentally responsible infrastructure systems. Table 2.15 tabulates various biosurfactant-related studies as corrosion inhibitors.

Table 2.15
Summary Of Previous Studies On Biosurfactants As Corrosion Inhibitors In Metals

Microorganism/biosurfactant	**Medium**	**Metal**	**References**
Coco Monoethanolamide (CMEA)	1 M HCl	Mild steel	Ganjoo et al., 2023
N-Dodecyl arginine, asparagine	Aqueous NaCl solution	Mild steel (MS 37-2)	Fawzy et al., 2021
Biosurfactant from Bacillus sp.	Oil	Carbon steel (ST-37)	Little et al., 2020
Glycolipid from Pseudomonas mosselii	Acid medium	Carbon steel	Parthipan et al., 2018
Marine bacteria from Marinobacter salsuginis	Alkaline medium	X80 pipeline steel	Khan et al., 2012
Bacillus subtilis and Bacillus licheniformis	Neutral	Aluminium	Örnek et al., 2002
RH produced by P. aeruginosa	Sea water	X70 carbon steel	Li et al., 2021
Rhamnolipid	CO_2 saturated oilfield	X65 carbon steel	Zhang et al., 2021
Phospholipids	Hydrochloric acid	Carbon steel	Lesik et al
Bacillus sp.	Injection water fromoilfield	Carbon steel (ST-37)	Gana et al., 2011
Brevibacillus brevis	Modified BAAR medium	Carbon Steel	Jayamaran et al., 1999
Glycolipid by *Rhizopus* oryzae and Fusarium oxysporum	1.0 M HCl	Carbon Steel	Amr Al-Kashef et al., 2018
Bacillus subtilis	Marine environment	Low alloy steel	Guo et al., 2017
Bacillus mycoides	Outdoor atmosphere	Zinc, aluminium and mild steel	Juzeliunas et al., 2006
Lipopeptides by Bacillus sp.	Oilfield-produced water	Carbon steel	Purwasena et al., 2019
Bacillus sp.	Nutrient-rich medium	Mild steel	Jayaraman et al. ,1999 & Zuo et al., 2004

Microorganism/biosurfactant	Medium	Metal	References
Rhamnolipids by Pseudomonas sp.	Synthetic acid rainwater	Alluminium alloy	Zin et al.,2018
Glycolipids by Pseudomonas mosselii	Acidic medium	Carbon steel	P. Punniyakotti et al., 2018
Pseudomonas cichorii	Phosphate-buffered basal salt solution	Mild steel	Chondar et al, 2005

2.7.2 Biosurfactant as Concrete Admixture

Reinforcing steel corrosion generally occurs when concrete is subjected to harsh environments, including high temperature, relative humidity, CO_2 concentration, and acidic or saline conditions (Asri et al., 2017). The porous nature of concrete allows for the infiltration of water and aggressive ions (Cl^-), which penetrate the matrix and compromise the passive protective film on steel surfaces. These environmental stressors can then undermine the protective mechanisms that typically safeguard the embedded steel. The corrosion of reinforcing steel is significantly influenced by concrete-related properties, such as w/c ratio, permeability, pH, cement type, concrete cover, and the quality of workmanship. Therefore, it is essential to analyse the factors influencing the strength and durability of the embedding concrete matrix, particularly the w/c ratio and the choice of appropriate admixtures. A lower w/c ratio generally leads to denser concrete with decreased permeability. This process thereby restricts the entry of aggressive agents that facilitate corrosion (Chu & Kwan, 2018). Likewise, admixtures [mineral-based materials (fly ash and silica fume)] enhance concrete durability by decreasing porosity and improving chloride ingress (Palanisamy, 2023).

Elsener et al. (1999) assessed the efficacy of a combined corrosion inhibitor in saturated $Ca(OH)_2$ solutions and mortar. The inhibitor demonstrated a capacity to postpone the initiation of pitting corrosion initiation in chloride-rich environments at elevated concentrations of 10% in 1 M sodium hydroxide (NaCl). Nonetheless, the performance decreased over time as a result of the evaporation of volatile components and the precipitation of non-volatile compounds in the presence of Ca^{2+}. Even though the inhibitor postponed the initiation of corrosion in chloride-contaminated mortar, it did not significantly affect the CR or performance under carbonated conditions. The

long-term effectiveness in real structures was also constrained, which was mainly due to the evaporation of active components.

He et al. (2020) investigated the impact of a biosurfactant from *Pseudomonas fluorescens* on slump loss, mechanical strength, capillary porosity, and bacterial colonisation in OPC-based mortar samples. The incorporation of 1.5% biosurfactant enhanced the plasticity and workability of fresh samples. Although f_c and f_s of mortars with biosurfactant were inferior to mortars without biosurfactant after a 28-day curing period, this biosurfactant increased the f_c of mortars after a 180-day curing period (the highest strength observed at a 1% biosurfactant concentration). The mortars containing biosurfactants also exhibited significantly lower capillary absorption coefficient A values ($P < 0.05$) compared to mortars without biosurfactants after 180 days. Consequently, reduced capillary porosity following extended curing periods was observed when the f_c of mortar samples was improved by the biosurfactant. A slower breakdown over time within the mortar due to higher resistance to biodegradation was also denoted by this biosurfactant, preventing deterioration and prolonging the lifespan.

Bruyako et al. (2021) explored the structural integrity of mineral matrices in mortar and concrete compositions. The study indicated that this integrity could be improved using *Rhodococcus erythropolis* in biocarbonisation through increased biotechnological treatments. A negative correlation was also demonstrated between microbial concentration (beyond 0.015% by weight) and mechanical strength. The bacterial cells caused a plasticising effect, contributing to this limitation. Another negative relationship was indicated between the concentration of *Rhodococcus erythropolis* and the rheological behaviour of sand-cement mortars. The flow properties of the w/c ratio mix were enhanced through higher bio-surfactant production when a lower w/c ratio was employed by the microorganisms operating similarly to surfactants. Overall, optimal microbial concentration was pivotal for improving performance. The study suggested that ineffective treatment or weakening of the mechanical and rheological performance of the mortar could be produced if insufficient or excessive bioactivity was observed, respectively.

Andalib et al. (2016) utilised *Bacillus megaterium*-based $CaCO_3$ to analyse its impact on the strength and durability of structural concrete. The study featured bacterial concentrations between 10×10^5 cfu/mL and 50×10^5 cfu/mL in various concrete samples (with and without bacterial inclusion). Compared to other concentrations, the 30×10^5 cfu/mL concentration sample revealed superior pore filling and microstructural

densification based on its highest $CaCO_3$ precipitation level. Despite the resistance of concrete to degradation was significantly improved by the microbially induced mineral precipitation, optimising bacterial concentration was still necessary. This recommendation was due to the negative strength and durability impacts on structural concrete when excessive amounts were used.

Kim et al. (2020) documented the link between biological admixtures [urea, nutrients, calcium lactate ($C_6H_{10}CaO_6$), and a ureolytic bacterium] from river sediment and hydration with the mechanical characteristics of Portland cement paste. During the curing process, $CaCO_3$ precipitation was facilitated when a vegetative state bacterium was added. A delay in hydration primarily attributed to nutrient content was also observed. Nonetheless, a lower porosity based on bacterial calcification was indicated owing to the higher mechanical strength. The study then concluded the beneficial influence of Ca on microbial activity and hydration through the higher increased f_c presented by specimens containing vegetative cells and $C_6H_{10}CaO_6$. Compared to control specimens, reduced porosity was observed for the bacterial mixes after 28 days. This outcome suggested that natural carbonation was less efficient than microbial calcification, with active bacterial participation confirmed by the high $CaCO_3$ levels. Hence, the negative impacts on hydration could be avoided by optimising nutrient composition with dosage and employing bioadmixtures in concrete.

Chahal et al. (2012) recorded the association between *Sporosarcina pasteurii* and the mechanical and durability properties of concrete. These concrete samples contained different fly ash amounts. The study then evaluated the f_c, water absorption, and rapid chloride permeability of the concrete mixes that were formulated using varying bacterial cell concentrations. Consequently, a 22% enhancement in f_c and an approximate eight-fold decrease in Cl^- permeability were exhibited by *Sporosarcina pasteurii* at an optimal concentration of 10^5 cells/mL. Even though increased strength and durability were reported, a negative implication on f_c was observed for high bacterial concentrations. This finding signified that effective performance enhancement necessitated dosage optimisation for effective performance enhancement (Mohammed et al., 2020).

Although most studies have examined mineral admixtures or microbial additives, research specifically addressing biosurfactants as concrete admixtures remains limited. Biosurfactants can theoretically modify the cementitious system through several mechanistic pathways:

i) Surface Tension Reduction

By lowering the surface tension of mixing water, biosurfactants improve wetting and dispersion of cement grains, enhancing early workability and potentially reducing the water demand required to achieve a given slump.

ii) Particle Dispersion and Deflocculation

Amphiphilic biosurfactant molecules adsorb onto cement particles, reducing van der Waals attractions and promoting a more uniform particle distribution. This process is analogous to the dispersing effect of conventional superplasticisers.

iii) Modification of Hydration Kinetics

Adsorption of biosurfactants on clinker phases may retard or accelerate hydration depending on molecular structure, influencing C–S–H formation, capillary porosity, and setting time.

iv) Interfacial Bonding at the Steel–Concrete Interface

The hydrophobic tail of biosurfactants may orient towards the pore solution while the hydrophilic head interacts with cement hydrates, potentially enhancing the microstructure adjacent to steel reinforcement and improving resistance to moisture and chloride ingress.

v) Pore Structure Refinement

Long-term curing may lead to reduced capillary porosity as dispersed particles hydrate more uniformly, consistent with the improvements reported by He et al. (2020).

Given the limited literature on biosurfactants, especially phospholipid-based biosurfactants derived from *Rhizopus sp.*, their role as multifunctional admixtures remains underexplored. In this study, a phospholipid biosurfactant from *Rhizopus sp.* was incorporated as a partial replacement for mixing water to investigate its dual functionality: (i) as a migratory corrosion inhibitor (MCI) applied to reinforcement surfaces prior to casting, and (ii) as an admixed corrosion inhibitor within the fresh concrete mix. The experimental programme evaluated its influence on flowability,

mechanical properties, pore structure refinement, and the protective quality of the hardened concrete matrix. Determining the optimal dosage was essential for maximising durability and structural performance.

2.8 *Rhizopus sp.* as a Biosurfactant Producer

The genus *Rhizopus* is part of the family Mucoraceae, which was introduced by Ehrenberg in 1820. In 1875, Van Tieghem identified several defining characteristics of the genus as follows:

i) Bearing stolons and rhizoids
ii) Formation of sporangiophores emerging from the locations where rhizoids are connected
iii) Sporangial form is typically globose, featuring columellae and apophyses
iv) Striation of spores

Rhizopus spp. (particularly *Rhizopus oryzae*) have been utilised in the fermentation of foods (tempeh and ragi) and more recently in the production of commercially significant metabolites [organic acids (lactic and fumaric acids), ethanol, and hydrolytic enzymes (Abe et al., 2003; Hartanti et al., 2015). *Rhizopus* spp. is also commonly referred to as bread moulds.

Many *Rhizopus* spp. demonstrate rapid growth and flourish across diverse environmental conditions. This species exhibits parasitism on a range of crops (potatoes, sweet potatoes, fruits), while particular species act as animal parasites (Taiji & Yoshito, 1964). These fungi can also inhabit dead and decaying organic material, such as leaves or soil. The fungi are widely distributed and can be located in several niches, including warm and humid regions of Southern Asia and cooler climates of Northern Europe. Despite optimal growth typically occurring between 30°C and 35°C, certain *Rhizopus* strains have been identified that can thrive at 45°C. Meanwhile, *Rhizopus* spp. exhibit optimal growth at a slightly acidic pH (~5.5). The growth remains relatively stable at pH levels between 3.5 and 4.0, with notable growth occurring at even lower pH values. *Rhizopus* spp. are facultative anaerobe fungi capable of thriving in both aerobic and anaerobic conditions. In contrast, aerobic growth is markedly superior to anaerobic growth. *Rhizopus* cultures are also relatively straightforward to maintain

and exhibit robust growth on potato dextrose agar (PDA) and yeast peptone dextrose (YPD) agar (Lennartsson et al., 2014).

The genus *Rhizopus* is easily recognised by its rapidly expanding, cotton-like mycelium that proliferates across solid media, often transitioning from white to grey or dark during sporulation. This structure comprises stolons, which are horizontal hyphae extending across the surface and rhizoids (root-like structures that penetrate downward to anchor the fungus and absorb nutrients). Sporangiophores (upright spore-bearing stalks) emerge at the locations of rhizoid formation, each culminating in a spherical sporangium that houses spores. A central swollen structure (columella) is usually indicated in these sporangia, generating distinct and striated sporangiospores (Abe et al., 2006). Furthermore, a highly branched coenocytic network is created owing to the hyphae of *Rhizopus* sp. being aseptate (lacking cross-walls) and multinucleate. Chitin and chitosan primarily form the cell wall, which confers structural integrity. Standard organelles [mitochondria, ribosomes, endoplasmic reticulum, and stored materials (glycogen and oil droplets)] are also located inside these cells. Thus, the swift growth and capacity to adjust to diverse environments of the organism is facilitated by these characteristics. Figure 2.15 presents the characteristic morphology of *Rhizopus oryzae*.

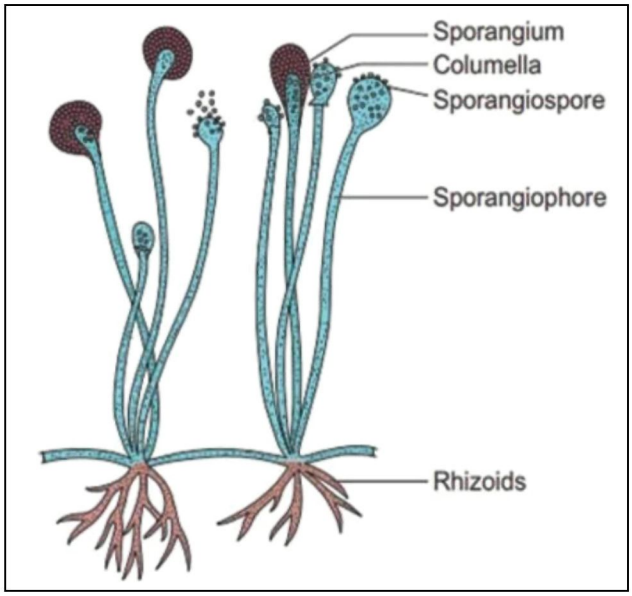

Figure 2.15 The Morphology Of *Rhizopus Oryzae*

Figure 2.16 presents microscopic observations of *Rhizopus sp.* cultures. The *Rhizopus arrhizus*, *Rhizopus delemar*, *Rhizopus microsporus*, and *Rhizopus stolonifer* were observed using 10× to 40× objective lenses on an Olympus BH-2

microscope (Gryganskyi et al., 2018). Gryganskyi et al. (2018) examined the micromorphological characteristics of sporangia, sporangiospores, and sporangiophores, along with the presence or absence of zygospores, rhizoids, and stolons. These morphological characteristics were utilised to identify the targeted strain in this study.

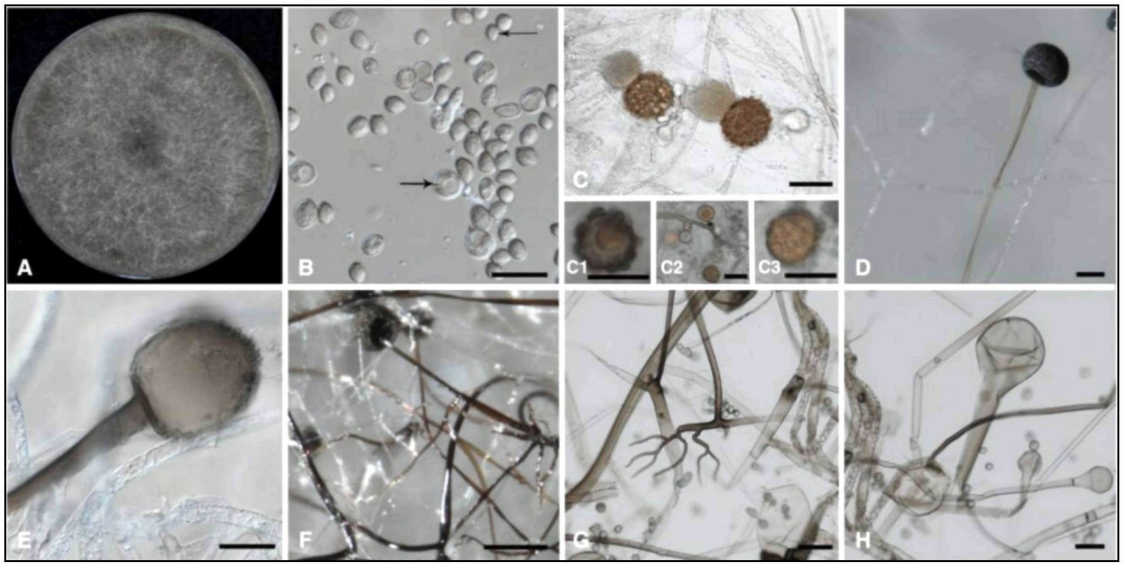

Figure 2.16 The Morphological Characteristics Of *Rhizopus sp* (a) Colony Observed On Malt Extract Agar (MEA) Following Three Days Of Cultivation At 30°C. (b) Intact And Germinating Sporangiospores Are Presented, With Arrows Denoting Spores Of Varying Sizes (Scale Bar = 10 Mm). (c) Zygospores Exhibiting Unequal Suspensors (Scale Bar = 10 Mm). (d) *S*porangiospore Release And Columella (Scale Bar = 10 Mm). (f) Sporangiophore, Rhizoids, And Pigmented Hyphae Of *Rhizopus Oryzae* (Scale Bar = 10 Mm). (g) Stolons (Scale Bar = 50 Mm). (h) Empty Sporangiophore (Scale Bar = 50 Mm)

Source: Gryganskyi et al. (2018)

Phylogenetic analysis indicates that the *Rhizopus* genus includes multiple species, such as *Rhizopus oryzae*, *Rhizopus microsporus*, *Rhizopus stolonifer*, *Rhizopus delemar*, and *Rhizopus arrhizus*. Specifically, *Rhizopus microsporus* represents the basal lineage (Gryganskyi et al., 2018). Among these species, *Rhizopus oryzae* and *Rhizopus microsporus* hold notable medical and biotechnological importance owing to their rapid growth, environmental resilience, and ability to produce synthesise compounds (biosurfactants) (Lennartsson et al., 2014). The *Rhizopus* genus also presents beneficial applications and notable drawbacks concerning food spoilage. One significant example is the considerable economic losses during the storage and

transportation of crops owing to *Rhizopus* spp. soft rot caused by *Rhizopus stolonifera*. Considering that this species exhibits significant thermal stability and retain activity after 40 minutes at 100°C, preventive treatments can be resisted by it.

Numerous studies have primarily explored *Rhizopus* spp.-based biosurfactants for their biodegradability, low toxicity, and effectiveness under extreme conditions. Compared to synthetic surfactants, several sectors have benefited from the employment of fungi-based biosurfactants as viable alternatives. These industries include bioremediation, wastewater treatment, pharmaceuticals, and agriculture. The strong cell wall structures and effective substrate conversion mechanisms of *Rhizopus* spp. fungi also produce greater amounts of biosurfactants than bacteria (Bhardwaj, 2013). Generally, *Rhizopus sp.*-based biosurfactants are categorised as secondary metabolites. In this biosurfactant type, the material is not directly associated with essential life-sustaining processes (growth or reproduction) and is generated during the stationary growth phase.

Under conditions requiring fungal adaptation to harsh surroundings or competition for limited resources, environmental stress or nutrient limitations cause this synthesis of biosurfactants. Therefore, the accessibility of hydrophobic nutrients is increased by *Rhizopus sp.*-based biosurfactants. This process involves emulsification, facilitating surface attachment or detachment, and offering a protective strategy against competing microorganisms (Pele et al., 2019). Consequently, *Rhizopus sp.*-based biosurfactants are useful for environmental remediation and industrial applications, given that they can flourish in varied and occasionally contaminated settings. The literature analysis conducted in this study presented few studies regarding *Rhizopus* spp. (see Table 2.16). Nonetheless, inadequate studies concerning phospholipid-based biosurfactant production by *Rhizopus sp.* have been observed. Research on mild steel corrosion for RC applications has also not been addressed using *Rhizopus*-derived biosurfactants.

Table 2.16
Production Of Secondary Metabolites By *Rhizopus Sp.*

Microorganism	BS. type	Substrates	Culture Type & Conditions	Characteristics of Biosurfactants	Reference
Rhizopus arrhizus	*Glycolipid*	Crude glycerol, Rice bran husks and corn steep liquor	Submerged fermentation	Surface tension reduced to 26.5 mN/m; E24 (palm oil) = 63.8%; biomass = 9.10 g/L	Freitas et al., 2012
Rhizopus arrhizus	*Glycoprotein*	Crude glycerol	submerged fermentation	Yield 1.74 g/L, Surface tension reduced to 28.8 mN/m, EI_{24} = 79.4 and 66.4 cm2 of oil displacement area	Pele et al., 2019
Rhizopus arrhizus	*Glycoprotein*	Soybean post-frying oil/sodium glutamate	submerged fermentation	Surface tension reduced to 38 mN/m, and 66.4 cm2 of oil displacement area	Pele et al., 2018
Rhizopus oryzae	*Glycolipid*	Sunflower oil cake and pineapple waste mixture	Solid state fermentation	Corrosion inhibitor in carbon steel	Kashef et al., 2018
Rhizopus nigricans	*Heteropolymer*	Deproteinised Juice, Soyabean and cauliflower	Submerged aerated fermentation	Bioemulsifier	Aulwar et al., 2016
Rhizopus oryzae	Not mentioned	Waste frying oil (WFO) and MSM	Submerged batch fermentation	Surface tension reduced from 72 to 31 mN/m; E_{24} (kerosene) = 55%; biosurfactant yield = 3.8 g/L	Ahmad et al., 2020
Rhizopus oryzae	Not mentioned	Soybean oil refinery waste	Submerged fermentation	E_{24} > 60%	Santos et al., 2019
Rhizopus sp.	Not mentioned	Palm oil mill effluent (POME)	Semi-solid fermentation	Demonstrated effective biosurfactant activity; details on yield and composition not fully reported	Ibrahim et al., 2021
Rhizopus sp.	Not mentioned	Potato Dextrose Broth	Submerged aerated fermentation	Inhibiting the bacterial growth of Klebsiella, Pseudomonas, Salmonella and Shigella	Farooq et al., 2023

2.9 Phospholipids -Based Biosurfactants

Phospholipids are amphiphilic molecules comprising a hydrophilic phosphate-containing head group and one or more hydrophobic fatty acid tails. Their amphipathic structure allows them to self-assemble into bilayers, micelles, and vesicles, enabling broad biological and industrial applications, including their use as biosurfactants. Beyond their natural role in stabilising cell membranes, phospholipid-based biosurfactants exhibit physicochemical characteristics that are highly relevant to corrosion mitigation. The corrosion inhibition mechanism of phospholipid biosurfactants arises from their ability to adsorb onto metal surfaces and form protective molecular films.

Adsorption of phospholipid molecules onto steel can occur via chemisorption or physisorption, depending on the functional groups and environmental conditions. Chemisorption typically enhances inhibition efficiency, as the phosphate groups form stable complexes with iron oxides or hydroxides within the passive film. This process improves film integrity and reduces the susceptibility of the metal surface to localized attack, such as pitting corrosion in chloride-rich environments. The hydrophobic orientation of the fatty acid chains further reduces surface wettability, limiting ionic transport across the metal–solution interface.

In cementitious systems, phospholipid biosurfactants may additionally influence the iron–concrete interface by modifying pore solution chemistry and improving the microstructural density around reinforcement. Their dual role as both surface-active molecules and potential hydration modifiers suggests that they can reduce moisture ingress while enhancing adhesion between cement hydrates and the steel surface. This multifunctionality positions phospholipid-based biosurfactants as promising eco-friendly corrosion inhibitors for reinforced concrete, particularly in environments where chloride ingress or carbonation presents significant durability challenges.

2.9.1 Classification of Phospholipids

The lipids in biological systems are classified into two categories: (ii) membrane and (ii) storage lipids. Even though cellular structure, function, and metabolism

necessitate both these lipids, the primary functions and locations within the cell are different. Further details on both these lipids are as follows:

1. Storage Lipid - Energy storage mainly involves the storage of lipids. This lipid type is accumulated in specialised organelles [adipocytes (fat cells)] or within adipose tissue. Storage lipids are also suitable for energy storage in a compact and efficient manner based on their high hydrophobicity and water insolubility. This lipid type can be further categorised into two groups as follows:

    i. Triglycerides (Triacylglycerols): A glycerol backbone that is esterified with three fatty acid chains is denoted as triglycerides (triacylglycerols). This compound is stored in lipid droplets within adipocytes, functioning as the primary energy storage in animals and plants.
    ii. The esters formed by long-chain fatty acids and long-chain alcohols or other hydrophobic are known as waxes. Various organisms require this compound for waterproofing and protective functions in the cuticles of plants, the exoskeletons of insects, and the skin of mammals.

2. Membrane Lipids - A diverse category that serves as the diverse group that forms the structural components of cell membranes and intracellular membranes is membrane lipids. The integrity, fluidity, and functionality of cellular membranes need these lipids to preserve their operations. Generally, the formation of bilayers in aqueous environments is enabled by the hydrophilic (water-attracting) and hydrophobic (water-repelling) regions observed in these amphipathic membrane lipids. Numerous functions are controlled by these lipids, including regulating the transport of substances across cell membranes, facilitating signal transduction, and supporting diverse membrane-related functions. These lipids can be further classified into three categories as follows:

    i. The predominant class of membrane lipids is phospholipids, constituting the fundamental architecture of the lipid bilayer. This lipid type demonstrates two fatty acid chains and a polar head group on the glycerol backbone and phosphate group, respectively.

ii. Glycolipids are lipids that include carbohydrate moieties alongside lipid components. In the outer leaflet of the plasma membrane, this lipid type is prevalent and is essential for cell recognition and communication.
iii. A non-conventional lipid that is pivotal for maintaining membrane stability and fluidity is cholesterol. The phospholipid bilayer contains this lipid type, which is correlated with its flexibility and permeability.

Phospholipids are usually distinguished by a phosphate head group and a glycerol backbone. These lipids are classified into three primary types according to their structural components as follows:

i. A lipid type presenting two fatty acid chains and a polar head group attached to the glycerol backbone and phosphate group, respectively, is known as glycerophospholipids (or phosphoglycerides). Most membrane phospholipids exhibit this structure, which is essential for the formation of lipid bilayers.
ii. Sphingolipids possess a sphingosine backbone, a single fatty acid chain attached linked to this backbone, and a polar head group. In the outer leaflet, membrane architecture and signalling processes are substantially influenced by these lipids as crucial constituents of the plasma membrane.
iii. Sphingophospholipids possess a structure akin to sphingolipids and are a subclass of sphingolipids. These lipids are distinguished by the presence of a phosphate group in their head group.

Overall, cellular integrity and complex biological processes (signal transduction and membrane trafficking are supported by structural lipids. These lipids aid in preserving membrane stability, flexibility, and functionality. Figure 2.17 illustrates the relationship between these lipid classes.

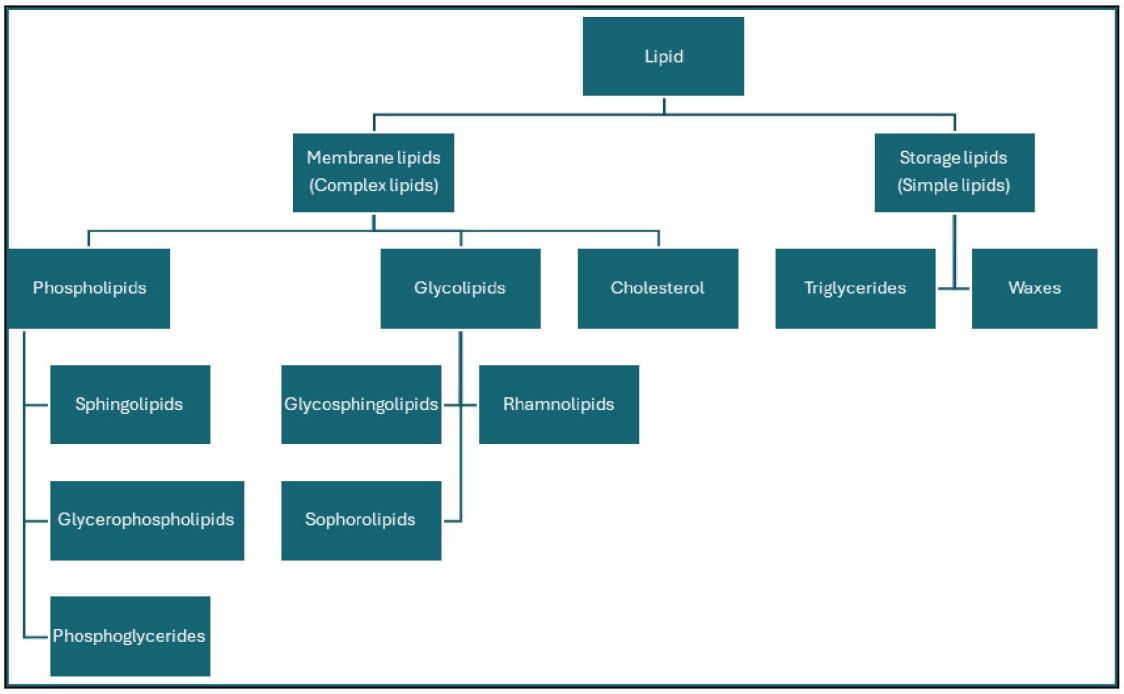

Figure 2.17 The Lipid Family Tree

2.9.2 Amphiphilic Properties and Self-Assembly

The shape and amphipathic nature of the lipid molecules cause them to form bilayers spontaneously in aqueous environments. For the above reason, lipid molecules spontaneously aggregate to bury their hydrophobic tails in the interior and expose their hydrophilic heads to water. Depending on their shape, they can do this in either of two ways: they can form spherical micelles, with the tails inward, or they can form bimolecular sheets, or bilayers, with the hydrophobic tails sandwiched between the hydrophilic head groups. Wedge-shaped lipid molecules form micelles, whereas cylinder-shaped phospholipid molecules form bilayers. The structure and amphipathic characteristics of lipid molecules lead to the spontaneous formation of bilayers in aqueous environments. Lipid molecules spontaneously aggregate to conceal their hydrophobic tails within the interior while exposing their hydrophilic heads to water. Depending on the shape, lipid molecules can achieve this process in two ways: (i) spherical micelles (tails orientated inward) and (ii) bimolecular sheets or bilayers (hydrophobic tails are positioned between the hydrophilic head groups. Lipid molecules with a wedge shape aggregate to form micelles. In contrast, phospholipid molecules with a cylindrical shape assemble into bilayers, and the inverted conical lipids aggregate into hexagonal tubes (Figure 2.18)

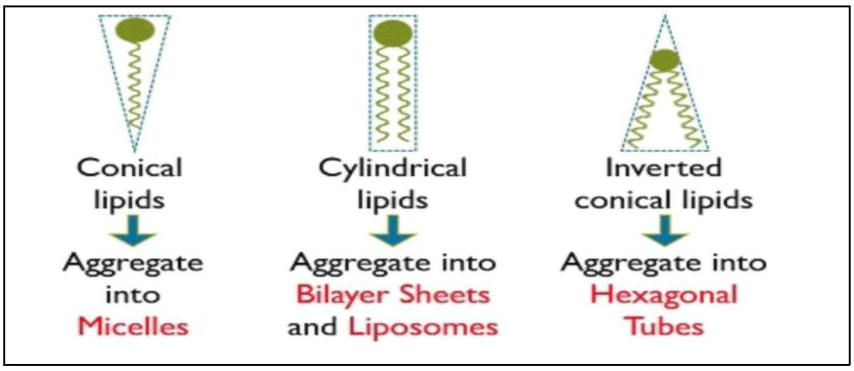

Figure 2.18 The Lipids Aggregates Based On Their Shapes

The structure of phospholipids biosurfactants also typically comprises a glycerol backbone, fatty acid moieties, and a phosphoric acid group. This configuration imparts surface activity due to the non-polar nature of the fatty acid tails and the polar nature of the phosphate head groups (see Figure 2.19). The amphiphilic properties of biosurfactants enable the groups to demonstrate interfacial activity at the boundaries between different phases, promoting emulsification, dispersion, and a reduction of surface tension across various systems.

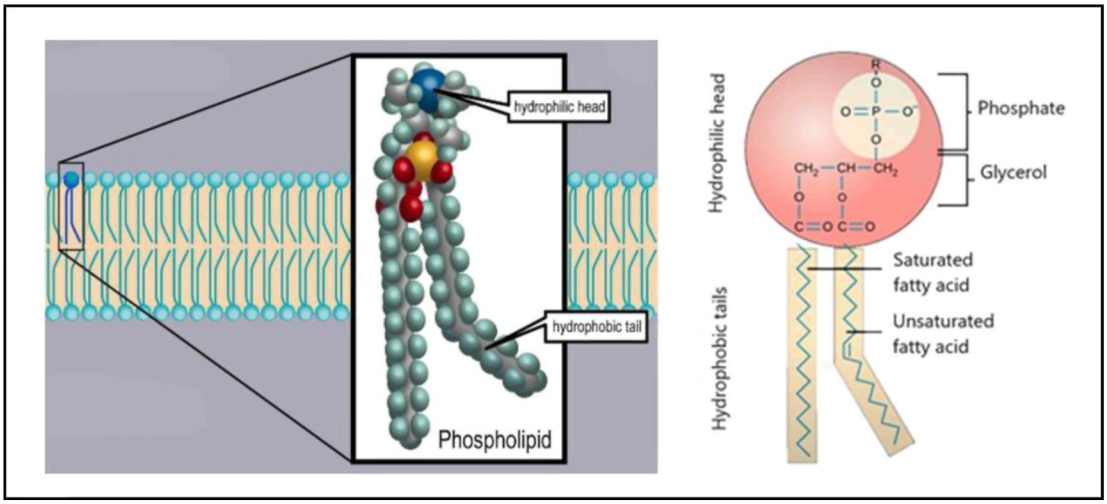

Figure 2.19 The Amphiphilic Molecules Of Phospholipids With Hydrophilic Heads And Hydrophobic Tails Of A Phospholipid Molecule

Phospholipid molecules, due to their cylindrical shape, can spontaneously assemble into bilayers in aqueous environments. In the bilayer configuration, phospholipids are arranged such that the hydrophilic heads are oriented towards the aqueous environments on both sides. On the contrary, the hydrophobic tails are directed inward towards the membrane. This phenomenon enables the establishment of a barrier

that delineates the cell from its environment. This phenomenon facilitating the formation of a barrier that separates the cell from its surroundings as depicted in Figure 2.20.

The amphipathic nature also facilitates the formation of the lipid bilayer and liposome, with hydrophilic head groups orientated towards the extracellular and intracellular environments. Alternatively, the hydrophobic tails are sequestered within the membrane interior. This configuration establishes a selective barrier that regulates the movement of substances into and out of the cell. Furthermore, spherical bilayers that encapsulate an aqueous compartment are referred to as vesicles or liposomes.

Phospholipids subjected to heat in an aqueous environment spontaneously aggregate into small spherical structures (micelles or liposomes). The architecture of liposomes also provides distinct benefits for multiple applications, such as drug delivery, gene therapy, and cosmetics. Hence, the ability of liposomes to encapsulate hydrophilic compounds in the aqueous core and hydrophobic compounds in the lipid bilayer renders them effective carriers for the targeted delivery of therapeutic agents within the body.

Various physicochemical factors cause the dynamic structural organisation of phospholipids regarding their capacity to exist in bilayer or micellar forms. Therefore, the factors requiring consideration include temperature, fatty acid chain saturation degree, head group chemical nature, pH, water content, and divalent cation presence. Despite the precise transition point that differs across various classes of phospholipids, an increase in temperature generally facilitates a transition from the bilayer to the micellar phase. A stable lamellar structure is also observed across a broad temperature range (0–100°C) for saturated phospholipids, which is largely unaffected by pH or cation concentration. Thus, optimising the application of biosurfactants in industrial contexts necessitates this phase behaviour that is influenced by environmental conditions and molecular composition (Li et al., 2015).

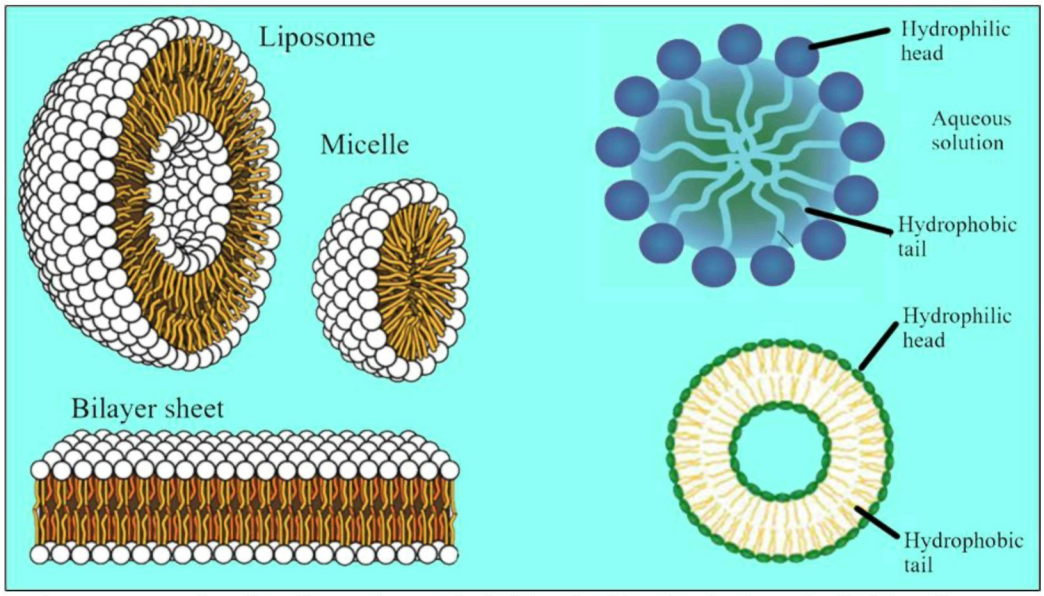

Figure 2.20 The Configuration Of Lipid Micelles And Phospholipids Bilayers Molecule

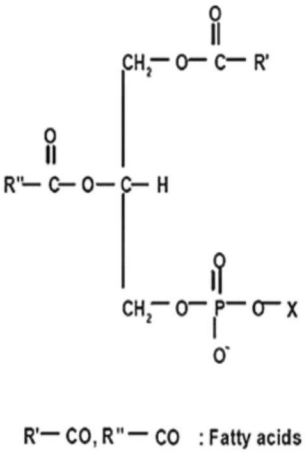

X = Phospholipid

Components of X = Phospholipid	
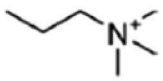 Phosphatidycholine	 Phosphatidic acid
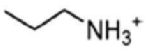 Phosphatidylethanolamine	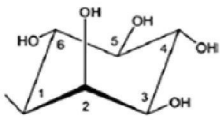 Phosphatidylinositol
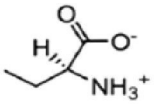 Phosphatidylserine	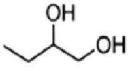 Phosphatidyglyserol

Figure 2.21 The Molecular Structure Of Phospholipid

Source: Adopted from Li et al. (2015)

2.9.3 Sources and Composition of Phospholipids

Phospholipids occur naturally in various biological systems and are commonly classified into phosphatidylcholine (PC), phosphatidylethanolamine (PE), phosphatidylinositol (PI), phosphatidic acid (PA), phosphatidylserine (PS), and phosphatidylglycerol (PG). Their molecular structures differ in head-group chemistry and fatty acid composition, which influence their surface activity and adsorption behaviour.

Although phospholipids can be derived from animal and plant sources, the significance for this study lies not in their nutritional role but in how variations in fatty acid chain length and saturation affect their performance as corrosion inhibitors. For example, oilseed-derived phospholipids are typically rich in palmitic, stearic, oleic, linoleic, and linolenic acids, contributing to stronger hydrophobic interactions and improved film-forming ability on steel surfaces. Conversely, phospholipids from animal-derived sources often contain long-chain polyunsaturated fatty acids, which may alter molecular packing density within the adsorbed layer.

Understanding these compositional differences is important because the hydrophilic head group controls the anchoring mechanism to metal surfaces, while the hydrophobic tails determine the compactness and protective quality of the resulting barrier film. Therefore, the variation in phospholipid profiles across biological sources provides insight into their potential effectiveness as corrosion-inhibiting biosurfactants, particularly in environments susceptible to chloride ingress or moisture exposure.

2.9.4 Functional Properties and Applications of Phospholipids

Phospholipids possess amphiphilic structures that confer strong surface-active behaviour, enabling adsorption at interfaces and reduction of surface and interfacial tension. These characteristics are directly relevant to corrosion inhibition, as the polar head groups interact with metallic surfaces while the hydrophobic tails orient away from the substrate to form a compact protective film. This adsorbed layer restricts the penetration of water, oxygen, and chloride ions, thereby decreasing both anodic dissolution and cathodic reduction reactions (Chen et al., 2017).

The ability of phospholipids to form stable lamellar structures and ordered molecular arrangements enhances barrier integrity on steel surfaces. Their antioxidative

tendencies also contribute to corrosion protection by limiting oxidative processes at the metal–electrolyte interface. Collectively, these functional properties position phospholipid-based biosurfactants as promising eco-friendly corrosion inhibitors, particularly in reinforced concrete systems where surface passivation and reduced ionic transport are critical for long-term durability.

2.9.5 Application of Phospholipids in Corrosion Inhibition

The drug delivery and membrane biology sectors have commonly utilised phospholipids due to their popularity. Nevertheless, limited studies on phospholipid-based corrosion inhibitors have been observed (Lesik et al., 2021). Considering that protective layers are formed by these compounds through interaction with metal surfaces (amphiphilic nature) to decrease corrosion rate, they should be explored. The molecular structure of these compounds is effective in inhibiting corrosion that is contingent upon specific conditions, presenting several benefits. These advantages include adsorption onto metal surfaces and the formation of self-assembled monolayers (SAMs) or barrier layers. Therefore, the following subsections explain the corrosion inhibition mechanisms of various biologically derived phospholipids, assess their effectiveness, and consider the influence of environmental factors on their performance.

2.9.5.1 Mechanisms of Phospholipid-Based Corrosion Inhibition

Corrosion mitigation can be performed via several mechanisms for phospholipids. These processes are chemisorption, barrier formation, and physisorption. Conversely, the molecular structure of the phospholipid and the metal surface with which it interacts can significantly impact these mechanisms. Further explanations of these mechanisms are delineated as follows:

i) Chemical adsorption - The establishment of robust chemical bonds between phospholipids and the metal surface is observed in chemical adsorption. Consequently, SAMs are established. Al-Badran and Mechler (2019) discovered stable SAM that exhibited corrosion resistance in an acetic acid (CH_3COOH) environment. The study chemically bonded di-myristoyl phosphatidic acid

(DMPA) to Fe surfaces. Additional metal oxidation and deterioration were then inhibited by the densely arranged monolayer serving as a protective barrier.

ii) Barrier Formation - Barrier formation is a corrosion inhibition mechanism commonly exhibited by many organic inhibitors; however, the effectiveness of this protective layer is strongly governed by molecular packing density and hydrophobic chain alignment. Conventional organic inhibitors such as plant extracts and amino acid–based compounds often generate discontinuous or loosely packed films, which permit the gradual penetration of aggressive species, particularly chloride ions (Cl^-), toward the metal surface (Al-Amier et al., 2024). This limitation compromises long-term protection, especially under chloride-rich environments. In contrast, phospholipids possess long hydrophobic hydrocarbon chains coupled with polar phosphate-based head groups, enabling the formation of highly ordered bilayer or multilayer structures on metal surfaces. These structured assemblies act as compact diffusion barriers, significantly restricting the transport of corrosive ions and moisture. Nascimento et al. (2024) demonstrated that a phospholipid coating based on 1-palmitoyl-2-oleoyl-sn-glycero-3-phosphoethanolamine (POPE) induced a positive shift in the electrochemical potential of Ti-6Al-4V alloy toward a more passive state, indicating enhanced corrosion resistance. This electrochemical stabilisation was attributed to the formation of a uniform shield-like coating that outperformed conventional organic coatings while simultaneously maintaining biological compatibility. Similarly, Lesik et al. (2021) reported that phospholipid-based inhibitors hindered the adhesion of wax crystals and prevented the development of tightly bound deposit layers on metal surfaces. The formation of a continuous hydrophilic protective film was observed, further supporting the superior barrier-forming capability of phospholipids compared with many low-molecular-weight organic inhibitors. Collectively, these findings highlight the enhanced barrier integrity and durability offered by phospholipid-based corrosion inhibitors.

2.9.5.2 Phospholipids and Metal Substrates

A significant correlation is observed between the effectiveness of phospholipids as corrosion inhibitors varies and the metal substrate, with distinct phospholipid types

providing differing degrees of protection across various metals. These metals were explained in previous studies as follows:

i) Carbon Steel: Lesik et al. (2021) tested phospholipids derived from vegetable oil waste on carbon steel in a hydrochloric acid solution. These phospholipids offered up to 86.5% protection individually, and up to 95% protection when combined with a cationic surfactant, highlighting their potential as corrosion inhibitors in aggressive environments.

ii) Ti-6Al-4V Alloy: Nascimento et al. (2024) denoted that the electrochemical stability of the Ti-6Al-4V alloy was enhanced by the phospholipid layer based on POPE. This process increased the biocompatibility of the material and inhibited the growth of bacterial cells, reducing CRs. Hence, phospholipid selection for specific metal substrates remained a critical aspect of optimal performance.

iii) Copper: Research by Sukul et al. (2018) demonstrated a thin layer of Phosphatidylcholine extracted from egg yolk, exhibits high corrosion inhibition efficiency when applied as a coating on copper in aqueous HCL.

Overall, phospholipid-based biosurfactants provide an effective and eco-friendly method for reducing metal corrosion by establishing protective layers via several mechanisms (chemisorption, physisorption, and barrier formation). Research has indicated that biologically derived phospholipids exhibit considerable potential as corrosion inhibitors for different metals. Nonetheless, the application of phospholipid-based biosurfactants on mild steel for RC has not been investigated. Therefore, additional research is necessary to examine the efficacy of phospholipid-based biosurfactants as corrosion inhibitors for mild steel in these environments.

2.10 Biocorrosion

The MIC (or biocorrosion) refers to the accelerated degradation of metals due to microorganisms on a metal surface. This interaction alters the rates and types of the electrochemical reactions involved in the corrosion processes (Beech & Sunner, 2004).

Typically, microorganisms on metal surfaces cause localised alterations in the concentration of certain electrolyte constituents, pH, and O_2 levels. Passive metals may experience localised corrosion, manifesting as pitting or crevice corrosion (Mansfeld & Little, 1991). These microbes generate detrimental substances that disrupt the standard electrochemical reactions associated with corrosion, such as organic acids, sulphides, and ammonia. Consequently, the by-products can modify local pH, O_2 levels, and electrolyte composition. This process frequently results in localised corrosion phenomena (pitting or crevice corrosion) in passive metals (Rao & Mulky, 2023).

Certain microbes are recognised for their ability to produce biofilm as a means of surface protection. Hence, uniformity, homogeneity, and non-porosity are essential characteristics for adequate biofilm protection. Despite this protective biofilm, which can be simulated in settings to suggest protection for metals, achieving this condition in real-world natural and industrial waters is challenging due to numerous variables (microorganisms present, substrate, water temperature, pH, flow rate, and dissolved O_2). Some studies indicated that biofilm formation may protect metals from corrosion by creating a barrier that limits contact between the metal surface and corrosive agents in the environment (Jayaraman et al., 1997; Zuo, 2007). Nonetheless, subsequent findings demonstrate that certain bacterial species can promote MIC instead of preventing it (A. Hisham, 2015). The MIC is primarily associated with pitting corrosion, which occurs when bacteria consistently colonise particular regions. This phenomenon of microbial corrosion was first identified in 1891, with early studies by Garrett and Zobell in 1941, emphasising the involvement of microorganisms and biofilms in the degradation of metals. Multiple factors are then denoted to contribute to MIC as follows:

i) Formation of O_2 and Fe concentration cells
ii) Fe and manganese (Mn)-oxidising bacteria activities
iii) Microbial synthesis of acids
iv) Conditions that are anaerobic and conducive to the activity of sulphate-reducing bacteria (SRB)

Environmental exposure to water, dust, and pollutants can result in the introduction of microbes onto surfaces, which can lead to corrosion. Generally,

corrosion processes involve mechanisms such as the formation of corrosive by-products, hydrogen embrittlement, metal ion deposition, and breakdown of protective inhibitors. Microbes also influence the metal-biofilm interface, either accelerating or decelerating corrosion based on the specific microbial strain involved. This MIC typically arises from intricate interactions among chemical, physical, mechanical, and biological factors. Moreover, the progression and intensity of MIC are affected by various interconnected parameters, such as temperature, pH, dissolved O2, sulphate levels, water composition, fluid dynamics, and operational maintenance practices. Bacteria are also significant among microorganisms due to their small size, high surface-to-volume ratio and rapid metabolic activity.

Little and Ray (2002) noted that the majority of research on biofilms for corrosion prevention was performed in controlled laboratory settings. Conversely, exposure of these biofilms to natural water environments frequently resulted in inadequate protection of the metal surfaces. Hence, a fundamental assumption in these studies was that biofilm formation could be anticipated and regulated. Lewandowski and Beyenal (2004) contested this assumption, as biofilms derived from pure microbial cultures in laboratory conditions exhibited structural variability over time, rendering them inconsistent and unreliable as protective barriers.

While biosurfactants are increasingly recognised for their environmentally benign corrosion inhibition potential, their application must be carefully evaluated to avoid unintentionally promoting microbiologically influenced corrosion (MIC). Therefore, comprehensive assessment incorporating both electrochemical and microbiological analyses is essential to confirm that biosurfactant-based systems inhibit corrosion without increasing MIC susceptibility.

2.10.1 Biosurfactant in Biocorrosion Mitigation

Microorganisms in specific scenarios can inhibit corrosion instead of promoting it through processes referred to as microbially influenced corrosion inhibition (MICI). These mechanisms are as follows:

i) Inhibition of Corrosive Microbes: Through the production of antimicrobial compounds that suppress corrosion-inducing strains.

ii) Consumption of Corrosive Agents: Aerobic microbes may consume oxygen, reducing the availability of this corrosive element at the metal surface.
iii) Formation of Protective Barriers: Excess production of extracellular polymeric substances can promote the development of a physical barrier that limits metal exposure.
iv) Multispecies Synergy: In complex biofilms, multiple microbial species may work synergistically to inhibit corrosion through a combination of the above mechanisms.

The MICI approaches also encompass the application of corrosion inhibitors, which may be classified as chemical or biological in nature. These inhibitors function by reacting with corrosive agents to render the environment less aggressive, forming adherent protective films on metal surfaces and acting as biocides, rapidly eliminating bacteria upon contact.

Corrosion inhibitors derived from plants contain various compounds (tannins, cellulose, and polycyclic structures), which demonstrate potential for improving film formation on metals. These natural extracts may fulfil dual roles: (i) chemical inhibition with biofilm disruption and (ii) preserving environmentally friendly characteristics. Biofilms also frequently pose difficulties for traditional antimicrobial agents due to their intricate structure and inherent resistance. Nevertheless, biofilms can facilitate the precipitation of protective compounds such as zinc hydroxide. This process inhibits specific forms of corrosion by creating stable passive layers on the metal surface, such as dezincification (Rao & Mulky, 2023). Furthermore, effective MICI application necessitates the selection of appropriate suitable biocides or microbial inhibitors based on efficacy across diverse microbes, biofilm penetration capability, environmental compatibility, biodegradability, safety, longevity, and cost-effectiveness (Deepalaxmi & Gayathri, 2018)

2.11 Corrosion Monitoring Techniques

Corrosion assessment in RC structures is crucial for evaluating structural durability and planning maintenance strategies. Numerous experimental techniques and methods have been utilised to examine corrosion activity, measure degradation, and analyse the interaction between steel and the surrounding concrete matrix. The

following subsections explore four primary methods employed for the corrosion monitoring of mild steel reinforcements. For biosurfactant-based corrosion inhibition studies, electrochemical impedance spectroscopy (EIS) is regarded as the most reliable and informative technique. EIS enables non-destructive, time-dependent evaluation of inhibitor performance by distinguishing charge transfer resistance, film resistance, and capacitive behaviour at the steel–concrete interface. This capability is particularly critical for biosurfactants, whose inhibition mechanism is strongly governed by adsorption stability, interfacial film formation, and long-term barrier integrity (Herrera Hernández et al., 2020).

2.11.1 Electrochemical Impedance Spectroscopy (EIS)

The EIS is a non-destructive and highly sensitive method utilised to investigate the corrosion behaviour of mild steel bars. This tool quantifies the impedance of a system over various frequencies, providing data concerning the electrochemical processes at the steel-concrete interface. Song and Saraswathy (2007) mentioned that the steel CR was significantly correlated with polarisation resistance and concrete resistivity. These variables could be measured through EIS. Different corrosion mechanisms can also be presented using this tool based on the equivalent circuit modelling of the impedance data. Additionally, the relationship between various environmental conditions (chloride ingress and carbonation) and corrosion monitoring could be understood using this tool (Poursaee & Hansson, 2007). In contrast, several constraints are observed that can impede field applicability, including ambient condition sensitivity (moisture and temperature) and data interpretation complexity.

2.11.2 Electrical Resistivity Testing

The corrosion condition of bare mild steel reinforcing bars before their application in concrete structures can be analysed using ER testing. This test serves as a practical, non-destructive method for obtaining relevant data. Typically, corrosion products (Fe_2O_3 and FeH_2O_2) exhibit low electrical conductivity. The amount of these products can increase when corrosion progresses. Thus, the ER of the metal surface becomes higher, indicating that an indirect measure of corrosion severity can be computed using resistivity values. Numerous studies have also noted a strong

correlation between resistivity measurements and the degree of corrosion when the steel is exposed to aggressive environments (chloride or acidic conditions). One notable example is steel bars exposed to salt spray or immersed in corrosive solutions, demonstrating increasing higher resistivity values over time. This outcome corresponds to the development of thicker corrosion layers. Consequently, this approach provides an efficient and straightforward strategy for assessing steel quality in both field and laboratory environments without causing damage to the specimens.

The ER readings are influenced by external variables, which may distort the results. These variables include surface moisture, ambient temperature, and surface contaminants. Hence, standardised test conditions and appropriate surface preparation are vital for acquiring reliable data. Although this technique lacks detailed information regarding the type or morphology of corrosion products, it serves as a valuable diagnostic tool. This approach can also be effectively integrated with complementary strategies to achieve a thorough corrosion assessment, such as visual inspection, gravimetric analysis, or SEM.

2.11.3 Weight Loss Measurement

The degree of corrosion in mild steel bars over a specified exposure duration is quantified using a direct technique utilised in laboratory settings known as the weight loss method. This technique determines the CR by the removal of corrosion products from the rebar and the measurement of its mass loss. Hence, the evaluation of protective coatings or inhibitors is facilitated through this gravimetric method for accelerated corrosion testing (Goyal et al., 2015). Nonetheless, this direct and quantitative approach does not adequately address localised corrosion phenomena (pitting or crevice corrosion). These issues can only be resolved if microscopic or surface characterisation techniques are complemented.

2.11.4 SEM-EDX for Surface Morphology and Elemental Analysis

An effective analytical method for assessing the surface morphology and elemental composition of corroded mild steel reinforcement and the adjacent concrete involves the SEM-EDX tool. High-resolution imaging of surface characteristics is presented through SEM, including cracks, voids, and corrosion products. On the

contrary, elemental analysis for the identification of significant elements (Cl, S, and Fe_2O_3) is conducted using EDX (Andrade & Alonso, 2004). Therefore, the corrosion mechanisms, protective treatments, and environmental exposure effects can be classified using this tool, specifically for post-exposure or forensic analysis.

However, despite its strong diagnostic capability, SEM–EDX is not a stand-alone corrosion monitoring technique. It is inherently destructive, provides post-exposure information, and does not capture time-dependent electrochemical processes or inhibitor adsorption dynamics. Consequently, SEM–EDX is most appropriately used to validate and support electrochemical findings, rather than to quantify corrosion rates or inhibition efficiency. This method can also fail to represent the overall condition of the rebar or concrete, which is attributed to the extensive sample preparation requirements, and only localised analysis can be utilised.

2.12 Strength and Durability Testing of Concrete

Numerous indicators necessitate data concerning the strength and durability of concrete. These indicators include structural reliability, service life, and sustainability. Currently, most studies and construction practices have evaluated the performance of concrete (fresh state and long-term behaviour) under service conditions based on a comprehensive testing regime. This process involves workability, mechanical strength, resistance, and environmental degradation tests. Furthermore, the three primary categories of testing are outlined as follows:

i) Slump flow and vertical slump tests (workability of fresh concrete)
ii) The f_c and f_s tests (mechanical properties of hardened concrete)
iii) The τ of rebars embedded in concrete (structural integrity and load transfer between concrete and reinforcement)

The evaluation of strength and durability parameters provides a direct and quantifiable means of assessing the influence of biosurfactant incorporation on concrete performance. In biosurfactant-modified concrete, mechanical tests such as compressive and flexural strength reflect changes in workability, particle dispersion, and cement hydration efficiency induced by the surface-active nature of biosurfactants. Concurrently, durability indicators including water absorption, permeability, and

resistivity offer insight into the ability of biosurfactants to refine pore structure, limit ingress of aggressive agents, and enhance the protective environment surrounding embedded steel reinforcement. Collectively, these tests enable a holistic assessment of whether biosurfactant modification improves concrete performance without compromising structural integrity, thereby establishing a critical link between fresh-state rheological behaviour, hardened-state mechanical properties, and long-term durability.

2.12.1 Slump Flow and Vertical Slump Tests for Fresh Concrete

High-performance and self-compacting concrete (SCC) formulations require understanding a vital characteristic known as workability. Hence, the consistency and flow characteristics of fresh concrete are frequently analysed using the slump and slump flow tests. Several information can be gathered from this process, including regarding the efficiency of concrete placement, compaction, and finishing processes. The vertical slump or subsidence of a concrete cone following the removal of the mould is also quantified by the standard slump test, which is detailed in MS 26-1-2:2009 [*Testing of Concrete - Part 1: Fresh Concrete - Section 2: Slump Test (Second Revision)*].

A rapid assessment of mix workability is provided by this test, in which lower or higher slump values suggest stiffer mixes or more fluid behaviour, respectively. Nevertheless, highly flowable concrete examinations demonstrate limitations using this test. One prominent example is self-consolidating concrete which may not indicate a significant vertical slump. To address these limitations, the slump flow test is used specifically for SCC and other high-flow mixtures. Consequently, the constraint is resolved using the slump flow test for SCC. The horizontal spread of concrete post-cone removal is often measured using this test as an indicator of its flowability. In addition, mix uniformity and segregation tendency are assessed in this test based on flow diameter and visual stability index (VSI).

The duration required for concrete to achieve a diameter of 50 cm or 500 mm within the slump flow test is represented by the T50 (or T500) slump flow metric. Given that the flowability and workability of the concrete are observed through this metric, it is pivotal for SCC. Thus, adequate filling and passing abilities through congested reinforcement without segregation or blockage can be ensured through this metric. A strong correlation was also demonstrated between the T50 value and rheological

properties of concrete (viscosity and yield stress). These properties are usually employed as a measure of SCC quality. Khayat et al. (2000) and EFNARC (2005) examined the performance of SCC using the slump flow test. Several critical data were then obtained, which was essential for gaining insights. These insights were associated with the filling ability, passing ability, and stability of SCC mixes during casting.

All of these elements are essential for reducing defects (voids, honeycombing, and uneven surface finish). Nonetheless, the slump flow results can still be impacted by environmental factors (ambient temperature and humidity and variations in mix design. This observation implies that standardised testing conditions must be maintained to ensure reliable and consistent outcomes.

2.12.2 Compressive Strength

The f_c test is considered the primary and most universally accepted measure of the quality of hardened concrete quality. This test serves as a key benchmark for structural design and quality assurance, providing a direct load-bearing capacity measurement of concrete under uniaxial compression. The test is typically conducted following MS EN 12390-4:2012 [*Testing Hardened Concrete - Part 4: Compressive Strength of Test Specimens (Second Revision)*]. This guideline standardises procedures for the f_c testing of hardened concrete specimens, ensuring consistency in specimen preparation, loading conditions, and failure evaluation. The f_c test also entails applying axial compressive loads to cylindrical or cubic concrete specimens until failure is achieved. A maximum load sustained is then utilised to determine the f_c (MPa). Neville (2011) established a significant correlation between f_c and the long-term durability and structural performance of concrete elements.

The f_c of concrete is affected by various material, environmental, and procedural factors as follows:

i) Proper curing conditions ensure sufficient moisture and temperature, which are critical for the ongoing hydration of cement and strength development. Otherwise, insufficient curing results in incomplete hydration and reduced strength.

ii) The w/c ratio is a crucial parameter in mix design. A lower w/c ratio generally results in enhanced f_c, which is attributed to decreased porosity and increased density of the hardened matrix.

iii) The size, shape, grading, and strength of aggregates significantly influence the packing density and load distribution in concrete, affecting its f_c.

iv) The composition of cement (blended cement or supplementary cementitious materials) influences the hydration rate and extent, thus affecting strength development over time.

v) Specimen size and shape significantly influence measured strength, with variations in dimensions (100 mm vs. 150 mm cubes) and geometry (cube vs. cylinder) affecting stress distribution and end restraint effects.

vi) The loading rate and machine calibration significantly affect the final test result, as both the speed of compressive load application and the precision of the testing equipment are critical factors. An accelerated or irregular loading rate can result in non-representative failures.

The f_c generally increases with age as a result of continued hydration processes. Standard tests are typically performed at 7, 14, or 28 days, with 28 days serving as the predominant benchmark. Table 2.11 presents the target f_c over time. The f_c test offers a reliable and quantifiable assessment regarding the capacity of a concrete mix to endure axial loads. Conversely, the test fails to account for other vital performance characteristics (R_m, f_s, or impact resistance), which are significant in structural applications. Hence, f_c must be evaluated alongside other mechanical tests and durability assessments to achieve a thorough understanding of concrete performance.

Table 2.17
Summary Of The Typical f_c Development Over Time

Age of Concrete	**Approximate % of 28-Day Target Strength**
7 days	65–70%
14 days	85–90%
28 days	100% (reference value)
100 days	110–120% (depending on mix and curing)

2.12.3 Flexural Strength

The capacity of concrete to withstand bending stresses can be analysed through the modulus of rupture (MR), which can be obtained from f_s testing (MS EN 12390-5: 2012). This test is pertinent for pavements, slabs, and beams. Thus, the stress in a material immediately prior to yielding in a flexure test is denoted as f_s. Other names for f_s are Modulus Rupture, bend strength, and fracture. Precisely controlled bending moments or loads are often applied to an RC beam specimen for the f_s test. This procedure is critical in structural design and evaluation for assessing the capacity of a beam to endure bending forces. The beam also generally consists of a rectangular concrete cross-section, which is reinforced with embedded steel bars. Therefore, the R_m and ductility of the beam are enhanced by these bars, which bolster the beam, reducing the natural weakness in the tension of concrete.

A progressively increasing load is applied at the midpoint of the beam in the f_s test. This process results in bending until fracture or yielding occurs. Considerable deformation or failure within the beam is then determined through the load level. The tensile and compression stresses also occur on the convex (bottom part) and concave sides (top part). Most materials experience tensile stress prior to experiencing compressive stress. Moreover, structural performance is systematically documented through the behavioural observations of the beam concerning deflection and cracking patterns. Numerous data can then be obtained through this examination, such as bending force resistance of the beam, stiffness, and capacity to distribute and bear loads effectively. Engineers utilise f_s test results to confirm adherence to design specifications and to guarantee the beam's safe and efficient application in diverse structural contexts. Neville (2011) proposed a general formula for estimating MR (f_s), aligning with ACI CODE-318-19(22): *Building Code Requirements for Structural Concrete and Commentary* and British Standard (BS) EN 1992-1-1 (Eurocode 2) standards as follows:

$$fs \approx \mathrm{k} \times \sqrt{f_c} \tag{2.4}$$

where k denotes empirical constant (typically ranging from 0.60 to 0.75 for normal weight concrete).

2.12.4 Pull-out Test

A crucial factor influencing the structural integrity and durability of RC elements is the τ between concrete and reinforcement. The overall performance of RC structures is affected by this factor, which governs load transfer, crack propagation, stress distribution, and corrosion resistance at the steel-concrete interface. Therefore, the τ between reinforcing steel and the adjacent concrete can be measured through the pull-out test. In this method, a steel bar is incorporated within a concrete specimen. This process is followed by the application of an axial tensile force until the bar experiences slippage or the surrounding concrete fails. The τ is also quantified by the maximum tensile load at failure divided by the embedded surface area of the bar. Improved adhesion between the concrete and reinforcement is presented in higher values, which is critical for structural stability.

A substantial relationship is observed between the reliability of the pull-out test and real-world construction conditions. This observation signifies that considerations must be placed on various elements, including concrete mix design (aggregate type, w/c ratio, and admixture content), curing regime, and specimen geometry (cover thickness, embedment length, and rebar diameter). Bond performance is also highly reliant on the surface condition of the rebar (smooth, deformed, epoxy-coated, or treated with corrosion inhibitors). Increased τ attributed to improved mechanical interlock is usually indicated in deformed bars (Shunmuga Vembu & Ammasi, 2023). Meanwhile, the guideline for executing pull-out tests is outlined as standardized procedures in ASTM A944 (*Standard Test Method for Comparing Bond Strength of Steel Reinforcing Bars to Concrete Using Beam-End Specimens*). These standards focus on measuring load-slip behaviour under escalating tensile loads, facilitating consistent comparisons of bond performance across various conditions and material combinations.

Substantial information concerning bond behaviour is observed from the load-displacement (or load-slip) curve produced during testing. The maximum τ is denoted as the peak load. On the contrary, the ductility and failure characteristics of the bond are illustrated by the descending branch. This response is also dependent on multiple parameters, including embedment length and loading rate. Higher or lower τ is observed from longer embedment (increased surface contact) or higher loading rates (dynamic effects). Likewise, the steel-concrete bond due to corrosion product formation or the

effectiveness of corrosion inhibitors can be examined using pull-out testing in corrosion research.

Almusallam et al. (1996) revealed that accumulation of expansive oxides at the interface during corrosion could produce smaller τ. The study noted that increased τ between the reinforcing bar and the surrounding concrete could be indicated in the early corrosion phase. This outcome was attributed to the produced mechanical pressure when expansive corrosion was formed. The process could improve the confinement of the bar and increase mechanical interlocking with the concrete. Enhanced friction and bond are also demonstrated when the surface of the bar is roughened by early corrosion. Nevertheless, the ongoing growth of corrosion products as corrosion advances beyond the initial phase results in cracking and deterioration of the adjacent concrete. Hence, τ between steel and concrete and confinement are negatively impacted by this deterioration, reduces confinement and weakens the τ between the steel and concrete. Figure 2.22 illustrates the relationship between corrosion level and the ultimate τ of reinforcement.

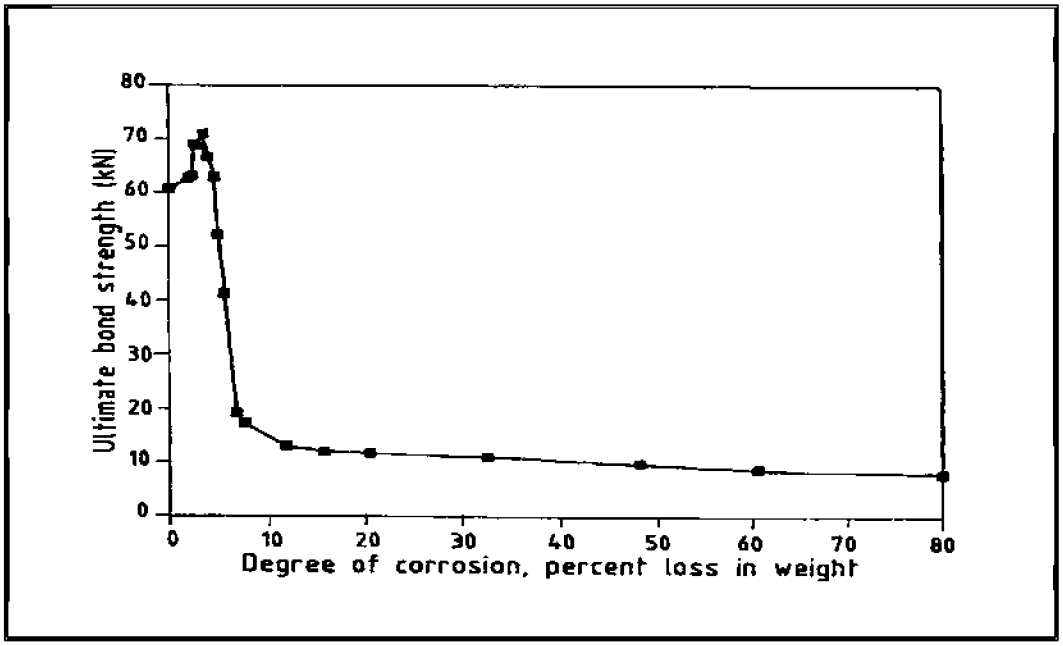

Figure 2.22 The Correlation Between Corrosion Level And Ultimate Bond Strength (τ) Of Reinforcement

Adapted from Ganjoo et al., (2023)

Numerous studies have examined the association between corrosion levels and τ in RC, yielding diverse outcomes influenced by corrosion intensity, specimen confinement, and testing methodologies. Cabrera and Ghoddoussi (2001) and Al-Sulaimani et al. (1990) noted that τ initially increased with corrosion up to approximately 1%. Nevertheless, the studies noticed a decline in τ as corrosion continued. Auyeung et al. confirmed this trend, observing that corrosion exceeding 1% corrosion resulted in a significant reduction in τ during axial tension pull-out tests. Almusallam et al. (1996) performed cantilever bond tests, employing open stirrups to mitigate shear failure. The outcomes were somewhat different, producing a 16% increase in τ at 4% weight loss. This finding was followed by a significant decline. At 8% corrosion (post-cracking stage), τ had decreased by nearly 30% relative to the uncorroded specimens. Although a certain degree of corrosion could initially enhance τ, continued corrosion resulted in a notable decline with the onset of cracking (Almusallam et al., 1996).

Fang et al. investigated the influence of confinement on τ through the examination of both confined and unconfined specimens. The findings indicated that confinement could significantly reduce bond loss at moderate corrosion levels (4–6% mass loss). Confined specimens, reinforced with stirrups, exhibited a mere 12% reduction in τ at 6% corrosion. In contrast, unconfined specimens demonstrated a considerably greater decline, with τ decreases between 30% and 65% at comparable corrosion levels. This observation highlighted the significance of structural confinement in preserving bond strength during corrosion. Williamson and Clark (2000) analysed various factors affecting τ, such as corrosion level, preload, cover depth, bar type, and specimen age. The study indicated that preloading exerted a negligible effect on τ, except in cases where deformed bars had a substantial concrete cover. Moreover, the extensive cracks at a 20% corrosion level, with a cover-to-diameter ratio of 2, indicated only a minor effect on τ compared to uncorroded specimens. This outcome suggested that additional factors, including concrete cover, could mitigate the adverse effects of corrosion on τ.

2.13 Concluding Remarks

This chapter has critically reviewed the fundamental concepts, mechanisms, and recent advances related to RC corrosion and the potential application of biosurfactants

as sustainable CI. The discussion on RC structures and corrosion mechanisms established the scientific basis for understanding steel degradation in alkaline and chloride-contaminated environments, thereby justifying the need for effective corrosion mitigation strategies tailored to RC systems. The review of conventional corrosion protection approaches, including coatings, admixtures, and organic inhibitors, highlighted their effectiveness as well as their inherent limitations, such as environmental toxicity, cost, and limited long-term performance. These limitations directly motivate the exploration of alternative, environmentally benign solutions, aligning with the overarching objective of this study.

The ability of Rhizopus-derived phospholipid biosurfactants to be produced from renewable waste substrates, together with their surface-active and adsorption properties, supports their potential application as green corrosion inhibitors. However, this chapter also highlights the need to evaluate these biosurfactants within a corrosion-specific framework, particularly with respect to inhibition efficiency, adsorption stability, and interaction with steel reinforcement under concrete-relevant conditions. The review of corrosion monitoring and testing methods established the framework for assessing both corrosion mitigation and structural performance, ensuring that biosurfactant incorporation improves corrosion resistance without compromising mechanical integrity

CHAPTER 3
RESEARCH METHODOLOGY

3.1 Introduction

This chapter outlines the research methodology adopted to achieve the objectives of the study, encompassing a systematic experimental framework from biosurfactant production to its application in corrosion protection and reinforced concrete (RC) performance. The overall research flow and experimental sequence are illustrated in Figures 3.1 and 3.2. The methodological framework was structured to address the following key stages:

i) Isolation, screening and identification of potential biosurfactant-producing fungi from contaminated environments for their ability to produce biosurfactants, and to optimise growth conditions to maximise biosurfactant yield

ii) Characterisation of the compounds, identification of functional groups, and determination of the biosurfactant class of the most efficient fungal strain, together with quantification of its inhibitory performance against mild steel corrosion.

iii) Evaluation of the corrosion inhibition efficiency of the biosurfactant on mild steel reinforcing bars using a migrating inhibitor approach, and establishment of the relationship between inhibitor dosage and electrochemical performance.

iv) Analysis of the effect of biosurfactant incorporation as a concrete admixture on the mechanical properties of fresh and hardened concrete.

v) Formulation of a corrosion protection strategy for RC that integrates both admixed and migrating applications of *Rhizopus*-derived phospholipid biosurfactants.

The methodological framework commenced with the isolation of indigenous fungi from contaminated environments, followed by screening and identification of potential biosurfactant-producing strains. The biosurfactant was produced via batch submerged fermentation in MSM under controlled conditions, with WFO as the sole carbon source. Isolated fungi were subjected to preliminary screening utilised drop collapse, oil displacement, and emulsification index (E_{24}) tests, which served as rapid and practical techniques for the preliminary identification of biosurfactant-producing fungi. These qualitative methods facilitated the selection of candidate strains for further analysis. Growth kinetics and biosurfactant yield were evaluated through optical density (OD) and dry cell weight (DCW) measurements during the biosurfactant production stage.

The fungal strains responsible for biosurfactant production were identified using microscopic examination and comparative analysis with existing literature and microbial databases. As identical fungal species may produce different biosurfactant classes depending on strain origin, fermentation conditions, and substrate composition, advanced characterisation was required. Liquid chromatography–quadrupole time-of-flight mass spectrometry (LC-QTOF-MS) was employed to determine the molecular structure and class of the biosurfactants produced. The identified biosurfactants were then assessed for their effectiveness in corrosion inhibition studies.

The performance of corrosion inhibition was assessed through various methods, such as weight loss measurements, ER testing, tensile testing, electrochemical impedance spectroscopy (EIS), and surface analysis [scanning electron microscopy (SEM) and energy-dispersive X-ray spectroscopy (EDX)]. Subsequently, biosurfactant concentrations between 5% (v/v) and 20% (v/v) in a 0.9% NaCl solution were employed for the mild steel bars. This process was conducted for 28 days to ascertain the optimal treatment concentration.

The compressive strength (f_c), flexural strength (f_s), tensile strength (R_m), and bonding strength (τ) tests were also conducted for the evaluation of RC strength. Furthermore, Tween 80 was employed as a commercial reference for comparative corrosion inhibition analysis.

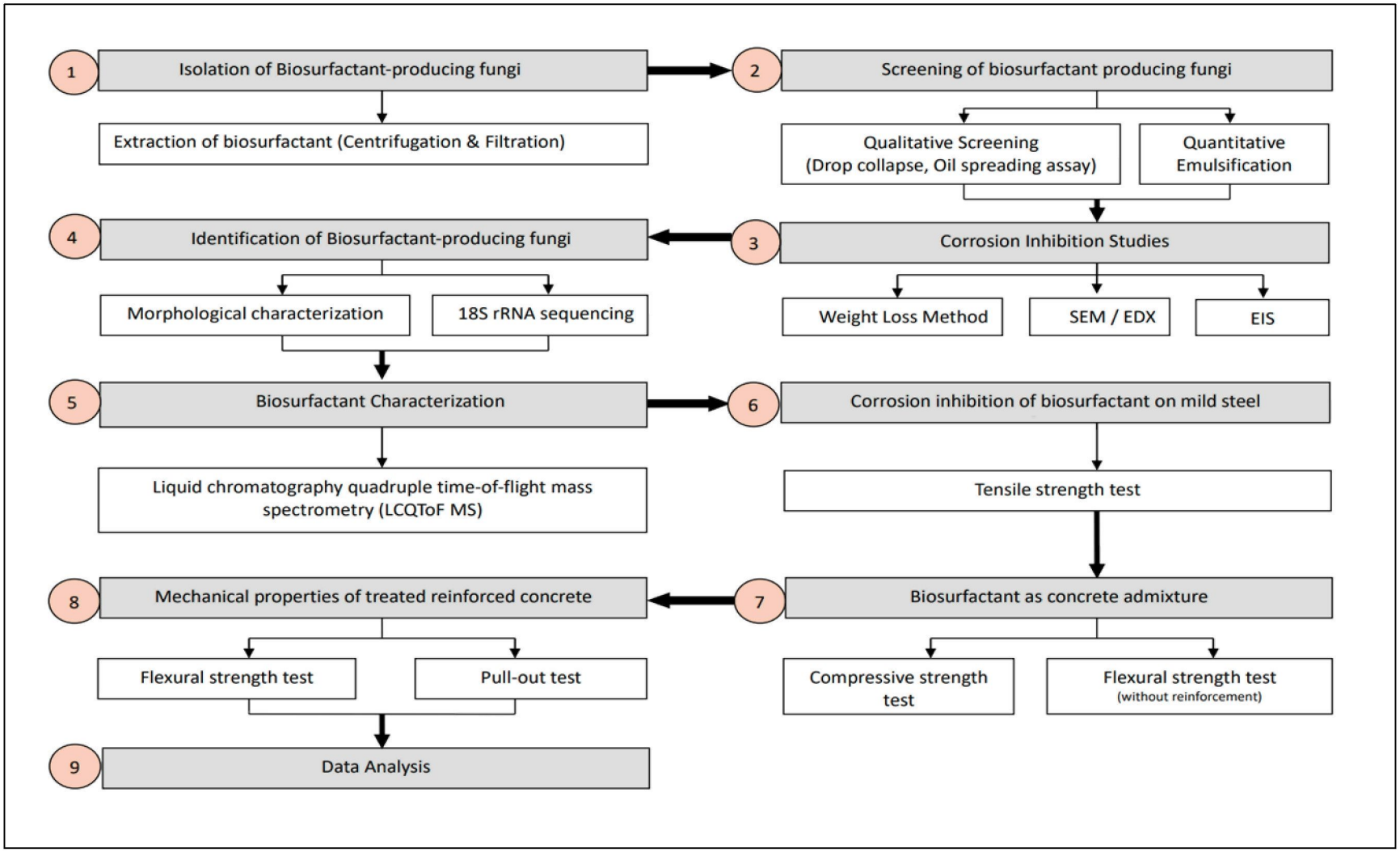

Figure 3.1 Flowchart Of Research Methodology

DESK STUDY

Purpose: Establish the research direction and develop the research methodology.

Activities:

1) Systematic Literature Review

2) Identification of research gap

3) Review suitable methods, consultation with experts, and develop research methodology

4) Design laboratory activities

LABORATORY ACTIVITIES

OBJECTIVE 1 — Biosurfactant Production and Screening

Stage 1A: Isolation of fungi from local municipal waste and petroleum sludge

Purpose:

To isolate indigenous fungi from municipal waste and petroleum sludge

Activities:

Samples taken from different dump sites and car garages at Kuching and Kota Samarahan, Sarawak

Serial dilution method and pour plate method for fungi isolation

Isolation on petri dish with potato dextrose agar (PDA) and malt extract agar (MEA) for 7-14 days at 30°C

Subcuture to obtain pure fungi strain

Stage 1B: Fermentation and enrichment of biosurfactant producers

Purpose:

To cultivate fungal mycelia from various genera for biosurfactant production

Activities:

Following multiple cultivation steps to obtain pure fungal cultures, the mycelia were transferred into conical flasks containing minimal salt medium (MSM) as the nitrogen source and waste frying oil (WFO) as the sole carbon source

The fermentation broth was enriched to enhance biosurfactant yield by manipulating key parameters, including the type and concentration of the carbon source, incubation period and size of the mycelia, pH, temperature, and fermentation duration.

Stage 1C: Screening of biosurfactant

Purpose:

To screen potential biosurfactant producing fungi using qualitative and quantitative screening methods

Activities:

Qualitative screening - Oil displacement assay & drop collapse method

Quantitative screening - Emulsification index (E_{24})

OBJECTIVE 2 — Fungi Identification and Biosurfactant Characterization

Stage 2A : Extraction of biosurfactant

Purpose:

To extract biosurfactant from fermentation broth

Activities:

Extraction of potential biosurfactant from the fermentation broth using centrifugation and filtration method

The supernatant was extracted from the fungal cells and particulates using a liquid-liquid separation method with N-hexane.

Stage 2B: Fungi Identification

Purpose:

To identify the biosurfactant-producing fungi by its morphology

Activities:

The mycological characteristics of the fungi were observed both macroscopically on agar plates and microscopically on glass slides using Acid Fuchsin staining.

The characteristics were compared with the known morphological features of the targeted strains to confirm their identities

Stage 2C: Biosurfactant Characterisation

Purpose:

To characterised the biosurfactant

Activities:

The extracted biosurfactant exhibiting the highest corrosion inhibition efficiency was characterised using LC-QTOF-MS analysis

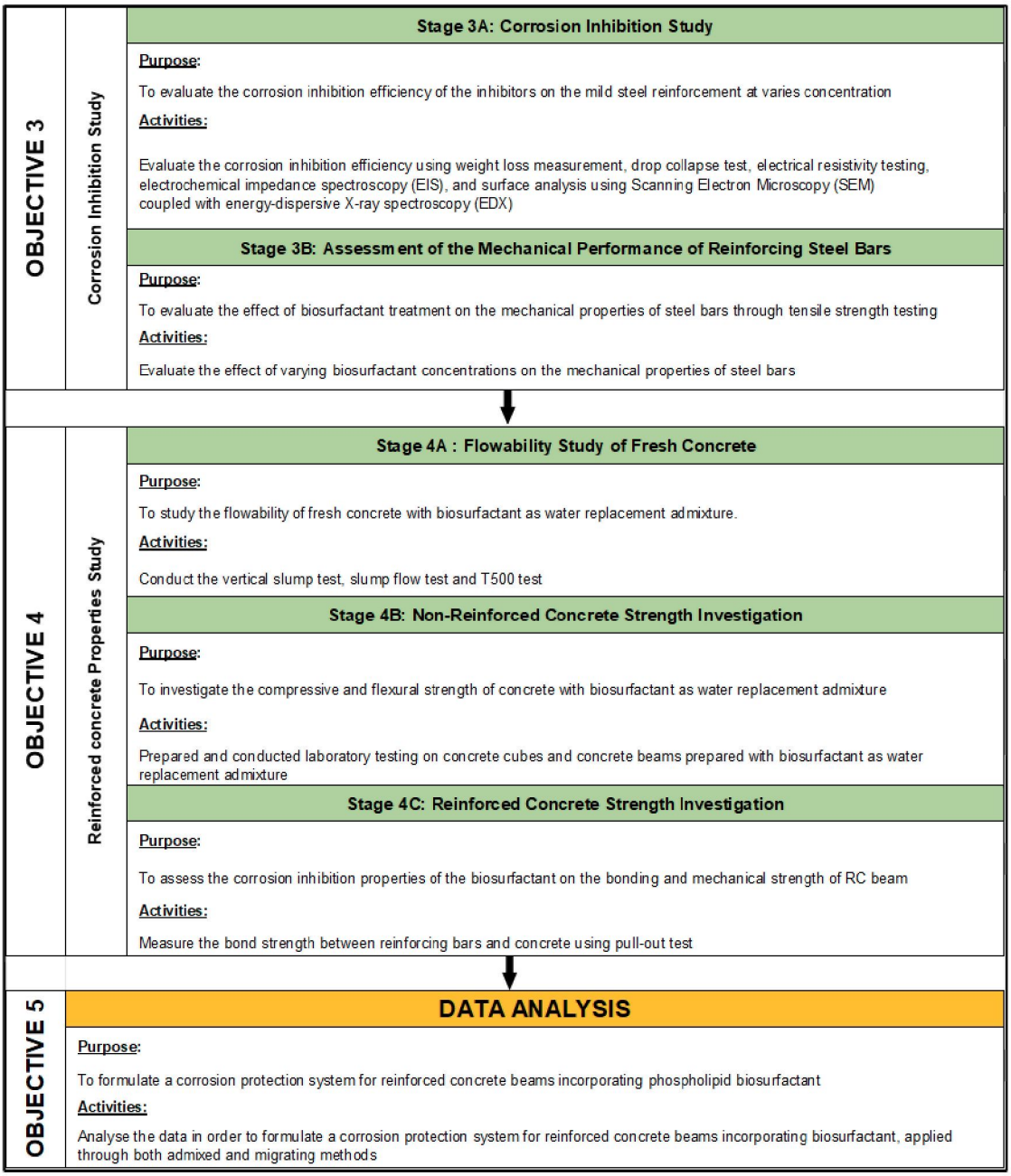

Figure 3.2 Summary Of Research Activities

3.2 Isolation of Biosurfactant-Producing Fungi

Fungi in natural environments generally exist in mixed populations that include various species and strain. Therefore, obtaining a pure culture is essential for analysing the properties of a specific organism within a mixed population. This study involved the isolation of biosurfactant-producing fungi from samples gathered at different locations. Soil samples were selected as the primary source for isolating biosurfactant-producing fungi due to their high microbial diversity and continuous exposure to

complex organic contaminants. Contaminated soils, particularly those impacted by hydrocarbons, oils, and industrial waste, create selective pressure that favours microorganisms capable of producing surface-active compounds to enhance substrate uptake and survival (Taylor & Sinsabaugh, 2015).

The process was followed by preliminary screening to identify biosurfactant production. Fungal mycelia were also isolated from soil samples and inoculated into an MSM, which was supplemented with WFO as substrates to facilitate biosurfactant production through submerged, batch, and anaerobic fermentation techniques. WFO was selected as the sole carbon source for fungal growth and biosurfactant production due to its abundance, low cost, and high lipid content, which is favourable for the synthesis of lipid-based biosurfactants (Nurul Fatihah Khairudin, 2016). The fatty acid composition of WFO further supports biosurfactant biosynthesis by providing essential precursors for amphiphilic molecule formation.

Meanwhile, cryotube cryovials were employed for the storage of master and working stocks. These cryovials were maintained in appropriately labelled glass bottles and stored at 4°C. Waste management also utilised distinct and clearly labelled biological waste bins, with all waste transport from the laboratories to the autoclave carried out by a dedicated technician familiar with laboratory operations and appropriate disposal protocols. Furthermore, biological waste bags were secured in the laboratory by folding the top of the bag and using autoclave tape. These bags were then transported to the autoclave within an autoclavable secondary container via a dedicated trolley.

All work areas were disinfected with 70% ethanol prior to and following use, which was in compliance with standard operating procedures (SOP). Contaminated waste was deposited into designated biowaste bags and subjected to autoclaving at 134°C for 20 mins. Liquid waste (fermentation broth residuals post-experiment) was disinfected through the addition of a 70% ethanol solution prior to autoclave transport. A programme was also established for the disposal of biological waste. Figure 3.3 depicts the stages involved in biosurfactant production.

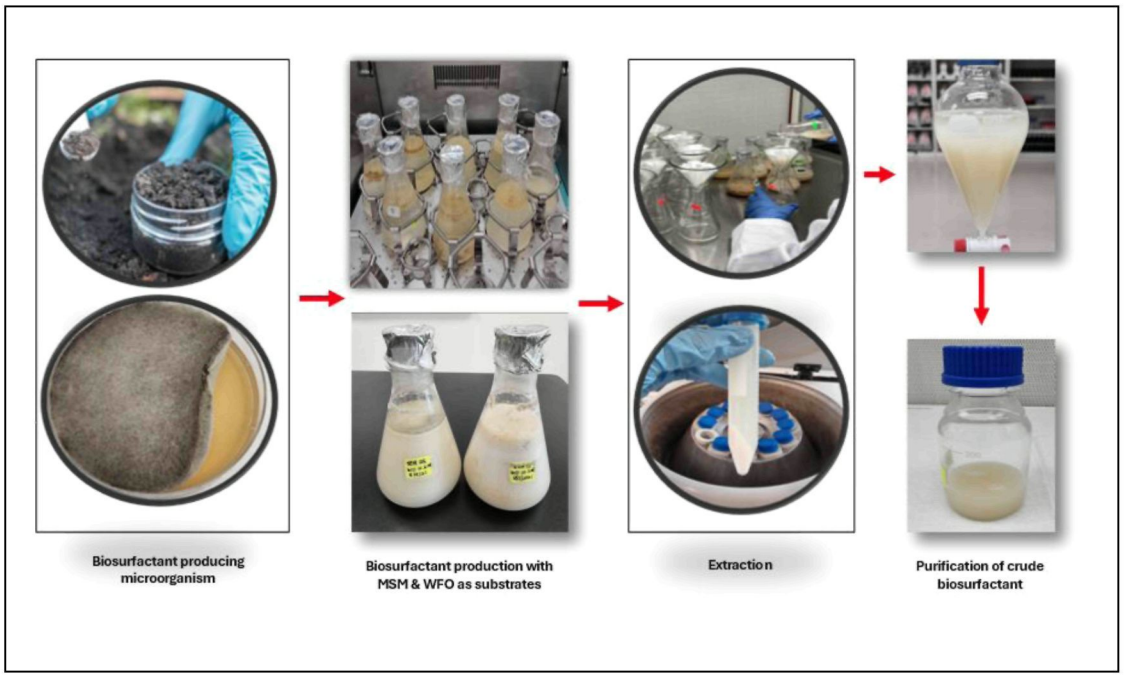

Figure 3.3 The Biosurfactant Production Stages For This Study

3.2.1 Environmental Screening for Biosurfactant-Producing Fungi from Contaminated Soils

Biosurfactants are secondary metabolites secreted by soil fungi isolated from contaminated locations in Kuching and Kota Samarahan, Sarawak. These areas were selected as sampling locations to isolate indigenous soil fungi from oil-impacted urban environments influenced by mixed residential and industrial activities, including municipal waste disposal sites and automobile workshops. Such environments impose selective pressure that favours the adaptation of native fungi capable of biosurfactant production, consistent with the mechanisms of microbial selection in hydrocarbon-contaminated soils discussed in Chapter 2.

A total of ten sampling locations were selected to balance ecological diversity and experimental feasibility. This number was sufficient to capture spatial variability across contaminated micro-environments and to enhance the likelihood of isolating diverse fungal strains with biosurfactant-producing potential, thereby strengthening the robustness of the screening process. Soil samples were excavated at a depth of approximately 20 cm, corresponding to the topsoil layer. This layer is also known as the root zone. Previous biosurfactant screening studies have consistently employed this depth range, as organic, inorganic and other soil nutrients tend to accumulate at this

layer. This depth has been shown to maximise the recovery of hydrocarbon-tolerant and biosurfactant-producing microorganisms, thereby enhancing screening efficiency and comparability with established literature (Abate, 2025; Samsu et al., 2020).

At each sampling location, approximately 500g of soil was collected by compositing subsamples from three nearby points within the same site to ensure representativeness. The samples collected in a polythene bag and wrapped in Aluminium foil. The temperature of composite samples was recorded promptly, whereas the pH levels, soil characteristics, and physical properties were examined. This analysis was pivotal for comprehending the ecological conditions that promoted the growth of fungal species.

The collected soil samples were air-dried for 24 h. Approximately 20 g of soil was then sieved into a 100 mL beaker, and 20 mL of sterile distilled water was incorporated. The suspension remained in effect for 30 mins. This suspension was periodically agitated to improve reaction equilibrium. The collected samples were finally labelled and stored at the Research Laboratory, Faculty of Applied Science, Universiti Teknologi MARA, Kampus 2, Kota Samarahan. Table 3.1 and Figure 3.4 provide a detailed account of the characteristics of the collected soil samples and their physical appearances, respectively.

Table 3.1
Summary Of The Sampling Locations And The Characteristics Of The Soil Samples Collected

Sample	Sources	Temperature on site (°C)	Soil Type	Soil Characteristic
S1	Aeroville Municipal Waste	31	Clay	Light brown, semi-solid
S2	Tabuan Jaya Municipal Waste	29	Chalky	Brown, semi-solid
S3	ILP Car Garage	29	Peaty	Dark brown, semi-solid
S4	Petrajaya Car Garage	29	Clay, loamy	Dark brown, semi-solid
S5	Tanjong Bako Municipal Waste	31	Sandy	Light grey, light sandy & drains quickly
S6	KBS Municipal Waste	30	Loamy	Greenish-dark brown, semi-solid
S7	Saberkas Car Garage	32	Loamy	Greenish brown, semi solid
S8	Riveria Municipal	31	Chalky	Reddish brown, semi

Sample	Sources	Temperature on site (°C)	Soil Type	Soil Characteristic
	Waste			solid, hard
S9	Riveria Car Garage	30	Silty loam	Greenish brown, semi-solid
S10	Permai Municipal Waste	29	Sandy clay	Light brown, sandy soil

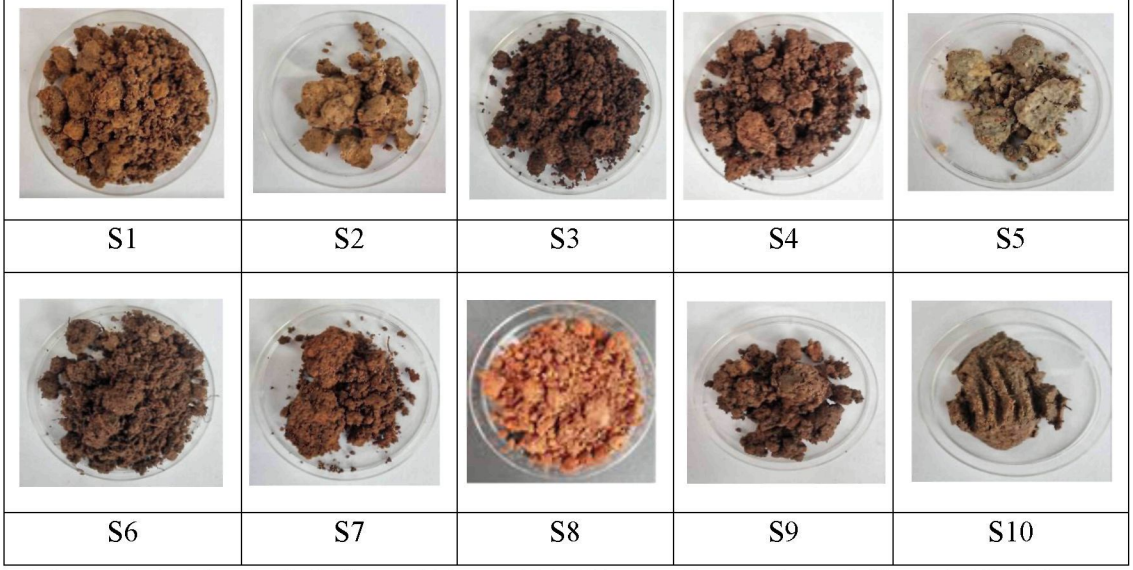

Figure 3.4 The Soil Collected From 10 Different Contaminated Sites At Kuching And Kota Samarahan

3.2.2 Isolation of Soil Fungi from Contaminated Environments

Isolation involves the extraction of a pure culture of fungi from a complex sample or environment. The main aim is to isolate and grow a particular fungal species or strain, enabling thorough investigation, characterisation, and application of that strain. Thus, serial dilution and pour plate techniques were employed for the isolation of potential microbes capable of biosurfactant production. The soil samples also underwent 10-fold dilutions in this study. Approximately 1 g of soil was placed into test tubes containing 9 mL of peptone water (Sena et al., 2018). The diluted sample in the initial tube was then transferred to a second tube containing 9 mL of peptone water. Subsequently, the diluted sample from the second tube was transferred into a third tube

containing 9 mL of peptone water. This dilution process was repeated 10 times (Sapkota, 2021). Figure 3.5 portrays the process of serial dilution.

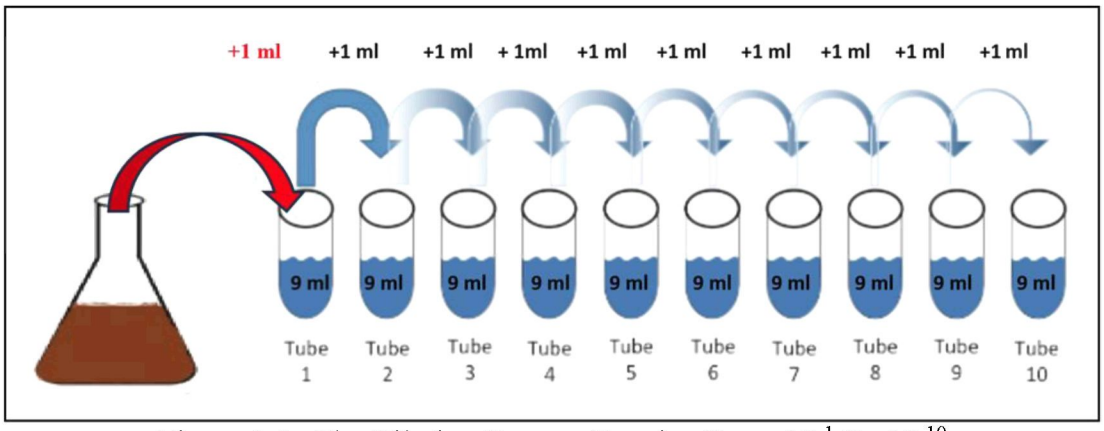

Figure 3.5 The Dilution Process Ranging From 10^{-1} To 10^{-10}

Figure 3.6 depicts that approximately 1 mL of each diluted sample from the 10^{th} tube is plated on Petri dishes containing sterilised MEA. The dishes were sealed prior to incubation for 7 to 14 days in laboratory incubator at a controlled temperature (27–30°C) to prevent solution migration. This process could promote the growth of microorganisms present in the samples. Fungal growth was monitored daily over a period of 4 to 14 days. Fungal growth observed on the plates after 7 days is depicted in Figure 3.7. The cultivated fungal strains were mesophilic and exhibited optimal growth at 30°C.

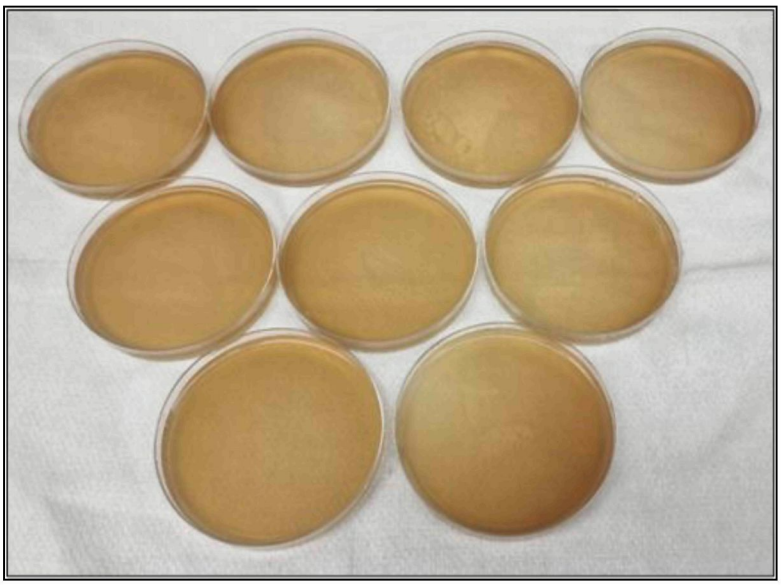

Figure 3.6 The Diluted Samples Poured On Sterilised Malt Extract Agar (MEA)

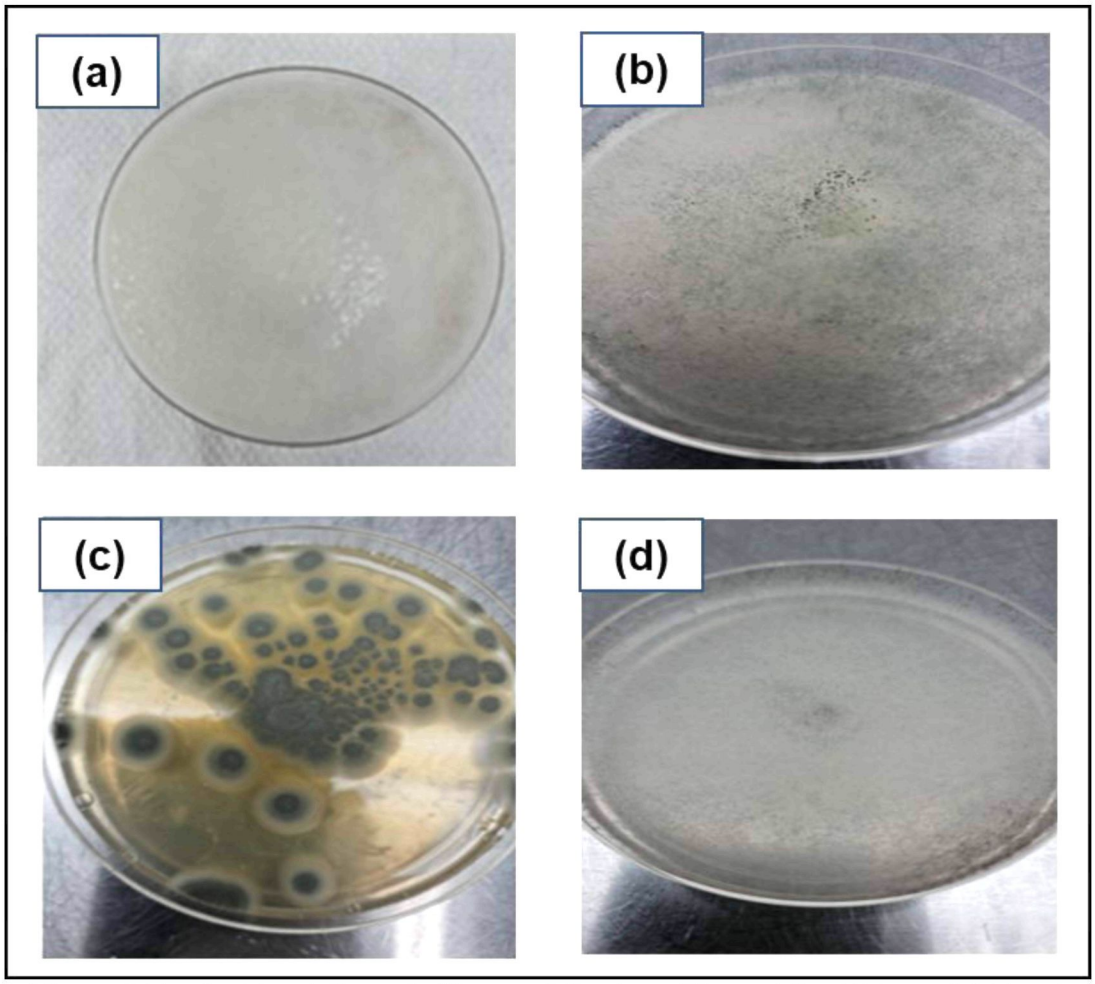

Figure 3.7 The Fungi Growth Observed On Agar Plates After 7 Days. (a) Fungi Isolated From Aeroville Municipals Waste- *Rhizopus Sp.* (b) Fungi Isolated From ILP Car Garage- *Pennicilium Sp.* (c) Fungi Isolated From KBS Municipal Waste -*Tricoderma Sp.* (d) Fungi Isolated From Riveria Car Garage - *Fusarium Sp.*

Figure 3.8 demonstrated that pure fungal cultures are obtained by sub-culturing mycelia from the four biosurfactant-positive isolates through repeated plating on MEA. All isolations were performed in triplicate to guarantee reproducibility. Daily monitoring of fungal cultures was also conducted, with selection limited to those demonstrating uniform mycelial growth were selected for further sub-culturing. This procedure was reiterated to remove contamination and verify the purity of the isolates. Only verified pure cultures were utilised for the submerged fermentation process. Subsequently, agar cubes with successfully isolated fungi were preserved as working stocks in glass bottles filled with autoclaved distilled water and were sealed correctly (see Figure 3.9). These working stocks were maintained at 4°C in a refrigerator to

suppress microbial activity. Master working stocks were also designed for utilisation within a two-year timeframe.

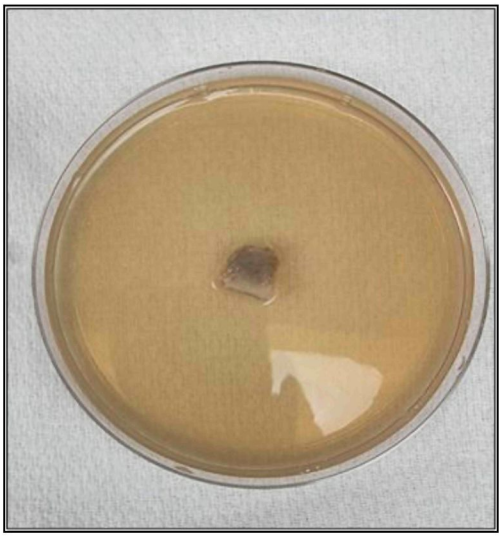

Figure 3.8 The Repeated Plating On MEA To Obtain A Pure Culture. This Sub-Culture Process Is Repeated At Least Twice For Every Strain

Figure 3.9 The Working Stocks That Are Cut From Agar Plates And Kept In Sealed Glass Bottles. These Strains Are The Biosurfactant-Producing Fungi

3.2.3 Cultivation of Potential Biosurfactant Producers

Biosurfactant production was carried out following the protocol described by Kosa et al. (2018). A liquid medium was prepared following the methodology established by Nur Afini Binti Wan Adlin et al. (2020). Fungal fermentation was initially performed in Erlenmeyer flasks containing 250 mL of MSM broth. Inoculums

from agar plates were then transported to the fermentation broth, which contained MSM as the nitrogen source. This process was supplemented with WFO as the sole carbon source. The WFO was subjected to double filtration using muslin cloth to remove solid waste. Previous study by Mumtaz et al., (2024) have shown that MSM promotes metabolite-driven microbial responses under nutrient-limited conditions, thereby supporting the induction of secondary metabolites such as biosurfactants when hydrophobic carbon sources are supplied.

Meanwhile, the MSM broth composed of distilled water containing 2.5 g/L (w/v) sodium nitrate ($NaNO_3$), 2.0 g/L (w/v) dipotassium phosphate (K_2HPO_4), 0.2 g/L (w/v) magnesium sulphate ($MgSO_4$), 0.2 g/L (w/v) NaCl, and 0.1 g/L (w/v) calcium chloride hexahydrate ($CaCl_2{\cdot}6H_2O$). This broth was sterilised through autoclaving at 121°C for 120 mins.

Medium optimisation was performed via a series of experiments in which a single variable was altered at a time. Other factors remained constant (see Table 3.2). A total of 7 key factors were also selected for analysis to enhance biosurfactant productivity: (i) nitrogen source, (ii) carbon ratio, (iii) inoculum concentration, (iv) initial pH of WFO, (v) temperature, (vi) agitation, (vii) and aeration. The concentration of WFO as the carbon source was then varied at 2%, 5%, 7%, and 10% (v/v) of MSM. The suitability of WFO pH levels 6.0 and 7.5 was also investigated. Moreover, fermentation temperature was maintained at 27°C and 30°C. These fermentation modes comprised aerobic (agitated) and anaerobic conditions. The shaking incubator was also set at 160 rpm.

Table 3.2
Summary Of The Initial Variables In The Fermentation Enrichment Process For Biosurfactant Production

WFO (%v/v)	Temperature (°C)	pH of WFO	Anaerobic and agitated	Aerobic	Biosurfactant production	
					7 days	14 days
2	27	6	✓		No	No
2	27	6		✓	No	No
2	27	7.5	✓		No	Yes
2	27	7.5		✓	No	Yes
2	30	6	✓		No	No
2	30	6		✓	No	No
2	30	7.5	✓		No	Yes
2	30	7.5		✓	No	Yes

WFO (%v/v)	Temperature (°C)	pH of WFO	Anaerobic and agitated	Aerobic	Biosurfactant production	
					7 days	14 days
5	27	6	✓		No	No
5	27	6		✓	No	No
5	27	7.5	✓		Yes	Yes
5	27	7.5		✓	Yes	Yes
5	30	6	✓		No	No
5	30	6		✓	No	No
5	30	7.5	✓		Yes	Yes
5	30	7.5		✓	Yes	Yes
7	27	6	✓		No	No
7	27	6		✓	No	No
7	27	7.5	✓		Yes	Yes
7	27	7.5		✓	Yes	Yes
7	30	6	✓		No	No
7	30	6		✓	No	No
7	30	7.5	✓		Yes	Yes
7	30	7.5		✓	Yes	Yes
10	27	6	✓		No	No
10	27	6		✓	No	No
10	27	7.5	✓		No	No
10	27	7.5		✓	No	No
10	30	6	✓		No	No
10	30	6		✓	No	No
10	30	7.5	✓		No	No
10	30	7.5		✓	No	No

The cultivation of fungi for biosurfactant production was carried out in Erlenmeyer flasks as depicted in Figure 3.10. The fungal culture was fermented in MSM broth for 14 days and was subsequently incubated in a shaking incubator at a consistent temperature of 30°C (agitation = 160 rpm). For upscale fermentation, the fungi were cultured within the 15 L bioreactor under batch fermentation conditions at room temperature for 45 days, utilising aerobic processes.

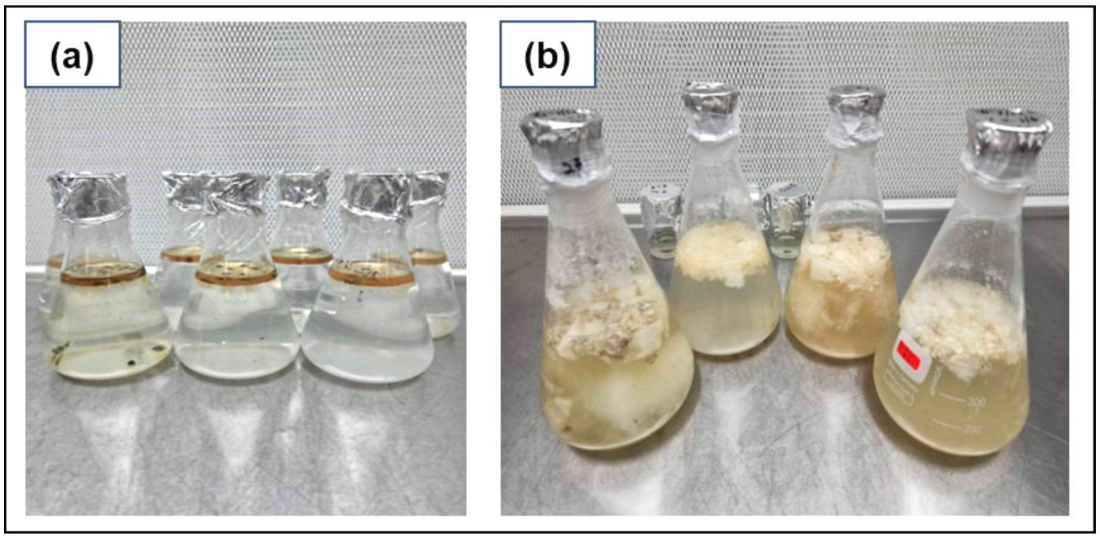

Figure 3.10 (a) The Fungi Mycelia Fermented In MSM Broth Supplemented With 5% WFO (v/v) In Erlenmeyer Flasks On Day 1 And (b) Fermentation Broth On Day 4 Of Batch Fermentation

3.3 Extraction and quantification of Biosurfactant

Following the completion of the fermentation process, the biosurfactant was extracted from the fermentation broth using an acid precipitation method, adapted from established protocols reported in the literature (George & Jayachandran, 2013; Nur Afini Binti Wan Adlin et al., 2020). This method was selected due to its suitability for crude biosurfactant recovery, scalability, and widespread application in studies involving microbial biosurfactants.

Centrifugation and filtration were initially utilised to separate the pellet from the fermentation broth, which was referred to as the supernatant. The supernatant was then subjected to liquid-liquid extraction with N-hexane as the solvent at a 1:1 ratio to isolate the unutilised substrate (WFO) from the biosurfactant. This liquid-liquid separation occurred in a separation funnel. Subsequently, the solvent and biosurfactant mixture was allowed to evaporate for 24 h. The biosurfactant derived from this process was finally employed in corrosion inhibition analysis.

To ensure the reliability and reproducibility of the extraction process, all extraction and quantification procedures were conducted in triplicate using independently prepared fermentation batches. Extraction efficiency was validated by calculating the coefficient of variation across replicates, with values below 10% indicating acceptable repeatability of the method. In addition, consistency of biosurfactant recovery was indirectly supported through repeated measurements of

surface tension reduction and emulsification index (E24), which exhibited minimal variation between replicates.

3.3.1 Centrifugation and Filtration

The initial phase of biosurfactant extraction entailed the removal of pellets containing fungal cells from the fermentation broth via centrifugation and filtration. Particularly, the fermentation broth was transferred to 15 mL centrifuge tubes and centrifuged at 10,000 rpm for 10 mins. This process successfully isolated the pellets containing fungal cells from the supernatant (see Figure 3.11). Figure 3.12 demonstrates the filtration step for enhancing the purity of the supernatant by eliminating residual particulate matter (unutilised substrates). The supernatant was filtered through 8 to 11 µm filter papers utilising a narrow neck filtering flask. This filtration was conducted under sterile conditions within a laminar flow hood to mitigate contamination risks. Figure 3.13 depicts the cell-free supernatant obtained from this process. The harvested supernatant was essential for subsequent steps in the extraction protocol. This extracted biosurfactant was applied for growth measurement based on DCW and OD procedures.

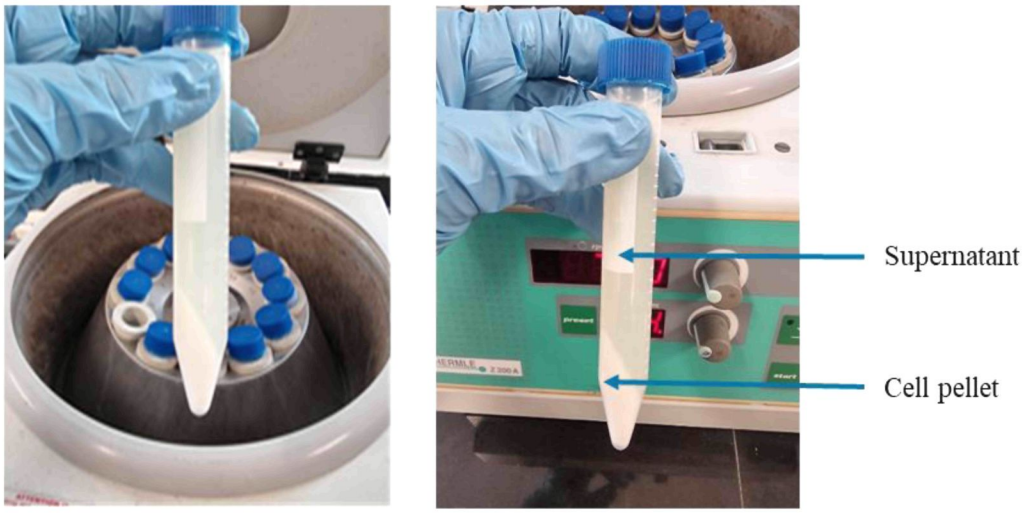

Figure 3.11 The Centrifugation Process To Separate The Supernatant From Pellet - Containing Cells And Unutilised Substrates

Figure 3.12 Further Extraction By Filtration Of Supernatant From Cell-Free Broth. This Process Was Performed After Centrifugation

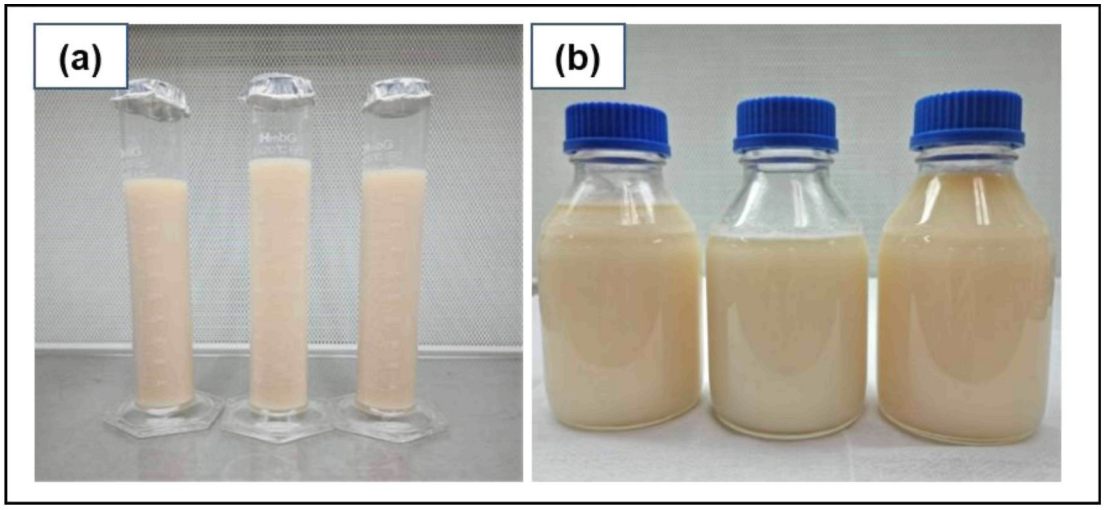

Figure 3.13 The Crude Biosurfactant Collected After Filtration

3.3.2 Liquid-to-Liquid Extraction

N-Hexane was selected as the extraction solvent due to its non-polar nature, immiscibility with water, and high selectivity toward lipid-based biosurfactants, enabling efficient phase separation and reproducible recovery. Ethyl acetate and chloroform are considered unsuitable for environmentally sustainable applications due to their toxicity and high solvent requirements, whereas n-hexane provides a

comparatively lower-risk alternative with comparable extraction efficiency. Ethanol was avoided due to its partial water miscibility and tendency to co-extract polar impurities, which can interfere with gravimetric quantification (Shen et al., 2019; Zhou et al., 2020).

Liquid-liquid extraction was performed on the supernatant to eliminate substrate residue after the removal of fungal cells and particulates. Equal volumes of supernatant and n-hexane (ratio 1:1) were combined in a separation funnel and shaken vigorously for 30 s to achieve complete mixing. This vigorous shaking promoted the transfer of biosurfactant molecules into the n-hexane layer, which was attributable to their amphiphilic characteristics (hydrophobic tails and heads). Following agitation, the mixture was permitted to stand for 24 h within a laminar flow cabinet, leading to the development of two separate layers. The lower aqueous layer contained the biosurfactant. Conversely, the upper layer consisted of residual cooking oil solubilised in N-hexane (see Figure 3.14). This residual oil constituted the unused substrate from the fermentation process. The two layers were meticulously separated, in which the biosurfactant-containing bottom layer was collected and evaporated over a 24-h period under ambient conditions to eliminate the solvent. Figures 3.15 and 3.16 present that the total elimination of n-hexane is verified by the lack of residual solvent, resulting in the purified biosurfactant in crystalline form (Sharma et al., 2014). From 1 L of culture broth, approximately 1.2 g L^{-1} of hexane-extracted crude biosurfactant fraction was recovered.

The yield of the biosurfactant was quantified gravimetrically following the evaporation step, expressed in grams per liter (g/L), offering a quantitative assessment of extraction efficiency (Chooklin et al., 2014). Ethyl acetate is frequently employed as an extraction solvent, independently or in combination with solvents (methanol and chloroform). Nonetheless, the application of this material is not recommended due to its toxicity and the substantial quantities needed (Radzuan, 2018; Liepins et al., 2021). Tang et al. (2018) proposed using N-hexane as a less harmful solvent, which was employed in this study.

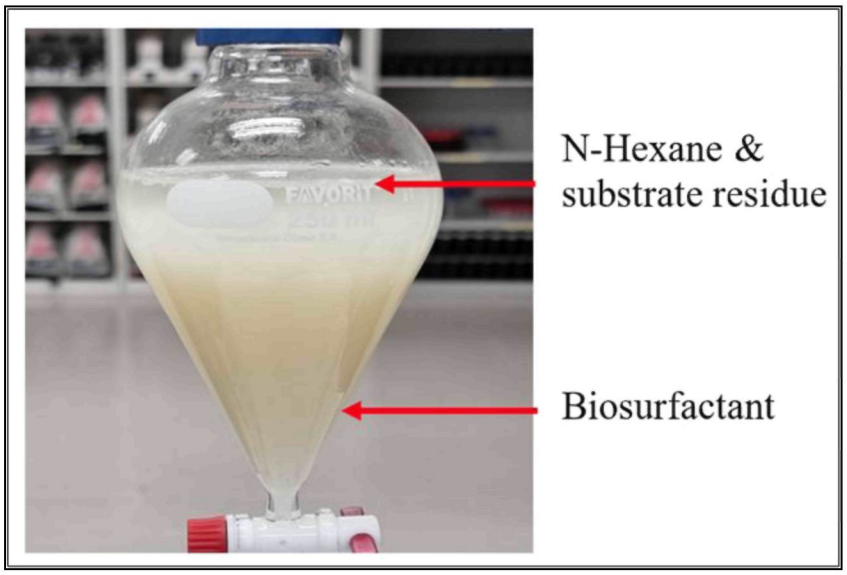

Figure 3.14 The Liquid-Liquid Extraction With N-Hexane

Figure 3.15 The Extracted Cell-Free Biosurfactant

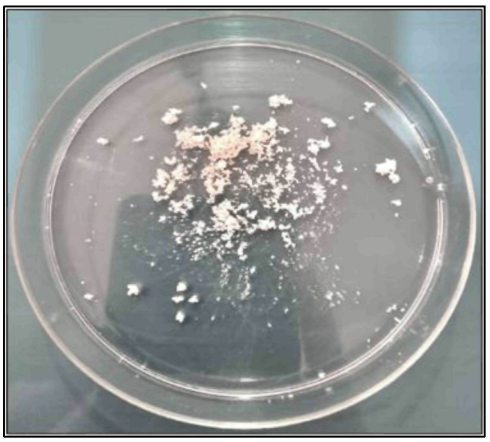
Figure 3.16 The Crystalized Biosurfactant After Evaporation

3.3.3 Growth Measurement with DCW and OD

Cell growth was quantified through DCW and OD analyses. The correlation between OD and DCW was established to ensure consistency and reliability in monitoring fungal growth, thereby validating the accuracy of biomass estimation during the determination of optimum biosurfactant production conditions. The OD of culture at a wavelength of 600 nm was measured using an Ultraviolet–visible spectrophotometry (UV-VIS) spectrophotometer. This OD was computed using distilled water as a blank reference. The blank medium was also calibrated to OD600 = 0. Measurements were conducted in triplicate to ensure result reliability. Meanwhile, the weight of the extracted crystallised biosurfactants was calculated using a high-precision weighing scale to determine the DCW (Radzuan, 2018). This dry weight of the biosurfactant is determined using the formula expressed as follows:

DCW = weight of the plate after drying - weight of empty plate (3.1)

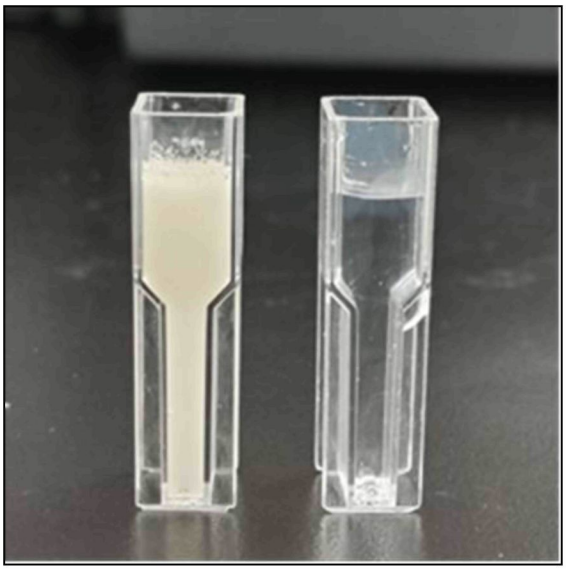

Figure 3.17 The Biosurfactant (Left) And Saline Solution (Right) For OD Measurement

3.4 Screening Tests for Biosurfactant Production

Biosurfactants are a diverse group of biomolecules that include amphiphilic compounds synthesised either intracellularly or exuded extracellularly (Apte & Padalia, 2018). These molecules possess hydrophobic and hydrophilic moieties, enabling the

microorganism to accumulate at fluid interfaces and reduce surface and interfacial tension (Radzuan, 2018). The identification of biosurfactant-producing strains primarily depends on the physicochemical properties of these surfactants. Three distinct screening assays were conducted to confirm the presence of biosurfactants in fermentation broth: (i) drop collapse, (ii) oil displacement, and (iii) E_{24} tests (Samsu et al., 2020). Table 3.3 delineates the methodologies for the screening processes, which are classified according to their distinct characteristics and intended functions. The screening for biosurfactant production was conducted on the 14th day of fungal cultivation. In all three screening tests performed, Tween 80 served as the positive control, while distilled water was utilised as the negative control.

Table 3.3
The Qualitative And Quantitative Method To Detect Biosurfactant Production By Soil Fungi

Category of Screening	Name of Screening Test	Observation / measurement
Qualitative	Drop Collapse Test	Surface activity
	Oil Displacement Test	Surface activity
Quantitative	Emulsification Index Test (E_{24})	Emulsifying ability

3.4.1 Drop Collapse Test

The drop collapse test effectively differentiates between producing and non-producing strains. This test is straightforward and does not necessitate specialised equipment, allowing it to be conducted with a minimal sample volume (Adnan et al., 2018). The drop collapse test evaluates the phenomenon of drop collapse upon contact with a hydrophobic surface. A directly proportional correlation exists between drop diameter and surfactant concentration, serving as a semi-quantitative indicator for the presence of biosurfactants (Bodour & Miller-Maier, 1998; Antoniou et al., 2015).

The drop collapse test was conducted following the methodology outlined by Płaza et al. (2006). This test was performed utilising a 96-well microplate. The microplate lids were composed of 96 circular wells featuring an internal diameter of 6 mm. Figure 3.18 depicts the specified 96-well along with its components. Approximately 2 µL of engine oil (SAE HD30 Pennzoil) was put into the wells and equilibrated at 37°C for 1 h to even coating of every well. Subsequently, 5 µL was taken from the culture supernatant of *Rhizopus sp.*, *Penicillium sp.*, *Trichoderma sp.*, and

Fusarium sp. A control (distilled water) and standard (Tween 80) were also pipetted into the centre of an oil-filled well using a 1–10µL micropipette. Drop results were then assessed visually at a standard time (1 min) through a magnifying glass (3× optical glass and 60 mm diameter). The collapse of the drop or a beaded drop in the presence of culture supernatant indicated a positive or negative result (absence of surfactant), respectively (Bodour & Miller-Maier, 1998). The drop collapsed within one minute is positive for the drop collapse test (Dhiman, 2016). Each experiment was conducted in triplicate. This process aimed to ensure the consistency of the results.

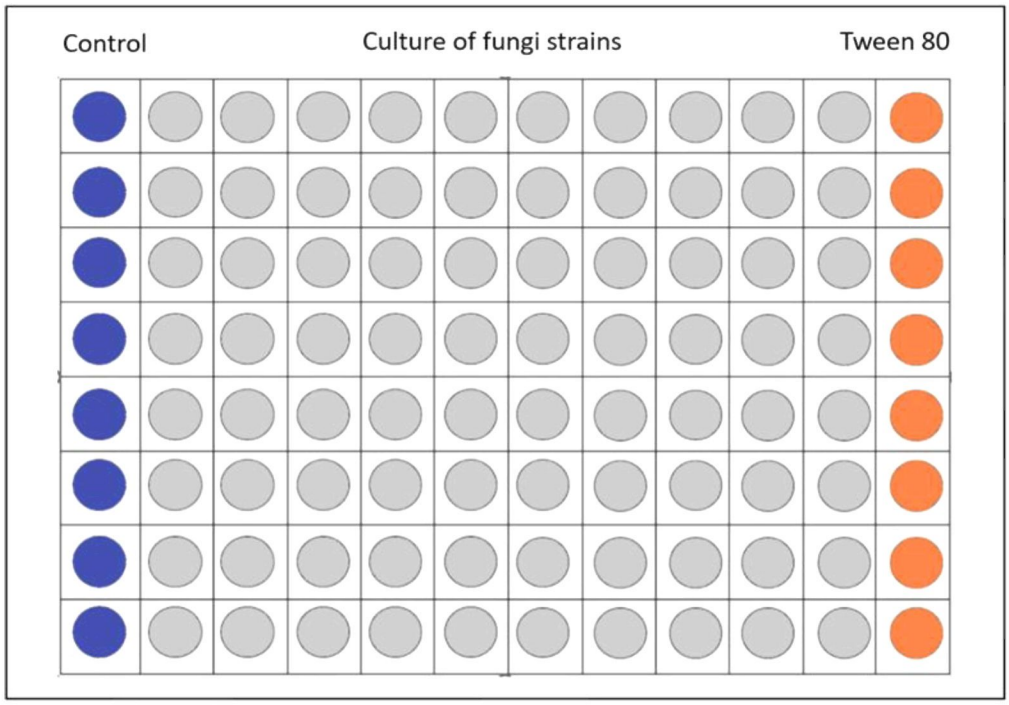

Figure 3.18 The Designated 96-Well Microplate And Its Component

3.4.2 Oil Displacement Test

Biosurfactant production is usually assessed using the oil displacement test (or oil spreading assay as a well-established method for measuring biosurfactant activity (Morikawa et al., 2000). This method utilises the principle of minimising interfacial tension between water and oil phases, which is indicative of biosurfactants that destabilise the water-oil interface and displace the oil volume on the surface (Youssef et al., 2004). The displacement of oil occurs in proportion to the concentration of biosurfactants as the repulsion between oil and water molecules diminishes. Therefore,

strains with the highest production potential are chosen based on a semi-quantitative variable (Asgher et al., 2020).

Several benefits are also indicated with this methodology, including high sensitivity, reliability, efficiency, and straightforward to implement. This study then introduced 2 mL of recycled used motor oil to 20 mL of distilled water (60 mm diameter × 20 mm depth borosilicate glass Petri dish) for the oil displacement test in creating a thin oil layer as shown in Figure 3.19. Approximately 1 mL of culture supernatant was then carefully added to the centre of the oil layer. When oil displacement and a clear zone occurred, the presence of biosurfactants was confirmed (Chakrabarti, 2013). The diameter of the clear zone formed on the oil surface is an indicator of surfactant activity. Larger displacement zones reflect greater surface tension reduction and therefore indicate higher biosurfactant activity (Shekhar et al., 2015).

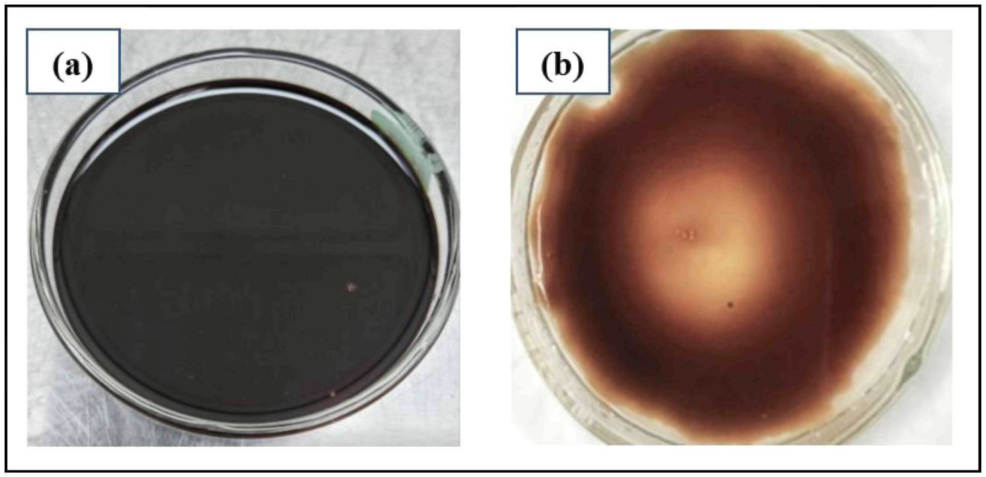

Figure 3.19 The Initial Surface Tension Of Motor Oil And (b) Reduction After 2 Mins With A Phospholipids-Based Biosurfactant

3.4.3 Emulsification Index (E_{24}) Test

The production of biosurfactants was evaluated using the E_{24} test, which was established by Cooper and Goldenberg (1987). This method assessed the emulsification capacity of biosurfactants by calculating the ratio of the emulsified volume to the total volume of the sample (see Figure 3.20). All isolates were examined for the presence of emulsifying properties in their produced metabolites. The experiment was conducted in triplicates for each isolate. 2 mL of culture supernatant was combined with 2 mL of motor oil in a centrifuge tube before vortexed at high speed for 2 mins. The vortexed

mixture was allowed to stand for 24 h. Measurement at 24 h minimises the influence of gravitational separation and secondary destabilisation phenomena that may occur at longer durations, while still providing a reliable indication of emulsifying capacity. Subsequently, the height of the stable emulsion layer was measured. Emulsification is considered significant when the emulsification index exceeds 50% (Rosenberg et al., 1988). The E_{24} was computed as the ratio of the height of the emulsion layer to the total height of the liquid as follows:

$$E24 = \frac{h_{emulsion}}{h_{total}} \times 100\% \quad (3.2)$$

where E_{24} correlates to the biosurfactant efficiency.

Emulsification activity was evaluated using the emulsification index after 24 h (E_{24}), where values $\geq$ 50% were considered indicative of effective biosurfactant production, as widely applied in biosurfactant screening studies.

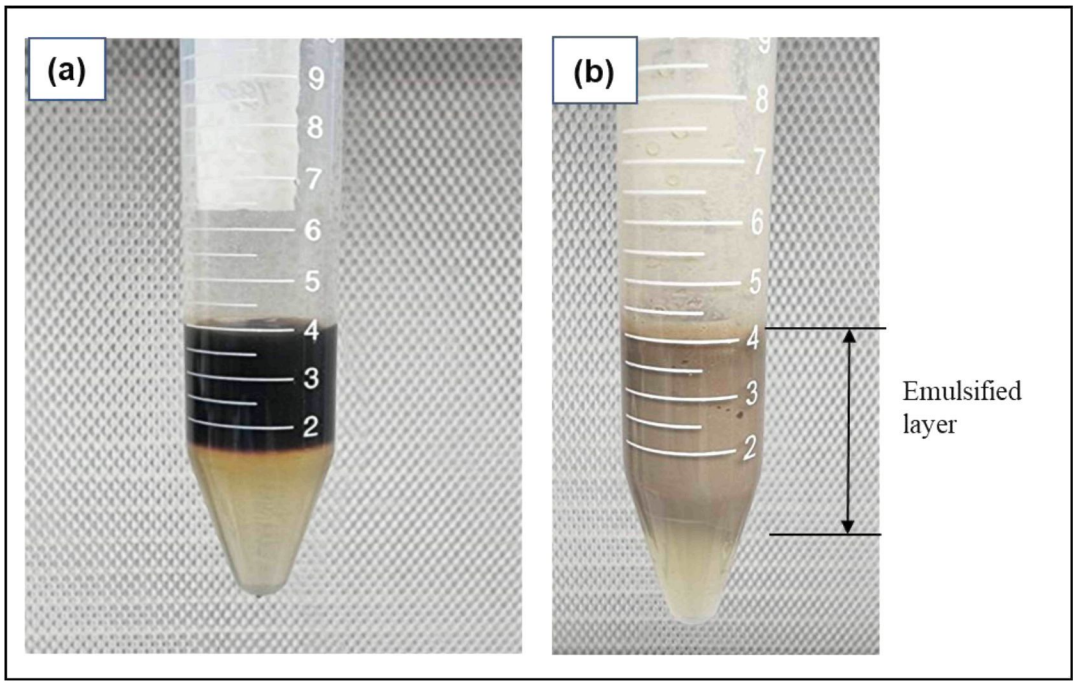

Figure 3.20 The Emulsification Test Involving (a) An Initial Biosurfactant-Motor Oil Mixture And (b) A Stable Emulsified Layer Based On Phospholipid-Based Biosurfactants After 24 H

3.5 Identification of Fungi and Biosurfactant Characterization

The genera of the four biosurfactant-producing fungi were determined through morphological properties. Additional characterisation of the biosurfactant with the highest corrosion IE was also performed using LC-QTOF-MS.

3.5.1 Macroscopic and Microscopic Identification of Fungal Strains

Fungal isolates were incubated on agar plates at 30°C for 14 days to facilitate optimal growth. The macroscopic characteristics of the fungal mycelia were systematically documented during the incubation period. Observations of colony height, diameter, margin type, surface texture, and pigmentation were then utilised for the preliminary identification of fungal genera. The samples were also stained with Acid Fuchsin (Sigma-Aldrich) and washed with distilled water to improve structural visibility prior to microscopic observation. A clean and dry glass slide was then prepared to remove contaminants. Subsequently, a small amount of fungal mycelium was meticulously transferred onto the slide with forceps and uniformly spread to create a thin smear. This smear was treated with Acid Fuchsin and allowed to stain for 1 min (see Figure 3.21). The excess stain was rinsed off with distilled water, and the stained smear was air-dried prior to microscopic examination using an Olympus CX31 microscope. The stained sample was also examined using a light microscope at 40× and 400× magnifications to evaluate its morphological properties. Figure 3.22 displays the micromorphological observations concerning the sporangium, spores, sporangiophore, hypha, and rhizoids. Characteristics of the fungal isolates were systematically compared with those of the targeted strains to verify their identities.

Figure 3.21 The Acid Fuchsin Used In Staining For Strain Identification

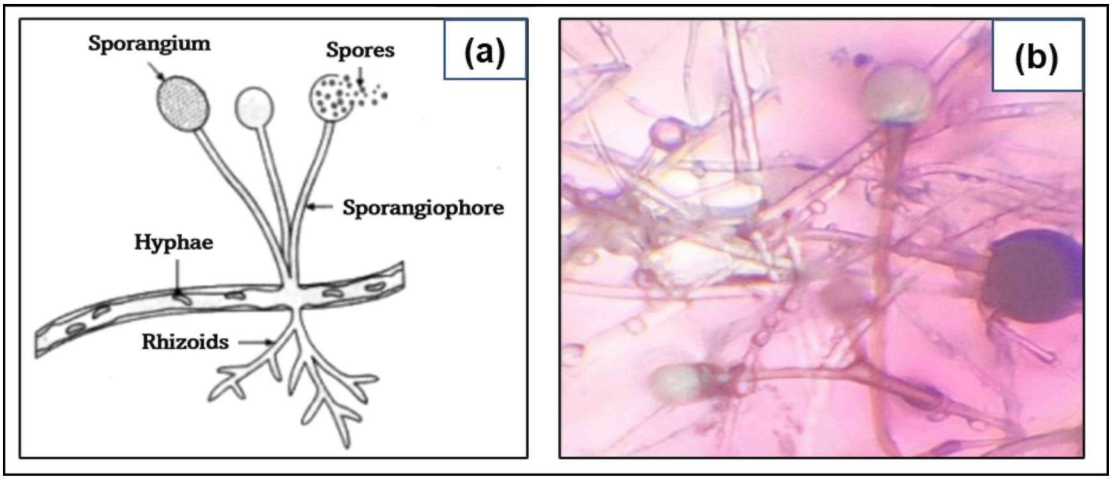

Figure 3.22 The Complex Structure Of *Rhizopus Sp.* (a) Illustration Adapted From Literature For Reference (b) Microscopic Image Captured At 400× Magnification Showing Hyphal And Sporangial Features Of The Isolated Strain

3.5.2 Biosurfactant Identification and Characterisation

Compounds were identified using LC-QTOF-MS in positive and negative ion modes. The mass spectrometer employed was the Vion IMS QTOF from Waters, USA. Acetonitrile (ACN) served as a blank to create the baseline and confirm that the detected peaks in the biosurfactant sample were derived from genuine compounds rather than impurities or background noise from the solvent system. This study then applied ACN, formic acid (HCOOH), and water phase in both positive and negative modes at varying concentrations (flow rate = 0.6 mL/min, duration = 20 mins, and injection volume = 10µL). Solvents A and B were composed of water containing 0.1% HCOOH and ACN

containing 0.1% HCOOH, respectively. Likewise, mass spectra were obtained in the range of 50 m/z to 2000 m/z. The analysis utilised an ACQUITY UPLC column measuring 100 mm × 2.1 mm, with a particle size of 1.8 µm. The capillary voltage was established at 2.50 kV, with the gas flow rate maintained at 800 L/h. This study then used varying temperature conditions for specific scenarios involving sample (20°C), column (40°C), and desolvation temperatures (550°C). A UNIFI software comprising a scientific library for compound matching and structural elucidation was then applied for compound identification.

Precise time-dependent solvent compositions were incorporated into a gradient elution programme. Initially, the composition consisted of 99% Solvent A and 1% Solvent B at 0.50 mins. This composition was then modified to 65% Solvent A and 35% Solvent B after 16.00 mins. The program shifted to 0% Solvent A and 100% Solvent B at 18.00 mins. Lastly, the composition reverted to 99% Solvent A and 1% Solvent B at 20.00 mins. Numerous parameters were used to identify the molecular components of the biosurfactant based on LC-QTOF-MS results, such as retention time (RT), peak intensity, and mass-to-charge ratio (m/z) values. A comparative analysis was then carried out between the acquired spectra and the scientific library in the UNIFI software. This process facilitated the identification of known compounds and the elucidation of structural characteristics. Biosurfactant components-based peaks and molecular structures were also determined using chromatograms and mass spectra fragmentation patterns, respectively.

Background noise was eliminated, and biosurfactant compound-based peaks were discerned for the blank solvent (ACN). Consistency in compound identification was also verified through a cross-reference process involving data from positive and negative ionisation modes. Subsequently, potential biosurfactant functions were identified through further analysis of the peaks exhibiting high intensity and matching fragmentation patterns. Compound distribution and intensities were then illustrated via graphical data [extracted ion chromatograms (EIC) and total ion chromatograms (TIC)]. The correlation between the predominant compounds in the biosurfactant sample and physicochemical properties was also assessed through RTs and peak areas.

3.6 Stability Studies of the Biosurfactant

Significant surface-active properties are indicated in biosurfactants as amphiphilic compounds synthesised by microorganisms. This feature renders biosurfactants applicable in diverse industrial and environmental contexts. Conversely, substantial relationships are observed between functionality and external conditions (temperature, time, and salinity). Multiple elements are then impacted by these correlations, including structural integrity, interfacial activity, and overall performance. Hence, the robustness of biosurfactants across diverse environmental conditions must be examined through stability analysis. This necessity can link to the role of biosurfactants in practical applications (concrete admixtures, bioremediation, and corrosion inhibition).

Varying thermal, time-dependent, and salinity conditions were then adopted in this study to evaluate the stability of the fungal-based biosurfactants. The effect of temperature was assessed to understand the thermal tolerance of the biosurfactant and its ability to maintain functionality at elevated or extreme temperatures. Moreover, the thermal tolerance of the biosurfactant and its capacity to retain functionality under elevated or extreme temperatures is investigated based on the time-dependent stability test. The efficacy of biosurfactants in high-salt conditions, which is significant for marine and saline-affected industrial systems, was also examined through salinity stability to evaluate the effectiveness in high-salt environments.

3.6.1 Effect of Temperature on Biosurfactant Properties

The sample was heated to 60°C to assess the correlation between temperature and biosurfactant activity. This sample was then cooled to room temperature. A comparative analysis was also performed between the sample and unheated crude biosurfactant via the E_{24} test to examine their effectiveness as an emulsifier. Sena et al. (2018) explained that emulsification activity was not affected for a biosurfactant at 100°C for 60 mins. The temperature ranges up to 60°C was selected based on the findings of Lesik et al. (2021), which demonstrated that phospholipid-based corrosion inhibitors retain high inhibition efficiency at this elevated temperature.

3.6.2 Time-Based Assessment of Biosurfactant Activity and Fungal Growth Impact

The relationship between shelf life and emulsification properties of the biosurfactant was assessed through a time-based analysis. This emulsification capacity was evaluated using the E_{24} test after storing the crude biosurfactant in a refrigerator at 4°C for 60 days. A comparative analysis was then conducted against the initial values to determine any changes that occurred throughout the storage period. This study also utilised Petri dishes containing PDA and 10 µL of crude biosurfactant to investigate the association between shelf life and fungal growth. These plates were incubated at room temperature (~25°C), and the growth of fungal mycelium was observed for 60 days. Fungal development variations were observed based on growth consistency and pattern.

3.6.3 Effect of High Salinity on Emulsification Properties

The NaCl was incorporated to reach a 30% v/v concentration for examining the correlation between salinity and emulsification properties of the biosurfactants. This process involved applying the E_{24} technique to the salinised biosurfactant. Finally, a comparative analysis was performed between the salinised biosurfactant and control (without NaCl). The NaCl concentration of 30% was selected following the findings of Sena et al. (2021), who reported that a semi purified biosurfactant remained stable after exposure to high ionic strength conditions, including the addition of 30% NaCl (w/v). In that study, Tween 80 (0.2% w/v) was employed as a conventional surfactant control, providing a benchmark for comparative performance. Accordingly, the adoption of a 30% NaCl condition in the present study enables evaluation of the biosurfactant's emulsification stability under severe salinity stress.

3.7 Toxicity Screening

A 14-day toxicity and compatibility analysis were conducted to evaluate the potential biological impact of the phospholipid-based biosurfactant derived from *Rhizopus sp.* based on aquatic and terrestrial biological models. This study investigated the relationships between biosurfactants, marine organisms, and plant health in an aquatic environment. Generally, developmental toxicity, general toxicity, and drug

screening are usually performed using zebrafish, which serve as a reliable vertebrate model (Lammer et al., 2009). Chahardehi et al. (2020) reported that the zebrafish model is a viable alternative to traditional laboratory animals (rats, mice, and rabbits) and provides relevant insight into both environmental and potential human health risks due to its conserved organ structure and metabolic functions. Notably, the three-lobed liver of zebrafish closely reflects human hepatic function, including the absorption, metabolism, and synthesis of lipids, vitamins, proteins, and carbohydrates. The study effectively assessed drug toxicity through zebrafish embryotoxicity tests. Thus, a valuable toxicology model for elucidating developmental toxicity mechanisms could be accomplished using zebrafish due to their phylogenetic proximity to mammals,

This study employed adult zebrafish (*Danio rerio*) due to their well-developed central nervous system (CNS) and intricate behavioural responses. Compared to embryos, adult zebrafish are more appropriate for evaluating long-term toxicity effects. Generally, neurotransmitter systems analogous to humans are presented in zebrafish, establishing their significance as a model for toxicity analysis. These systems include glutaminergic, cholinergic, serotonergic, dopaminergic, and Gamma-aminobutyric acid (GABA)ergic pathways. Considering that adult zebrafish are a less sentient species, they adhere to the principles of the 3Rs principles (replacement, reduction, and refinement). Consequently, vertebrate testing-related issues can be mitigated. The relevance of zebrafish in evaluating biosurfactant toxicity is also denoted in most behavioural and neurotoxicology-related studies (Faria et al., 2018). Meanwhile, the ecological impact of chemical substances necessitates prediction through plant-based toxicity assessments. This process can confirm that the use of newly developed biosurfactants does not negatively impact terrestrial ecosystems by examining their toxicity regarding environmental applications (Pele et al., 2019). Hence, this study assessed potential health risks to living organisms and ecological impacts on the environment for the *Rhizopus sp.*-based biosurfactant through a 14-day toxicity analysis on fish and plants.

Monstera adansonii and Syngonium podophyllum were selected as test species because of their high tolerance to indoor and aqueous growth conditions, making them suitable for controlled laboratory toxicity screening. Their ability to survive and grow in water-based systems allows direct assessment of biosurfactant exposure under simplified hydroponic conditions, which is relevant for evaluating potential environmental impacts associated with waterborne release.

3.7.1 Toxicity Screening Using Zebrafish

A 14-day chronic toxicity test involving adult zebrafish was conducted under controlled laboratory conditions to assess the toxicity of the biosurfactant. Under a 14:10 h light and dark cycle prior to exposure, healthy adult zebrafish (3–6 months) were acclimated for seven days in aerated distilled water (27 ± 1°C). A semi-static exposure regime was employed, whereby fish were introduced into individual 2 L test tanks containing the biosurfactant at a concentration of 20% (v/v). Simultaneously, a negative control (distilled water) was prepared. A total of 10 fish were in each concentration group, which was maintained in individual 2 L tanks equipped with oxygenators.

These fish were observed daily for mortality, behavioural changes, physiological responses, and sublethal effects during the 14-day exposure period. Examples of observed elements included swimming patterns, feeding behaviour, gill movement, body colour changes, and fin damage. The stable environmental conditions were also validated by examining the water quality parameters (pH, dissolved O_2, and temperature). Subsequently, the sublethal toxicity impacts were investigated by documenting the fish mortality and physiological responses. This study also ensured that ethical considerations were adhered to by implementing humane endpoints. Fish exhibiting severe distress were promptly euthanised following approved protocols (OECD, 2013). This methodology was modified based on established protocols for aquatic toxicity testing (OECD, 2013; Faria et al., 2018)

3.7.2 Toxicity Screening with Monstera adansonii and Syngonium podophyllum

This study introduced two 1 L glass beakers containing 900 mL of solution, comprising a 20% biosurfactant and negative control (distilled water), respectively. This study also involved potted plants of two species: (i) *Monstera adansonii* and (ii) *Syngonium podophyllum* as depicted in Figure 3.23. The physiological stress indicators in the plants spanning 14 days were then systematically monitored, such as wilting and chlorosis. Phytotoxicity signs were also examined daily through visual inspections. Moreover, any negative impacts related to biosurfactant exposure were determined through a qualitative evaluation of plant health based on photographic documentation. A calibrated pH metre was also utilised to measure the pH of the water periodically.

Thus, any fluctuations in acidity or alkalinity resulting from biosurfactant interaction could be identified through this process (Kristen, 1997). The samples were then examined for alterations in the plants at the conclusion of the 14-day period. These monitored changes included wilting or yellowing of the leaves, root elongation, and leaf growth.

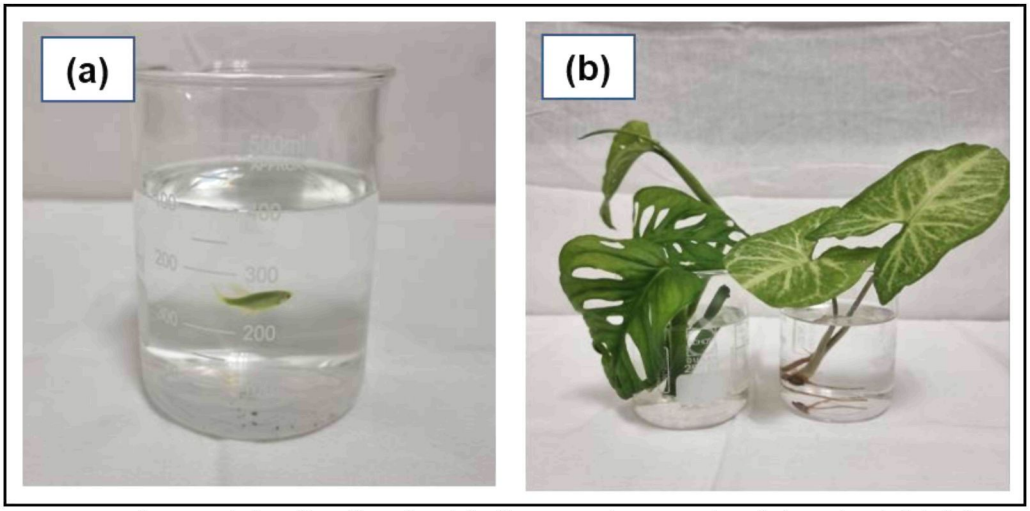

Figure 3.23 The Toxicity Studies On (a) Green Zebra Danio Fishes And (b) *Monstera Adansonii* With *Syngonium Podophyllum*

3.8 Corrosion Inhibition Study

The efficiency of corrosion inhibition was assessed through weight loss and ER methodologies for biosurfactants produced by four fungal genera: (i) *Fusarium sp.*, (ii) *Rhizopus sp.*, (iii) *Trichoderma* sp., and (iv) *Penicillium sp.* Among these biosurfactants, the *Rhizopus sp.*-based biosurfactant exhibited the greatest corrosion inhibition. Additional corrosion inhibition analysis was then performed using EIS to identify the optimal concentration for effective corrosion prevention. The surface morphology of the treated samples was also evaluated using a SEM-EDX tool. Table 3.4 presents a summary of the conducted tests.

Table 3.4
Summary Of Experimental Methods For Corrosion Inhibition Analysis

Fungal Strain	Gravimetric Measurement	Electrical Resistivity	EIS	SEM & EDX
Rhizopus sp.	✓	✓	✓	✓
Penicillium sp.	✓	✓	✗	✗

Fungal Strain	Gravimetric Measurement	Electrical Resistivity	EIS	SEM & EDX
Trichoderma sp.	✓	✓	X	X
Fusarium sp.	✓	✓	X	X

3.8.1 Preparation of Materials and Inhibitor Solutions

The Tween 80 (P8074) served as a positive control synthetic surfactant in this study, which was obtained from Sigma Aldrich, USA. Mild steel bars were procured from a local supplier and was manufactured by Ann Joo Steel Sdn. Bhd (see Figure 3.23).

3.8.1.1 Mild Steel Bars

Mild steel bars (MS144:2014, G250) with the chemical composition presented in Table 3.5 and Figure 3.24 were used throughout this study. The use of plain, non-ribbed steel bars allows for a more precise evaluation of the effect of corrosion inhibitors on the intrinsic bonding properties between steel and concrete. This study aims to assess the fundamental bonding mechanism between steel and concrete without the influence of mechanical interlocking provided by ribs. Ribbed bars enhance anchorage, which could complicate the interpretation of results. Therefore, plain bars provided a uniform surface, reducing experimental uncertainties linked to variations in rib height, spacing, or orientation that could influence τ.

Test specimens were also prepared using a series of emery papers for abrasion, ranging from coarser (220) to finer (1200) grades. These specimens were subjected to a comprehensive cleaning and degreasing procedure utilising distilled water, acetone, and deionised water. Considering that the cleanliness of mild steel bars directly affects measurements, weight assessments, and corrosion inhibition testing, the cleaning process was essential for removing contaminants. The images in Figure 3.25 provide a visual representation of the pre-treated specimens, emphasizing their condition before further experimentation.

Table 3.5
Chemical Composition Of Mild Steel Bar (MS144:2014) Grade 250

Chemical	C	Si	Mn	P	S	V	Cu	Ni	Cr	Mo	Nb	C_{eq}
Composition	×100			×1000			×100				×10000	×100
(%)	19	17	66	21	18	3	19	6	12	1	50	34

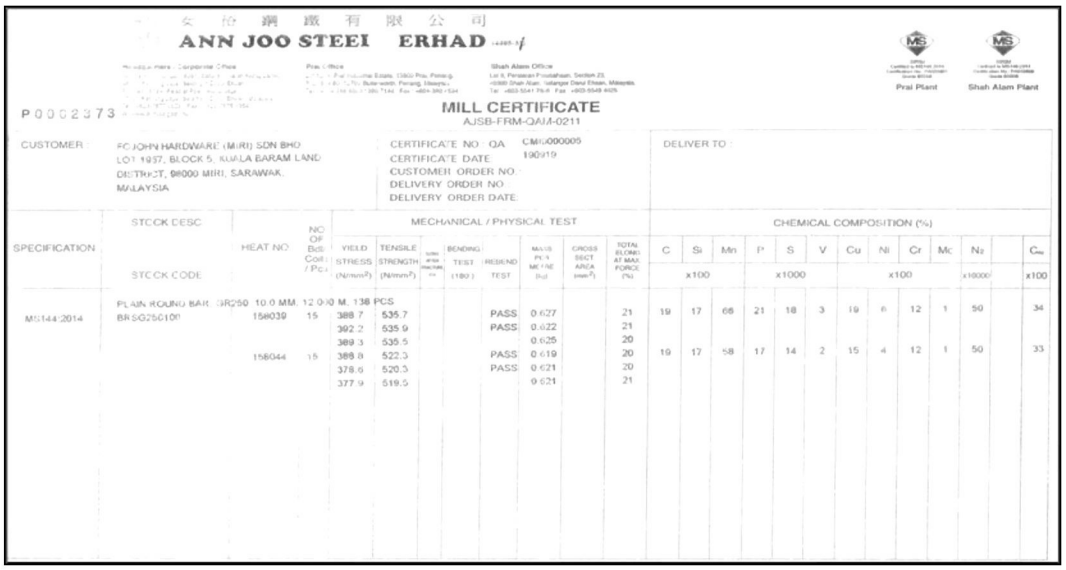

Figure 3.24 The Mill Certificate Of The Mild Steel Bars Used In The Corrosion Inhibition Analysis

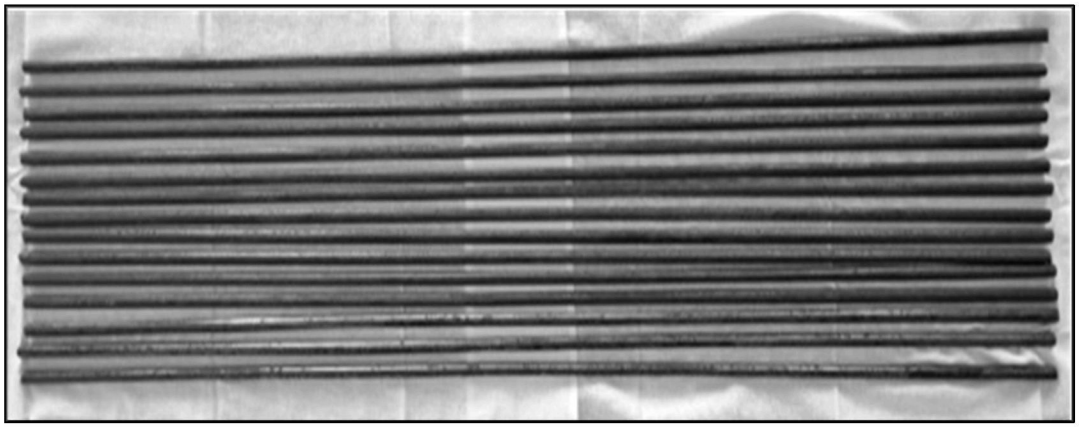
Figure 3.25 Mild Steel Bars Used For The Corrosion Inhibition Studies

3.8.1.2 Tween 80 Surfactant

Tween 80 is a high-viscosity, non-ionic synthetic surfactant, which is also referred to as polyoxyethylene sorbitan monooleate (Wahyuni et al., 2020). El-Nabey et al. (2017) demonstrated that the addition of 0.01 M Tween 80 into a zinc phosphate

coating solution markedly improved the corrosion resistance of steel. This process resulted in a 90% IE and a decrease in coating porosity from 49.2% to 10.5%. The study noted that a barrier to corrosive agents (moisture and aggressive ions) was created on the metal surface. Hence, direct metal exposure and corrosion were effectively mitigated. Wahyuni et al. (2020) recorded improved viscosity and energy activation when asphalt emulsion contained Tween 80. A chemisorption mechanism is often observed to be more prominent than simple physisorption, which is based on the Tween 80 adsorption adhering to the Flory-Huggins and kinetic-thermodynamic models through thermodynamic analysis. Abd-El-Nabey, El-Housseiny, and El-Kshlan (2017) and Li et al. (2009) published similar outcomes based on their SEM and EDX analyses. These studies concluded enhanced corrosion resistance for Tween 80-treated metal surfaces due to lower roughness and improved coating integrity. Wang et al. (2021) underscored the synergistic effect of Tween 80 on inhibitor performance. The study enhanced corrosion IE by 24.2% for grape seed proanthocyanidin extract containing Tween 80. Overall, Tween 80, as an effective positive control surfactant in corrosion inhibition analysis, was indicated by all these previous studies. This conclusion was based on the improved steel protection owing to significant surface adsorption and film-forming capabilities.

Stable emulsions are demonstrated when Tween 80 is combined with water or other liquids. Therefore, this observation indicates that the compound is a water-soluble non-ionic surfactant. Lower surface tension and improved uniform dispersion of hydrophobic with hydrophilic components can also be observed owing to the amphiphilic nature of this compound. Consequently, mixtures that would typically separate can be effectively stabilised (Gutiérrez-Méndez et al., 2022). The dispersion of cement particles and enhanced workability of the fresh mix in concrete mixtures can also be attained through this compound functioning as a plasticiser. A more uniform and cohesive mixture is presented when internal friction between particles is lowered due to increased flowability (Wahyuni et al., 2020). Additionally, positive relationships are demonstrated between the hydration of cement, setting time, and overall mechanical properties of hardened concrete when surfactants are incorporated (Unosson et al., 2016). These characteristics render surfactants (Tween 80) appropriate for use as positive control surfactants and concrete admixtures.

3.8.2 Weight Loss Measurements

The weight loss measurement represents the most prevalent and straightforward among corrosion monitoring techniques. This method entails subjecting a material specimen (the coupon) to a process environment for a specified duration. The procedure is followed by specimen removal for analysis (Speight, 2014). Thus, the weight loss measurements in this study were conducted on mild steel coupons immersed in solutions with varying biosurfactant concentrations based on four fungal strains (*Penicillium* sp., *Rhizopus sp.*, *Trichoderma sp.*, and *Fusarium sp.*). A commercially available surfactant (Tween 80, product code 8074) was employed to evaluate the efficacy of biosurfactants relative to their synthetic counterpart as suggested by El-Nabey, El-Housseiny and El-Kshlan in their previous research (B. A. Abd-El-Nabey, S. El-Housseiny, H. M. El-Kshlan, 2017). This study then utilised a 0.9% NaCl solution devoid of any added biosurfactant as the negative control group while simulating the typical salinity of marine water in Sarawak.

The plain mild steel bars (15 mm in length and 10 mm in diameter) were also cut from a single mild steel bar to maintain uniform chemical consistency. Subsequently, coupons without defects were chosen to prevent pitting or localised corrosion, which could influence the outcomes. The surface of the specimens was then abraded with emery papers, advancing from coarser (220) to finer (1200) grades to obtain a smooth finish.

Thorough rinsing with distilled water was conducted on these coupons following abrasion. This process was followed by degreasing with acetone and washing with deionised water. The cleaned specimens were then air-dried for 30 mins at room temperature. This study also indicated that the cleaning process was crucial for preparing specimens for immersion in inhibitor solutions while removing contaminants. Given that cleaning was significantly correlated with the precision of weight measurements and the efficacy of corrosion inhibition testing, this process in mild steel bars was critical. Furthermore, individual weight assessments were carried out to determine the densities of these specimens before immersion (Parthipan et al., 2018).

Figure 3.26 reveals the condition of pre-treated specimens prior to subsequent experimentation. Certain cleaned and air-dried specimens were immersed in 0.9% NaCl solution without biosurfactants (negative control). In contrast, the remaining specimens were placed in a similar solution containing 5%, 7.5%, 10%, 12.5%, 15%, 17.5% and

20% biosurfactants and Tween 80 (positive control). Each piece of specimen was affixed with a thread to facilitate its suspension in the medium. All the solutions were maintained at room temperature. Table 3.6 provides a detailed overview of the solutions and their respective concentrations.

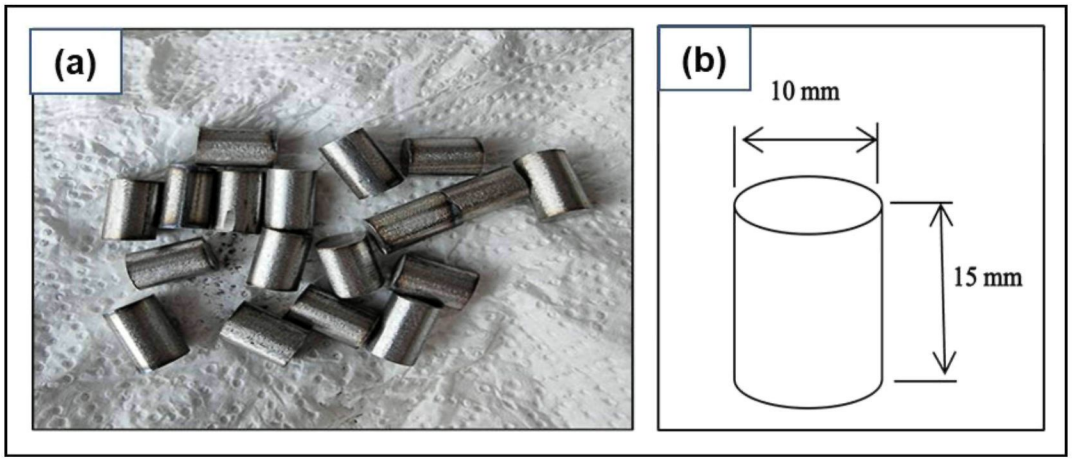

Figure 3.26 (a) The Cleaned Mild Steel Bars And (b) Dimension Of The Specimens

Table 3.6
Summary Of The Biosurfactant Concentrations Used In Corrosion Inhibition Analysis

Solution	**Concentration (%)**						
0.9%NaCl	100.0						
BS 01	5.0	7.5	10.0	12.5	15.0	17.5	20.0
BS 02	5.0	7.5	10.0	12.5	15.0	17.5	20.0
BS 03	5.0	7.5	10.0	12.5	15.0	17.5	20.0
BS 04	5.0	7.5	10.0	12.5	15.0	17.5	20.0
Tween 80	5.0	7.5	10.0	12.5	15.0	17.5	20.0

Specimens were then extracted from the solution after immersion periods of 14^{th}, 28^{th}, and 100^{th} days to capture the short, medium, and long-term corrosion behaviour of the steel specimens. Each bar was also cleaned with a microfibre cloth and fine brush before weighing to remove any traces of rust, ensuring accurate measurements. A 30-min air-drying period at room temperature was conducted prior to the weighing process. Likewise, the pH value of corrosion solutions was monitored during the gravimetric test. The pH value of corrosion solution containing biosurfactant samples consistently exceeded 8. In civil engineering applications, the protective passive layer of steel must maintain a pH value exceeding 10.5 to inhibit corrosion

(Ai et al., 2016). All experiments were also conducted in triplicate to ensure reliability, and the average weight loss of the specimens was carefully recorded.

The percentage of IE can be determined using an equation expressed as follows (Hussin & Kassim, 2011):

$$\text{IE}\ (\%) = \frac{\text{Wo} - \text{W}'}{\text{Wo}} \times 100 \tag{3.3}$$

where Wo and $W^{'}$ denote the weight loss values without and with the inhibitor, respectively. The CR (mm/year) is also computed as follows (G. Płaza & Achal, 2020):

$$CR = \frac{87600 \times C}{AtD} \tag{3.4}$$

where C represents the weight loss (g) that is calculated by subtracting the final weight from the initial weight; A represents the surface area of the specimen (cm^2); t represents the exposure time (h); and D represents the density of the material (g/cm^3).

3.8.3 Surface Morphology and Physical Characteristic Observations

The specimens were systematically removed and examined for corrosion deposits after the immersion period. Several indicators were observed on these specimens, including their colouration, distribution, intensity, and biofilm formation on the surfaces. Subsequently, a fine brush and a soft microfibre cloth were employed to remove the loose corrosion products carefully. The examination of the specimens was then repeated to assess alterations in surface colouration, corrosion patterns, and localised or uniform corrosion traces. Meanwhile, corrosion activity signs were identified in the immersion solutions based on several indicators. These indicators included corrosion deposits, coagulation, and solution clarity changes. Consequently, the correlations between biosurfactants, the surrounding environment, and potential ecological implications could be examined based on these assessments.

3.8.4 Electrical Resistivity Test

The ER changes of a metal element subjected to a corrosive environment can be quantified using the ER method (Sabri et al., 2012). Typically, an increase in ER is observed when the cross-sectional area of a metal reduces due to progressing corrosion. This observation suggested a relationship between resistance and metal loss, which the temporal rate of change can indicate the CR (Speight, 2014). Therefore, ER testing was applied on the specimens utilised in the weight loss method for evaluating the corrosion inhibition properties of biosurfactants at 100 days. A comparative analysis was also performed between biosurfactants (test inhibitor), Tween 80 (positive control), and 0.9% NaCl (negative control). The ER of corroded mild steel specimens was examined using a Kyoritsu Insulation-Continuity Tester Model 3005A. (Sabri et al., 2012) validated that the tool provided enhanced sensitivity and reading accuracy compared to a standard digital multimeter. Consequently, the association between corrosion and inhibitor performance on the electrical conductivity of the steel bars was identified. This tester was set on continuity (Ω) mode for resistance measurement. Specifically, the 0–200 Ω range was selected as the resistance range for specimens exhibiting moderate corrosion based on the onset of oxide layer formation.

This study established the methodology outlined by (Brodňan et al., 2017) as the framework for the experimental procedure. A delicate soft brush and a clean cloth were used on the specimens before each test to eliminate surface contaminants that could influence the accuracy of the readings. The resistance values for each specimen were also obtained by connecting the tester probes to both ends of the specimen. Thus, the current application and voltage measurement enabled accurate determination of resistance values. Measurements were also conducted in triplicate to ensure the reliability and consistency of the data. Generally, the ER method relies on the principle that alterations in ER are associated with cross-sectional area changes of the specimen due to corrosion. The ER of specimens can be determined using an equation formulated as follows:

$$R = \frac{L}{A} \cdot r \tag{3.5}$$

where R signifies the measured resistance (Ω); r signifies the specific resistance (Ω mm^2 m^{-1}); A signifies the cross-sectional area of the specimen; and L signifies the length of the specimen

The resistance values were then examined to determine CRs. Higher resistance values implied increased oxidation, corrosion products, and reduced electrical conductivity due to inhibitor performance. Lower resistance values suggested minimal corrosion and good electrical continuity.

3.8.5 Electrochemical Impedance Spectroscopy (EIS)

Mild steel bars (7 mm in length and 10 mm in diameter) were cleaned and abraded using 100, 400, 600 and 1200-graded emery papers. This process was followed by acetone degreasing and rinsing with distilled water. Subsequently, the mild steel bar was soldered to establish a connection between the mild steel surface and the copper conductor wire. The soldered mild steel was positioned in a small pipe tube, and epoxy was applied to fill the void space within the tub. This steel was then dried at room temperature overnight. Figures 3.27 and 3.28 portray that the bottom surface of mild steel remains uncovered for the purpose of corrosion analysis.

Likewise, the EIS was conducted using a Gamry Instrument Reference 600 Potentiostat/ Galvanostat/ZRA (Gamry instrument, USA) over a frequency range of 10^{-2} to 10^5 and 5 mV signal amplitude. Initially, open circuit potential (OCP) measurement was conducted for 30 mins as a prerequisite step. This analysis utilised jacketed three-electrode cells [counter electrode = carbon rod, reference electrode = silver rod, and working electrode = mild steel (10mm × 7 mm)], which were immersed in 40 mL of 0.9% NaCl solution (pH = 4.75).

The acquired EIS data was represented as a Nyquist plot. This plot was fitted into an equivalent electrical circuit through the Gamry Echem Analyst software to derive various electrochemical impedance parameters (see Figures 3.30 and 3.31). These parameters were solution resistance (R_s), double layer constant phase element, (CPE_{dl}), charge-transfer resistance (R_{ct}), surface heterogeneity factor (n), Warburg diffusion element (W_d), and IE. The IE can be measured as follows (Hussin & Kassim, 2011):

$$IE\% = \frac{Rct}{R'ct} X\ 100 \tag{3.6}$$

where R'_{ct} and R_{ct} represent the charge-transfer resistance (Ω cm^2) of mild steel in the presence and absence of biosurfactant or Tween 80, respectively.

Figure 3.27 The Soldered Mild Steel Before EIS Analysis

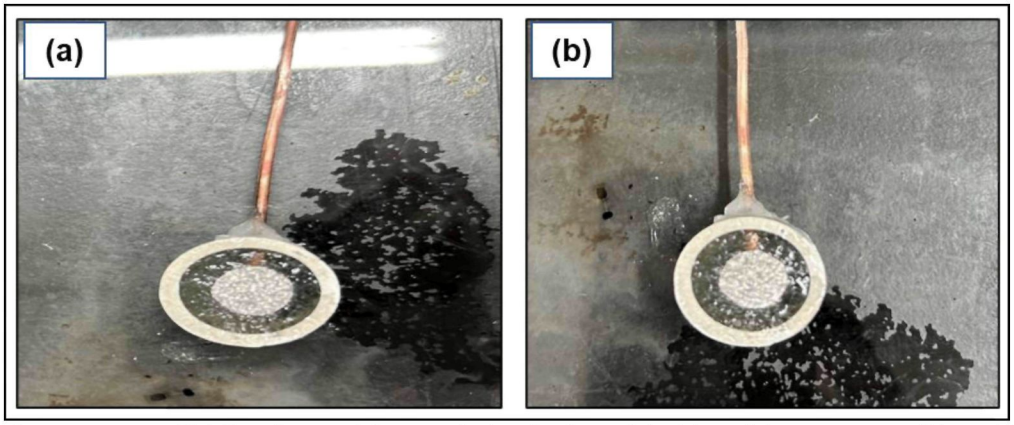

Figure 3.28 Mild Steel Bar After EIS Analysis With (a) 10% Tween 80 (b) 10% Biosurfactant

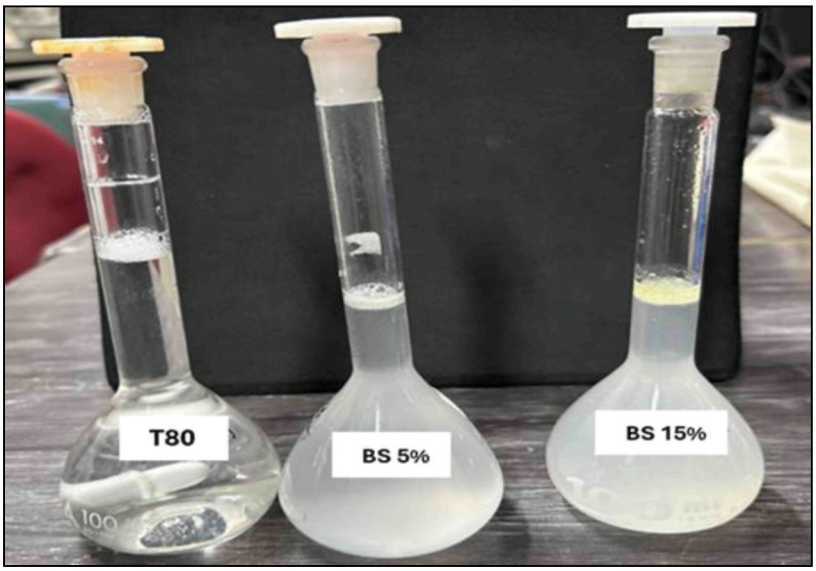

Figure 3.29 The 10% Tween 80, 5% Biosurfactant, And 10% Biosurfactant In 0.9 % NaCl Solution

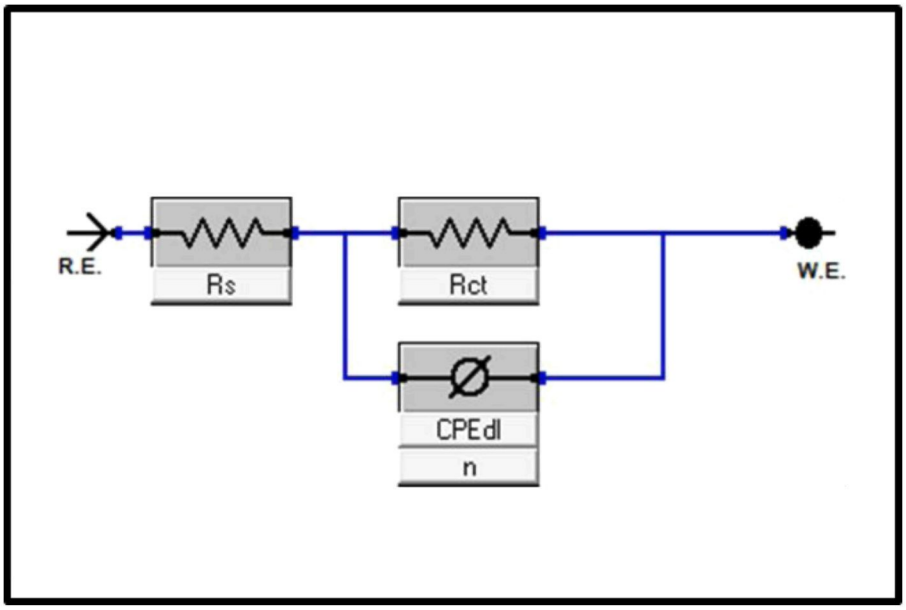

Figure 3.30 The Randle's Constant Phase Angle Element (CPE) Equivalent Circuit For Blank Mild Steel (Control)

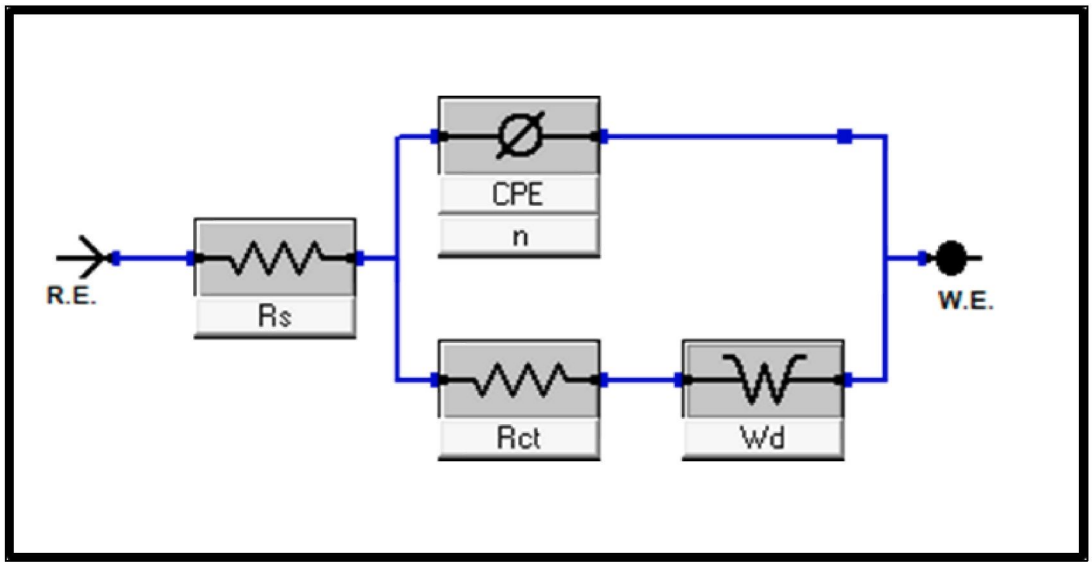

Figure 3.31 The Proposed Equivalent Circuit To Fit Nyquist Plot Of EIS Data For The Mild Steels In The Presence Of Biosurfactant Displaying Warburg Impedance

3.8.6 SEM and EDX

The surface morphology of the corrosion products from mild steel specimens was assessed using the SEM-EDX tool. The specimens subjected to these analysis were the same specimens from the weight loss analysis, which exhibited the highest efficiency of corrosion IE. The specimens were submerged in phospholipid biosurfactants at concentrations of 5%, 10% and 15%, 10% Tween 80 (positive control), and a blank (without the inhibitor). These specimens were extracted from their respective solutions and underwent a cleaning process that included gentle brushing to remove surface rust and biofilm following a 100-day immersion period. The process succeeded by rinsing with deionised water and air drying prior to conducting weight loss measurement and ER test.

Initially, specimens were mounted on carbon stubs with double-sided adhesive tape for the SEM analysis. This process involved examining the surface characteristics of the treated specimens based on a scanning electron microscope (QUANTA FEI 650) at 500× and 1000× magnifications. The areas displaying evident corrosion and surface modifications were focused as the designated regions of interest (ROIs). Subsequently, a comprehensive analysis was conducted for regions exhibiting certain characteristics. These features were rust formation, pitting, or discernible alterations resulting from the treatments that were targeted for detailed analysis. Consequently, a focused

examination of the region most vulnerable to corrosion was facilitated by this method. This analysis involved an Oxford Instruments X-Max model, in which the elemental composition of mild steel specimens was computed based on an electron beam voltage of 10 kV. Overall, this comprehensive analysis sought to correlate observed morphological changes with elemental composition, offering information into the corrosion IEs of the tested inhibitors.

3.8.7 R_m Test of Biosurfactant-Coated Reinforcement Bars

The tensile properties of steel bars treated with biosurfactants were assessed through a tensile test to evaluate the potential enhancement in mechanical strength resulting from the application of the biosurfactant. The assessment was limited to the determination of R_m as this parameter provides a direct indicator of material integrity and load-bearing capability following corrosion exposure. Fatigue testing was not considered in this study because it involves long-term cyclic loading and service-life performance evaluation, which falls beyond the scope of the present investigation that focuses on the short-term mechanical implications of corrosion inhibition treatment.

The tensile test was conducted in accordance with Malaysian Standard MS ISO 15630-1:2012 for reinforcing and prestressing steel using a Universal Testing Machine (UTM). The reinforcement bars employed were mild steel bars conforming to MS 144:2014 (Grade G250), with their chemical composition detailed in Table 3.5. Ribbed steel bars with a nominal diameter of 10 mm (R10) were sectioned into specimens of 600 mm length prior to testing.

Surface preparation of the steel bars was performed to ensure uniformity and repeatability. The specimens were abraded sequentially using emery papers of increasing fineness (220, 400, 500, 800, and 1200 grit), followed by rinsing with distilled water, degreasing with acetone, and final washing with deionised water. The cleaned specimens were air-dried at room temperature for 30 minutes to remove residual moisture. All reinforcement bars were verified to be straight and free from deformation, and proper axial alignment was ensured in accordance with the recommendations of Shaffer (2015). Each test condition was conducted in triplicate to enhance the reliability and reproducibility of the results.

The Phospholipids biosurfactant was used in this study. To simulate a corrosive environment, a 0.9%NaCl saline solution was used as the corrosive medium to expedite

corrosion. Following surface preparation and initial weighing, the steel bars were immersed in the saline solution solutions with and without biosurfactant addition, representing the experimental and negative control conditions, respectively. Biosurfactant concentrations were varied from 5%, 10%, 15%, to 25% (v/v). During immersion, plastic spacers were employed to suspend the steel bars within the solution, ensuring uniform exposure on all surfaces. The conditioning setup is illustrated in Figure 3.32(a–b).

After an exposure period of 28 days, the steel bars were retrieved from the solutions, and corrosion products were carefully removed using soft cloths and fine brushes to avoid surface damage. The mass loss of each specimen was then measured to quantify corrosion severity. Subsequently, the specimens were air-dried and subjected to tensile testing for the determination of R_m testing.

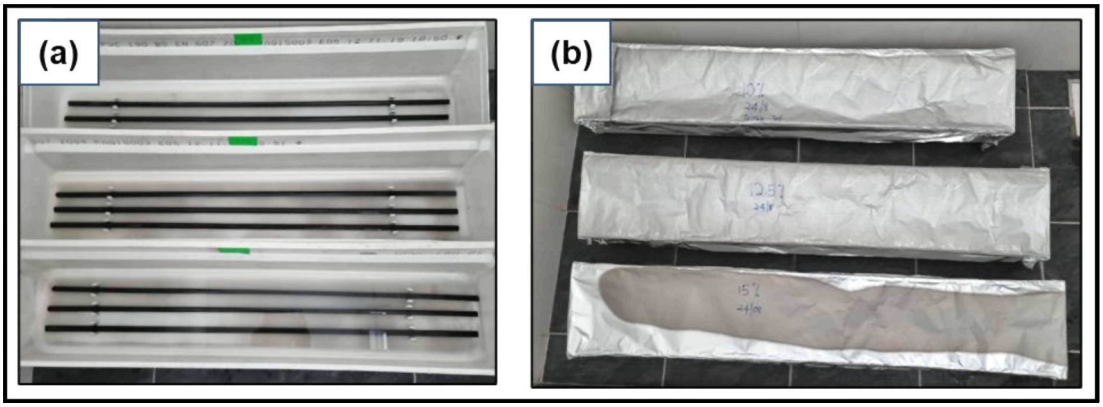

Figure 3.32 (a – b). The Conditioning Of Steel Bars With Different Biosurfactant Concentrations

The tensile tests were performed using the Universal Testing Machine (UTM), in which each bar was subjected to tensile force until failure to ascertain the ultimate R_m. The maximum applied load was set at 45 kN. Several parameters were then measured, including R_e (N/mm^2), R_m (N/mm^2), ultimate stress (N/mm^2), nominal breaking stress (N/mm^2), actual breaking stress (N/mm^2) and percentage of elongation (%). Figure 3.33 (a -b) depicts the tensile testing procedure conducted on the steel bars.

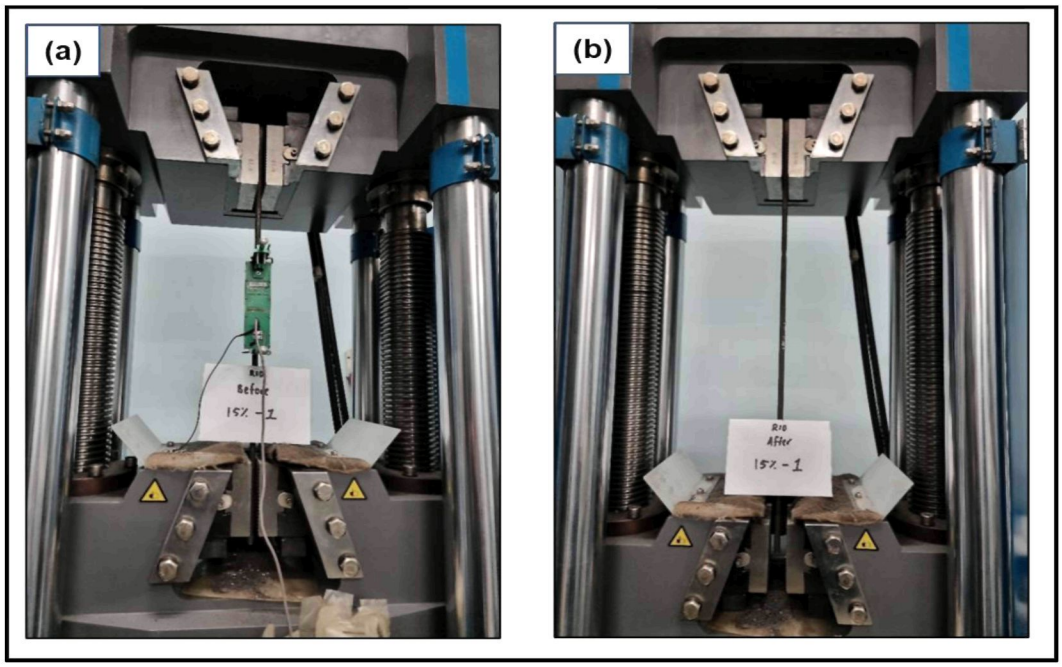

Figure 3.33 The Tensile Test On The Reinforcement (a) Before And (b) After Applied Force

3.9 Mechanical Performance Evaluation of RC with Biosurfactant as Admixture

Multiple tests were performed to assess the influence of biosurfactants on the performance of fresh and hardened RCs. The tests conducted included flowability, f_c, f_s, and τ tests. These tests aimed to evaluate the impact of phospholipid-based biosurfactants from *Rhizopus oryzae* on the characteristics of RC and non-RC when utilised as a bio-admixture. Initially, the workability of fresh concrete with and without Tween 80 and biosurfactant was analysed using the flowability test (vertical slump, slump flow, and T50 tests). A comparative analysis concerning flowability was then carried out between Tween 80 with biosurfactant and plain concrete (negative control sample). Consequently, the correlation between biosurfactants and fresh concrete properties could be comprehended through this test. These properties included placement ease, compaction, and homogeneity. A lower probability of voids and defects could then be indicated that superior concrete consolidation occurred under enhanced workability.

A comparison between biosurfactant-admixed concrete and control samples was observed by measuring the strength of concrete cubes in the f_c test. The link between biosurfactants and compressive properties of concrete could be obtained through this

test for examining the structural integrity and load-bearing capacity of RC. Meanwhile, the bending capacity and ductility of steel-RC and non-RC beams were evaluated using the f_s test. The association between biosurfactants and mechanical behaviour could be provided through the f_s and elasticity parameters. This data was useful for exploring the resistance of the specimens to deformation and failure. Alternatively, the τ between biosurfactant-coated steel bars and the concrete cover was assessed via the τ test. The τ between the concrete cover and reinforcement could be gathered to comprehend the impact of biosurfactant treatment on the durability and integrity of the RC structures.

This study employed two conditioning techniques: (i) admixed and (ii) migrating biosurfactant treatments. The fresh concrete mix was integrated with the biosurfactant in the admixed method as a bio-admixture. This process facilitated the assessment of its impact on both fresh and hardened concrete properties. In the migrating method, steel reinforcement bars were treated with biosurfactant through total immersion, utilising optimised conditions derived from previous studies. This method could improve the characteristics of the steel-concrete interface regarding the τ and corrosion resistance. The following subsections outline the experimental procedures for each test and the methodologies employed to evaluate the flowability and mechanical performance of biosurfactant-treated RC structures.

3.9.1 Selection of Concrete Materials

Concrete is a composite commonly used in construction, consisting of a mixture containing cement, water, fine aggregates (such as sand), coarse aggregates (such as gravel or crushed stone), and occasionally admixtures. The combination of these components results in a paste that hardens over time, attaining considerable strength and durability. Cement serves as the primary binder in concrete, undergoing a chemical reaction with water (hydration). This process produces a hardened matrix that unites the aggregates. The materials utilised for concrete mixing in this study were obtained and manufactured locally. Mixing and batching were also performed in the laboratory under regulated conditions.

3.9.1.1 Cement

The OPC 42.5N manufactured by Cahya Mata Cement Sdn. Bhd. was used in this study (See Figure 3.34). The physical and chemical features of the cement utilised in this study were derived from the chemical composition of OPC in Malaysia, as stipulated by MS 197-1: 2014 Specification for Portland Cement. Tables 3.7 and 3.8 summarise the composition of the materials (Ayob et al., 2016).

Figure 3.34 The OPC Is Manufactured By CMS Cement Industries Sdn. Bhd. In Sarawak

Table 3.7
Summary Of The Physical Properties Of The OPC 42.5N Used In This Study According To MS 197-1:2014

Physical Property	**Specification**
Fineness	Minimum 300 m^2/kg (Blaine)
Setting time	Initial setting time: not less than minutes, Final setting time: 160 minutes
Soundness	Maximum autoclave expansion: 10 mm
Compressive strength	Minimum 16 MPa at 7 days Minimum 32.5 MPa to maximum 52.5 Mpa at 28 days

Table 3.8
Summary Of The Major Chemical Constituent Of The OPC Based On MS 197-1:2014

Chemical Constituent	**Percentage composition (%)**
Lime (CaO)	68.85
Silica (SiO_2)	15.00

Chemical Constituent	Percentage composition (%)
Alumina (Al_2O_3)	4.30
Sulfur trioxide (SO_3)	4.00
Iron Oxide (Fe_2O_3)	3.96
Potassium oxide (K_2O)	1.08
Magnesia (MgO)	1.30
Barium oxide (BaO)	0.34
Titanium dioxide (TiO_2)	0.34
Others	0.73

3.9.1.2 Coarse and Fine Aggregates

This study utilised crushed granite as coarse aggregates, with particle sizes ranging between 10 mm and 20 mm (see Figure 3.35). The materials were obtained from a local quarry located in Jangkang, Sebuyau. The aggregates then underwent thorough washing with tap water to remove impurities (dirt, clay, dust, and loam) use, which could negatively impact the bond between the aggregate and cement paste (Ayob et al., 2016). Following washing, the aggregates were air-dried and stored in airtight plastic bags until the casting process commenced. The fine aggregates also consisted of uncrushed quartzite natural river sand, exhibiting a maximum particle size of 1.6 mm. These aggregates were similarly washed to ensure the removal of contaminants.

Coarse and fine aggregates were in a surface-saturated dry (SSD) condition to maintain consistency in the w/c ratio during the preparation of the mix. Table 3.9 summarises the physical properties of crushed coarse aggregates and fine aggregates.

Figure 3.35 The Crushed Granite Obtained From A Quarry At Jangkang, Sebuyau

Table 3.9
Summary Of The Physical Properties Of The Aggregates Used In Concrete Mixing

Aggregate	**Maximum size (mm)**	**SSD Specific gravity**	**Water adsorption (%)**
Natural fine aggregate	1.6	2.55	1.07
Natural coarse aggregate	20	2.63	1.26

SSD : Saturated-surface dry

3.9.1.3 Water

The concrete mix was prepared using potable water, which was pivotal in concrete production. This water utilised for concrete adhered to the cleanliness standards and was devoid of contaminants (dirt and organic matter). Small amounts of acidic substances in water could significantly degrade concrete. In contrast, oil presence could diminish strength and impede the setting process.

3.9.1.4 Reinforcing Bars

The reinforcing bars employed in the f_s and pull-out τ tests were mild steel bars (MS144:2014, G250) with a nominal diameter of 10 mm. Notably, the R_e and R_m were 388 N/mm^2 and 535 N/mm^2, respectively. The utilisation of plain and non-ribbed steel bars also facilitated a more precise evaluation of the effects of corrosion inhibitors on the fundamental bonding characteristics between steel and concrete.

3.9.2 Concrete Trial Mixes

Trial mixes were performed to ascertain the optimal proportions of concrete constituents (cement, water, fine aggregates, and coarse aggregates) necessary to achieve the specified strength and desired slump. Each mixture was formulated to reach a target characteristic strength of 30 N/mm^2 (MPa) after 28 days of curing. This process was vital for ensuring the concrete attained the necessary strength and workability for further applications in this study. Table 3.10 lists the nominal design requirements, and the materials are proportioned based on these figures. The quantities of materials were measured by weight in accordance with the JKR Standard Specification for Building Works 2014 (JKR, 2021). Four trial mixes were also formulated with different compositions (see Table 3.11). The cube specimens for each batch were then prepared in triplicate to ensure reliability.

Table 3.10
Summary Of The Nominal Design Requirement

Specified characteristic strength at 28 days	30 N/mm^2
Proportion defective	5% (k=1.64)
Standard deviation	8 N/mm^2
Cement type	OPC
Coarse aggregate	Crushed
Fine aggregate	Uncrushed
Water cement ratio	0.50 – 0.60
Vertical sump	75 mm (±25mm)
Maximum aggregate size	20 mm
% fine aggregate passing 600μm sieve	65%
Relative density / specific gravity of aggregate	2.70

Table 3.11
Summary Of The Mix Design For Concrete Grade 30 (kg/m^3)

Materials (kg/m^3 concrete)	**Design Mix 1**	**Design Mix 2**	**Design Mix 3**	**Design Mix 4**
W/C ratio	0.50	0.55	0.60	0.55
Water (kg)	205	205	205	225
Cement (kg)	410	373	342	409
Coarse Aggregate (kg)	1151	1174	1194	1110

Materials (kg/ m^3 concrete)	Design Mix 1	Design Mix 2	Design Mix 3	Design Mix 4
Fine Aggregate (kg)	654	668	679	631

Steel moulds measuring 150 mm × 150 mm × 150 mm were adequately prepared by tightening, cleaned of debris, and coated with a layer of motor oil on the inner surface. This procedure could inhibit water seepage from the mixture and ensure proper adhesion of concrete to the mould. Figure 3.36 displays that a free-fall concrete mixer is utilised for mixing the concrete. Coarse aggregates were combined with one-third of the mixing water for 2 mins. Cement and sand were then incorporated and mixed for 2 mins. This process was followed by the addition of the remaining mixing water. Prior to conducting slump tests, the concrete mixture was examined to confirm that all components were thoroughly blended for a uniform distribution. Subsequently, a substantial volume of concrete mixes was extracted for the vertical slump test, which was conducted within 10 mins to prevent alterations in the fresh concrete composition (See Figure 3.37). This slump test was performed in compliance with MS 26-1-2:2009, *Testing of concrete – Part 1: Fresh concrete – Section 2: Slump test (second revision).*

Figure 3.36 The Concrete Ingredients Mixed Within A Concrete Mixer In Batches According To Their Admixture Compositions

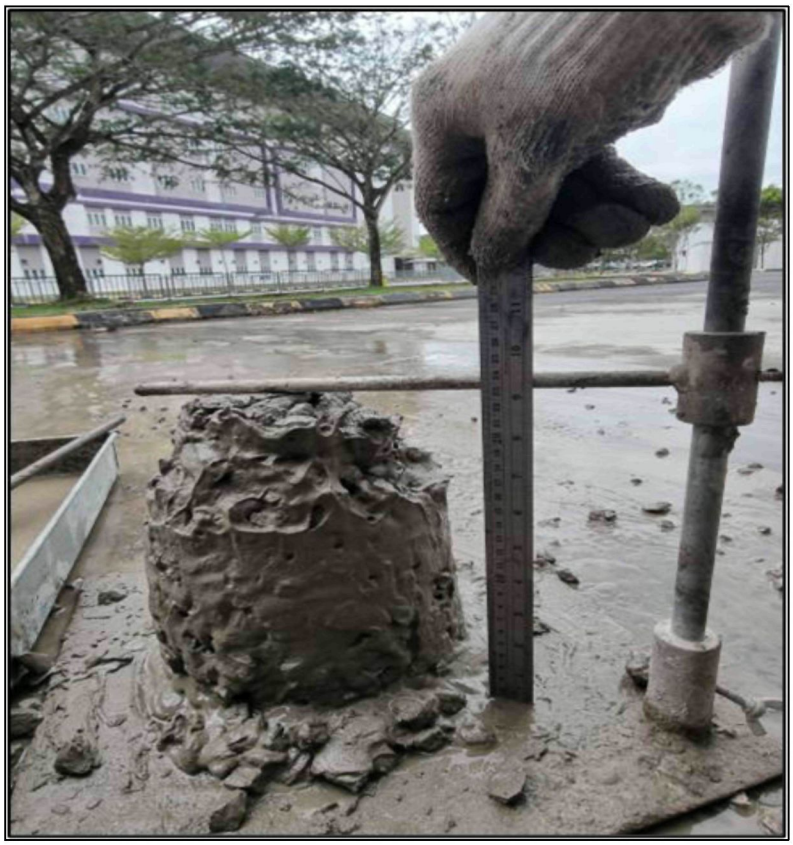

Figure 3.37 The Slump Test For Design Mix 1 Involves A Vertical Slump Of 70 Mm, Which Is Below The Required Slump For G30. The Low Slump Value Indicates A Dense Mix With High Aggregate Content, Making It Unsuitable As A Control Mix

The moulds were filled with three layers of concrete, each approximately 50 mm in depth. Every layer of concrete was tamped 25 times with a standard 16 mm steel rod as the tamping rod. Effective compaction then achieved consistent density and reduced air voids, in which the upper surface of each cube was rendered level and smooth. These moulds were stored in a cool and dry environment at room temperature for 24 h that was covered with moist gunny sacks. Following a 24-h period, the cubes were demoulded, labelled, and cured in a curing tank until the testing date.

The cured specimens were also tested for f_c on the 7^{th} and 28^{th} days following MS EN 12390-3:2012, *Testing hardened concrete - Part 3: Compressive strength of test specimens (Second revision).* One cube from each sample batch was evaluated for f_c over a period of seven days (JKR, 2021). Table 3.12 presents the data from these trials, encompassing vertical slump values and f_c. All tests were performed in triplicate, and the mean values were reported.

The findings demonstrated a distinct correlation between w/c ratio and performance characteristics of the concrete mixes. In the vertical slump test, these mixes improved with an increase in the w/c ratio. Particularly, Design Mix 4 (w/c ratio = 0.55) exhibited the highest predicted slump of 90 mm, signifying enhanced workability for applications requiring placement ease. On the contrary, Design Mix 1 (w/c ratio = 0.50) denoted the least slump of 70 mm, indicating a stiffer mix. The elevated coarse aggregate content in Design Mix 1 also resulted in diminished workability.

A negative correlation was observed between the w/c ratio and f_c. The maximum f_c of 39.3 MPa at 28 days was presented by Design Mix 1 (lower w/c ratio and higher cement content). Therefore, applications requiring higher structural capacity could benefit from Design Mix 1. Conversely, the lowest predicted f_c of 32 MPa was observed for Design Mix 3 [highest w/c ratio (0.60) and the lowest cement content].

Design Mix 4 demonstrated the required vertical slump and attained the highest f_c at 7 and 28 days. This mix demonstrated a vertical slump of 90 mm, indicating excellent workability suitable for applications where ease of placement, proper compaction, and minimal segregation are critical. This level of workability is particularly advantageous for casting in complex formwork, congested reinforcement areas, or when using pumpable concrete techniques, ensuring uniform placement without compromising quality.

This interplay between workability and strength highlights the trade-off inherent in concrete design. Lower w/c ratios enhance compressive strength by reducing the water content and resulting voids in the hardened concrete. However, this reduction negatively impacts workability, making the mix less fluid and more challenging to handle. Conversely, higher w/c ratios improve workability by increasing fluidity but at the cost of reduced strength, consistent with Abrams' law.

Table 3.12
Fresh And Hardened Concrete Properties For Trial Mix Designs

Design Mix	**Vertical Slump (mm)**	***f*c (MPa) 7-day**	***f*c (MPa) 28-day**
Design Mix 1	70	25.3	39.3
Design Mix 2	85	22.7	34.6
Design Mix 3	90	21.0	32.0
Design Mix 4	90	25.0	38.2

Design Mix 4 was selected for this study based on its superior balance between workability and strength, which aligns with the research objectives and practical requirements for concrete Grade 30. This Design Mix attained a 28-day f_c of 38.2 MPa, which aligns with the target characteristic strength for Grade 30 concrete as outlined in the JKR Standard Specification for Building Works 2014. This standard generally specifies that the minimum characteristic cube strength for Grade 30 concrete is 37 N/mm^2. The average strength of the three tested cubes must also be at least 30 N/mm^2 at 28 days. Meanwhile, the strength on seven days should be a minimum of two-thirds of the 28-day f_c (JKR, 2021).

Although Design Mix 4 exhibited slightly lower compressive strength than Design Mix 1, the difference remains within acceptable limits and does not compromise structural integrity for most applications. Its higher workability, combined with compliance with strength requirements, makes it a more practical choice, especially compared to mixes with lower slump values that may present handling and placement challenges. The higher water content in Design Mix 4 (w/c ratio = 0.55) not only enhances workability but also facilitates better hydration of cement particles, contributing to uniform strength development. Furthermore, the proportions of fine and coarse aggregates in this mix are well-balanced, supporting improved cohesiveness and resistance to segregation during mixing and pouring. This ensures consistent quality in both fresh and hardened states of the concrete.

3.9.3 Proportion of Concrete Materials for Flowability & Strength Studies

Design Mix 4 was functioned as the baseline for concrete components in the preparation of test specimens for f_c, f_s, and τ tests. Thus, the mechanical and rheological properties of concrete were assessed by preparing mixtures with consistent proportions of cement, coarse aggregate, and fine aggregate in accordance with Design Mix 4. The main variable was the water-admixture ratio, enabling the analysis of the impact of the admixtures on the mechanical and rheological properties of the concrete. Considering the capacity of the free-fall concrete mixer, the concrete volume necessary for casting cubes and beams was determined. The concrete volume was increased by 10% to mitigate potential losses during mixing and testing.

Biosurfactant and Tween 80 were incorporated at concentrations of 0%, 5%, 7.5%, 10%, 12.5%, 15%, 17.5%, and 20% by weight of water in each mixture. Tween

80 (synthetic corrosion inhibitor recognised for its ability to enhance fluidity and viscosity) served as a positive control (Unosson et al., 2016) (B. A. Abd-El-Nabey, S. El-Housseiny, H. M. El-Kshlan, 2017) (Wahyuni et al., 2020). Alternatively, the control batch lacked both biosurfactant and Tween 80, functioning as the negative control. Table 3.13 outlines the mix proportions for producing 1 m^3 of Grade 30 concrete involving the quantities of cement, coarse aggregate, fine aggregate, water, biosurfactant, and Tween 80 utilised in each batch.

Table 3.13
The Design Mix Proportions For Every 1 M^3 Of Concrete G30

Mix ID	Admixture	% of Admixture	Admixture (kg)	Water (kg)	Cement (kg)	Fine Aggregate (kg)	Coarse Aggregate (kg)
Control	None	0.0	0.0	225.0	409	631	1110
B-1	Biosurfactant	5.0	11.3	213.8	409	631	1110
B-2	Biosurfactant	7.5	16.9	208.1	409	631	1110
B-3	Biosurfactant	10.0	22.5	202.5	409	631	1110
B-4	Biosurfactant	12.5	28.1	196.9	409	631	1110
B-5	Biosurfactant	15.0	33.8	191.3	409	631	1110
B-6	Biosurfactant	17.5	39.4	185.6	409	631	1110
B-7	Biosurfactant	20.0	45.0	180.0	409	631	1110
T-1	Tween 80	5.0	11.3	213.8	409	631	1110
T-2	Tween 80	7.5	16.9	208.1	409	631	1110
T-3	Tween 80	10.0	22.5	202.5	409	631	1110
T-4	Tween 80	12.5	28.1	196.9	409	631	1110
T-5	Tween 80	15.0	33.8	191.3	409	631	1110
T-6	Tween 80	17.5	39.4	185.6	409	631	1110
T-7	Tween 80	20.0	45.0	180.0	409	631	1110

3.9.4 Fresh Concrete Workability Test

The vertical slump, slump flow, and T500 tests were conducted to assess the rheological properties of fresh concrete, both with and without the addition of biosurfactants. This vertical slump test assessed the flowability or consistency of a concrete mix. The slump flow and T500 tests examined the fluidity and viscosity related to the filling ability of fresh concrete. These tests were performed within 10 mins post-mixing to prevent alterations in the concrete properties (Rawat & Khan, 2022). The tests were also conducted in accordance with MS 26-1-2:2009 (Testing of Concrete - Part 1: Fresh Concrete - Section 2: Slump Test (Second Revision).

3.9.4.1 Slump Test

Flowability tests were performed on a clean and levelled steel plate base. The slump cone (Abram's cone) that was standardised at a height of 300 mm was meticulously cleaned prior to each test to eliminate any foreign materials that might influence the data. Fine and coarse aggregates were then subjected to sieving and grading in accordance with the mix design. The OPC, aggregates, water, and biosurfactant were also measured and prepared accordingly. Subsequently, the concrete mix was formulated based on Design Mix 4, incorporating biosurfactant and Tween 80 added as partial water substitutes at levels of 5%, 7.5%, 10%, 12.5%, 15%, 17.5% and 20% of the total water weight. These ingredients were mixed thoroughly ensuring uniform distribution of the ingredients. The slump cone was also positioned on a levelled steel base plate and filled with fresh concrete in three equal layers, each approximately 100 mm thick. Every layer underwent compaction through 25 tamping actions with a standard tamping to achieve uniformity in compaction. Excess concrete was removed following filling, and the top surface was levelled. The cone was then lifted vertically within 5 ± 2 s to permit the concrete to slump freely.

The vertical slump and the final diameter of the horizontal concrete spread were measured, and the slump type was documented. Concurrently, a stopwatch was initiated to measure the duration required for the concrete to reach a 500 mm diameter spread (T500 time) (Alyamaç & İnce, 2010). This observed slump was categorised into three categories: (i) true, (ii) shear, (iii) and collapsed slumps. Detailed explanations of these slumps are as follows:

i) True slump occurs when concrete retains its form while subsiding uniformly. The slump value (S) can be assessed using the following method:

$$S = 300\,mm - H_t \tag{3.7}$$

where H_t denotes the highest point of the slumped concrete (mm).

ii) Shear slump happens when concrete exhibits greater slumping on one side, signifying inadequate cohesion. The S can be determined as follows:

$$S = 300\,mm - H_s \tag{3.8}$$

where H_s refers to the highest displaced point of the slumped concrete (mm). Upon the occurrence of excessive leaning, the test was considered invalid. This outcome necessitates a remix and subsequent retest of the mixture.

iii) A collapse slump occurs when concrete completely loses its shape and spreads uncontrollably owing to excessive fluidity. The S can be assessed as follows:

$$S = 300\,mm - H_c \tag{3.9}$$

where H_c is the new central height of the spread-out concrete (mm).

This study discovered that the majority of the mixes demonstrated collapse slump behaviour, which could be attributed to the self-compacting effects of Tween 80 and the biosurfactant.

3.9.4.2 T500 Test

The T500 test quantified the duration needed for fresh concrete to spread to a diameter of 500 mm following the lifting of the slump cone. The same equipment as the slump test was utilised, and the recorded time presented the viscosity and flowability of the mix. A higher T500 value indicates higher viscosity and greater resistance to flow,

whereas a lower T500 time suggests higher flowability. Typically, the T500 measurement for SCC falls between 2 s and 10 s (Sani & Osman, 2010). The slump flow diameter (D) is visualised in Figure 3.38 and can be determined as follows:

$$D = \frac{D1 + D2}{2} \tag{3.10}$$

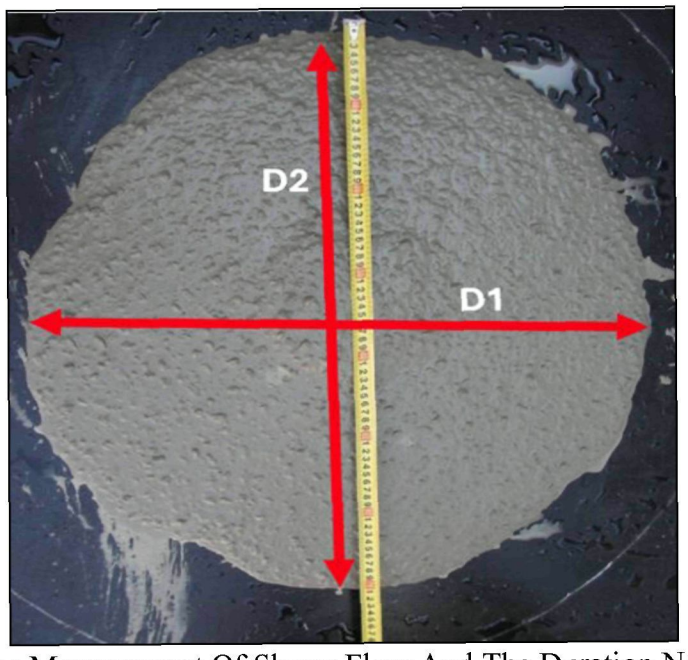

Figure 3.38 The Measurement Of Slump Flow And The Duration Needed For The Flow To Reach A 500 mm Diameter Marking

3.9.5 Hardened Concrete Strength Assessment

The f_c, f_s, and τ tests were performed to assess the influence of biosurfactants as a water replacement bio-admixture on the performance of RCs. The biosurfactant and Tween 80 was added into fresh concrete as a partial water substitutes at 5%, 7.5%, 10%, 12.5%, 15%, 17.5% and 20% of the total water weight.

3.9.5.1 The fc of Concrete with Water Replacement Admixture

The concrete materials were prepared and mixed in accordance with the proportions specified in Table 3.13 and the procedures outlined in Section 3.9.3. Figure 3.39 depicts that the mixed concrete is poured into steel moulds measuring 150 mm ×

150 mm × 150 mm. Each mould was filled in three layers, with each layer compacted through 35 rodding actions. The sides of the moulds were also tapped to remove any entrapped air voids. Subsequently, the upper surface of each specimen was meticulously levelled and polished to guarantee uniformity. These moulds were stored in a controlled environment at room temperature for 24 h, covered with damp gunny sacks to mitigate premature moisture loss.

Following a 24-h period, the concrete specimens were demoulded, labelled, and placed in individual curing tanks (see Figure 3.40). The segregation of specimens based on their respective admixture compositions was implemented to inhibit solution migration during curing. A total of six concrete cubes were prepared for each batch, with three specimens allocated for f_c testing on Day 7 and the other three on Day 28. The testing was conducted in triplicate to verify the consistency and reliability of the data. Furthermore, the mean f_c of the three specimens was documented for each batch.

Figure 3.39 The 150 mm × 150 mm × 150 mm Cube Mould Used In This Study

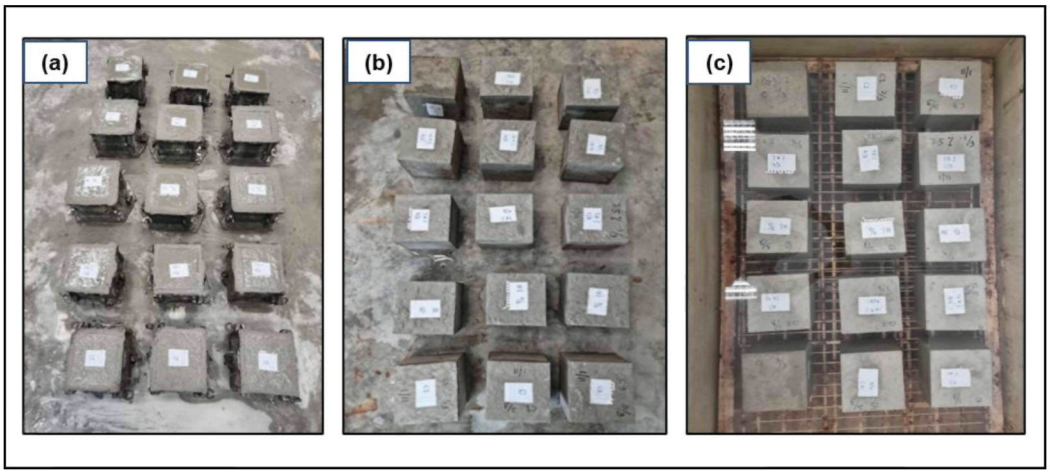

Figure 3.40 The Preparation Of Concrete Cubes (a) After Casting (b) Demoulding After 24 H (c), And In The Curing Tank For 7 And 28 Days

On the specified testing days (7 and 28 days), the concrete cubes were taken from the curing tanks and permitted to air dry at room temperature for 24 h. Before testing, dust or residual surface particles were eliminated using soft cloths and brushes. The dimensions and weights of each specimen were then documented to evaluate their density. This study implemented the f_c test following the Malaysian Standard MS EN 12390-3:2012, *Testing Hardened Concrete – Part 3: Compressive Strength of Test Specimens (Second Revision).* The specimens underwent testing with a concrete compression testing machine, which possessed a maximum load capacity of 2000 kN (see Figure 3.41 and Figure 3.42). A continuous loading rate of 6.8 kN/s (equivalent to 140 kg/cm^2 per min) was maintained until the specimen failed. The primary parameters assessed were the failure load (kN) and f_c (N/mm^2). In addition, the maximum load sustained and the failure mode were observed and documented to analyse the fracture characteristics of each specimen. This f_c is determined using an equation as follows (Prasad et al., 2019):

$$f_c = \frac{P}{A} \tag{3.11}$$

where P represents the ultimate load resisted by concrete (N); P represents the surface area of specimen that carry the load (mm^2).

Likewise, the water absorption and density of specimens are computed as follows:

$$Density = \frac{Weight\ of\ specimen}{Volume\ of\ specimen} \tag{3.13}$$

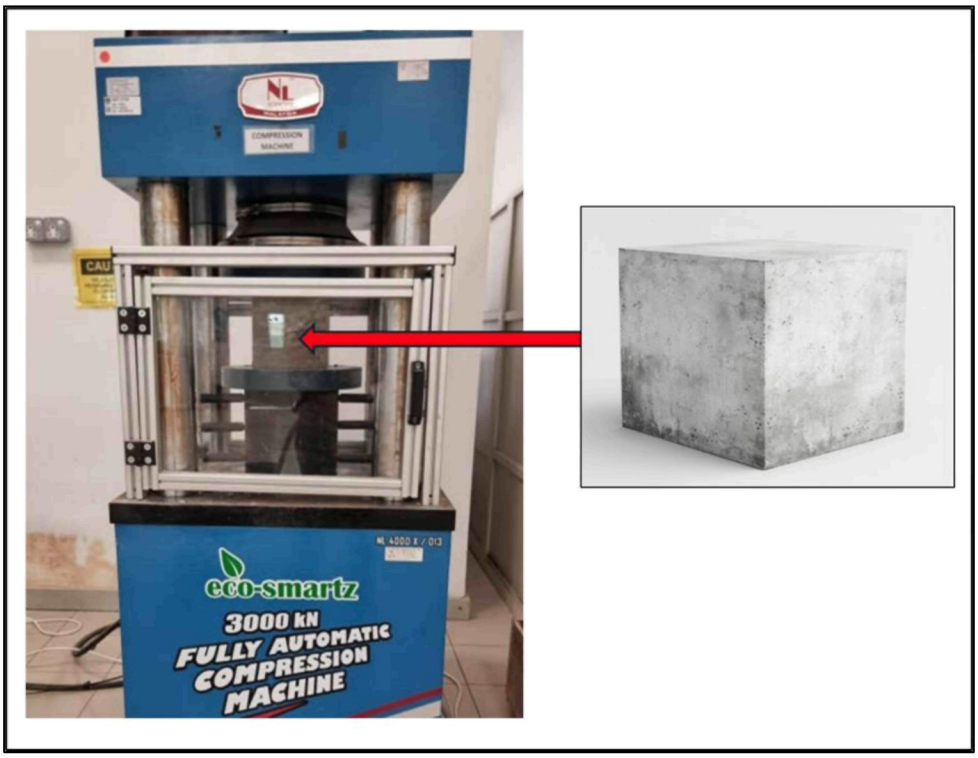

Figure 3.41 The Measurement Setup Of The Concrete Cube f_c

Figure 3.42 The f_c Test For Concrete Cubes (a) Before And (b) After The Test

3.9.5.2 The f_s of Non-RC Beams

The f_s denotes the maximum stress that a material can endure prior to failure. The concrete f_s test (or MR test) assesses the R_m of concrete under bending forces. Although concrete demonstrates significant f_c, it possesses relatively low R_m. Therefore, the f_s of concrete is a critical parameter, as it reflects its capacity to withstand breaking or bending applied forces. This study conducted the testing procedure following MS EN 12390-5:2012, *Testing hardened concrete - Part 5: Flexural strength of test specimens (Second revision).*

The f_s test on the non-RC beams was performed to evaluate the effects of biosurfactant and Tween 80 on the f_s of concrete as a matrix, providing information into how these admixtures influenced the tensile performance of the concrete matrix. Specifically, phospholipid-based biosurfactants and Tween 80 were incorporated as partial water replacement concentrations of 5%, 7.5%, 10%, 12.5%, 15%, 17.5%, and 20% of the water weight in the design mix. Negative control specimens (without admixture) were also included. The concrete mix was formulated for Grade 30, aiming for a f_c of 30 MPa at 28 days. Each specimen group was established in triplicate to guarantee statistical reliability. Furthermore, the dimensions of the beam were 100 mm × 100 mm × 500 mm. Table 3.14 presents the material proportions for each mix.

Table 3.14
Summary Of The Specimen Details And Composition Of Materials For 1 m^3 Concrete Grade 30 Used In The f_s Test

Mix ID	Admixture Type	% of Admixture	Admixture (kg)	Water (kg)	Cement (kg)	Fine Aggregate (kg)	Coarse Aggregate (kg)
Control	None	0.0	0.0	225.00	409	631	1110
B-1	Biosurfactant	5.0	11.3	213.75	409	631	1110
B-2	Biosurfactant	7.5	16.9	208.13	409	631	1110
B-3	Biosurfactant	10.0	22.5	202.50	409	631	1110
B-4	Biosurfactant	12.5	28.1	196.88	409	631	1110
B-5	Biosurfactant	15.0	33.8	191.25	409	631	1110
B-6	Biosurfactant	17.5	39.4	185.63	409	631	1110
B-7	Biosurfactant	20.0	45.0	180.00	409	631	1110
T-1	Tween 80	5.0	11.3	213.75	409	631	1110
T-2	Tween 80	7.5	16.9	208.13	409	631	1110
T-3	Tween 80	10.0	22.5	202.50	409	631	1110
T-4	Tween 80	12.5	28.1	196.88	409	631	1110
T-5	Tween 80	15.0	33.8	191.25	409	631	1110

Mix ID	Admixture Type	% of Admixture	Admixture (kg)	Water (kg)	Cement (kg)	Fine Aggregate (kg)	Coarse Aggregate (kg)
T-6	Tween 80	17.5	39.4	185.63	409	631	1110
T-7	Tween 80	20.0	45.0	180.00	409	631	1110

Concrete was poured into clean, degreased moulds (See Figure 3.43) in two distinct layers. Each layer underwent compaction through 25 uniformly distributed roddings. This process was accompanied by gentle tapping on the mould exteriors to reduce air voids. The top surface of the specimens was then levelled and smoothed. Moreover, the beams were initially cured by being covered with damp gunny sacks for 24 h at room temperature. After the initial curing period, the specimens were demoulded, labelled, and immersed in curing tanks maintained kept at 25 ± 2°C for 7 and 28 days prior to testing. Distinct curing tanks were also allocated for each admixture composition to avoid solution migration (Figure 3.45). The specimens were then removed from the curing tanks and air-dried at room temperature for 24 h before testing. Each beam was weighed individually to ascertain its density. Three-point bending tests were performed on the treated specimens after 7 and 28 days (Anggraini et al., 2017).

Testing was performed utilising a UTM. These beams were arranged in the loading assembly with the top surface orientated sideways and centred. The f_s was then assessed through a central point loading test (three-point bending test). In this procedure, each beam was positioned on two roller supports with a 400 mm span (centre to centre) as depicted in Figure 3.46. The axial load was applied at a rate of 180 kg/min at the mid-span until failure. Subsequently, the load when each specimen exhibited cracking was documented. The test was also performed in triplicate, and an average reading was obtained. Typically, the f_s is quantified as the Modulus of Rupture (MR), representing the maximum tensile stress at the point of rupture. The f_s in a three-point bending test was determined using an equation expressed as follows (Prasad et al., 2019):

$$f_s = \frac{PL}{bd^2}, when\ a\ >\ 133\ mm \tag{3.14}$$

In the four-point bending test, f_s is determined using the following formula (Anggraini et al., 2017):

$$f_s = \frac{3PL}{2bd^2}, when\ 100\ mm\ <\ a\ <\ 133\ mm \tag{3.15}$$

where a signifies the distance between the line of fracture and the nearest support (see Figure 3.47); b signifies the width of the beam (mm); d signifies the failure point depth (mm); L signifies the span length between the support points (mm); and P signifies the maximum load applied to the beam (N). The f_c of concrete also serves as a foundation for employing empirical formulas to determine f_s as follows:

$$f_s = 0.7 \times \sqrt{f_c} \tag{3.16}$$

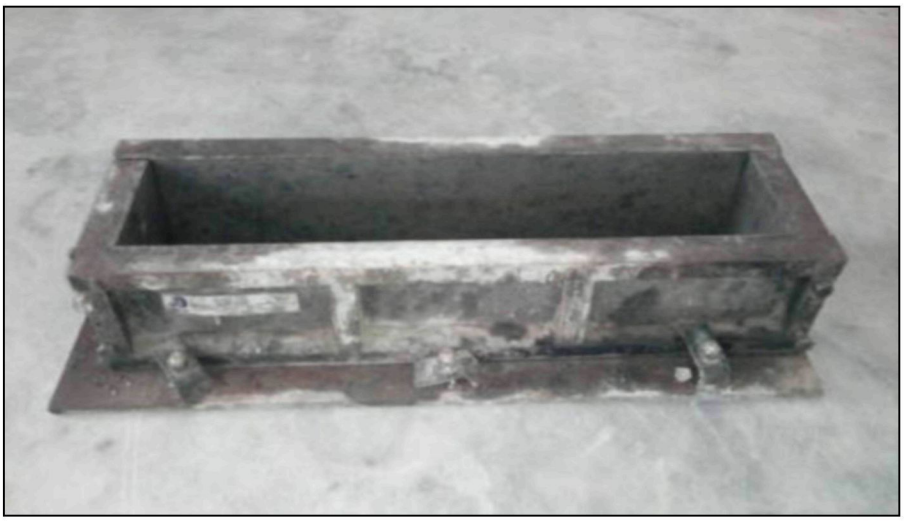

Figure 3.43 The Beam Mould (500 mm × 100 mm × 100 mm) Used For Specimen Preparation

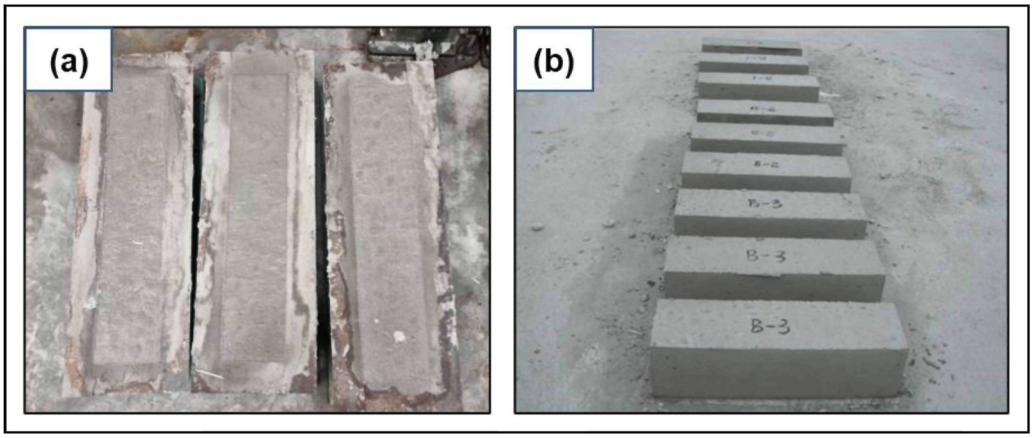

Figure 3.44 (a-b) The Grade 30 Concrete Beam Specimens Prepared For The f_s Test

Figure 3.45 The Specimens in the Curing Tank At 25 ± 2°C For 28 Days

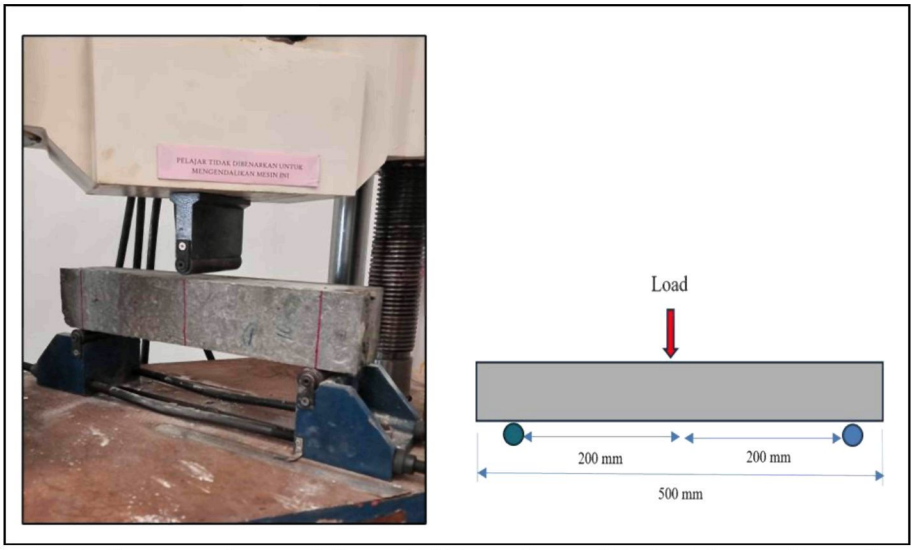

Figure 3.46 The Experimental Setup With A Central Point Flexural Loading Test Using A UTM

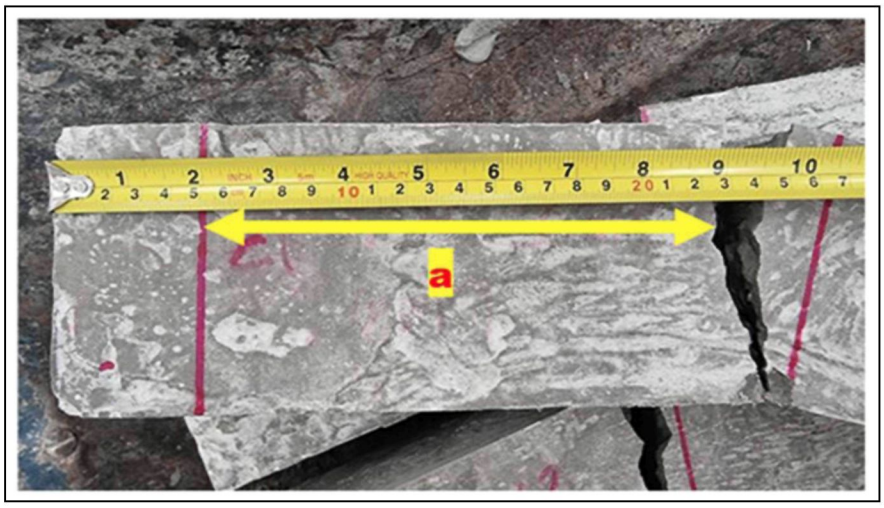

Figure 3.47 The Measurement Of The Distance Of a = Line of Fracture To The Nearest Support

3.9.5.3 The f_s of Single Reinforced Concrete Beams

This study assessed the f_s of single-RC beams to determine the impact of biosurfactant used as a water replacement admixture and corrosion inhibitor on structural performance. The test specimens were prepared according to standard procedures, featuring beam dimensions of 100 mm × 100 mm × 500 mm. Each beam was reinforced with a 450 mm R10 mild steel bar. Concrete mixtures were also designed using three distinct biosurfactant dosages (7.5%, 10%, and 12.5%) as a partial substitute for mixing water by weight (kg) alongside a control mix (0%) for comparative analysis (See Table 3.15). These dosage levels were selected based on prior studies indicating their efficacy in enhancing the f_c and f_s of non-RC. All reinforcing steel bars (except for those utilised in the control specimens) were treated with 10% biosurfactant (v/v) to ensure uniformity in corrosion protection. Conversely, the control specimens utilised untreated reinforcement as a reference for comparative analysis. These steel bars were cut to a length of 450 mm, abraded with emery papers (grades 220 to 1200) to eliminate surface impurities, rinsed with distilled water, degreased with acetone, and finally cleaned with deionised water to ensure the thorough removal of contaminants.

The prepared bars (excluding control specimens) were immersed in 10% biosurfactant (v/v) in distilled water for 14 days at room temperature. Plastic spacers were also employed to suspend the bars, ensuring full immersion and preventing contact with the container, as presented in Figure 3.48. In contrast, Tween 80 was excluded from this experiment due to previous studies demonstrating its incompatibility. These

bars were then extracted from the inhibitor solution following the 14-day treatment, cleaned with a microfibre cloth to eliminate excess solution, and transported into a desiccator containing silica gel at 25 ± 2°C between 24 h and 48 h. This process efficiently absorbed residual moisture while inhibiting oxidation or undesirable reactions prior to incorporation into the concrete beams.

Figure 3.49 illustrates a beam subjected to a three-point bending test, which was supported at two lower points. Simultaneously, a concentrated load was applied at the mid-span by the upper actuator until failure occurred. When a visible crack first appeared at the mid-span, the onset of failure was indicated. This outcome was accompanied by a minor deflection as the applied load intensified. The ultimate load-bearing capacity was then recorded and examined to evaluate the effect of biosurfactant dosage on the flexural performance of RC beams while ensuring a uniform corrosion protection approach for the steel reinforcement.

Table 3.15
Summary Of The Mix Design And Corrosion Inhibitor Treatment For Single-RC Beams

Mix ID	Admixture (%)	WC Ratio	Admixture (kg)	Water (kg)	Cement (kg)	Fine Aggregate (kg)	Coarse Aggregate (kg)	Corrosion Inhibitor (%)
Control (B0)	0	0.55	0	225	409	631	1110	Untreated Steel Bar
B-1	5	0.55	11.3	213.8	409	631	1110	10%
B-2	7.5	0.55	16.9	208.1	409	631	1110	10%
B-3	10	0.55	22.5	202.5	409	631	1110	10%
B-4	12.5	0.55	28.1	196.9	409	631	1110	10%
B-5	15	0.55	33.8	191.3	409	631	1110	10%

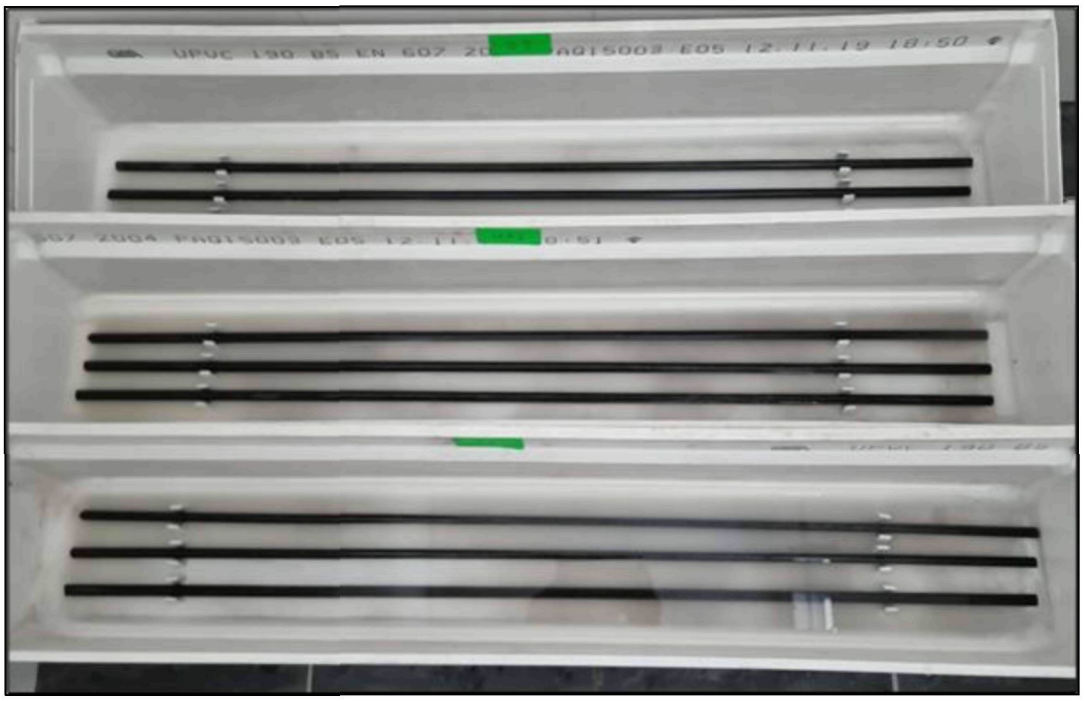

Figure 3.48 The Treatment Of Reinforcing Bars In Inhibitor Solution

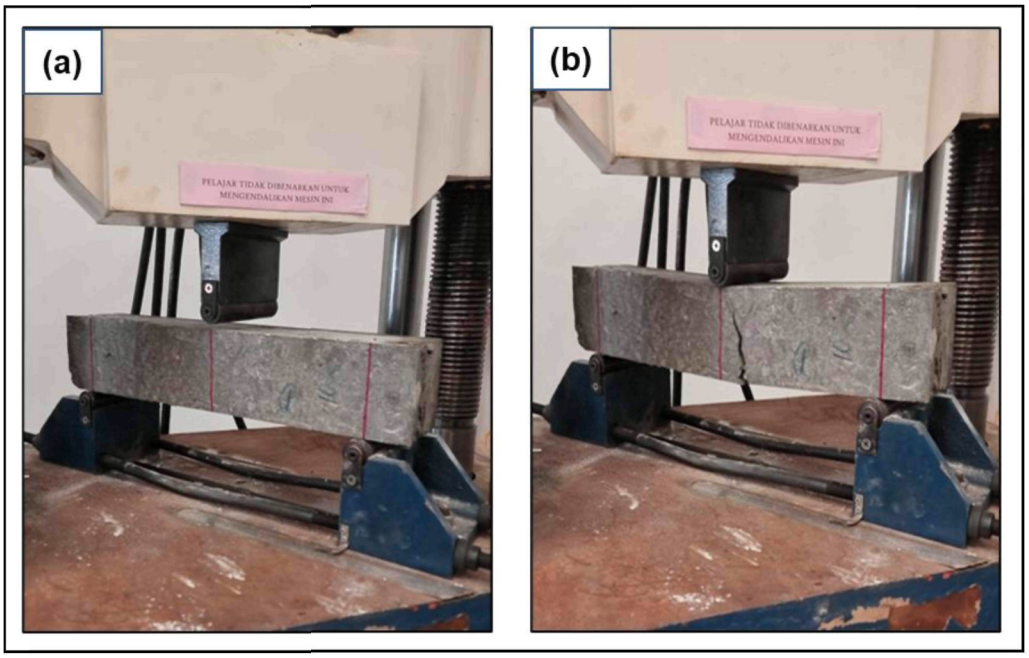

Figure 3.49 The Flexural Failure Of The Concrete Beam Under The Three-Point Bending Test (a) Before Testing And (b) After Failure

3.9.5.4 Pull-out Test

The pull-out test was conducted to assess the τ between reinforcement and concrete by applying a tensile force to pull out a steel bar embedded in a concrete cube.

This study focused on evaluating the effect of time on τ in RC incorporating biosurfactant both as a corrosion inhibitor and as an admixture. The τ was calculated by dividing the maximum applied force by the embedded surface area of the bar. A stronger bond indicates superior adhesion between concrete and reinforcement, which is crucial for the overall structural integrity of reinforced concrete elements.

The corrosion inhibition analysis revealed that mild steel bars submerged in distilled water with 10% biosurfactant (v/v) demonstrated the greatest corrosion IE. Data from the f_c and f_s tests also suggested that substituting 10% of the water content with phospholipid-based biosurfactants increased the f_c of concrete cubes and the f_s of RC and non-RC beams. Therefore, a 10% phospholipid-based biosurfactant (v/v) was chosen for the pull-out tests to evaluate its impact on the τ between reinforcement and concrete. This concentration was selected due to its effectiveness in corrosion inhibition and its enhancement of the mechanical properties of concrete.

A comprehensive understanding was also established by this study concerning the influence of biosurfactants on RC durability and structural integrity. This outcome was attained by ensuring consistent dosage across various performance evaluations. Testing was performed to assess the impact of time on τ at five distinct curing durations: (i) 14, (ii) 28, (iii) 60, (iv) 100, and (v) 120 days. The intervals were selected to capture both early-age and long-term bonding behaviour between reinforcement and concrete (Almusallam et al., 1996; Zhao et al., 2013; Zhang et al., 2016; Lin et al., 2019). This study utilised Grade 30 concrete, with the experimental design outlined in Table 3.16.

Table 3.16
Mix Proportion Of Concrete Grade 30 For Test Specimens

Admixture (%)	**WC Ratio**	**Admixture (kg)**	**Water (kg)**	**Cement (kg)**	**Fine Aggregate (kg)**	**Coarse Aggregate (kg)**	**Corrosion Inhibitor (%)**
0	0.55	0	225	409	631	1110	Untreated Steel Bar
10	0.55	22.5	202.5	409	631	1110	10%

A plain mild steel bar with a diameter of 10 mm (R10) and length of 600 mm was employed for each specimen. These bars were embedded 50 mm into concrete cubes measuring 100 mm × 100 mm × 100 mm (see Figure 3.50). This experiment utilised only straight, non-deformed reinforcement bars, adhering to the methodology

established by Shaffer (2015). The effectiveness of biosurfactant as a corrosion inhibitor was assessed by pre-treating steel bars through submersion in a solution of distilled water containing 10% (v/v) biosurfactant. Plastic spacers facilitated the suspension of the bars, guaranteeing complete immersion in the solution. The bars were submerged for 14 days to facilitate adequate interaction with the inhibitor. Following a 14-day treatment period, the specimens were extracted, and residual rust was carefully removed with soft cloths and fine brushes to prevent damage. These bars were then air-dried prior to embedding them in the concrete specimens. On the contrary, untreated steel bars functioned as the negative control group, establishing a baseline for comparison.

Concrete cube moulds (100 mm × 100 mm × 100 mm) were prepared, with a single steel bar centrally embedded along the vertical axis of each mould. An embedment length of 50 mm was uniformly preserved across all specimens to ensure consistent τ calculations. Concrete was poured into the moulds in two distinct layers. Each layer underwent compaction through 15 rodding actions and tapping of the mould sides to remove air voids. The top surface of the concrete was levelled and smoothed to ensure uniformity. Following casting, the specimens were maintained at room temperature (covered with damp gunny sacks) for 24 h to mitigate moisture loss. These specimens were demoulded after 24 h. After demoulding, the specimens were placed in saline water (25 ± 2°C) to expedite the corrosion process in the concrete. All specimens were also cured under uniform environmental conditions to maintain consistency in experimental conditions during the study period. These specimens were extracted from the curing tank 24 h prior to testing and permitted to air-dry at room temperature to maintain uniform moisture conditions.

The testing procedures adhered to Malaysian Standard MS ISO 6892:2016 and MS ISO 15630-1:2012, which outlined the guidelines for testing steel reinforcement and prestressing materials used in concrete. These tests were performed using fully automatic UTM, with three repetitions for each condition. The embedded rebar was then extracted vertically from the specimen, and the maximum pull-out load at failure was documented.

Typically, improved τ indicates a lower CR and higher corrosion inhibition efficiency (Shunmuga Vembu & Ammasi, 2023). The τ was then determined using the maximum pull-out load at failure and the surface area of the embedded bar. This process reflected an average stress over the bonded length of the reinforcement (Lee et al., 2002).

The τ can be computed using the following equation (Lee et al., 2002; Rahim et al., 2020):

$$\tau = \frac{P}{A} \tag{3.17}$$

where P denotes the maximum pull-out load at failure (N); and A denotes the embedded surface area of the steel bar (mm^2). The A can also be measured as follows:

$$A = \pi dL \tag{3.18}$$

where d is the diameter of the steel bar (mm); and L is the embedded length (bonded length) (mm).

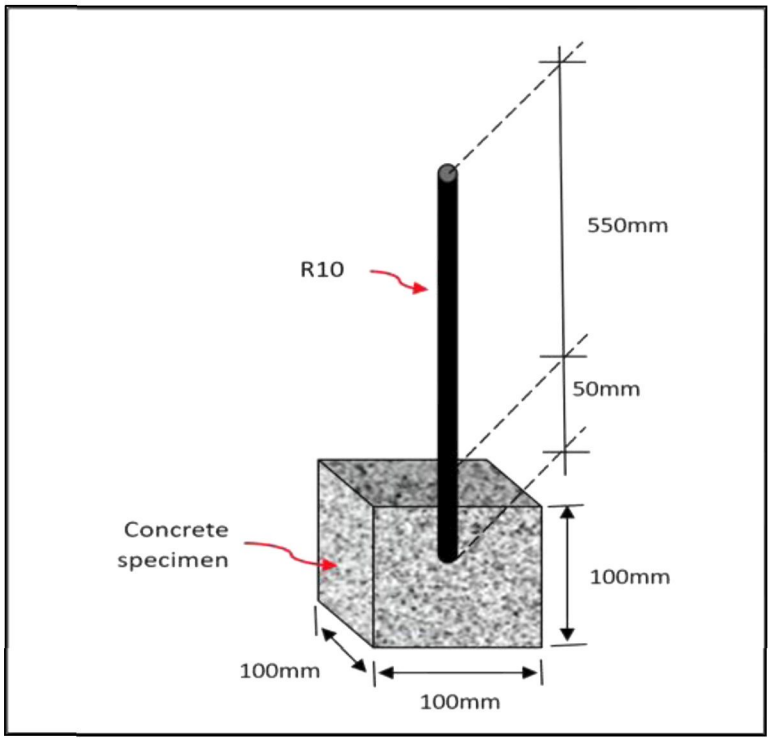

Figure 3.50 The τ Details Of The Test Specimen

CHAPTER 4
RESULT AND DISCUSSION

4.1 Introduction

This chapter presents and discusses the experimental results obtained in this study in direct relation to the established research questions (RQ1–RQ5) and research objectives. The findings are organised into three main thematic areas, each addressing specific research questions.

The first section focuses on biosurfactant production and characterisation, addressing RQ1 and RQ2, which examine the feasibility of producing phospholipid biosurfactants using Rhizopus sp. and the optimisation of production conditions to achieve consistent yield and stability. The results presented in this section provide quantitative and qualitative evidence of biosurfactant synthesis efficiency and production reliability.

The second section evaluates the corrosion inhibition performance of the biosurfactant, directly addressing RQ3 and RQ4. These results assess the effectiveness of the biosurfactant in mitigating steel reinforcement corrosion under simulated aggressive environments and elucidate the associated inhibition mechanisms. The findings are discussed in terms of inhibition efficiency, surface protection behaviour, and electrochemical performance.

The final section examines the mechanical performance of reinforced concrete incorporating the biosurfactant as an eco-admixture, addressing RQ5. This section evaluates the influence of biosurfactant incorporation on the fresh and hardened properties of concrete and assesses whether corrosion mitigation is achieved without compromising structural integrity and mechanical reliability.

Collectively, the results presented in this chapter provide an integrated assessment of the phospholipid biosurfactant's dual functionality as a corrosion inhibitor for steel reinforcement and as an environmentally sustainable admixture for reinforced concrete applications.

4.2 Isolation of Biosurfactant-Producing Fungi

Four soil samples containing fungi underwent a minimum of two sub-culturing rounds on MEA and PDA to isolate pure fungal cultures. This procedure isolated a single fungal genus per plate, improving the precision of subsequent identification. The process was also essential to verify the isolate responsible for biosurfactant production, which was consistent with the research objectives. Pure fungal cultures were initially cultivated in an MSM broth, with WFO serving as the sole carbon source (under batch anaerobic fermentation conditions). Following a 14-day fermentation period, the extracellular metabolites were evaluated for their surfactant characteristics. Only genera exhibiting significant surfactant activity were chosen for corrosion inhibition analysis. Of the four genera subjected to corrosion inhibition testing, the fungus demonstrating the highest IE was selected for further examination regarding its potential to enhance the strength of RC.

4.2.1 Screening of Fungi from Contaminated Soils

Table 4.1 summarises the characteristics of the collected soils. The pH levels of the soil samples varied between 5.5 and 7.5, reflecting minor differences in acidity and alkalinity across various locations. This data indicated that the soils were predominantly mildly acidic to neutral, with a subset exhibiting slight alkalinity. Out of the ten soil samples screened, fungal growth was successfully observed in four samples (S1, S3, S6, and S9), corresponding to 40% of the total samples analysed. The absence of fungal isolates in the remaining 60% of samples suggests that contamination alone does not guarantee fungal colonisation, as fungal presence is strongly influenced by additional environmental factors such as moisture content, soil texture, nutrient availability, aeration, and microbial competition.

A closer examination of soil properties revealed that fungal isolates were predominantly recovered from soils with pH values between 6.5 and 7.5, supporting the observation that near-neutral pH conditions favour fungal activity. Furthermore, positive fungal isolation was associated with clay, peaty, loamy, and silty soils, which typically exhibit higher moisture retention and organic matter content. In contrast, no fungal growth was detected in sandy and saline soils, which are characterised by rapid drainage, low nutrient retention, and reduced water-holding capacity. These conditions

are generally unfavourable for sustained fungal growth. This outcome was consistent with the outcome reported by Lin et al. (2017) and Classen et al. (2015). The studies stated that fungi thrived in warm temperatures and required moisture for growth. Additionally, Taylor and Sinsabaugh (2015) reported that the presence of fungi in contaminated soils reflects their ecological role in decomposing organic matter and utilising plant-derived carbon sources, particularly in environments where nutrient cycling is active.

Overall, the quantitative screening results demonstrate that only a subset of contaminated soils supports fungal colonisation, underscoring the importance of soil physicochemical characteristics in the successful isolation of biosurfactant-producing fungi. These findings justify the targeted selection of positive samples for subsequent biosurfactant production and characterisation stages in this study.

Table 4.1
Physicochemical Characteristic Summary Of Soil Samples And Fungal Growth Assessment On MEA

Sample	**Source**	**Temperature on site (°C)**	**pH of the Soil**	**Characteristic**	**Fungi growth**
S1	Aeroville Municipal Waste	31	6.5	Light brown, semi-solid	(+ve)
S2	Tabuan Jaya Municipal Waste	29	6.5	Brown, semi-solid	(-ve)
S3	ILP Car Garage	29	6.5	Dark brown, semi-solid	(+ve)
S4	Petrajaya Car Garage	29	6	Dark brown, semi- solid	(-ve)
S5	Tanjong Bako Municipal Waste	31	5.5	Light grey, sandy soil	(-ve)
S6	KBS Municipal Waste	30	6.5	Greenish-dark brown, semi-solid	(+ve)
S7	Saberkas Car Garage	32	6.5	Greenish brown, semi-solid	(-ve)
S8	Riveria Municipal Waste	31	7	Reddish brown, semi-solid	(-ve)
S9	Riveria Car Garage	30	7.5	Greenish brown, semi-solid	(+ve)
S10	Permai Municipal Waste	29	6.0	Light brown, sandy soil	(-ve)

4.2.2 Isolation of Soil Fungi

The isolation of fungi from soil samples was performed utilising the serial dilution and pour plate techniques. Among the ten soil samples collected, four demonstrated fungal growth following a seven-day isolation period. The mycelium underwent sub-culturing through successive plating on fresh MEA and PDA to guarantee the isolation of pure cultures. This process was conducted a minimum of twice to achieve a single-coloured mycelium, aiming to eliminate contaminants and ensure fungal purity. Figure 4.1 illustrates the fungus growth on PDA following a seven-day isolation period at a controlled temperature of 30°C. The outcomes indicated significant differences between MEA and PDA as culture media, in which the fungi presented the highest growth on PDA.

Figure 4.2 illustrates the morphological characteristics of *Rhizopus sp.* obtained after 14 days of isolation on MEA in an incubator at a controlled temperature of 30°C. The mycelia exhibited a thick, soft, and cottony white appearance. Figure 4.2(a) presents the surface morphology of the fungal colony, characterised by dense, cottony mycelial growth with uniform radial expansion, which is a typical macroscopic feature associated with *Rhizopus* species. The rapid colony coverage observed within the incubation period suggests strong adaptability of the isolate to nutrient-rich agar media. Figure 4.2(b) highlight the three-dimensional mycelial architecture and colony thickness, demonstrating the extensive aerial hyphae development and compact mycelial mat formed during prolonged incubation, provides visual evidence of vigorous biomass accumulation and hyphal density, indicating fungal metabolic activity and growth robustness. Such morphological traits are commonly associated with filamentous fungi capable of producing extracellular metabolites, including biosurfactants, under suitable growth conditions.

This species also demonstrated a survival rate of up to 60 days on MEA at room temperature (~25°C), but after 60 days, the mycelia exhibited a gradual colour change to greyish and blackish (see Figure 4.3).

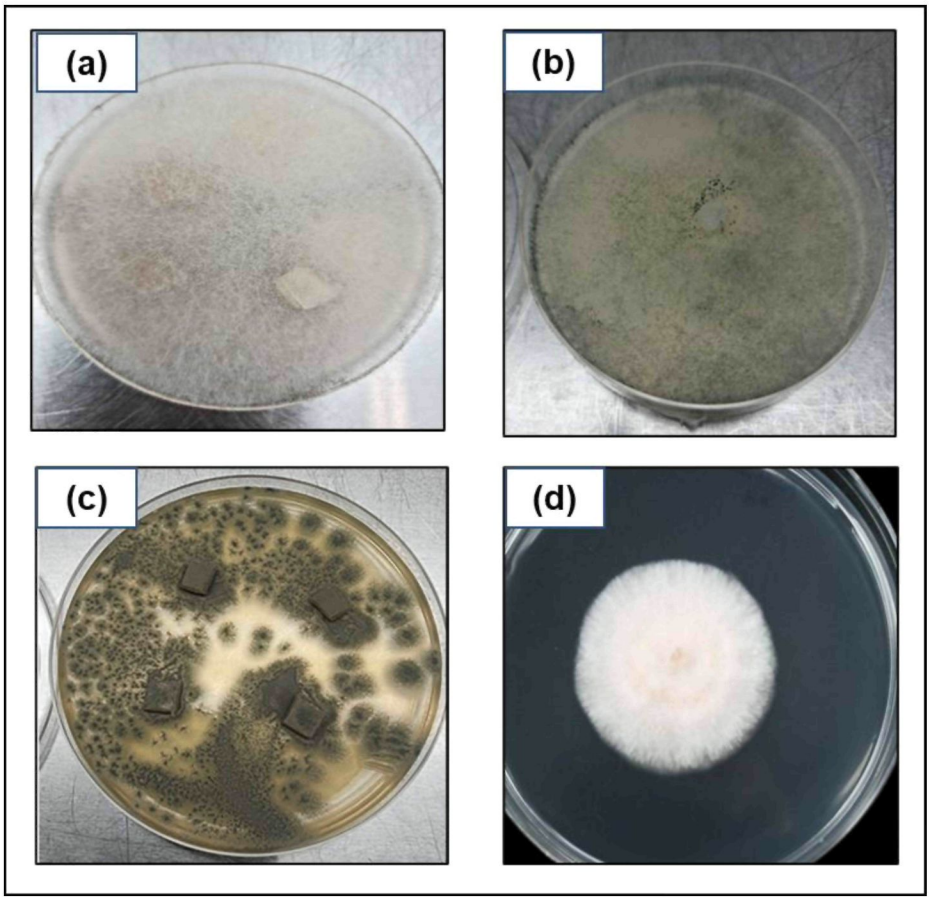

Figure 4.1 The Morphological Features Of (a) S1 (*Rhizopus sp.*), (b) S2 (*Pennicilium Sp.*), (c) S3 (*Tricoderma Sp.*), and (d) S4 (*Fusarium Sp.*) Observed On PDA Plates After Seven Days Of Isolation At A Controlled Temperature Of 30°C

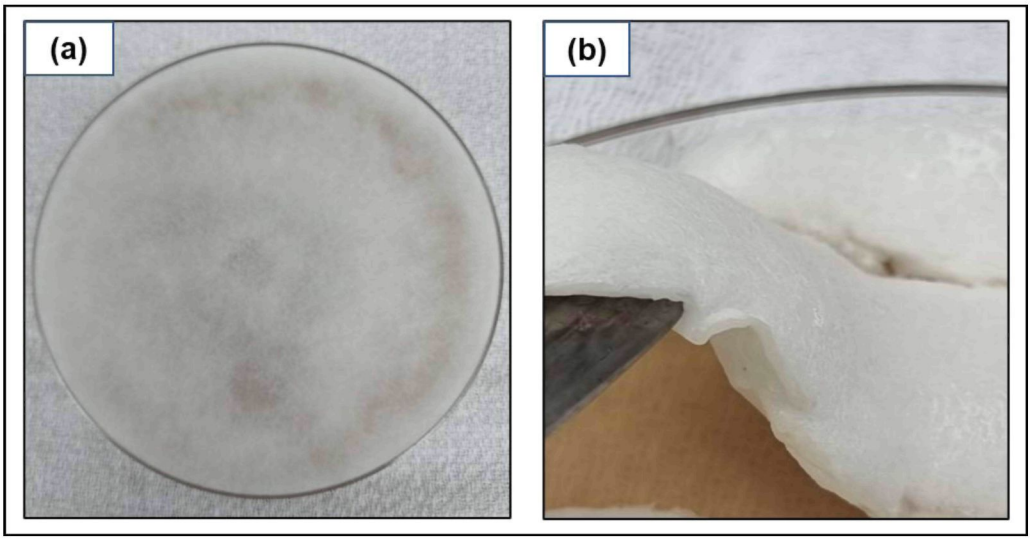

Figure 4.2 (a) The *Rhizopus Sp.* Growth On The MEA After 14 Days Of Isolation At A Controlled Temperature Of 30°C And (b) Three-dimensional Mycelial Of *Rhizopus Sp.*

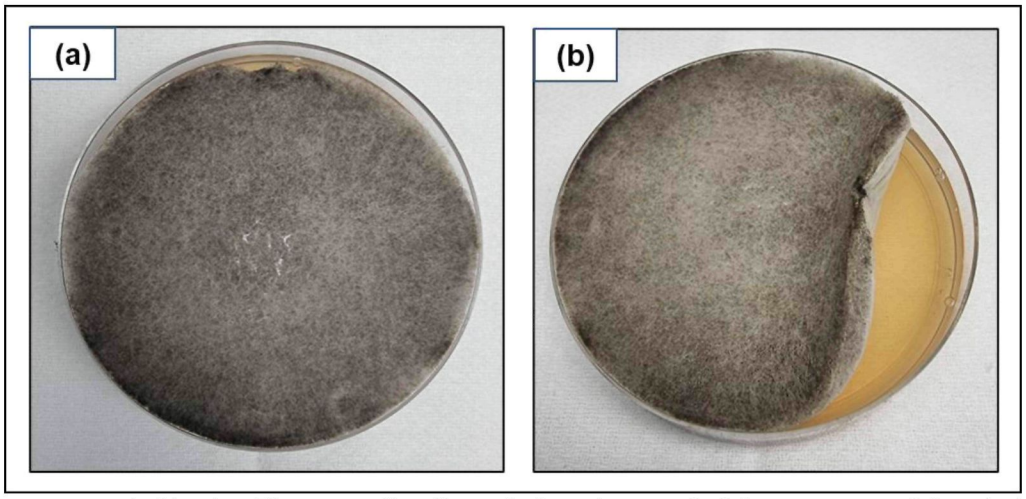

Figure 4.3 (a-b) The *Rhizopus Sp*. Growth On The MEA After 60 Days Of Isolation At Room Temperature (~25°C)

4.2.3 Fermentation and Enrichment of Potential Biosurfactant Producers

The optimisation studies indicated that the maximum biosurfactant yield occurred at 30°C in both aerobic and anaerobic (agitated) conditions. All four tested fungal isolates were identified as facultative anaerobes. These isolates could grow in the presence or absence of O_2. Likewise, the optimal volume of WFO as a carbon source was established at 5%, with a pH above 7.0. A minimum fermentation duration of 14 days was also required for optimal biosurfactant yield. Table 4.2 lists these outcomes that summarise the variables influencing biosurfactant production during fermentation. For upscale fermentation, these fungi were cultured in a 15 L bioreactor under batch fermentation conditions at room temperature for 45 days, utilising aerobic processes.

Table 4.2
Summary Of The Variables Affecting Biosurfactant Production

Variable	Condition Tested	Optimal Condition
WFO Concentration	2%, 5%, 7%, 10%	5%
WFO pH	5.0 to 9.0	Above 7.0
Temperature	25°C to 30°C	30°C
Fermentation Mode	Aerobic and anaerobic	Both (with proper aeration)

Figure 4.4 portrays the culture broth at the onset of fermentation. Conversely, Figure 4.5 demonstrates fungal growth in the broth following 14 days of fermentation. The fermentation process resulted in the emulsification of the solution and a decrease

in WFO levels, implying fungal growth and metabolite production. Biosurfactant production measurements were also quantitatively and qualitatively assessed on days 7 and 14. Notably, cell growth was evaluated via OD, which correlated with DCW (see Section 3.3.3).

Among the isolates, *Rhizopus sp.* demonstrated the earliest sustained emulsification, with a stable milky emulsion forming by Day-3 and persisting continuously until Day-14, corresponding to a ≥64% stability duration relative to the total cultivation period. In addition, a consistent reduction in the WFO phase was observed from Day-3 onward, indicating uninterrupted biosurfactant activity over time. Table 4.3 summarises the visual characteristics of the metabolites produced by each fungal isolate.

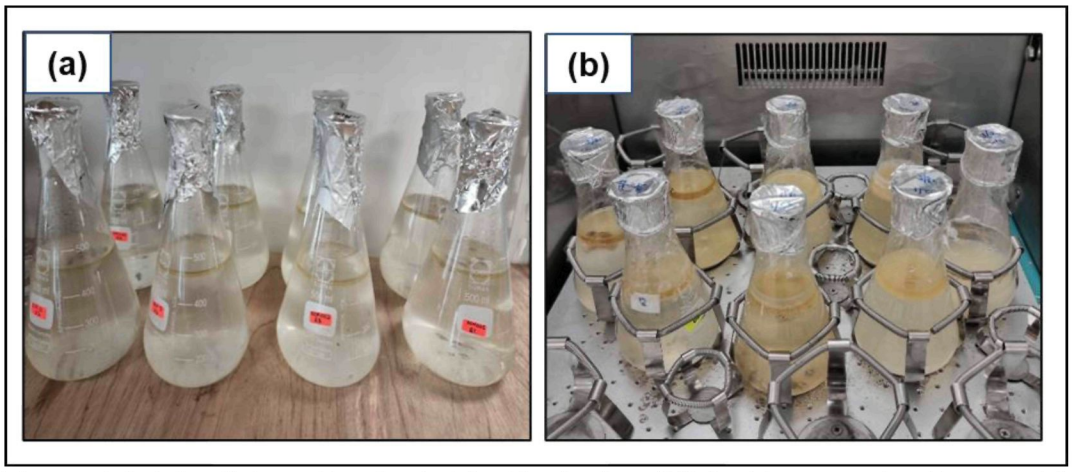

Figure 4.4 The Culture Broths At The Beginning Of The Fermentation Process (a) The MSM Broth Is Supplemented With 5% WFO (b) The Shake Flask Fermentation Setup Used For Biosurfactant Production

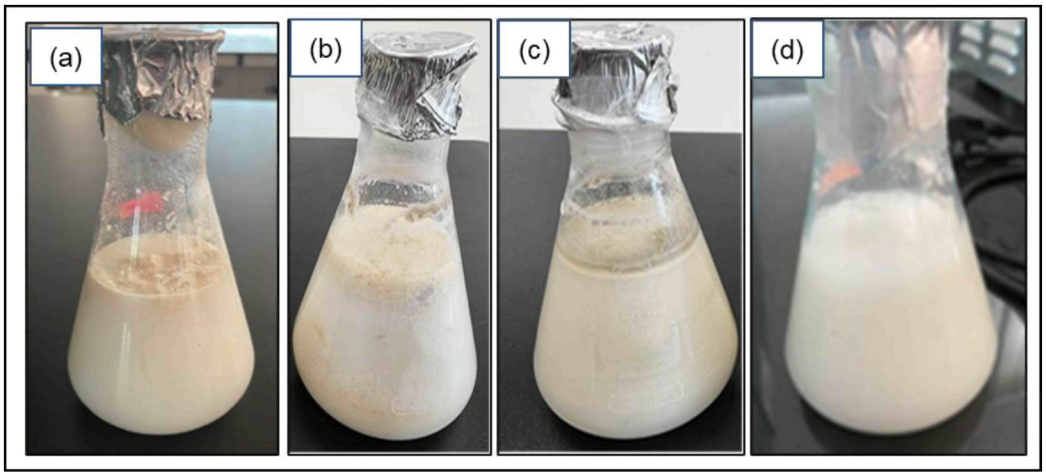

Figure 4.5 The Emulsified MSM Broth Containing Metabolites Secreted By (a) *Rhizopus Sp.* (b) *Penicillium Sp.* (c) *Trichoderma Sp.*, And (d) *Fusarium Sp.*, After 14 Days Of Cultivation In Erlenmeyer Flasks Under Anaerobic And Agitated Conditions

Table 4.3
Visual Characteristic Summary Of The Metabolites Produced By Each Fungal Isolate Observed In The Fermentation Broths As Presented In Figure 4.5

Isolates	**Observation in the Culture Medium**
Rhizopus sp. (a)	A distinct milky and stable emulsified broth was observed, with visible thick mycelial aggregation suspended in the medium. A marked reduction in WFO layer was evident from the third day of fermentation, indicating effective emulsification and metabolite production.
Pennicilium sp. (b)	The culture medium appeared cloudy and weakly emulsified. Partial reduction of the WFO phase was observed from the third day, suggesting moderate metabolite secretion with limited emulsion stability compared to *Rhizopus* sp.
Tricoderma sp. (c)	A light-coloured milky appearance observed. Although a reduction in WFO level was observed from the third day, the emulsion formed was less uniform, indicating comparatively lower surface-active metabolite production.
Fusarium sp. (d)	A light milky suspension was observed, accompanied by a noticeable but lower reduction in WFO level from the third day of fermentation, suggesting limited emulsification efficiency relative to *Rhizopus* sp.

4.2.4 Screening Test for Biosurfactant Production

The production of metabolites and their surfactant properties were assessed through qualitative and quantitative screening assays (oil displacement, drop collapse, and E_{24} tests).

4.2.4.1 Drop Collapse Test

Table 4.4 and Figure 4.6 display the drop collapse results for biosurfactant producers, control (distilled water), and standard (Tween 80). All four isolates exhibited a positive outcome in the drop collapse test, signifying the presence of biosurfactants. Among the four isolates, S1 (*Rhizopus* sp.) presented the largest drop diameter. On the contrary, the control (distilled water) exhibited no collapse while retaining a beaded shape, confirming the absence of surfactants. The use of recycled SAE HD30 Pennzoil and visual evaluation using a magnifying glass yielded consistent and reproducible outcomes, validating the methodology for identifying biosurfactants in culture supernatants.

Table 4.4
Summary Of The Drop Collapse Test Results

Sample	Genus	Visual Observation	Diameter of Drops
S1	*Rhizopus sp.*	Collapsed	1.28
S3	*Penicillium sp.*	Collapsed	1.27
S6	*Trichoderma sp.*	Collapsed	1.26
S9	*Fusarium sp.*	Collapsed	1.18
Negative Control	Distilled water	Beaded	1.12
Positive control	Tween 80	Collapsed	1.48

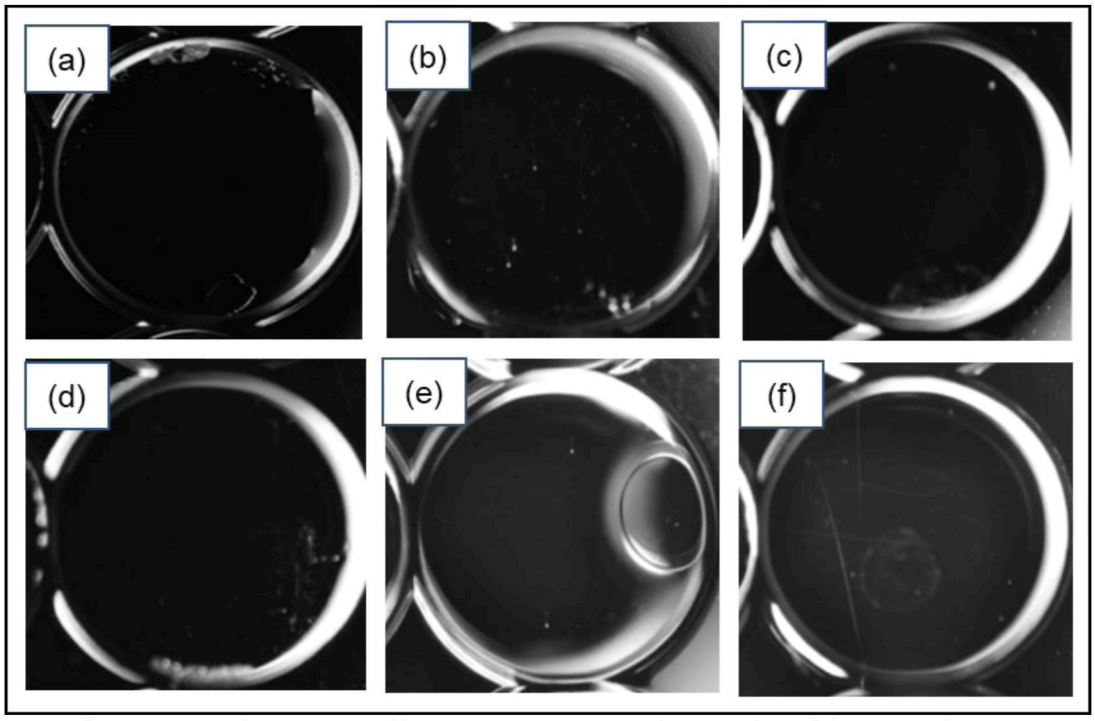

Figure 4.6 The Drop Collapse Assays. Negative And Positive Results Are Characterised By The Presence Of Beaded Droplets Of Culture Supernatant On The Oil Surface Or The Absence Of Beaded Droplets (Drops Appearing Collapsed). (a) *Rhizopus* Sp., (b) *Penicillium Sp.*, (c) *Trichoderma Sp.*, and (d) *Fusarium Sp.* Indicates Collapsed Droplets. (e) Distilled Water (Negative Control) Suggests Beaded Droplets. (f) Tween 80 (Positive Control) Presents Collapsed Droplets

4.2.4.2 Oil Displacement Test / Oil Spreading Assay

The confirmation of biosurfactant-producing fungi was achieved through the oil spreading test. Particularly, *Fusarium* sp., *Rhizopus* sp., *Trichoderma* sp., and *Penicillium* sp. displayed oil-spreading abilities. Table 4.5 tabulates the percentage of clear zone areas and the time required for oil displacement. Figure 4.7 demonstrates the capacity of these biosurfactants to disperse a layer of recycled used motor oil in comparison to Tween 80 (positive control). Dispersion activity was also not observed on the plate with distilled water. Consequently, *Rhizopus* sp. demonstrated the most excellent biosurfactant activity, producing the largest clear zone in the least amount of time. This observation suggested that *Rhizopus* sp. possessed the highest potential for biosurfactant production. The incorporation of Tween 80 as a positive control also confirmed the reliability and sensitivity of the oil displacement test.

Table 4.5
Summary Of The Oil Displacement Areas By Biosurfactants, Distilled Water, And A Synthetic Surfactant (Tween 80)

Sample	Isolates	Clear zone (%)	Displacement time (s)
S1	Rhizopus sp.	80	90
S3	Penicillium sp.	70	120
S6	Tricoderma sp.	60	150
S9	Fusarium sp.	60	300
Positive control	Tween 80	90	20
Negative control	Distilled water	Negative	Negative

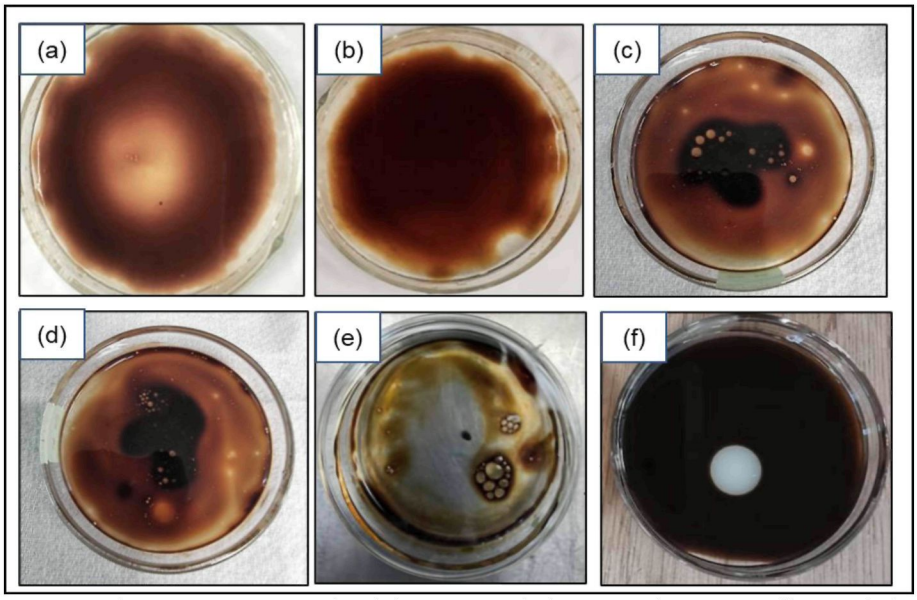

Figure 4.7 The ODAs In Petri Dishes Containing Used Motor Oil Involving (a) *Rhizopus Sp.* (b) *Penicillium Sp.* (c) *Tricoderma Sp.* (d) *Fusarium Sp.* (e) Tween 80 And, (f) Distilled Water

4.2.4.3 E_{24} Test

Table 4.6 presents the E24 results, demonstrating the emulsification efficiency of the biosurfactants generated by each isolate. All E24 measurements were conducted in triplicate (n = 3) for each isolate to ensure reproducibility and statistical reliability. The results are reported as mean values with corresponding standard deviations. Among

the tested isolates, *Rhizopus sp.* exhibited the highest mean E_{24} value of 75 ± SD%, indicating superior emulsification efficiency compared to the other isolates. This performance was comparable to the T80 tested under identical conditions. The relatively low standard deviation observed for *Rhizopus sp.* further reflects the consistency and stability of its biosurfactant production. As illustrated in Figure 4.8, the E_{24} index provides a quantitative measure of emulsification capability, corroborating the trends observed in the oil displacement test. Overall, the statistical treatment of the E_{24} data confirms discernible differences in emulsification performance among the isolates and reinforces the significant potential of *Rhizopus sp.* as a robust biosurfactant-producing strain.

Table 4.6
Summary Of The E_{24} Results For Biosurfactant Production

Sample	**Emulsion Layer Height (cm)**	**Total Liquid Height (cm)**	**E_{24}**
Fusarium sp.	2.2	4	55%
Rhizopus sp.	3.0	4	75%
Tricoderma sp.	2.4	4	60%
Pennicilium sp.	2.6	4	65%
Tween 80	3.7	4	93%

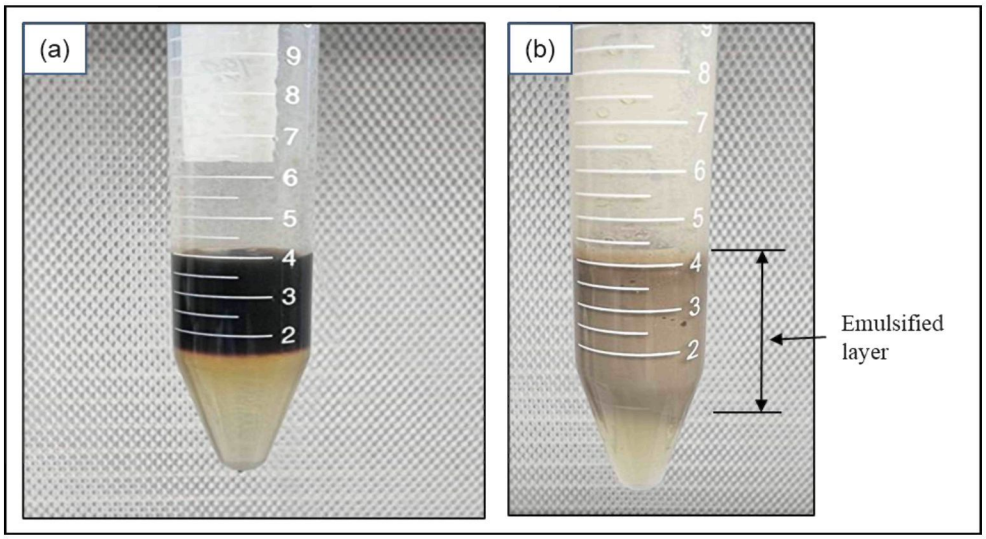

Figure 4.8 The E_{24} Of A Phospholipids-Based Biosurfactant Produced By *Rhizopus Sp.* (a) Initial Mixture Of Biosurfactant And Used Motor Oil (b) A Stable Emulsified Layer Of Biosurfactant After 24 H

4.2.5 Growth Measurement and Quantification of Biosurfactant

The cell growth and biosurfactant production capabilities of *Fusarium* sp., *Rhizopus sp., Trichoderma* sp., and *Penicillium* sp. were assessed using OD and DCW measurements.

4.2.5.1 OD Measurements

The OD measurements at 600 nm for the crude biosurfactants were recorded on days 10 and 14 of fermentation. These values indicated the efficiency of cell growth and biosurfactant production in the culture medium (dos Santos et al., 2018). Table 4.7 summarises the results of this process. Consequently, the growth and biosurfactant production potential of *Fusarium sp.*, *Rhizopus sp.*, *Trichoderma sp.*, and *Penicillium sp.* were indicated through pH and OD data analysis. This assessment was performed under submerged fermentation utilising WFO as the sole carbon source. The most significant increase in OD was then produced by *Rhizopus sp.* under neutral pH conditions (7.10), escalating from 1.764 (day 10) to 2.498 (day 14). Therefore, the most promising isolate for biosurfactant production was *Rhizopus sp.* based on its effective substrate utilisation and strong metabolic activity. Likewise, *Fusarium sp.* exhibited substantial growth, with OD rising from 1.175 to 2.1371. This sample flourished in mildly acidic conditions (pH = 6.37). Hence, the capacity to employ WFO as a substrate demonstrated the potential of the sample for biosurfactant synthesis. *Trichoderma sp.* and *Penicillium sp.* also revealed moderate growth under neutral (pH = 7.05) and slightly acidic (pH = 6.65) conditions, with OD increases from 1.571 to 2.214 and from 1.010 to 2.290, respectively. Nonetheless, the substrate utilisation and growth rates of these samples were relatively inferior to those of *Rhizopus* sp. and *Fusarium sp.*

Table 4.7
Summary Of The ODs For The Crude Biosurfactants Taken On Days 10 And 14 Of The Fermentation Process

Isolate	pH	OD (Day 10)	OD (Day 14)	Change in OD
Fusarium sp.	6.37	1.175	2.1371	+ 0.9621
Rhizopus sp.	7.10	1.764	2.498	+ 0.734
Trichoderma sp.	7.05	1.571	2.214	+ 0.643
Penicillium sp.	6.65	1.010	2.290	+ 1.28

4.2.5.2 Dry Cell Weight (DCW) Measurement

The DCW data corroborated the observations regarding the growth potential of the fungal isolates and facilitated the quantification of biosurfactant yield. This DCW of crystallised biosurfactants was determined using a high-precision scale, and the measurement was performed following the extraction process. Table 4.8 portrays the DCW values. *Rhizopus sp.* demonstrated the DCW at 0.8509 g/L, signifying the most significant biomass yield among the tested isolates. This outcome was associated with the maximum increase in OD, implying that *Rhizopus sp.* efficiently utilised the WFO substrate for growth and biosurfactant production.

Table 4.8
Summary Of The DCW Values Of The Crystallised Biosurfactants

Isolate	***Fusarium* sp.**	***Rhizopus* sp.**	***Tricoderma* sp.**	***Pennicilium* sp.**
DCW (g/L)	0.4669	0.8509	0.7018	0.7868

Moderate DCW values were presented by *Penicillium* sp. (0.7868 g/L) and *Trichoderma sp.* (0.7018 g/L). Thus, *Rhizopus sp.* outperformed both these samples, indicating their subdued growth. Likewise, the lowest biomass production was produced by *Fusarium sp.* (DCW = 0.4669 g/L).

Overall, the most enhanced growth and biosurfactant yield was generated by *Rhizopus sp.* based on the OD and DCW measurements. Although biosurfactant production could still benefit from these isolates, less efficient substrate utilisation or reduced growth rates were exhibited by *Fusarium* sp. And *Trichoderma* sp. This

conclusion was based on the lower DCW values. These results reinforce the suitability of Rhizopus *sp*. for biosurfactant production under the tested conditions.

4.3 Identification of Biosurfactant Producing Fungi

The fungi isolate capable of producing biosurfactants was examined for morphological properties through microscopic assessment. These fungal isolates presented distinct macroscopic features on PDA plates following a 14-day incubation at 30°C. Every isolate then produced distinct characteristics in terms of height, size, margin surface, and mycelium colour that enabled their identification. Consequently, all these data were recorded and compared to the established traits of target isolates based on their morphological features. Table 4.9 lists the morphological properties of the isolated fungi. Figure 4.9 to 4.12 illustrate the macroscopic morphology and micromorphological properties of biosurfactant-producing fungi following a 14-day isolation period on PDA.

Based on comparative assessment with authoritative morphological keys and reference images, the isolates exhibited characteristic features consistent with *Rhizopus sp*. (Kwon et al., 2011), Penicillium sp. (Samson et al., 2004), Trichoderma sp. (Sandle, 2014), and Fusarium sp. (Thrane, 2014). The concordance between the observed colony morphology, hyphal structures, and sporulation patterns and those reported in previous studies supports the validity of genus-level identification. While molecular confirmation would further strengthen taxonomic resolution, the integrated use of macroscopic and micromorphological comparison provides a scientifically acceptable basis for fungal screening and selection in biosurfactant-oriented studies.

Table 4.9
Summary Of The Macroscopic Morphological Characteristics Of Biosurfactant-Producing Fungi

Isolate	Macroscopic Characteristics	Micromorphological Characteristics	References
Fusarium sp.	Floccose to cottony texture, white to pink color, smooth margin, moderate height, extensive growth on agar plate	Oval to kidney-shaped microconidia, sickle-shaped, thin-walled and delicate macroconidia, a single terminal chlamydospore.	(Fourie et al., 2011) (Thrane, 2014)
Rhizopus sp.	Fluffy, white to grey mycelium, lobate margins, significant height, large spread on the agar plate	Long, upright, stalk-like sporangiophore arose from the hyphae and supported the sporangium (round, dark brown sac-like structure located at its tip).	(Hartanti et al., 2015) (Gryganskyi et al., 2018)
Trichoderma sp.	Green mat of conidia with concentric rings. Mycelium on PDA appears powdery, greenish white and bright green compact tuff. Relatively low height. Light to dark brown pigmentation appeared at the bottom of the plate,	Branched and paired conidiophores with radial phialides and globose to sub-globose shaped conidia.	(Jambhulkar et al., 2024) (Sandle, 2014) (Sudantha & Suwardji, 2021)
Penicillium sp.	Velvety colonies, blueish grey green conidia, clear zonation, undulate margin, low to moderate height, dense conidiophores	Smooth conidiophore, globose & smooth walled conidia	(Houbraken et al., 2010) (Samson et al., 2004)

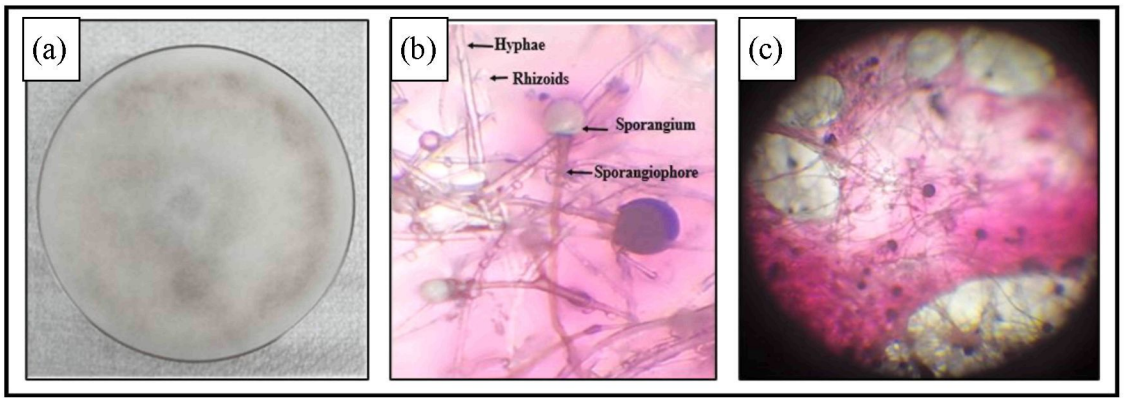

Figure 4.9 Macroscopic And Micromorphological Characteristics Of *Rhizopus Sp.* Following 14 Days Of Incubation on PDA At 30 °C: (a) Macroscopic Morphology On PDA Plate, (b) Micromorphological Features Showing Hyphae, Rhizoids, Sporangiophore, and Sporangium Observed Under Light Microscope At 400×, And (c) Microscopic View Illustrating Sporangial Structures And Hyphal Network Observed Under Light Microscope At 40× Magnification.

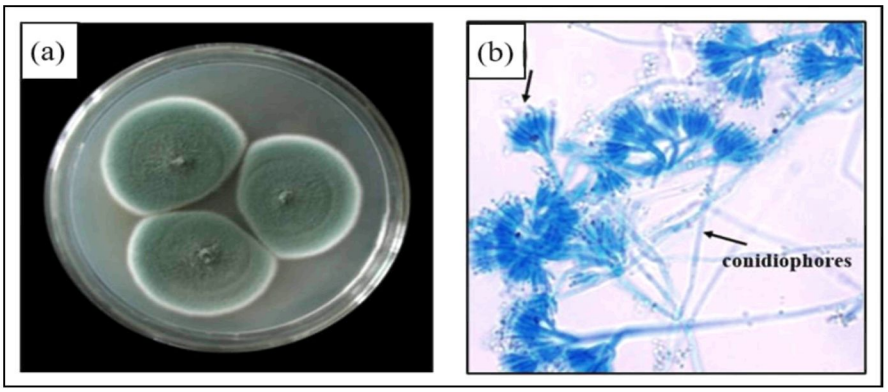

Figure 4.10 Macroscopic And Micromorphological Characteristics Of *Penicillium Sp.* Following 14 Days Of Incubation On Potato Dextrose Agar (PDA) At 30 °C. (a) Macroscopic Colony Morphology On PDA Plate And (b) Micromorphological Features Showing Conidiophores And Conidia Under Light Microscopy At 400× Magnification.

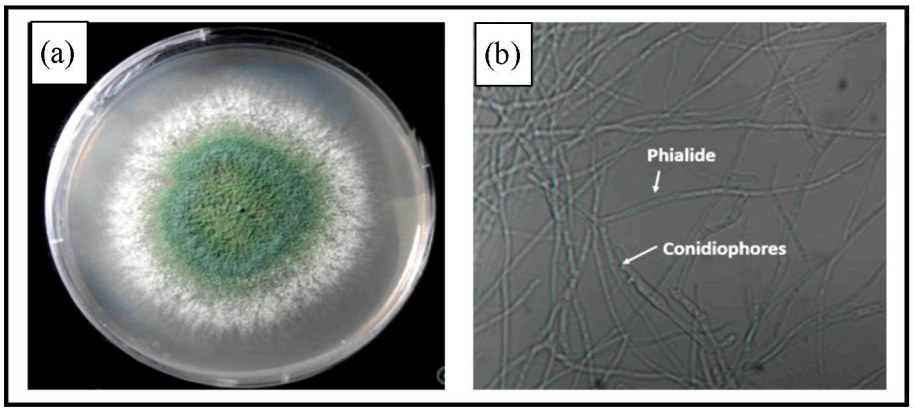

Figure 4.11 Macroscopic And Micromorphological Characteristics Of *Trichoderma Sp*. Following 14 Days Of Incubation On PDA At 30 °C. (a) Macroscopic Colony Morphology Exhibiting A Dense Green Conidial Surface With A Distinct White Marginal Zone, Characteristic Of *Trichoderma Sp*. And (b) Micromorphological Features Showing Branched Conidiophores Bearing Phialides.

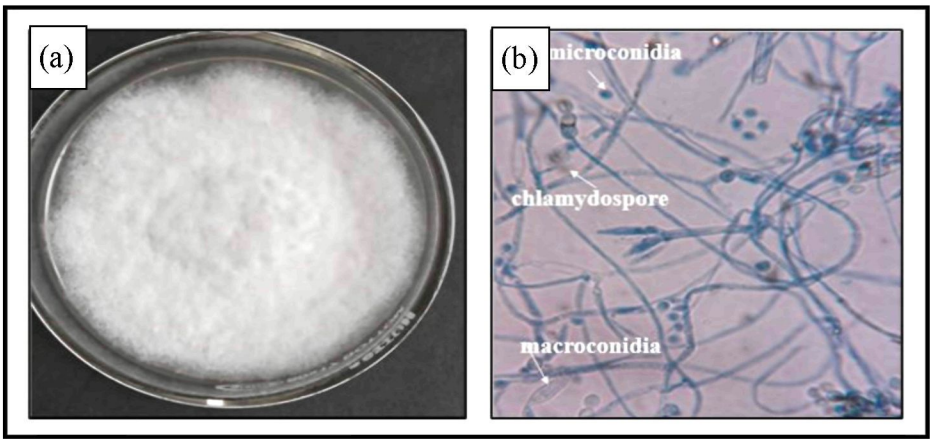

Figure 4.12 Macroscopic And Micromorphological Characteristics Of *Fusarium Sp.* Following 14 Days Of Incubation On PDA At 30 °C. (a) Macroscopic Colony Morphology Showing Abundant White, Cottony Aerial Mycelium; And (b) Micromorphological Features Illustrating Septate Hyphae With Characteristic Macroconidia, Microconidia, And Chlamydospores.

Figure 4.13 illustrates the microscopic structure of the genus *Rhizopus* mycelium at various magnifications, detailing its hyphal network (broad, coenocytic hyphae and sporangiophores). The plate also emphasised the structural components (sporangia, columella, and rhizoids), providing a more precise visualisation of their morphological characteristics.

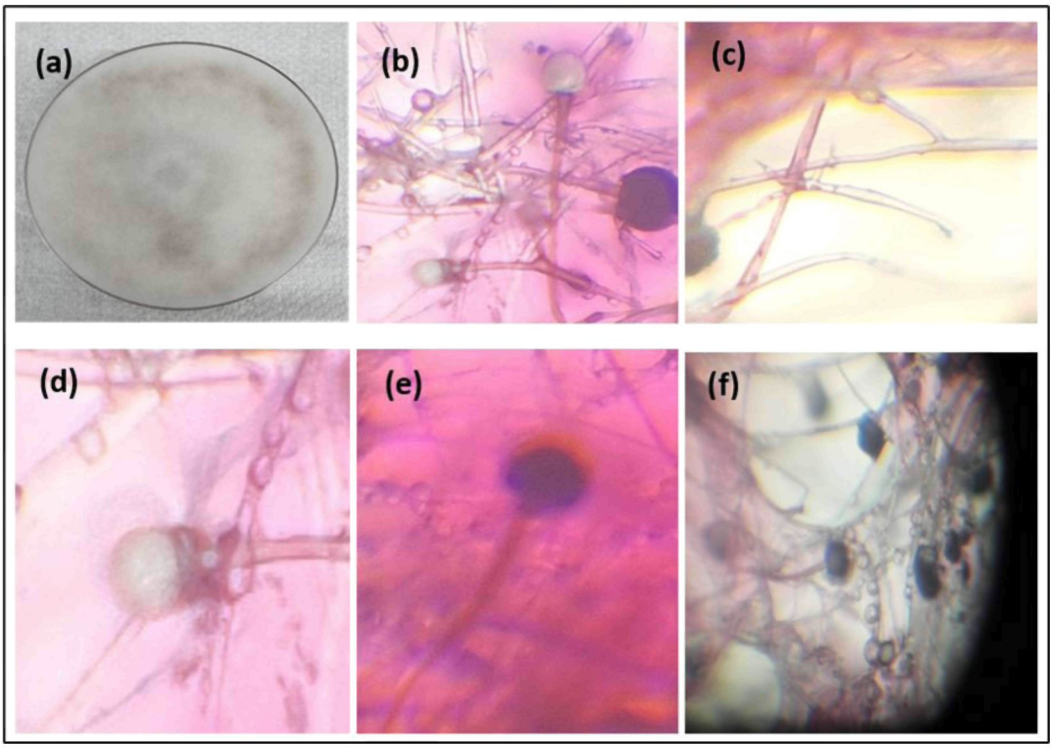

Figure 4.13 The *Rhizopus Sp*. Morphology. (a) The Colony On MEA Following 14 Days Of Cultivation At 30°C. (b) Sporangiophore, Rhizoids, and Pigmented Hyphae of *Rhizopus Sp*. (c) Stolons, (d) Empty Sporangiophore, (e) Sporangiophore With Columella, And (f) Intact With Germinating Sporangiospores

4.4 Biosurfactant Characterization Using LC-QTOF-MS Analysis

The characterisation of biosurfactants was analysed using LC-QTOF-MS via positive and negative ion modes. The LC-QTOF-MS analysis of the biosurfactant sample revealed the presence of compounds predominantly classified as phospholipids, including glycerophosphoethanolamines (PE), lysophosphatidylethanolamines [LPE (20:3)], glycerophosphoinositols (PI), and glycerophosphoserines (PS), consistent with previous reports on microbial phospholipid biosurfactants by Tan et al. (2020) and Ermolenko et al. (2022). The molecular composition and dominance of specific phospholipid species play a key role in governing the adsorption-driven corrosion inhibition mechanism observed in this study.

4.4.1 Positive Ion Mode

Figure 4.14 presents chromatograms from the photodiode array involving a comparative analysis between a blank sample (ACN) and a biosurfactant sample. The

LC-QTOF-MS in positive ion mode was employed for this process. Both chromatograms contained an absorbance range from 190 nm to 500 nm and RTs for the significant peaks. Hence, the unique compounds in the biosurfactant sample could be identify while differentiating them from background noise or contaminants. The solvent front or minimal system noise was then observed for the ACN plot via a single small peak at 0.46 mins. Nevertheless, no notable peaks were detected after the 2-min mark. This finding indicated that the analysis was not significantly interfered with by ACN, creating a establishes a reliable baseline for comparison with the biosurfactant sample.

Likewise, low molecular weight compounds or minor impurities that eluted rapidly were denoted at 0.39 mins and 0.69 mins for the biosurfactant sample. Distinct peaks appeared at retention times of 16.42 mins, 16.75 mins, 18.49 mins, and 18.51 mins, corresponding to the principal biosurfactant compounds determined through LC-QTOF-MS. This outcome was attributed to the phospholipids, fatty acid, and glycolipid-based biosurfactants. The presence of these peaks validated the successful detection of key biosurfactant components in the sample.

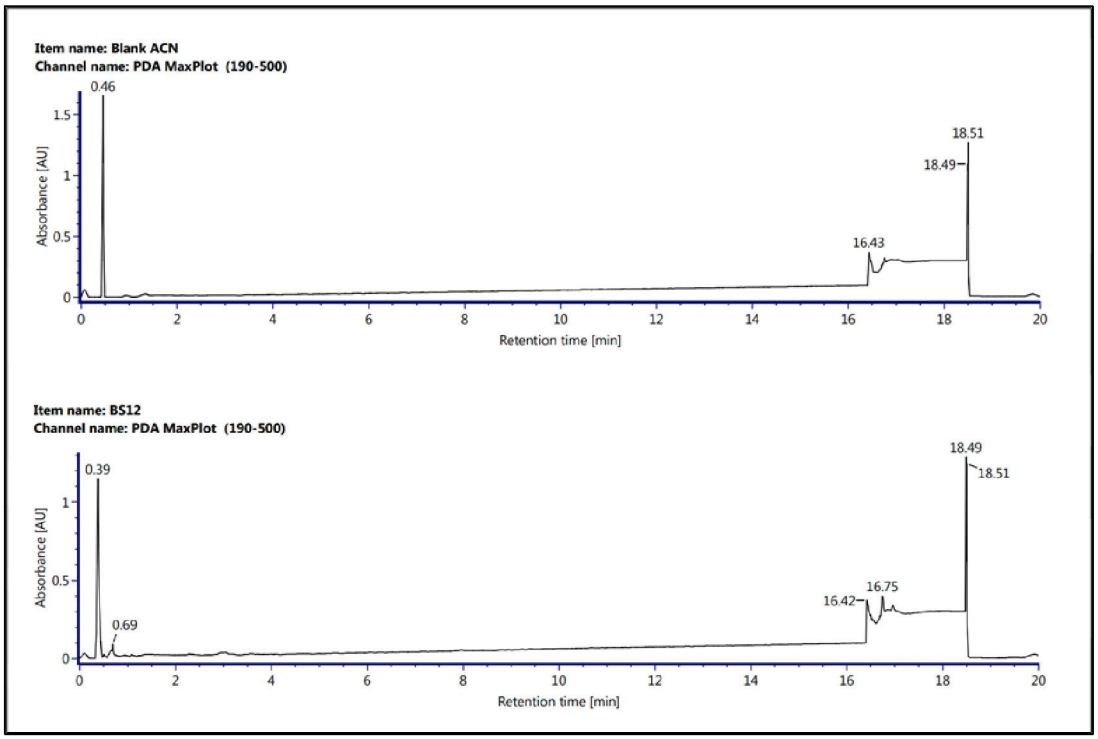

Figure 4.14 The Photodiode Array Chromatograms Comparing A Blank Sample (ACN) With A Biosurfactant Sample Analysed In The Positive Ion Mode. The Absorbance Was Recorded Over A Wavelength Range Of 190–500 nm

Figure 4.15 illustrates the LC-QTOF-MS peak intensity distribution of the compounds identified in the biosurfactant extract analysed in positive ion mode. The markedly higher intensities observed for phospholipid species indicate their dominance within the biosurfactant matrix. The most intense signals are observed at retention times between 16.94 and 18.51 min, corresponding primarily to phosphatidylethanolamine (PE)-type phospholipids, with PE 28:2 exhibiting the highest peak intensity, followed by PE(P-36:2). The longer retention times of these compounds reflects increased hydrophobicity associated with longer or more saturated fatty acid chains (Tapfuma et al., 2019). Their high signal intensities indicate that these phospholipid species are the dominant constituents of the biosurfactant extract.These compounds are characterised by amphiphilic molecular architectures consisting of polar head groups and hydrophobic fatty acid tails, which are critical determinants of adsorption behaviour at metal–solution interfaces.

The dominance of phospholipids with relatively longer hydrophobic tails, as inferred from their retention times and high signal intensities, suggests enhanced hydrophobic interactions with the steel surface. Such interactions promote dense molecular packing and increased surface coverage, facilitating the formation of a compact adsorbed film that acts as an effective barrier against corrosive species. Concurrently, the polar head groups of these phospholipids can interact with charged or electron-deficient sites on the steel surface through electrostatic attraction or coordination bonding, thereby strengthening adsorption stability.

In addition, the presence of fatty acids such as palmitic acid and myristic acid, although detected at lower relative intensities, may contribute synergistically to inhibition by enhancing hydrophobicity and supporting film continuity within the adsorbed layer. The combined effect of dominant phospholipid species and auxiliary hydrophobic components supports a mixed adsorption mechanism, where both physical adsorption and chemisorption processes contribute to corrosion protection.

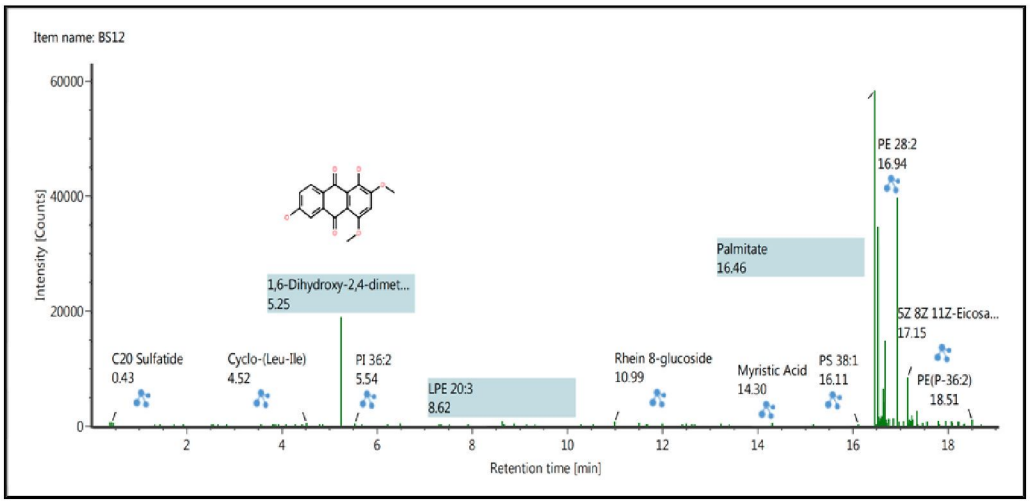

Figure 4.15 The Identified Compounds In The Biosurfactant Sample Obtained Via The Positive Mode Of LC-QTOF-MS Analysis

Table 4.10 summarises the compounds identified in the biosurfactant extract using LC-QTOF-MS operated in positive ion mode. For comparative interpretation, emphasis was placed on the observed *m/z*, mass error (ppm), retention time, and response intensity, as these parameters are most relevant for assessing compound identity, relative abundance, and physicochemical behaviour. Retention time was used as an indicator of relative hydrophobicity, while response intensity served as a semi-quantitative measure of compound dominance. Other parameters, including drift time and collision cross-section (CCS), were retained as supporting evidence to strengthen confidence in compound assignment but were not used as primary comparison metrics.

The analysis conducted detected phospholipids compounds such as Glycerophosphoethanolamines, Glycerophospholipids, and Glycerophosphoinositols, Glycerophosphoserines, In addition to phospholipids, fatty acids such as palmitate (C16:0), palmitoleic acid (C16:1), and myristic acid (C14:0) were identified, indicating the coexistence of fatty acid-derived surface-active components (Gope & Mauro, 2025). Although these compounds were present at lower relative abundances, their hydrophobic chains may contribute synergistically to surface activity and adsorption behaviour by enhancing hydrophobic interactions within the adsorbed layer.

The detection of quinoid compounds, including 1,6-dihydroxy-2,4-dimethoxy anthraquinone and rhein-8-glucoside, suggests the presence of secondary metabolites associated with fungal metabolism. These compounds have been reported to exhibit surface-active or interfacial properties, potentially contributing to the overall emulsification performance of the biosurfactant mixture.

From a corrosion inhibition perspective, the dominance of phospholipid compounds with relatively long hydrophobic tails, as indicated by their higher peak intensities and longer retention times, suggests strong adsorption onto the metal surface. The hydrophobic tails promote close contact with the steel through physical attractive forces, enabling extensive surface coverage, while the polar head groups assist in anchoring the molecules to the steel surface via electrostatic interactions or coordination with active surface sites.

These interactions allow the biosurfactant molecules to form a compact and continuous protective layer on the steel surface. This adsorbed layer acts as a physical barrier that restricts the penetration of corrosive species such as chloride ions, oxygen, and moisture, thereby reducing the corrosion rate. Overall, the molecular composition and dominance of specific phospholipid species play a key role in governing the adsorption-driven corrosion inhibition mechanism observed in this study.

Table 4.10
Summary Of The Identified Compounds Obtained Via The Positive Mode Of LC-QTOF-MS Analysis.

Component Name	Observed Neutral Mass (Da)	Observed m/z	Mass Error (mDa)	Mass Error (ppm)	Observed RT (min)	Observed Drift (ms)	Observed CCS (Å²)	Response	Item Tags
Palmitate	256.2406	274.2745	0.4	1.4	16.46	6.17	188.37	58314	Lipids, Fatty Acids
PE 28:2	631.4165	649.4504	-4.8	-7.3	16.94	8.81	263.6	39754	Lipids, Glycerophosphoethanolamines
Palmitate	256.2405	274.2743	0.3	0.9	16.52	6.2	188.95	34577	Lipids, Fatty Acids
1,6-Dihydroxy-2,4-dimethoxyanthraquinone	300.0624	323.0516	-1	-3	5.25	5.44	167.75	18863	Quinonoids, Bajitian, Morindae Officinalis Radix
5Z 8Z 11Z-Eicosatrienoic Acid	306.2570	324.2908	1.1	3.4	17.15	6.58	199.24	8447	Fatty Acyls, Lipids
PE(P-40:4)	779.5836	797.6174	0.7	0.8	17.24	10.55	317.29	1782	Lipids, Glycerophospholipids
PE(P-36:2)	727.5513	745.5851	-0.3	-0.4	17.26	10.18	305.7	1120	Lipids, Glycerophospholipids
PE 36:2	743.5477	761.5816	1.2	1.6	17.19	10.41	312.73	1095	Lipids, Glycerophosphoethanolamines
PE(P-36:2)	727.5536	745.5874	2	2.7	18.51	10.3	309.19	1047	Lipids, Glycerophospholipids
Palmitoleic Acid	254.2251	272.2589	0.5	1.9	16.52	6.02	184.12	977	Lipids, Fatty Acids
PI 38:4	886.5590	887.5662	1.8	2.1	17.95	10.49	315.77	972	Lipids, Glycerophosphoinositols
PE(P-40:4)	779.5828	797.6166	-0.1	-0.1	17.22	10.32	310.22	960	Lipids, Glycerophospholipids
PE(P-36:2)	727.5534	745.5872	1.8	2.4	17.79	10.35	310.73	907	Lipids, Glycerophospholipids

Component Name	Observed Neutral Mass (Da)	Observed m/z	Mass Error (mDa)	Mass Error (ppm)	Observed RT (min)	Observed Drift (ms)	Observed CCS (Å²)	Response	Item Tags
PE 36:2	743.5480	761.5818	1.5	2	17.14	10.31	309.65	827	Lipids, Glycerophosphoethanolamines
PE(P-38:3)	753.5681	771.6020	0.9	1.2	17.07	10.51	315.95	808	Lipids, Glycerophospholipids
LPE 20:3	503.3009	526.2901	-0.3	-0.5	8.62	7.05	212.18	805	Lipids, Glycerophosphoethanolamines
Rhein 8-glucoside	446.0857	447.0930	0.8	1.9	10.99	6.84	206.08	673	Quinonoids, Folium Sennae, Fanxieye
C20 Sulfatide	835.5844	853.6182	0	0	0.43	5.71	176.71	615	Lipids, Sphingolipids
PE(P-40:1)	785.6312	808.6204	1.3	1.6	0.39	7.33	221.09	578	Lipids, Glycerophospholipids
PI 34:0	838.5588	839.5661	1.7	2	0.41	5.58	173.21	573	Lipids, Glycerophosphoinositols
Cyclo-(Leu-Ile)	226.1672	249.1564	-1	-3.8	4.52	5.01	157.03	547	Ophiopogonis Radix, Maidong, Peptides
Myristic Acid	228.2107	246.2445	1.8	7.2	14.3	5.79	178.26	497	Lipids, Fatty Acids
C24 Sulfatide	891.6455	914.6347	-1.4	-1.5	0.42	7.99	240.64	463	Lipids, Sphingolipids
PI 36:2	862.5561	880.5899	-1	-1.2	5.54	5.7	176.85	416	Lipids, Glycerophosphoinositols
PE 38:4	767.5472	785.5810	0.7	0.8	0.39	5	157.84	383	Lipids, Glycerophosphoethanolamines

Component Name	Observed Neutral Mass (Da)	Observed m/z	Mass Error (mDa)	Mass Error (ppm)	Observed RT (min)	Observed Drift (ms)	Observed CCS (Å²)	Response	Item Tags
PE 40:3	797.5952	820.5845	1.8	2.2	0.4	5.3	165.78	376	Lipids, Glycerophosphoethanolamines
PE 40:5	793.5602	816.5494	-1.9	-2.4	0.4	5.17	162.26	347	Lipids, Glycerophosphoethanolamines
PI 36:2	862.5570	880.5909	-0.1	-0.1	0.4	5.39	168.58	344	Lipids, Glycerophosphoinositols
PI 36:2	862.5590	880.5928	1.9	2.1	0.42	5.75	178.13	319	Lipids, Glycerophosphoinositols
PI 36:2	862.5561	880.5899	-1.1	-1.2	0.39	7.42	224.05	311	Lipids, Glycerophosphoinositols
PS 38:1	817.5833	835.6171	0	0	16.11	5.78	178.65	264	Lipids, Glycerophosphoserines

4.4.2 Negative Ion Mode

Figure 4.16 illustrates that the blank ACN chromatogram exhibits a small RT of 0.47 mins, which is likely due to solvent impurities or column void volume effects. Major peaks were also observed at RTs of 16.42 mins, 18.49 mins, and 18.51 mins. The presence of these peaks in the blank suggested they could arise from residual column contamination, system noise, or non-sample-related artefacts. Thus, the blank acted as a control, verifying the absence of significant interfering compounds from the solvent. Conversely, the biosurfactant sample chromatogram displayed several peaks not observed in the blank sample.

This finding signified the presence of distinct compounds in the biosurfactant extract. Notably, distinct peaks appeared at RTs of 16.43 mins, 16.75 mins, and 16.97 mins, indicating possible biosurfactant-derived compounds (phospholipids, glycolipids, or fatty acid derivatives). A minor peak at RT of 0.69 min was also computed (absent in the blank), potentially indicating a highly polar impurity or a small molecule in the sample. In contrast, the peaks at RTs of 18.49 mins and 18.51 mins were present in the blank and sample, indicating that they were not associated with the biosurfactant and could represent elution artefacts or column residues.

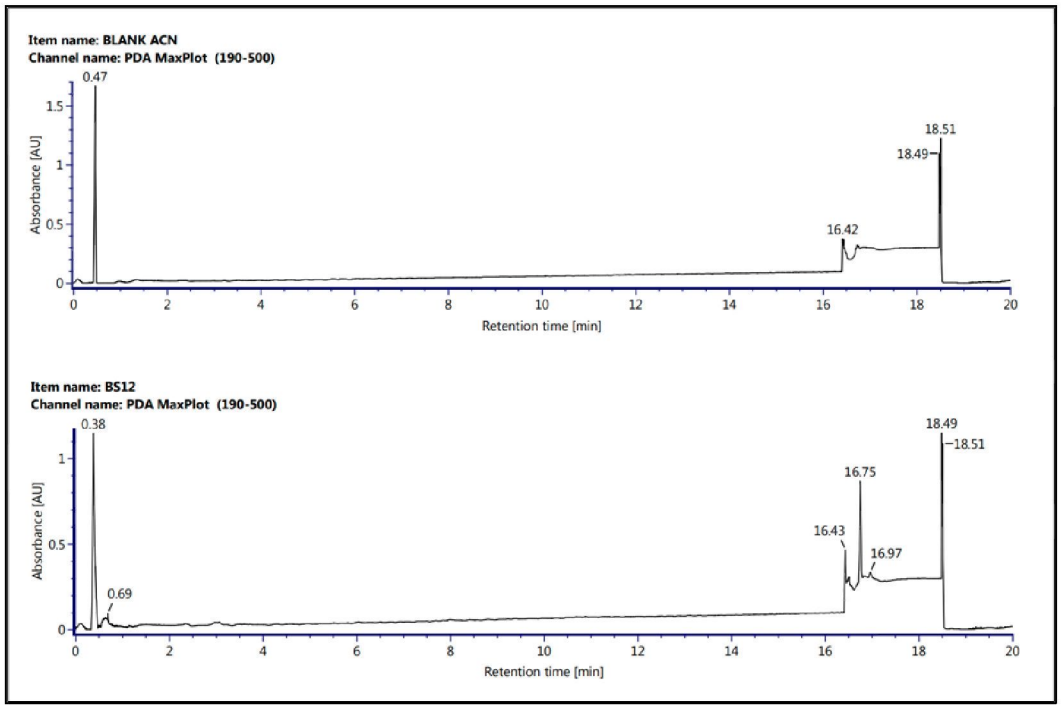

Figure 4.16 The Photodiode Array Chromatograms Comparing a Blank Sample (ACN) With A Biosurfactant Sample Analysed In The Negative Ion Mode. The Absorbance Was Recorded Between 190 nm and 500 nm

Figure 4.17 and Table 4.11 display that the LC-QTOF-MS analysis of the biosurfactant sample in negative mode presents numerous primary compounds. These identified compounds were C24 sulfatide, thymoquinone, 2-acetylemodin-1, PI (34:2, phosphatidylinositol), 10E-heptadecen, taurocholic acid, and taurodeoxycholic acid. The compounds also mostly corresponded to the phospholipid group, in which the primary classes detected included glycerophosphoinositols (PI), glycerophosphoglycerols (PG), glycerophosphoethanolamines (PE), glycerophosphoserines (PS), sphingolipids (C24 sulfatide), and steroid-derived lipids (taurocholic and taurodeoxycholic acids). Meanwhile, glycerophosphoinositols [PI (36:2), PI (34:0), and PI (34:2)] were demonstrated to be the main components among the phospholipids. Several compounds were also prevalent in microbial biosurfactants, contributing to the reduction of interfacial tension. These compounds were glycerophosphoglycerols [PG (40:4), PG (34:1), and PG (32:0)], glycerophosphoethanolamines [LPE (16:0)], and glycerophosphoserines [PS (28:00], supporting the phospholipid properties of the biosurfactant.

In addition to phospholipids, sulfated lipids, particularly C24 sulfatide, were detected. Sulfatides are known for their enhanced hydrophilicity, which improves their surface-active properties. The detection of fatty acid-derived biosurfactants, such as 10E-heptadecenoic acid, suggests the presence of additional amphiphilic components commonly associated with microbial surfactants. Furthermore, the identification of steroid-derived lipids, including taurocholic acid and taurodeoxycholic acid, indicates the presence of bile acid-based biosurfactants. These compounds function as natural detergents, aiding in emulsification and micelle formation.

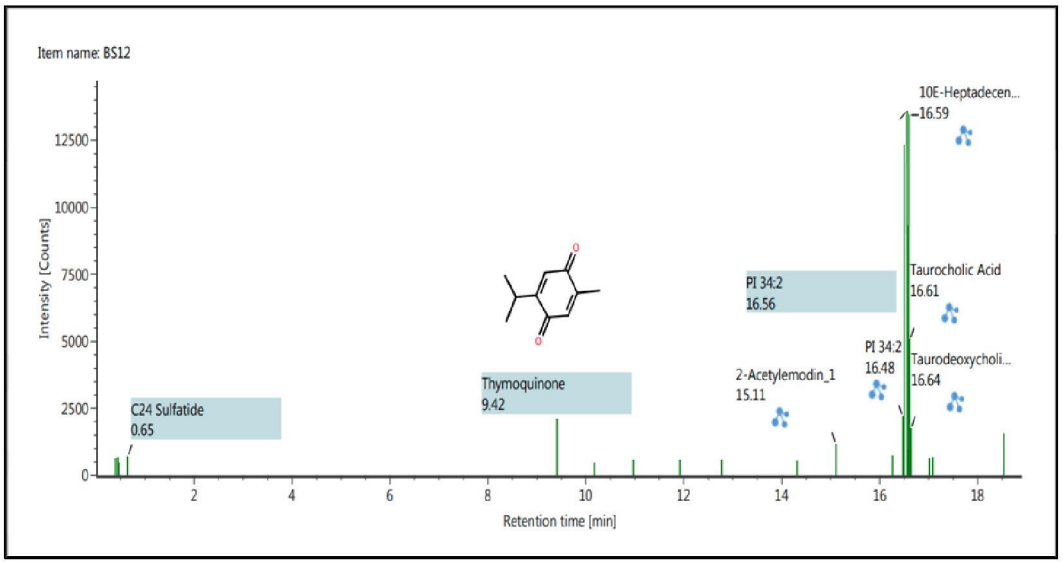

Figure 4.17 The Identified Compounds In The Biosurfactant Sample Via The Negative Mode Of LC-QTOF-MS

Table 4.11
Summary Of The Identified Compounds Obtained Via The Negative Mode Of LC-QTOF-MS

Component name	Observed neutral mass (Da)	Observed m/z	Mass error (mDa)	Mass error (ppm)	Observed RT (min)	Observed drift (ms)	Observed CCS (Å²)	Response	Item tags
PI 36:2	862.5562	861.5489	-1	-1.1	0.4	5.51	162.17	625	Lipids, Glycerophosphoinositols
PI 34:0	838.5563	883.5545	-0.8	-0.9	0.43	5.76	168.41	651	Lipids, Glycerophosphoinositols
PG 40:4	826.571	871.5692	-1.4	-1.6	0.48	5.63	165.09	473	Lipids, Glycerophosphoglycerols
C24 Sulfatide	891.6467	936.6449	-0.2	-0.2	0.65	6.06	176.21	698	Lipids, Sphingolipids
PI 34:2	834.5222	833.5149	-3.6	-4.4	16.48	10.59	309.61	2189	Lipids, Glycerophosphoinositols
LPE 16:0	453.2854	452.2782	-0.1	-0.2	16.49	7.61	221.05	474	Lipids, Glycerophosphoethanolamines
PS 28:0	679.4428	678.4355	0.4	0.5	16.5	9.23	267.18	479	Lipids, Glycerophosphoserines
1-18:1-LysoPE	479.3013	478.294	0.1	0.2	16.55	7.83	226.85	1133	Lipids, Glycerophosphoethanolamines
PI 34:2	834.5241	833.5168	-1.8	-2.1	16.56	10.59	309.78	13603	Lipids, Glycerophosphoinositols
PG 34:1	748.5235	747.5163	-1.9	-2.5	16.56	10.23	298.58	1137	Lipids, Glycerophosphoglycerols
10E-Heptadecenoic Acid	268.2397	313.2379	-0.5	-1.7	16.59	6.26	185.55	13451	Fatty Acyls, Lipids
Taurocholic Acid	515.2912	514.2839	-0.5	-1	16.61	8.06	233.33	5062	Lipids, Steroids

Component name	Observed neutral mass (Da)	Observed m/z	Mass error (mDa)	Mass error (ppm)	Observed RT (min)	Observed drift (ms)	Observed CCS (Å²)	Response	Item tags
PG 32:0	722.5117	721.5045	2	2.7	16.61	10.05	292.82	892	Lipids, Glycerophosphoglycerols
PE 34:2	715.5149	714.5076	-0.3	-0.4	16.61	10.05	292.79	446	Lipids, Glycerophosphoethanolamines
Taurodeoxycholic Acid	499.2953	498.288	-1.5	-3	16.64	8.02	232.34	1747	Lipids, Steroids
PI 34:2	834.5277	833.5205	1.9	2.3	18.54	10.65	311.7	1533	Lipids, Glycerophosphoinositols

4.5 Stability Studies of the Biosurfactant

Several parameters were varied to evaluate the suitability of *Rhizopus sp.* phospholipid-based biosurfactants for practical applications. These parameters included temperature, time, and salinity conditions. The functionality across varying temperatures was examined through the thermal stability test. Likewise, the longevity during prolonged storage periods was assessed through the time-dependent test. The biosurfactant efficiency in high-salt environments was also investigated through a salinity test. This test replicated the conditions observed in marine and industrial systems. Consequently, the physicochemical resilience of the biosurfactant and its applicability in practical contexts could be obtained through these analyses.

4.5.1 Effect of Temperature

To assess the impact of temperature on the biosurfactant activity, the biosurfactant was heated to 60°C and subsequently cooled to room temperature. The E_{24} test was employed to examine the emulsification capacity. Figure 4.18 depicts good stability under moderate heat treatment for the heated and unheated biosurfactants based on their comparable emulsification activity. This aligns with Sena et al. (2018), who reported that heating biosurfactants at 100°C for 60 minutes did not significantly affect their emulsification activity (Sena et al., 2018).

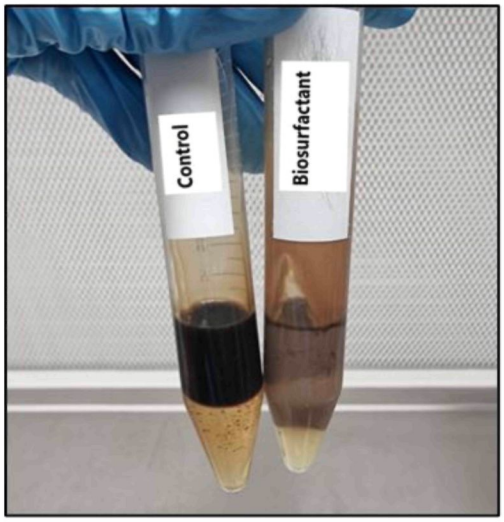

Figure 4.18 The Emulsified Layer Of Biosurfactant In Cooking Oil After Heating At 60°C

4.5.2 Time-Based Assessment on Fungal Growth and Biosurfactant Activity

The stability of the crude biosurfactant over time was tested by refrigerating it at 4°C for 60 days. Its emulsification ability was then assessed with the E_{24}, and compared to the initial values to determine any changes over the 60-day storage period. Table 4.12 tabulates the emulsification activity of the biosurfactant before and after refrigeration. The Emulsification Index (E_{24}) decreased slightly from 75% to 72% indicates that the biosurfactant maintained a high level of emulsification ability over the storage period. This outcome indicated that the crude biosurfactant possessed stable emulsification activity. Additionally, the biosurfactant retained its fungal growth-promoting properties, as evidenced by the consistent mycelium growth observed over the 60-day period as shown in Figure 4.19. These results suggest that the crude biosurfactant maintains its functional properties over prolonged storage, making it a reliable candidate for applications in corrosion inhibition.

Table 4.12
Summary Of The Relationship Between Shelf Life And Emulsification Activity Of The Crude Biosurfactant

Crude biosurfactant	**Emulsification Index (E_{24})**
Initial	75%
After refrigeration for 60 days	72%

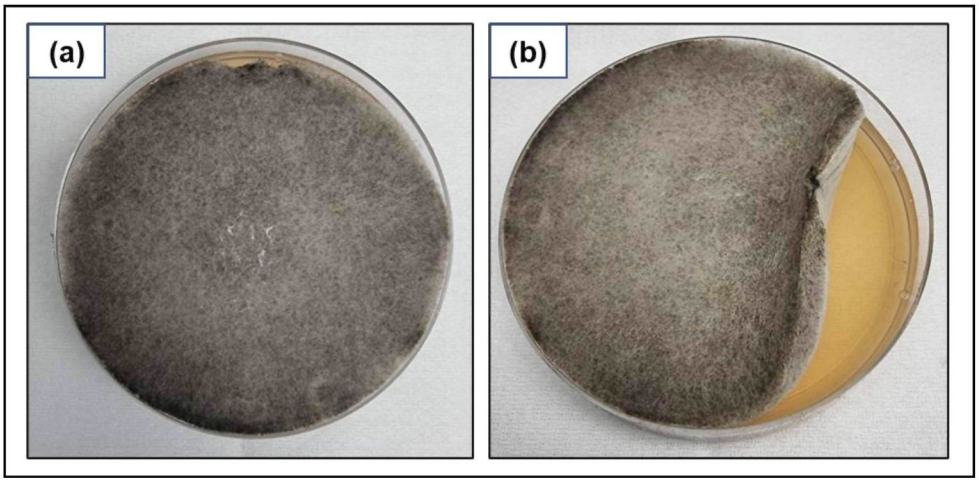

Figure 4.19 (a-b) The *Rhizopus Sp.* Growth On MEA Following 60 Days Of Isolation In Room Temperature (~ 25°C)

4.5.3 Effect of High Salinity on Biosurfactant Activity

Table 4.13 presents the association between salinity and biosurfactant efficiency of the crude biosurfactant. A comparative analysis was implemented between the phospholipid-based biosurfactant under high salinity conditions (30% NaCl) and the control sample, presenting E_{24} values of 65% and 75%, respectively. Thus, increased salinity levels caused a lower emulsification efficiency based on the observed 10% reduction in E_{24}. This outcome suggested that salinity fluctuations and the potential applications across various environmental contexts must be examined owing to the negative correlation recorded between salt concentration and biosurfactant performance.

Table 4.13
Summary Of The Relationship Between Salinity And Emulsification Activity Of The Crude Biosurfactant

Sample	Emulsification Index (E_{24})
Control (No NaCl)	75%
Salinised Biosurfactant (30% NaCl)	65%

4.6 Toxicity Analysis of the Biosurfactant

The correlation between biological impact and *Rhizopus*-derived phospholipid-based biosurfactants was examined using aquatic and plant models. The evaluation aimed to determine the biosurfactant's effects on marine life and plant health in an aqueous environment over a 14-day period. Green Zebra Danio (*Danio rerio*) fish and potted plants (*Monstera adansonii* and *Syngonium podophyllum*) were then employed in this study. The results of this evaluation are presented in Table 4.14 and Table 4.15.

Throughout the 14-day period, only 10% mortality (1 out of 10) was observed in the Green Zebra Danio fish, indicating the minimum of toxicity. Additionally, the fish exhibited normal gill movement, fin condition and feeding patterns. Mild discoloration was observed on the body of deceased fish. Water pH dropped to 6.3, which remains within the safe range for most aquatic organisms, suggesting no immediate harmful acidification effects. Dissolved O_2 (DO) decreased to 6.3 mg/L due to microbial O_2 consumption (Ibrahim & Kutty, 2013). The biosurfactant promoted

microbial growth, leading to an increased O_2 demand, which contributed to DO depletion. The observed minor decrease in swimming activity could be attributed to a combination of lower dissolved O_2 levels, higher microbial activity, potential biofilm formation, and mild biosurfactant exposure-related physiological stress. Nonetheless, the effect on fish locomotion was sublethal rather than critical based on the feeding behaviour, which was essentially unchanged. This response may also be influenced by experimental conditions, including the limited water volume and the absence of water flow, which could further constrain oxygen exchange and natural movement patterns.

Meanwhile, no observable stress indicators (leaf wilting or chlorosis) were recorded during the study period for *Monstera adansonii* and *Syngonium podophyllum*. High biocompatibility was then demonstrated by the biosurfactant in an aqueous environment, which was attributed to the healthy appearance and standard growth patterns presented by both plant species. Notably, the *Rhizopus*-derived phospholipid-biosurfactant was non-toxic and could promote certain aspects of plant growth. This conclusion was based on the improved secondary root development and leaves of these plants.

Table 4.14
Summary Of The Physiological And Behavioural Responses In Fish Exposed To Biosurfactant Solution For 14 Days

Parameter	**Control Group (Distilled Water)**	**Biosurfactant-Treated Group (20%)**
Mortality Rate (%)	0	10%
Swimming Pattern	Slightly reduced activity	Slightly reduced activity
Feeding Behaviour	Normal, regular feeding	Normal, regular feeding
Gill Movement	Normal	Normal
Body Colour Changes	No significant changes	Mild body discoloration observed in deceased fish
Fin Condition	Intact	Intact
Water pH	7	6.3
Dissolved O_2 (mg/L)	7.5 mg/L	6.3 mg/L (16% reduction)
Temperature (°C)	25°C	25°C

Table 4.15
Observations Summary Of Plant Health And Water Quality Over 14 Days

Parameter	Day 0 (Initial Condition)	Day 14 (Final Observation)
Plant Condition	Healthy	Healthy
Monstera adansonii	No wilting or yellowing of leaf	No wilting or yellowing Elongation of secondary roots and new leaf growth occurring
Syngonium podophyllum	No wilting or yellowing of leaf	No wilting or yellowing Elongation of secondary roots and new leaf growth occurring
Water pH	7	6.3
Dissolved Oxygen (mg/L)	7.5	6.8 (9.33% reduction)

4.7 Corrosion Inhibition Analysis

The weight loss and ER measurements were utilised to examine the corrosion IE by biosurfactants derived from *Fusarium sp.*, *Rhizopus sp.*, *Trichoderma sp.*, and *Penicillium* sp. Table 4.16 outlines that the greatest corrosion IE among the four fungal isolates is the *Rhizopus sp.*-based biosurfactant. This study then assessed the corrosion inhibition properties of *Rhizopus* sp.-based biosurfactant using EIS. The surface morphology of the treated specimens was also analysed using an SEM-EDX tool to evaluate the elemental composition and surface modifications caused by the biosurfactant.

Table 4.16
Corrosion Inhibition Studies Assessing The Corrosion Inhibition Efficiency Of Biosurfactants Produced By The Four Fungal Isolates

Isolate	Weight Loss Measurement	Electrical Resistivity	EIS	SEM & EDX
Rhizopus sp.	Conducted	Conducted	Conducted	Conducted
Penicillium sp.	Conducted	Conducted	Conducted	Conducted
Trichoderma sp.	Conducted	Conducted	Not Conducted	Not Conducted
Fusarium sp.	Conducted	Conducted	Not Conducted	Not Conducted

4.7.1 Weight Loss Measurement

This study assessed the corrosion IE of four classes of biosurfactants through weight loss measurement, using a 0.9% NaCl solution as the negative control and Tween 80 as the positive control. The findings then demonstrated that the corrosion IE of biosurfactants and Tween 80 increased with higher concentrations. This pattern has been frequently noted in corrosion inhibition-related studies, in which higher inhibitor concentrations generally improve corrosion protection. Figure 4.20 provides the graphical representation of the result obtained, illustrating the effectiveness of the biosurfactants and Tween 80 at different concentrations. Tables 4.17 to 4.22 list the results for each biosurfactant and the synthetic surfactant.

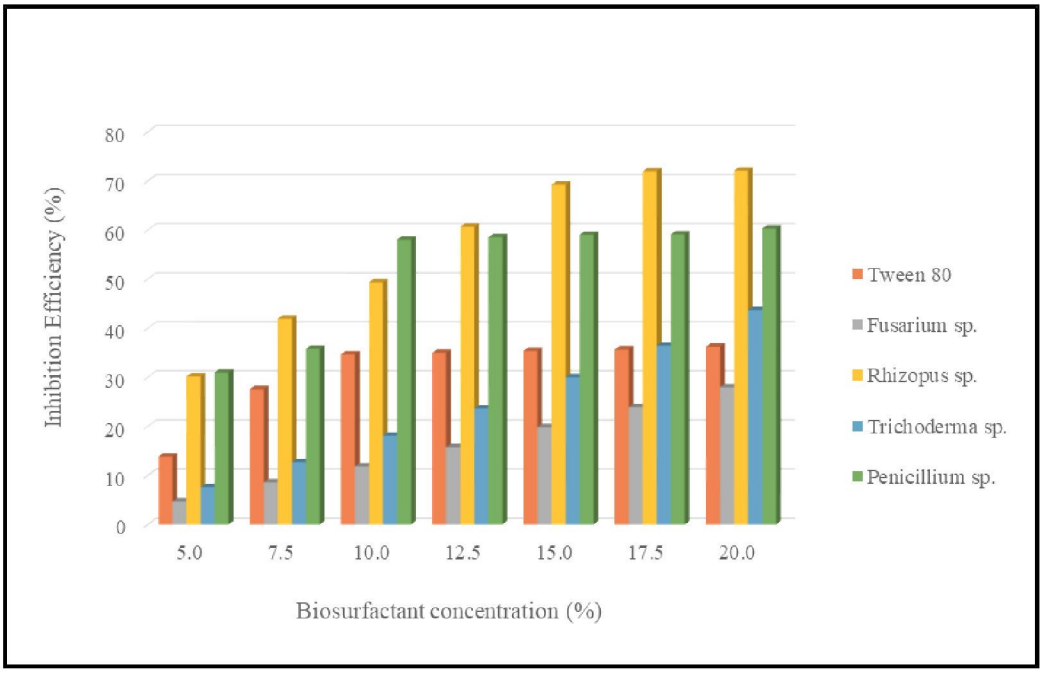

Figure 4.20 The Corrosion Inhibition Efficiency Of Biosurfactants and Tween 80 At Various Concentrations

Table 4.17
Summary Of The Weight Loss Measurement Test Results For Tween 80

Concentration (%)	**Initial pH Value**	**Initial Weight (W_i) gram**	**Weight at Day 14 (gram)**	**Weight at Day 28 (gram)**	**Final weight (W_f) at Day 100 (gram)**	**Weight Loss (W_f-W_i)**	**Corrosion Rate (Cr) mm/year**	**Inhibition Efficiency (ηg %)**
Control	7.17	9.3075	9.3030	9.2928	9.2055	0.1020	0.0716	0.0000
5.0	6.58	8.5884	8.5855	8.5812	8.5056	0.0828	0.0618	13.7955
7.5	6.52	8.5638	8.5621	8.5584	8.4946	0.0692	0.0519	27.5403
10.0	6.38	8.7208	8.7193	8.7154	8.6576	0.0632	0.0468	34.6268
12.5	6.24	9.0326	9.0240	9.0154	8.9679	0.0614	0.0442	34.9466
15.0	6.10	9.3702	9.3617	9.3532	9.3038	0.0605	0.0422	35.3654
17.5	5.96	9.4972	9.4890	9.4808	9.4306	0.0586	0.0405	35.6446
20.0	5.82	9.5360	9.5279	9.5198	9.4685	0.0578	0.0391	36.2029

Table 4.18
Summary Of The Weight Loss Measurement Test Results For *Fusarium Sp.*-Derived Biosurfactant

Concentration (%)	**Initial pH Value**	**Initial Weight (W_i) gram**	**Weight at Day 14 (gram)**	**Weight at Day 28 (gram)**	**Final weight (W_f) at Day 100 (gram)**	**Weight Loss (W_f- W_i)**	**Corrosion Rate (Cr) mm/year**	**Inhibition Efficiency (ηg %)**
Control	7.17	9.3075	9.303	9.2928	9.2055	0.1020	0.07160	0.0000
5.0	7.65	8.9988	8.9855	8.9723	8.9040	0.0948	0.06830	4.6621
7.5	7.82	8.5742	8.5617	8.5492	8.4850	0.0892	0.06550	8.5758
10.0	7.86	8.6162	8.6041	8.5920	8.5300	0.0862	0.06320	11.8138
12.5	7.87	8.8333	8.8217	8.8100	8.7500	0.0833	0.06040	15.7327
15.0	7.89	8.6424	8.6315	8.6205	8.5642	0.0782	0.05750	19.7904
17.5	7.90	9.0949	9.0842	9.0736	9.0189	0.0760	0.05450	23.8586
20.0	8.02	9.2298	9.2197	9.2096	9.1577	0.0721	0.05160	27.9310

Table 4.19
Summary Of The Weight Loss Measurement Test Results For *Rhizopus Sp.*- Derived Biosurfactant

Concentration (%)	**Initial pH Value**	**Initial Weight (W_i) gram**	**Weight at Day 14 (gram)**	**Weight at Day 28 (gram)**	**Final weight (W_f) at Day 100 (gram)**	**Weight Loss (W_f- W_i)**	**Corrosion Rate (Cr) mm/year**	**Inhibition Efficiency (ηg %)**
Control	7.17	9.3075	9.3030	9.2928	9.2055	0.1020	0.0716	0.0000
5.0	7.78	9.1674	9.1637	9.1550	9.0972	0.0702	0.0500	30.1537
7.5	7.95	9.0848	9.0816	9.0739	9.0267	0.0582	0.0416	41.9129
10.0	7.99	9.2283	9.2260	9.2191	9.1769	0.0514	0.0363	49.3226
12.5	8.00	9.1684	9.1623	9.1562	9.1292	0.0434	0.0312	60.6329
15.0	8.02	9.2265	9.2209	9.2153	9.1956	0.0400	0.0285	69.2164
17.5	8.03	9.0860	9.0812	9.0763	9.0590	0.0345	0.0257	71.9405
20.0	8.15	9.3090	9.3047	9.3003	9.2817	0.0310	0.0227	72.0801

Table 4.20
Summary Of The Weight Loss Measurement Test Results For *Trichoderma Sp.*-Derived Biosurfactant

Concentration (%)	**Initial pH Value**	**Initial Weight (W_i) gram**	**Weight at Day 14 (gram)**	**Weight at Day 28 (gram)**	**Final weight (W_f) at Day 100 (gram)**	**Weight Loss (W_f - W_i)**	**Corrosion Rate (Cr) mm/year**	**Inhibition Efficiency (ηg %)**
Control	7.17	9.3075	9.303	9.2928	9.2055	0.1020	0.0716	0.0000
5.0	7.20	8.5988	8.5864	8.5739	8.5100	0.0888	0.0662	7.5718
7.5	7.30	8.6875	8.6757	8.6638	8.6030	0.0845	0.0626	12.6792
10.0	7.35	8.8479	8.8366	8.8254	8.7676	0.0803	0.0587	18.0814
12.5	7.40	9.0452	9.0345	9.0239	8.9691	0.0761	0.0547	23.6068
15.0	7.44	9.3829	9.3728	9.3628	9.3110	0.0719	0.0502	29.9903
17.5	7.60	9.5098	9.5006	9.4914	9.4440	0.0658	0.0455	36.4175
20.0	7.65	9.5488	9.5404	9.5321	9.4891	0.0597	0.0403	43.6792

Table 4.21
Summary Of The Weight Loss Measurement Test Results For *Penicillium Sp*-Derived Biosurfactant

Concentration (%)	**Initial pH Value**	**Initial Weight (W_i) gram**	**Weight at Day 14 (gram)**	**Weight at Day 28 (gram)**	**Final weight (W_f) at Day 100 (gram)**	**Weight Loss (W_f- W_i)**	**Corrosion Rate (Cr) mm/year**	**Inhibition Efficiency (ηg %)**
Control	7.17	9.3075	9.3030	9.2928	9.2055	0.1020	0.0716	0.0000
5.0	7.60	8.8914	8.8894	8.8830	8.8235	0.0679	0.0495	30.9442
7.5	7.72	8.5168	8.5157	8.5129	8.4556	0.0612	0.0460	35.7745
10.0	7.76	8.6557	8.6544	8.6539	8.6153	0.0404	0.0297	58.0159
12.5	7.78	8.7656	8.7599	8.7532	8.7249	0.0407	0.0297	58.4862
15.0	7.80	8.6592	8.6536	8.6481	8.6195	0.0397	0.0294	59.0159
17.5	7.81	8.8235	8.8180	8.8126	8.7845	0.0390	0.0293	59.0977
20.0	7.82	8.8654	8.8599	8.8544	8.8260	0.0394	0.0285	60.2717

Table 4.22
Effect Of Biosurfatants Concentration On Corrosion Inhibition Of Mild Steel Specimens After 100 Days Of Exposure In 0.9% NaCl Solutions

Concentration (%)	**Tween 80**	***Fusarium sp.***	***Rhizopus sp.***	***Trichoderma sp.***	***Penicillium sp.***
5.00%	13.8	4.66	30.15	7.57	30.94
7.50%	27.54	8.58	41.91	12.68	35.77
10.00%	34.63	11.81	49.32	18.08	58.02
12.50%	34.95	15.73	60.63	23.61	58.49
15.00%	35.37	19.79	69.22	29.99	59.02
17.50%	35.64	23.86	71.94	36.42	59.1
20.00%	36.2	27.93	72.08	43.68	60.27

Figures 4.20 indicate a significant positive correlation between biosurfactant concentration and corrosion IE. With increasing concentration, all evaluated biosurfactants demonstrated higher IE. This observation was due to the adsorption of biosurfactant molecules on the metal surface, which created a protective barrier that diminished exposure to corrosive agents and decelerated the corrosion process. The increased IE observed with higher biosurfactant concentration also indicated a greater adsorption capacity, which correlated directly with the concentration of the inhibitors (Al-Kashef et al., 2018). Among the four biosurfactants, the one secreted by *Rhizopus* sp. exhibited superior performance. A consistent increase in IE was denoted, reaching the highest effectiveness at the maximum concentration evaluated. Al-Kashef et al. (2018) recorded similar findings, in which Glycolipid biosurfactants derived from *Rhizopus oryzae* notably improved the corrosion inhibition properties of carbon steel.

Even though a pronounced initial increase in corrosion IE was presented by the *Penicillium* sp.-based biosurfactant, a plateau at elevated concentrations was observed. This finding implied that performance could not be increased above a saturation point for this biosurfactant type. Olivia et al. (2023) propounded similar patterns regarding their *Penicillium*-derived biosurfactants relative to synthetic inhibitors (Tween 80). Intriguingly, an IE closely approaching that of 17.5% Tween 80 was demonstrated by the *Trichoderma* sp.-based biosurfactant. Hence, this biosurfactant was a viable alternative owing to its consistent behaviour across different concentrations (albeit its performance was not on par with Rhizopus *sp.* or *Penicillium sp.*-based biosurfactants). A moderate increase in IE was also recorded for the *Fusarium sp.*-based biosurfactant. Nevertheless, the levels achieved by this isolate were much weaker than the other three biosurfactants. Another interesting observation involved the superior performance compared to Tween 80 in *Rhizopus sp.* and *Penicillium sp.*-based biosurfactants at lower concentrations (5% biosurfactant). Sundaram et al. (2024) asserted that the eco-friendly and cost-effective benefits at reduced concentrations were critical. The study stated that this feature could improve surface-active properties and adsorption efficiency of fungal-based biosurfactants.

Figure 4.21 illustrates the relationship between the concentration of phospholipid biosurfactant produced by *Rhizopus sp.* (ranging from 5% to 20%) and its corrosion inhibition efficiency after 100 days of immersion in the inhibitor solution. At lower concentrations (5% to 15%), inhibition efficiency rises significantly, from 30.45% at 5% concentration to 69.22% at 15% concentration. This indicates that

increasing the biosurfactant concentration enhances corrosion inhibition by forming a protective layer on the metal surface. Conversely, increases in biosurfactant concentration beyond 15% resulted in only slight marginal enhancements in IE. The IE then achieved 71.94% (17.5% biosurfactant) and stabilised at 75.08% (20% biosurfactant). This finding indicated a saturation effect, wherein further increases in biosurfactant did not substantially improve corrosion protection. Lesik et al. (2021) reported similar trends, in which phospholipids in experimental settings conferred protective properties of up to 86.5%.

Equation 4.1 indicates a logarithmic relationship between y (IE) and x (concentration) as follows:

$$y = 23.625ln(x) + 27.694 \quad (4.1)$$

where:

y = corrosion inhibition efficiency, and

x = biosurfactant concentration

As the concentration of biosurfactant increased, the inhibition efficiency rose (albeit at a diminishing rate). The coefficient of determination (R^2) was also 0.9704, signifying a strong and statistically significant correlation between biosurfactant concentration and IE. Likewise, the logarithmic trend observed indicated that IE increased significantly at lower concentrations of biosurfactant. This value eventually stabilised after reaching a certain threshold, suggesting a saturation effect. Specifically, the optimal concentration was approximately 15% biosurfactant, beyond which further addition of biosurfactant yields negligible enhancement in corrosion inhibition. This plateau effect was due to adsorption saturation, where the metal surface was covered entirely, resulting in minimal additional protection from further biosurfactant molecules.

When concentrations surpassed 15% biosurfactant, the incremental improvement in IE decreased as a result of molecular crowding. Thus, an increase in biosurfactant concentration resulted in elevated solution viscosity, which impeded uniform dispersion and caused inconsistent protection across the metal surface. This non-uniform coverage could also lead to specific regions exhibiting diminished IE (Sari et al., 2018). Overall, elevating the biosurfactant concentration beyond 15 to 20%

(according to the logarithmic equation) was both ineffective and impractical, resulting in resource wastage and potential adverse effects. This observation implied that optimising the biosurfactant concentration within the effective range was essential for achieving optimal corrosion inhibition while ensuring cost-effectiveness and stability.

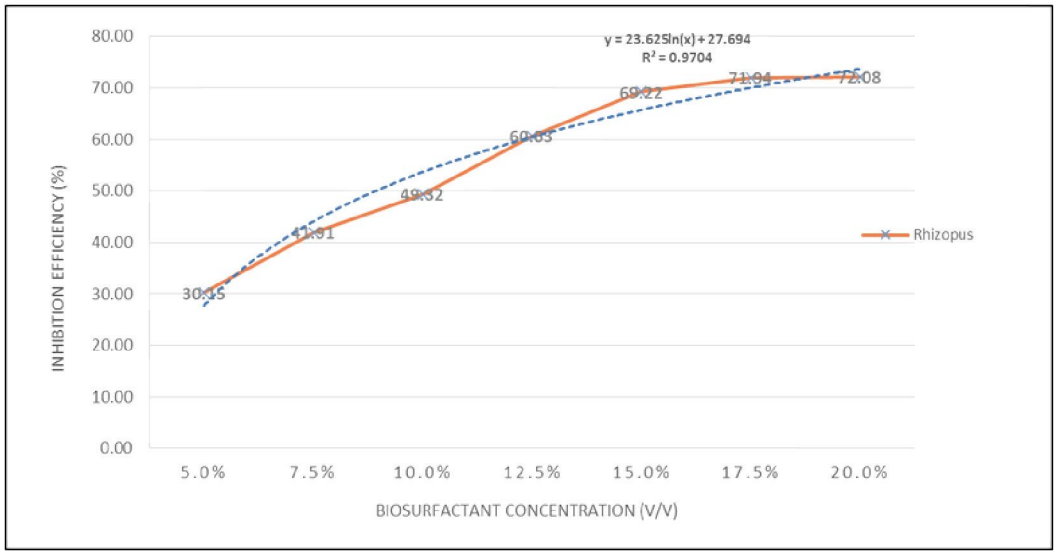

Figure 4.21 The Corrosion IE of *Rhizopus Sp*. Phospholipid-Based Biosurfactant At Concentrations From 5% To 20% After 100 Days Of Mild Steel Specimen Immersion In The Inhibitor Solution

4.7.2 Surface Morphology and Physical Characteristics of Inhibitor Solutions

Figure 4.22 to Figure 4.24 illustrate the physical appearance of the mild steel specimens extracted from the 0.9% NaCl solution, both with and without corrosion inhibitors. The specimens underwent submersion for 100 days. Specimens immersed in the negative control solution (0.9% NaCl) exhibited a brownish-orange coloured corrosion product characteristic of iron oxide layers formed due to chloride-induced corrosion. In contrast, specimens treated with Tween 80 demonstrated partial coverage of orange-coloured spots. No biofilm formation was detected on the surfaces of any specimens. Specimens treated with the *Rhizopus sp.*-based biosurfactant also depicted no observable corrosion or biofilm attachment on their surfaces.

Following cleaning with a fine brush and soft microfiber cloth, the negative control specimens exhibited a dark black coloration accompanied by relatively uniform corrosion features. This appearance is commonly referred to as *black rust*, which consists predominantly of iron oxides formed under low-oxygen conditions. This

corrosion behaviour is characteristic of steel exposed to oxygen-deficient environments and indicates uniform corrosion rather than localized pitting.

Specimens treated with Tween 80 showing sign of localised corrosion following removal of loosely adherent corrosion products. Meanwhile, specimens treated with the phospholipid-based biosurfactant showing minimal corrosion features and uniform surfaces, demonstrating superior corrosion protection.

Visual observations demonstrated that the *Rhizopus* sp.-based biosurfactant possessed markedly enhanced corrosion inhibition capabilities in comparison to Tween 80. This finding was consistent with the research conducted by Ishaq et al. (2015), which evidenced the efficacy of *Aspergillus flavus*-based biosurfactants in the removal of biofilms. Furthermore, Hisham (2015) highlighted the role of passive films in mitigating corrosion by serving as barriers to anodic oxidation and cathodic reduction reactions, further corroborating the observed efficacy of biosurfactants.

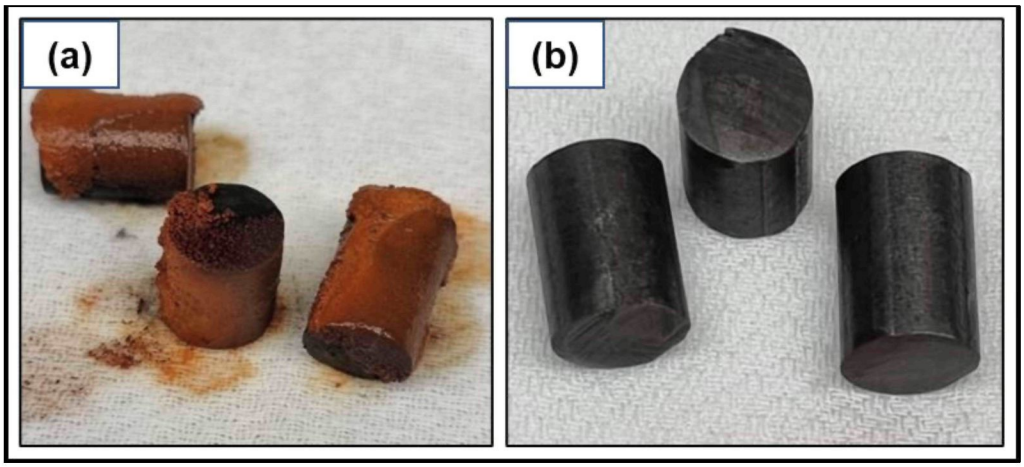

Figure 4.22 The Mild Steel Specimens In A 0.9% NaCl Solution Without Corrosion Inhibitors (a) Before Cleaning, Showing The Formation Of Thick Brownish-Orange Corrosion Products (b) After Cleaning With A Fine Brush And A Microfibre Cloth, Revealing A Black-Coloured Surface

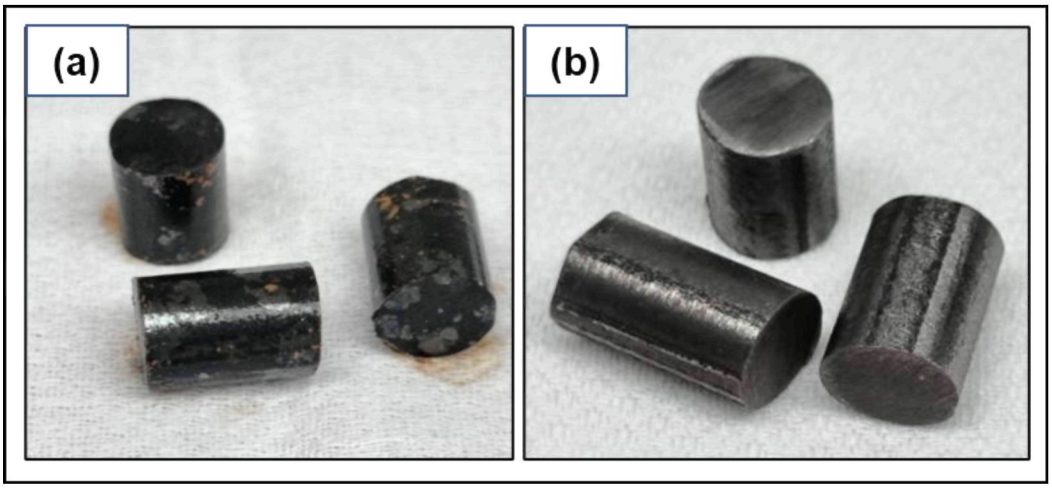

Figure 4.23 The Mild Steel Specimens In A 0.9% NaCl Solution With 20% Tween 80 (a) Surface Condition Of Mild Steel Specimens Before Cleaning, Exhibiting Black Rust Formation With Orange Traces (b) Cleaned Steel Surfaces Showing Sign Of Localised Corrosion

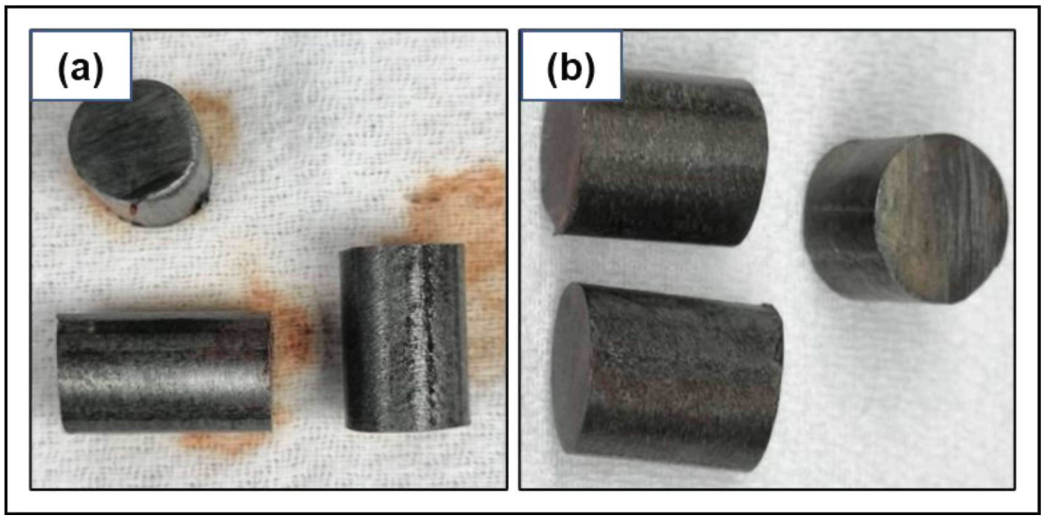

Figure 4.24 The Mild Steel Specimens In A 0.9% NaCl Solution With 20% Phospholipid-Based Biosurfactant. (a) Images Before And (b) Specimens After Cleaning, Exhibiting Minimal Corrosion Features And Uniform Surfaces

Upon extraction of the specimens from their respective solutions, distinct differences in the physical appearance of the solutions were noted (See Figure 4.25 to Figure 4.28). The 0.9% NaCl solution exhibited a yellowish hue, with rust sediment observed at the bottom of the beaker. This outcome implied substantial corrosion activity. Likewise, the solution with Tween 80 displayed dark orange discolouration, indicating a chemical interaction between the metal specimens and the solution. This solution resulted in persistent stains on the beaker, necessitating further effort for

removal with phospholipid-based biosurfactant. On the contrary, the solutions with biosurfactants remained clear, with only biofilm residue flocculating at the bottom. These biosurfactant solutions did not stain the beakers and were easily cleaned by rinsing with tap water, demonstrating the effectiveness of the phospholipid-based biosurfactant in reducing corrosion while being environmentally friendly. The observed clarity also resulted from decreased metal ion release and limited byproduct formation, underscoring the effectiveness of the biosurfactant in corrosion inhibition over prolonged durations.

This study also verified that environmentally sustainable and efficient corrosion inhibitors could be created through biosurfactant-treated solutions exhibiting effective cleaning properties and did not result in staining. Marajan (2020) noted a significant connection between these characteristics and the bioremediation potential of biosurfactants.

Barnita Ghosh and Ray (2011) and Hugo Leon-Santiesteban (2008) documented outcomes identical to this study. These studies examined a toxic environmental contaminant known as pentachlorophenol (PCP). Consequently, PCP was degraded and tolerated by *Rhizopus oryzae* metabolites (strain ENHE). Hugo Leon-Santiesteban (2008) also published that melanin biosynthesis and organic compound degradation-related oxidation reactions produced by tyrosinase caused PCP degradation. The study also attributed this outcome to an extracellular enzyme that breaks down complex organic molecules (lignin peroxidase). Furthermore, *Rhizopus oryzae* for bioremediation applications was verified by both studies regarding the non-toxic nature of these enzymes necessary for biotransformation and removal of PCP. Dinakarkumar et al. (2024) also contended that the bioremediation of heavy metals and remediation of contaminated soils could be improved using *Rhizopus oryzae*-based mycoremediator.

Overall, several advantages were denoted through *Rhizopus sp.*-based biosurfactants compared to synthetic surfactants. These benefits were corrosion inhibition, corrosion products removal, ease of cleaning, and environmental sustainability. Therefore, corrosion prevention and bioremediation could significantly benefit from this biosurfactant class.

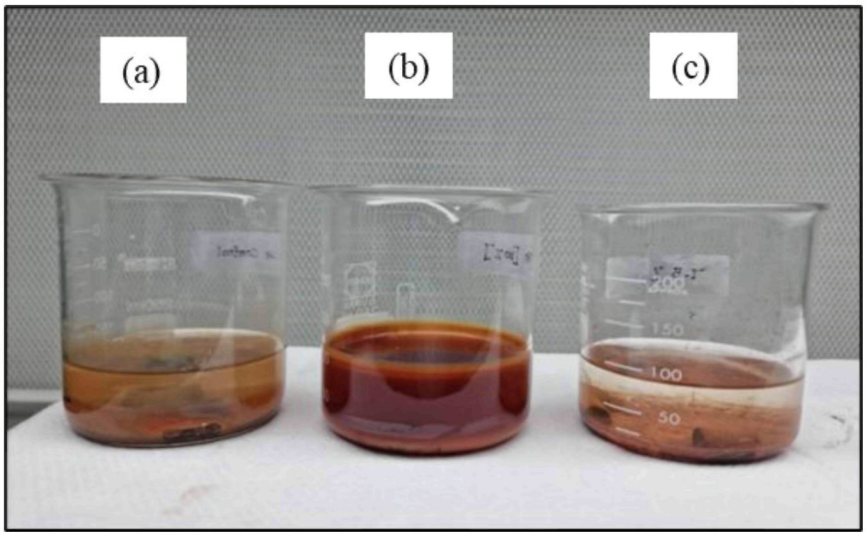

Figure 4.25 The Physical Observation Of The Solutions Involving (a) Positive Control (Tween 80), (b) Negative Control (Distilled Water), and (c) Phospholipid-Based Biosurfactant

Figure 4.26 The 0.9% NaCl (Negative Control) Solution After Immersion Of Mild Steel Bars Coupons For 100 Days

Figure 4.27 The Tween 80 Solutions After Immersion Of Mild Steel Bars Coupons For 100 Days (Positive Control)

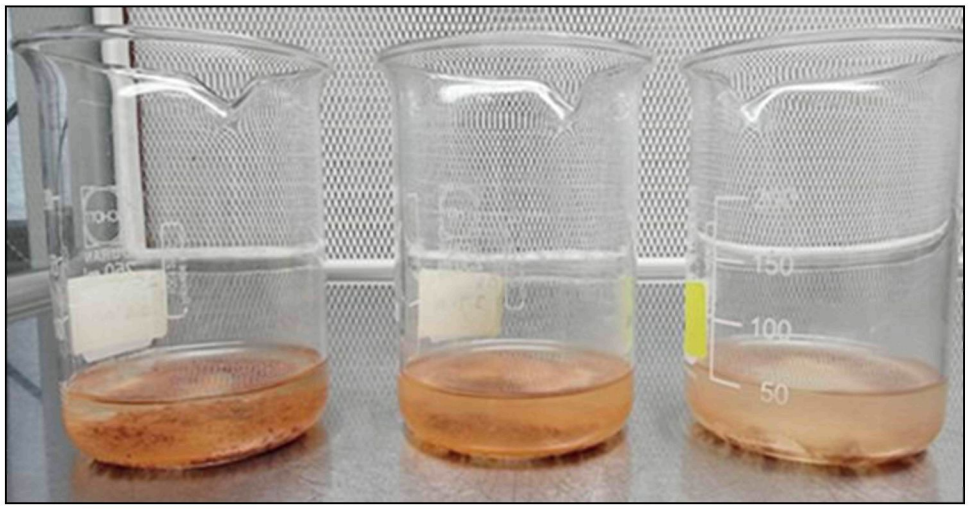

Figure 4.28 The Clear Appearance Of The 0.9% NaCl Solutions Containing Phospholipid-Based Biosurfactants 100 Days Of Immersion Of Mild Steel Bar Coupons

4.7.3 Electrical Resistivity Test

The ER test was performed to assess the efficacy of different inhibitors (Tween 80, *Fusarium sp., Rhizopus sp., Trichoderma sp., and Penicillium sp.*) in preventing corrosion. Previous studies have established a correlation between ER and various concrete durability parameters, including the degree of water saturation, chloride diffusivity and corrosion (Layssi et al., 2015; Márquez & Nokken, 2015; Mukhti et al., 2023). The ER value of mild steel specimens was measured across a range of inhibitor concentrations (5.0–20.0%) added to 0.9% NaCl. Table 4.23 demonstrates a trend of decreasing ER as inhibitor concentration increased, indicating improved corrosion protection. Particularly, *Rhizopus sp.* displayed the most substantial reduction in resistivity, decreasing from 3.31 Ω (5.0% biosurfactant) to 0.73 Ω (20.0% biosurfactant), indicating effective strong inhibition performance. *Penicillium* sp. also exhibited a significant reduction from 3.30 Ω (5.0% biosurfactant) to 1.44 Ω (20.0% biosurfactant), reinforcing its role as an effective corrosion inhibitor. Additionally, *Fusarium* sp. and *Trichoderma* sp. exhibited comparable trends, presenting reductions in resistivity relative to *Rhizopus sp.* and *Penicillium sp.* The declines of *Fusarium sp.* and *Trichoderma sp.* were from 4.88 Ω (5.0% biosurfactant) to 3.45 Ω (20.0% biosurfactant) and from 4.70 Ω (5.0% biosurfactant) to 2.48 Ω (5.0% biosurfactant) respectively. Consequently, a lower corrosion IE was confirmed.

Tween 80 exhibited a consistent decrease in resistivity from 4.15 Ω (5.0% biosurfactant) to 2.50 Ω (20.0% biosurfactant), indicating its effectiveness in corrosion inhibition. Nonetheless, the IE of Tween 80 was considerably inferior to that of biosurfactant-based inhibitors, particularly *Rhizopus sp*. and *Penicillium sp.* The rate of resistivity reduction was also slower than the biosurfactants, suggesting that although Tween 80 provided corrosion protection, its effectiveness was inferior to that of fungal-based biosurfactants. Overall, a significant relationship between biosurfactant concentration and electrical conductivity of mild steel specimens was concluded. Higher conductivity and lower resistivity could be accomplished when the concentrations were higher. Specifically, the highest IE was demonstrated by *Rhizopus sp*.-based phospholipids (minimum resistance value of 0.73 Ω at 20% biosurfactant) (see Figure 4.29 and 4.30). Sabri et al. (2012) presented similar findings, in which a notable association between metal CRs and ER was validated.

Table 4.23
Summary Of The ER Values For Mild Steel Specimens Exposed To Tween 80 And Fungal-Based Biosurfactants In 0.9% NaCl Solution At Varying Inhibitor Concentrations

Inhibitors Concentration (%)	**Tween 80**		***Fusarium sp.***		***Rhizopus sp.***		***Trichoderma sp.***		***Penicillium sp.***	
	Resistivity (Ω)	**Inhibition efficiency**	**Resistivity (Ω)**	**Inhibition efficiency**	**Resistivity (Ω)**	**Inhibition efficiency**	**Resistivity (Ω)**	**Inhibition efficiency**	**Resistivity (Ω)**	**Inhibition efficiency**
5.0	4.15	13.80	4.88	4.66	3.31	30.15	4.70	7.57	3.30	30.94
7.5	3.83	27.54	4.64	8.58	2.58	41.91	4.39	12.68	2.68	35.77
10.0	3.40	34.63	4.44	11.81	2.13	49.32	4.05	18.08	1.80	58.02
12.5	3.20	34.95	4.20	15.73	1.43	60.63	3.71	23.61	1.70	58.49
15.0	2.95	35.37	3.95	19.79	0.90	69.22	3.32	29.99	1.60	59.02
17.5	2.70	35.64	3.70	23.86	0.75	71.94	2.92	36.42	1.55	59.10
20.0	2.50	36.20	3.45	27.93	0.73	72.08	2.48	43.68	1.44	60.27

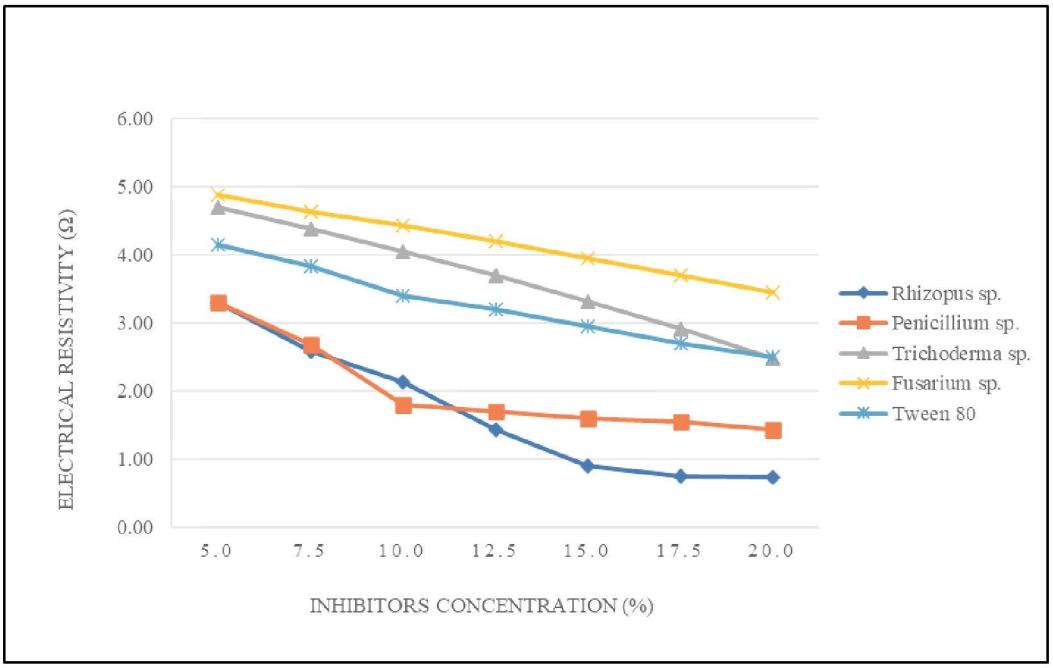

Figure 4.29 The Relationship Between ER And Inhibitor Concentration For Tween 80 And Fungal-Based Biosurfactants (*Fusarium Sp.*, *Rhizopus Sp.*, *Trichoderma Sp.*, And *Penicillium Sp.*). The ER Consistently Decreased With Increasing Inhibitor Concentration, Indicating Improved Corrosion Inhibition

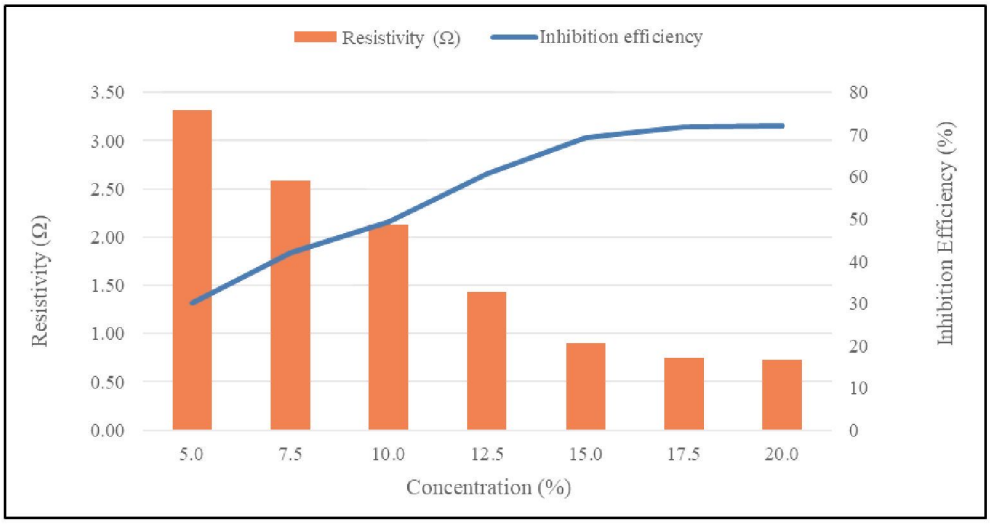

Figure 4.30 The Correlation Between Resistivity And IE Of *Rhizopus Sp.* -Based Biosurfactant At Varying Concentrations

4.7.4 Electrochemical Impedance Spectroscopy (EIS)

This section synthesises the findings from the electrochemical impedance spectroscopy (EIS) analysis, highlighting the differences in corrosion inhibition performance between Tween 80 and phospholipid biosurfactants at varying

concentrations. Characterisation of the steel–electrolyte interface involved the determination of polarisation resistance (R_p), corrosion rate (CR), and the underlying electrochemical mechanisms governing the corrosion process. The acquired data enabled alternating current (AC) impedance analysis, which was modelled using an equivalent electrical circuit to represent the corrosion behaviour of mild steel (Hussin & Kassim, 2010). Accordingly, the formation of protective films, adsorption behaviour, and inhibition effectiveness were evaluated to assess the potential of phospholipid-based biosurfactants as corrosion inhibitors.

The experimental Nyquist plots were fitted using an equivalent circuit comprising solution resistance (R_s), charge transfer resistance (R_{ct}) associated with the interfacial corrosion reaction, a constant phase element representing the double-layer capacitance (CPE_{dl}), and the CPE exponent (n). The incorporation of CPE_{dl} in place of an ideal capacitor is widely adopted to account for surface heterogeneity, roughness, and non-uniform adsorption of inhibitor molecules at the steel surface. An increase in R_{ct} values in the presence of inhibitors indicates enhanced resistance to charge transfer reactions, reflecting effective suppression of corrosion kinetics through surface adsorption.

Table 4.24 summarises the impedance parameters derived from the Nyquist plots for specimens treated with 10% Tween 80 and 5% and 10% phospholipid-based biosurfactants. The phospholipid-treated specimens exhibited significantly higher R_{ct} values than Tween 80 at equivalent concentrations, indicating the formation of a more compact and protective interfacial film. Concurrently, the reduction in CPE_{dl} values suggests a decrease in double-layer capacitance due to inhibitor adsorption and increased surface coverage, which restricts electrolyte access to the steel surface (Zhang et al., 2008). These findings confirm that corrosion inhibition is governed primarily by an adsorption-controlled barrier mechanism.

Figures 4.31 to 4.34 present the EIS spectra of mild steel specimens exposed to the corrosive medium with and without inhibitors. The observed increase in the diameter of the Nyquist semicircles with increasing inhibitor concentration further indicates the strengthening of the protective film and enhanced corrosion resistance (Jain & Kassim, 2010).

Table 4.24
Electrochemical Impedance Parameters Of Mild Steel Samples In 0.9%NaCl Solution In The Absence And Presence Of Inhibitors At 303K (29.85°C)

Inhibitor	Concentration	Rs (Ω cm^2)	Rct (Ω cm^2)	CPE_{dl} (mF cm^{-2})	*n*	IE (%)
Control	Blank	11.54	436.3	1.270	0.733	N/A
		11.11	433.5	1.660	0.726	N/A
Tween 80	10%	13.70	1440	0.240	0.636	69.90
		13.40	1180	0.607	0.623	63.26
Phospholipids	5%	13.54	358	0.185	0.799	N/A
		15.38	534	0.138	0.713	18.82
Phospholipids	10%	24.40	621	0.080	0.794	30.19
		12.80	625	0.112	0.900	30.64

Note: Rs, Rct, CPEdl, *n* and IE are referred as solution resistance, charge-transfer resistance, double layer constant phase element, surface heterogeneity factor, and inhibition efficiency, respectively.

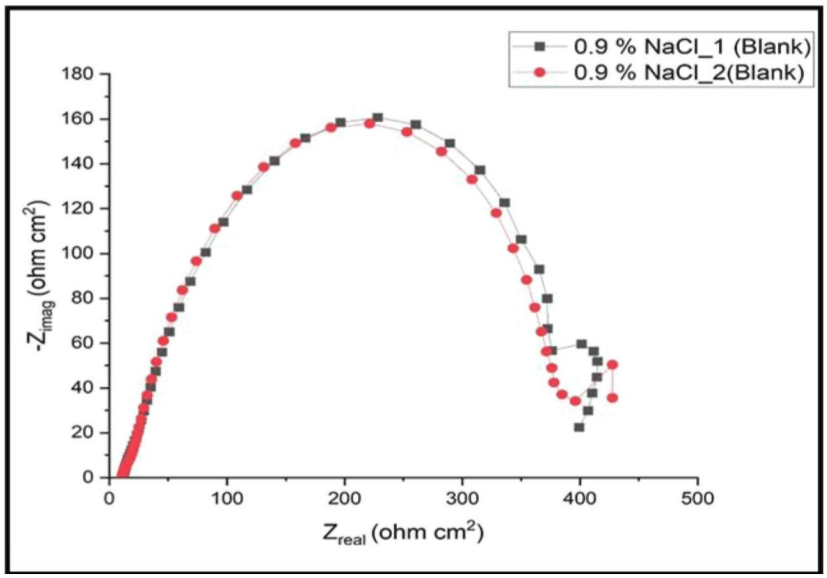

Figure 4.31 The Nyquist Plot Of Mild Steel (Referred As BK_1 and BK_2) in 0.9 % NaCl Solution (As Negative Control) At 303 K

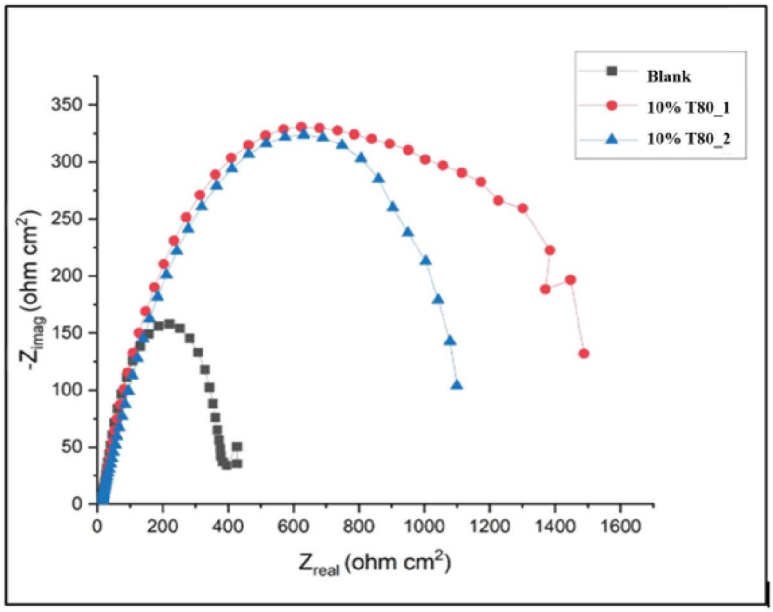

Figure 4.32 The Nyquist Plot Of Mild Steel In The Presence Of 10% Tween 80 And A Blank Control (BK_2) In A 0.9 % NaCl Solution At 303 K

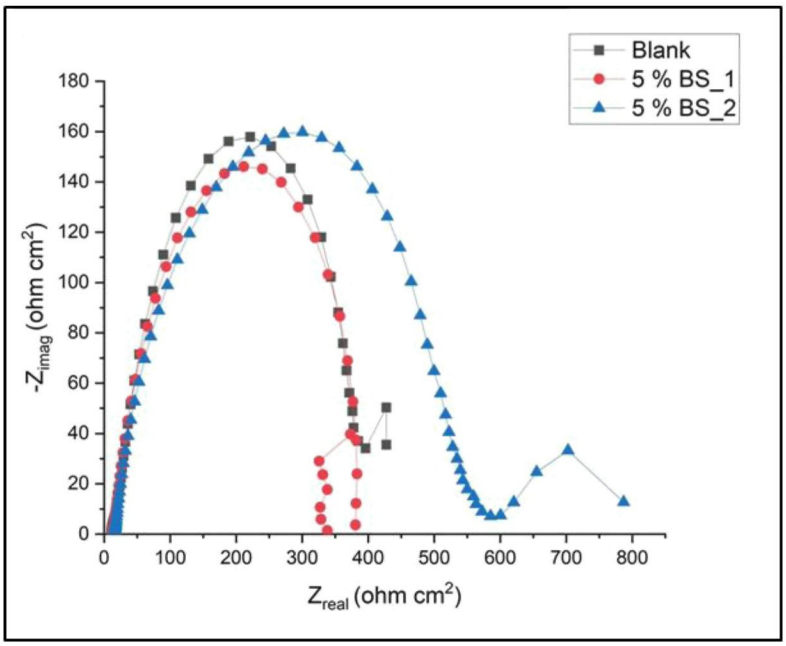

Figure 4.33 The Nyquist Plot Represents The Electrochemical Impedance Behavior Of Mild Steel In The Presence Of 5% Phospholipids-Based Biosurfactant (BS_1 And BS_2) And Blank Control (BK_2) In A 0.9% NaCl Solution At 303 K.

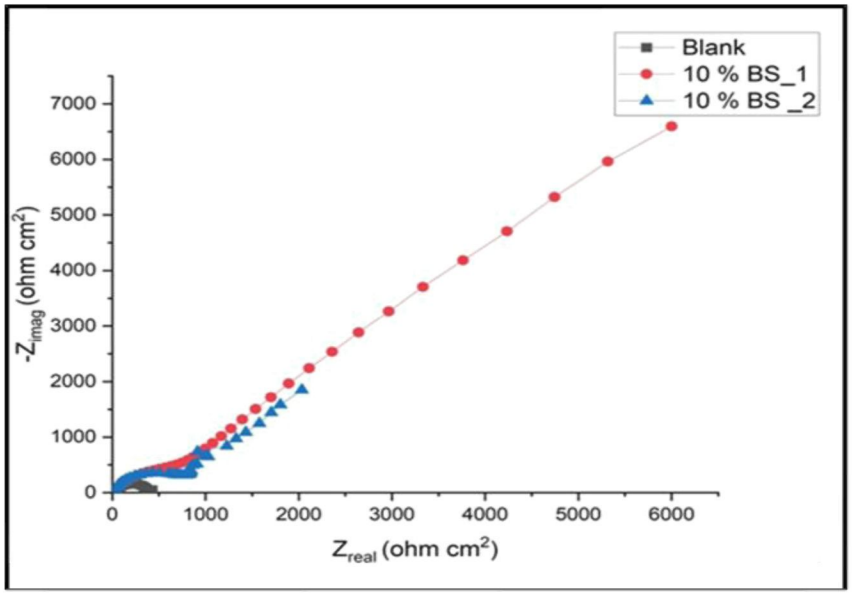

Figure 4.34 The Nyquist Plot Represents The Electrochemical Impedance Behavior Of Mild Steel In The Presence Of 10 % Phospholipids-Based Biosurfactant (BS_1 and BS_2) And Blank Control In A 0.9% NaCl Solution At 303 K.

The CPE was regarded as a surface irregularity of the electrode, resulting in a more pronounced depression in the Nyquist semicircle diagram (the metal-solution interface functioned as a capacitor with irregular surface). When the electrode surface was homogeneous and planar, the *n* equalled 1. This process caused the meta-solution interface to function as a capacitor with a regular surface. Subsequently, the simulation of Nyquist plots with Randle's model containing CPE_{dl} (in place of capacitance and R_{ct}) demonstrated strong concordance with experimental data (Jain Kassim et al., 2010). The rise in charge R_{ct} and the decline in CPE_{dl} then suggested a decrease in the corrosion rate (B. A. Abd-El-Nabey, S. El-Housseiny, H. M. El-Kshlan, 2017). This outcome implied that the formation of a protective layer on the metal surface (produced from inhibitor adsorption) hindered the charge transfer processes and active surface area exposed to the corrosive medium. The reduced value of *n* also revealed that surface inhomogeneity arose from the roughening of the metal surface due to corrosion.

The negative control specimens displayed the lowest R_{ct} of 436.3 Ω cm^2 and 433.5 Ω cm^2, indicating no IE. The 10% Tween 80 then exhibited the highest corrosion inhibition, with R_{ct} of 1440 Ω cm^2 and 1180 Ω cm^2. These values resulted in IEs of 69.90% and 63.26%, respectively. Likewise, the CPE_{dl} exhibited a significant decrease, indicating effective adsorption of Tween 80 molecules on the steel surface. The highest IE (18.82%) was then observed for the 5% biosurfactant. Nonetheless, the IE for the

repetition (second specimen) was not computed owing to the R_{ct} value of the control specimen (BK_2) exceeding that of the tested specimen (R'_{ct}). This observation indicated that additional repetition tests were required to achieve an accurate value for IE. Elevating the phospholipid concentration to 10% also resulted in a notable increase in the R_{ct} values to 621 Ω cm^2 and 625 Ω cm^2, which correspondingly enhanced the IEs to 30.19% and 30.64%, respectively. This observation signified that increased biosurfactant concentration enhanced corrosion inhibition.

The results indicated that elevating the biosurfactant concentration from 5% to 10% improved corrosion inhibition, suggesting a concentration-dependent enhancement of its protective effects on the mild steel surface. Despite the IE of the phospholipid-based biosurfactant being lower than that of Tween 80, its n value was higher at both 5% and 10% biosurfactants. This larger n value implied a more homogeneous and smoother surface, which could be attributed to the development of a protective biofilm (Jain Kassim et al., 2010). Overall, the results demonstrated that biosurfactants significantly improved corrosion inhibition due to their efficient adsorption and protective film formation on the steel surface. Nevertheless, the finer molecular structure of the Tween 80 enabled deeper penetration into mild steel, enhancing its efficacy in inhibiting internal corrosion.

4.7.5 Scanning Electron Microscope (SEM) and Energy Dispersive X-ray Spectroscopy (EDX)

The SEM-EDX tool was employed to examine the CR of mild steel specimens treated with Tween 80 and phospholipid-based biosurfactant at different concentrations. Information concerning the surface morphology and elemental composition of the steel surfaces was obtained following a 100-day immersion period in inhibition solutions. Notably, the relationship between corrosion inhibitors and the corrosion behaviour of mild steel was presented through the surface morphology analysis conducted using SEM micrographs.

4.7.5.1 SEM

EM–EDX analysis was employed to characterise the surface morphology and elemental composition of mild steel specimens exposed to 0.9% NaCl solutions

containing different inhibitor concentrations after 100 days of immersion. Observations at 1000× magnification enabled correlation between inhibitor adsorption, surface degradation features, and the resulting corrosion behaviour of the steel, as illustrated in Figure 4.35(a–f).

Plate 4.35(a) illustrates the surface condition of the fresh mild steel specimen prior to exposure to any corrosive medium, exhibiting a smooth and intact surface morphology. In contrast, Plate 4.35(b) represents the mild steel specimen exposed to a saline environment (0.9% NaCl) without any protective inhibitor. The control specimen shows pronounced surface degradation characterised by a roughened texture, widespread general corrosion, and distinct pitting features. These morphological characteristics indicate sustained and uncontrolled corrosion activity in the absence of corrosion inhibitors.

Figure 4.35(c) to 4.23(f) present the surface analysis of mild steel specimens treated with inhibitors. Specimens subjected to 10% Tween 80 solution displayed irregular surface morphologies characterised by localised corrosion. Conversely, the extent and severity of pitting were considerably lower than those observed in the control specimen. Specimens immersed in 5% biosurfactant solution exhibited significantly smoother surface morphology. This finding implied decreased corrosion activity, even at low biosurfactant concentrations. An increase in biosurfactant concentration to 10% then resulted in a progressively more uniform mild steel surface displaying fewer pits and improved microstructure. At 15% biosurfactant, the mild steel exhibited minimal indications of corrosion-related damage. The enhanced surface morphology also revealed a lower susceptibility to pitting and general corrosion, reinforcing and supporting the increased inhibition effectiveness of the biosurfactant at elevated concentrations.

These findings indicate that while Tween 80 demonstrated a higher inhibition efficiency of 34.63% at a 10% concentration in the Weight Loss Measurement method, compared to 30.15% for phospholipid-based biosurfactant at 5%, its ability to provide surface protection was inferior. This conclusion is supported by the presence of residual surface damage, suggesting that the phospholipid biosurfactant at 5% concentration offered better surface integrity despite its slightly lower inhibition efficiency. The SEM analysis demonstrated that specimens treated with phospholipid-based biosurfactants exhibited significantly improved surface morphology compared to negative control

specimens or specimens treated with 10% Tween 80. The surface enhancement was positively correlated with the increasing concentration of the biosurfactants.

Distinctive molecular structure and adsorption properties were two primary factors contributing to the improved corrosion inhibition by phospholipid-based biosurfactants. Generally, biosurfactants adsorb onto metal surfaces and create protective films that inhibit corrosion. This process is attributed to the hydrophilic and hydrophobic moieties of the amphiphilic molecules. Sivakumar et al. (2024) propounded that biosurfactants in corrosion mitigation operated by this mechanism. Previous studies also agreed that the corrosion IE of biosurfactants was highly dependent on their concentration (Zin et al., 2018; Sivakumar et al., 2024). Notably, multilayered protective films and micelle structures on the metal surface were observed when concentrations were higher. This procedure eventually enhanced the barrier against corrosive agents. Hence, this concentration-dependent improvement corresponded with the SEM findings, indicating that higher biosurfactant levels were associated with improved surface preservation.

Numerous studies have proved that phospholipid-based biosurfactant treatment could improve surface quality. Lesik et al. (2021) stated that carbon steel surfaces contained protective layers when plant material-based phospholipids were utilised to lower CRs. Overall, superior corrosion protection could be accomplished with higher phospholipid-based biosurfactant concentrations based on the SEM data. The protective barriers against corrosion, as demonstrated by previous studies, occur when biosurfactants adsorb onto metal surfaces.

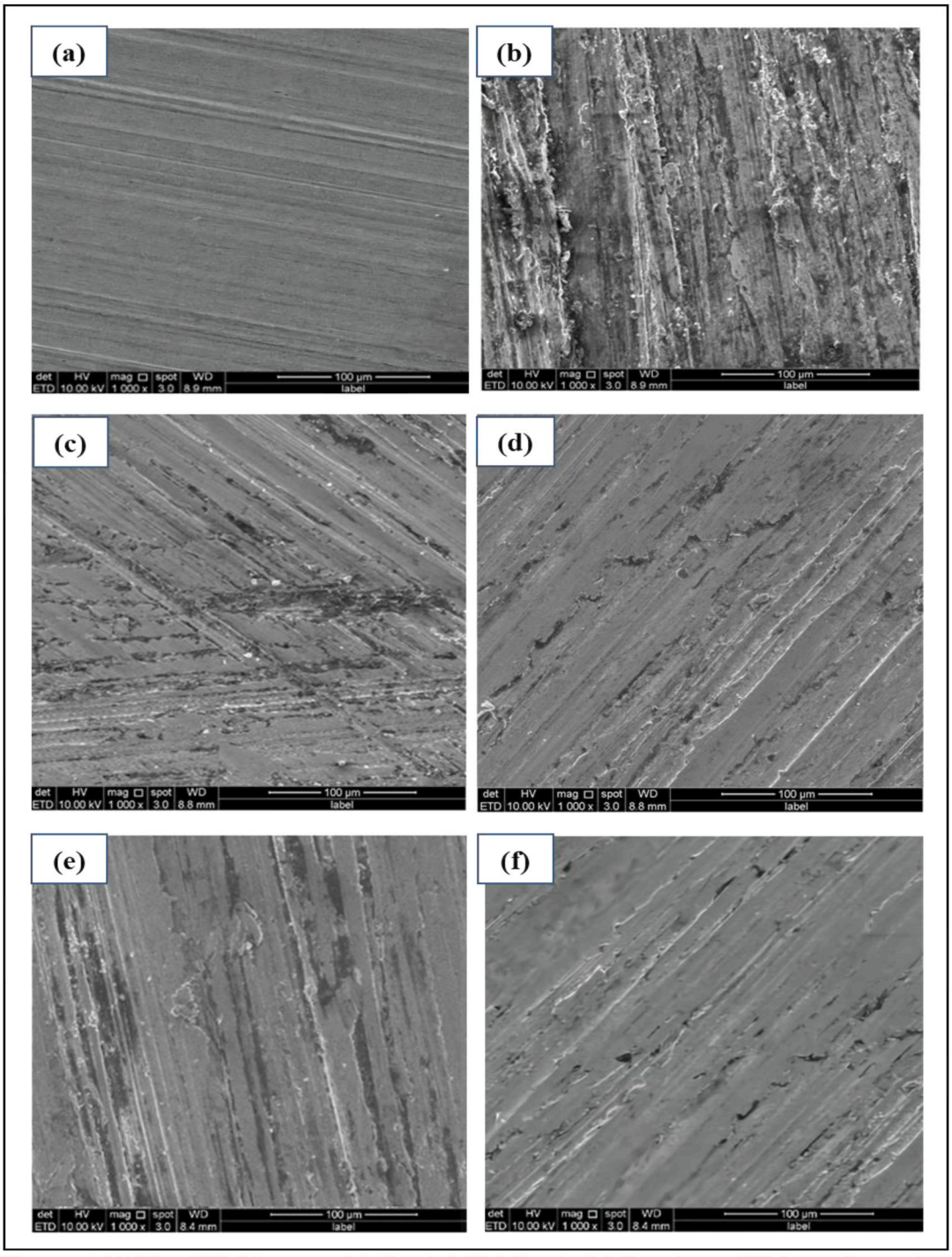

Figure 4.35 The SEM Images (a) Fresh Mild Steel, (b) Specimen Without Corrosion Inhibitor, (c) Specimen Treated With 10% Tween 80, (d) Specimen Treated With 5% Biosurfactant, (e) Specimen Treated With 10% Biosurfactant, And (f) Specimen Treated With 15% Biosurfactant.

4.7.5.2 EDX

Figure 4.36 to Figure 4.41 provide EDX spectra of mild steel specimens. The dominance of these peaks reflects the direct exposure of the steel substrate, with

minimal surface coverage by corrosion products or adsorbed species. SEM–EDX analysis provides a comprehensive comparison of surface condition and elemental composition of mild steel under different exposure and inhibition scenarios. Fresh mild steel (Figure 4.36) exhibited high-intensity Fe peaks with minimal oxygen contribution, confirming an unoxidised metallic surface. In contrast, steel specimens immersed in 0.9% NaCl without inhibitor (Figure 4.37) showed a marked reduction in Fe peak intensity accompanied by pronounced oxygen signals, indicating extensive oxide formation and active corrosion in the chloride-rich environment. The presence of corrosion products partially masked the underlying iron substrate, consistent with severe surface degradation observed in SEM morphology.

Figure 4.38 show steel treated with 10% Tween 80 exhibited relatively higher Fe peak intensity and reduced oxygen signals compared with the uninhibited specimen, indicating partial suppression of corrosion through surface adsorption of the surfactant. However, the persistence of oxygen and carbon peaks suggests that Tween 80 provides only moderate protection, allowing some oxide formation and incomplete surface coverage.

In comparison, phospholipid-based biosurfactant-treated specimens (5–15%) demonstrated progressively enhanced corrosion protection. At 5% concentration, a clear reduction in oxygen peak intensity and stabilisation of Fe signals were observed, indicating effective adsorption of phospholipid molecules and limitation of oxide growth. Increasing the biosurfactant concentration to 10% and 15% resulted in further suppression of oxygen-related signals, with minimal differences between these two concentrations, suggesting near-complete surface coverage and perceived saturation of the protective film at approximately 10%. The detected carbon peaks are attributed to the organic phospholipid layer adsorbed on the steel surface, which acts as a compact barrier restricting chloride ingress and oxygen diffusion.

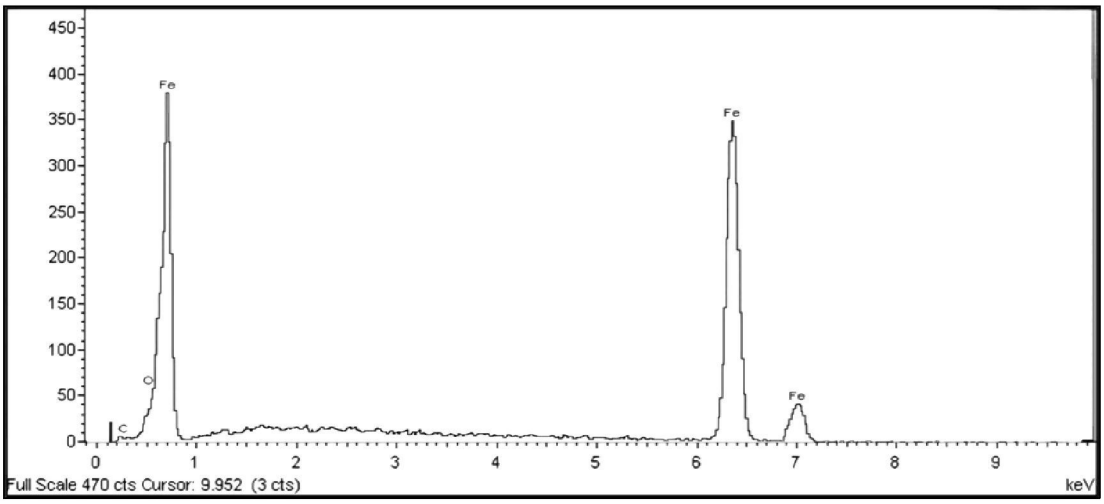

Figure 4.36 The EDX Spectrum Of Fresh Mild Steel

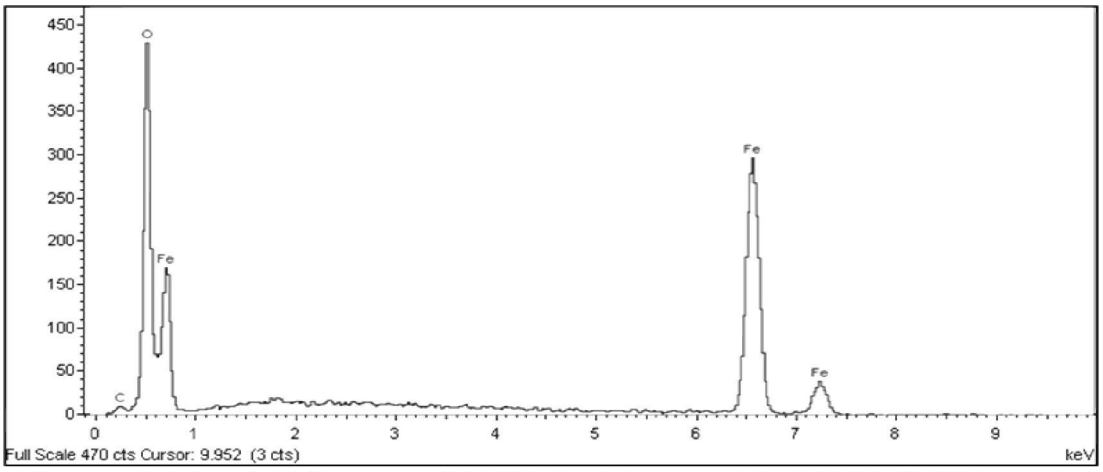

Figure 4.37 The EDX Spectrum Of Mild Steel Immersed In 0.9%NaCl Without An Inhibitor

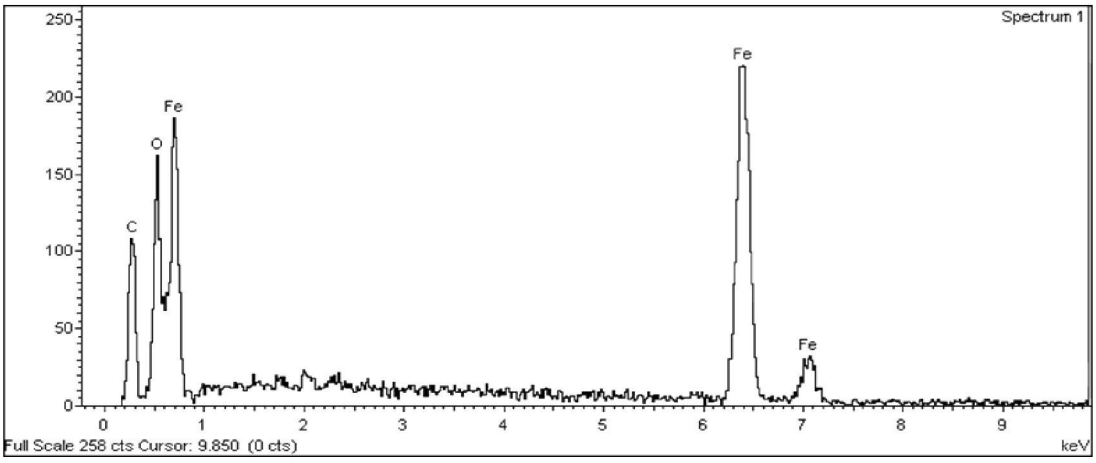

Figure 4.38 The EDX Spectrum Of Mild Steel Immersed In 0.9%NaCl With 10% Tween 80

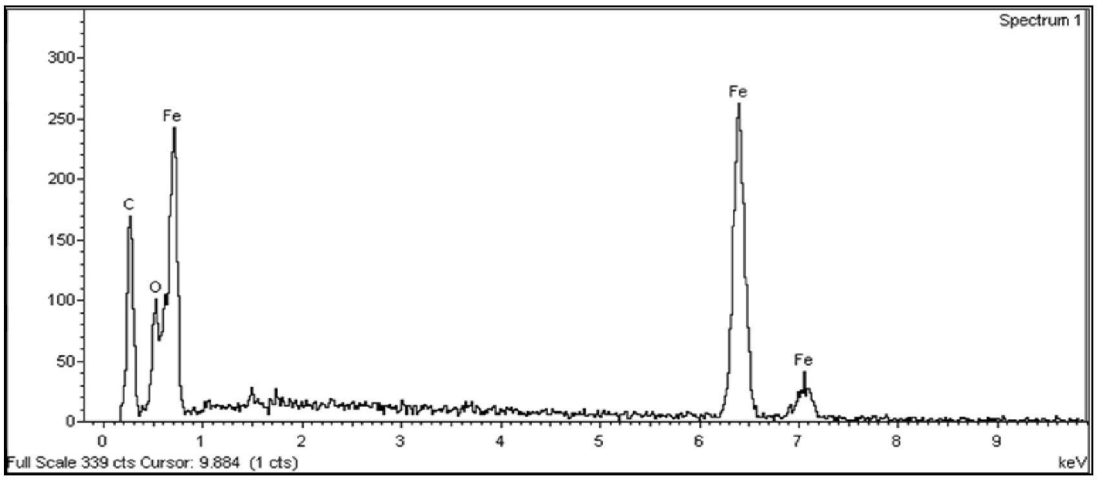

Figure 4.39 The EDX Spectrum Of Mild Steel Immersed In 0.9%NaCl With 5% Phospholipids-Based Biosurfactant

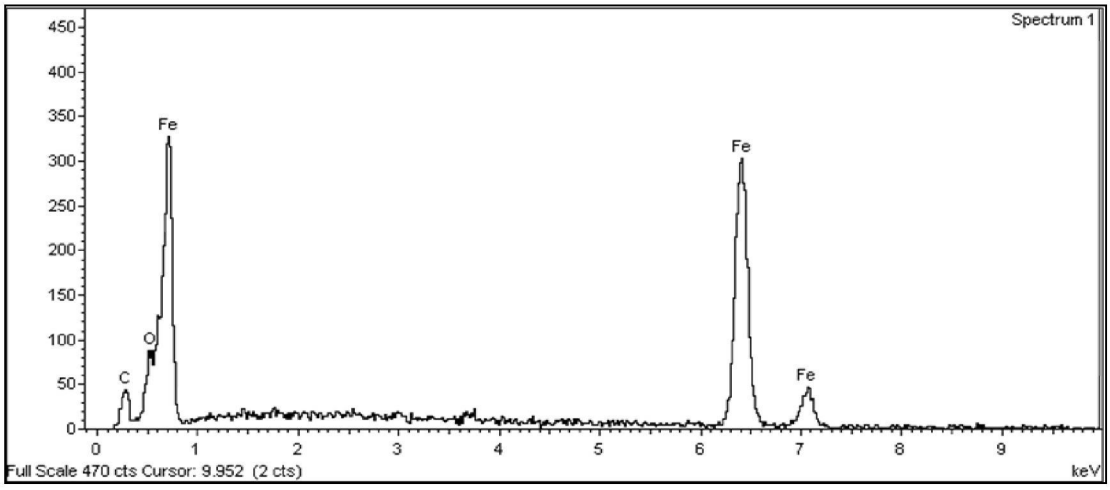

Figure 4.40 The EDX Spectrum Of Mild Steel Immersed In 0.9%NaCl With 10% Phospholipids-Based Biosurfactant

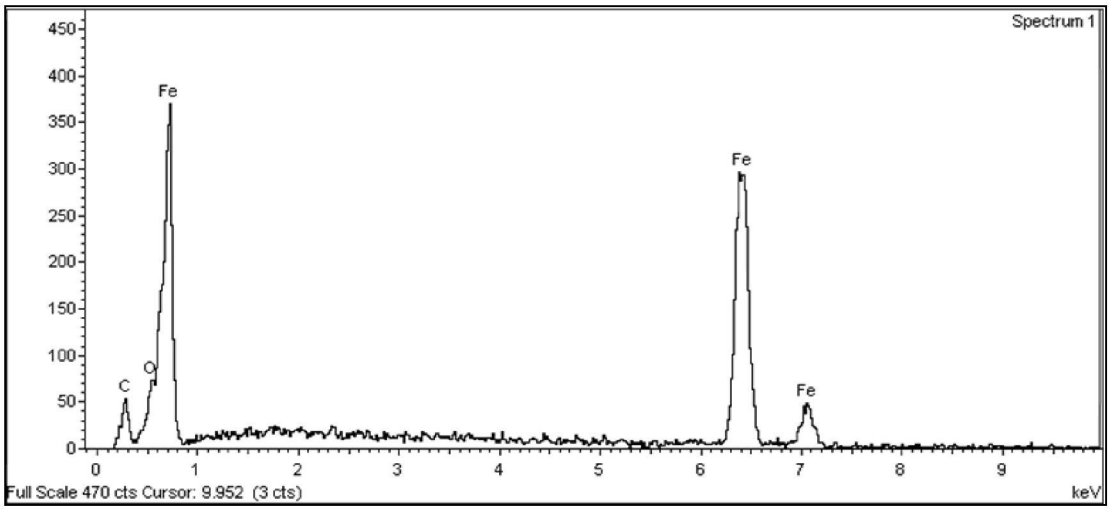

Figure 4.41 The EDX Spectrum Of Mild Steel Immersed In 0.9%NaCl With 15% Phospholipids-Based Biosurfactant

The elemental composition of corrosion products on the surface of the specimens as summarised in Table 4.25. These data show the percentage of iron (Fe), oxygen (O), and carbon (C), which provide insight into the corrosion process. This process entailed the loss of Fe through its reaction with O_2 to form Fe_2O_3 (Iron oxide), commonly referred to as rust. The presence of C on the surface also implied organic residues, which resulted from the adsorption of corrosion by-products or protective films. Furthermore, the corroded specimen denoted a higher percentage of O due to the formation of $Fe(OH)_2$ and other oxide precipitates. In treated specimens, the biosurfactant lowered O content, indicating a decrease in CR. The notable content reduction in O also revealed the efficacy of this inhibitor (Jain Kassim et al., 2010).

A significant atomic percentage of O was observed from the mild steel (without an inhibitor) EDX spectrum. This observation confirmed the extensive formation of corrosion products. As the biosurfactant concentration increases, the spectra show a reduction in O_2 intensity and a corresponding rise in iron content. This suggests that the inhibitor effectively slows down iron dissolution and shields the steel surface from corrosion(Hussin et al., 2015). From the EDX evaluation, it is clear that the upraising value of O_2 is due to the formation of the $Fe(OH)_2$, whereas, for C, it is due to the presence of biosurfactant that acts as the active inhibitor and complexes with the mild steel surface (Hussin & Kassim, 2010).

Among the treated samples, steel exposed to 15% biosurfactant exhibited the highest Fe content, indicating minimal corrosion. The lower O_2 content signifies reduced Fe_2O_3 formation, while the higher C percentage suggests the accumulation of a biofilm, acting as a protective barrier. Notably, the elemental composition of specimens treated with 10% and 15% biosurfactant showed minimal variation, with the 10% concentration achieving IE comparable to the 15% treatment.

The steel treated with 5% biosurfactant exhibited reduced Fe content, indicating heightened metal loss attributable to corrosion. The higher O and C levels suggested the occurrence of rust and organic corrosion by-products, implying that this concentration was inadequate for corrosion inhibition. Similarly, steel treated with Tween 80 exhibited moderate Fe loss along with increased O_2 and C levels, demonstrating only limited protective effects. In conclusion, higher biosurfactant concentrations effectively mitigate corrosion by minimizing Fe loss and restricting O_2 participation in rust formation.

Table 4.25
Summary Of The Elemental Composition (Weight And Atomic Percentages) Of Mild Steel Specimens Obtained Through The EDX Analysis

Element (%)	C		O		Fe	
	Weight	Atomic	Weight	Atomic	Weight	Atomic
Fresh mild steel	0.72	1.24	1.94	3.12	97.34	95.64
Mild Steel Without inhibitor	2.51	4.68	50.65	74.46	46.84	20.86
Mild Steel with 10% Tween 80	8.6	29.67	28.97	38.08	62.42	32.25
Mild Steel with 5% biosurfactant concentration	9.46	30.03	18.29	32.69	72.25	37.28
Mild Steel with 10% biosurfactant concentration	11.96	32.94	7.89	13.29	80.16	53.77
Mild Steel with 15% biosurfactant concentration	12.86	36.52	5.09	7.14	82.06	56.34

4.7.6 R_m of Plain Mild Steel in 0.9% NaCl Solution with Corrosion Inhibitors

This study investigated the mechanical properties of plain mild steel following immersion in a 0.9% NaCl solution containing varying biosurfactant concentrations (5–20%) and 5% Tween 80. The primary parameters examined were R_m, R_e, elongation at maximum force, maximum load, R_m/R_e ratio, and ductility (R_e/R_m). This study then examined the effect of inhibitor concentration on the corrosion-induced performance of mild steel.

Table 4.26 and Figure 4.42 present the obtained results. The average tensile properties reported in Table 4.26 were calculated using the arithmetic mean of three replicate specimens tested under identical conditions. Although some scatter is observed at higher inhibitor concentrations, particularly at 15% biosurfactant dosage (Rm = 574, 506, and 519 N/mm^2), all recorded values fall within the expected mechanical performance range for mild steel exposed to corrosive environments and subsequently tested after immersion. The observed variability is attributed to inherent material heterogeneity, minor surface condition differences after immersion, and sensitivity of tensile response to localised corrosion effects and gripping alignment during testing. No statistical outliers were excluded, as none of the results exhibited abnormal failure behaviour or deviation from ductile tensile response, as supported by consistent elongation values and stable Rm/Re ratios across all concentrations. Fracture

surface analysis was not conducted in this study, as the primary objective of the tensile test was to evaluate macroscopic mechanical performance retention rather than microstructural fracture mechanisms.

The BS 449:88 and MS 146:2014: *Steel for the reinforcement of concrete,* stipulate that the tensile-to-yield strength ratio (R_m/R_e) for mild steel bars must be no less than 1.10 and 1.05, respectively, with a minimum R_e of 250 N/mm². Additionally, another Malaysian Standard, MS 144:2014: *Steel wire for the reinforcement of concrete products - Specification (Fourth revision)* mandates a minimum R_e of 250 N/mm² for hot-rolled plain steel bars (R10), R_m/R_e ratio of no less than 1.15, and a minimum elongation of 5%, as certified by the Standards and Industrial Research Institute of Malaysia, SIRIM (Steel, 2022).

The analysis of tensile test data indicated a distinct trend of R_m enhancement correlated with rising inhibitor concentration. Particularly, R_m increased from 452 MPa (5% biosurfactant) to 573 MPa (20% biosurfactant), demonstrating that the inhibitor improved the strength of the material. Similarly, R_e increased from 315 MPa (5% biosurfactant) to 398 MPa (20% biosurfactant), indicating that the steel exhibited enhanced resistance to plastic deformation with increasing inhibitor concentration. Nonetheless, a reduction in elongation at maximum force was noted, declining from 18.00% (5% biosurfactant) to 14.33% (20% biosurfactant). This outcome implied a reduction in ductility. Even though the inhibitor enhanced the strength of the steel, it reduced its flexibility to some extent. The maximum load also exhibited a comparable trend, increasing from 35.33 kN (5% biosurfactant) to 45.00 kN (20% biosurfactant). This observation meant that the material could withstand greater force with rising inhibitor concentration. Surprisingly, the R_m/R_e ratio and ductility presented stability with a range from 1.42 to 1.47 and 0.69 to 0.70, respectively. This finding suggested that the inhibitor did not significantly impact the structural integrity of the material.

The variability in elongation noted in biosurfactant-treated specimens could occur from multiple factors. The R_m and R_e exhibited a distinct improvement with rising biosurfactant concentration. In contrast, elongation was affected by both microstructural and mechanical properties of the material, which could differ due to treatment variations (heterogeneous microstructural modifications and inconsistencies in isolate-hardening behaviour). The formation of thin protective layers was also established when the surface chemistry of steel reinforcement bars was modified by the biosurfactants. Uneven stress distribution during tensile loading could then take place

due to the interaction between these layers and the underlying metal. Hence, increased brittleness could be observed in specific regions owing to the localised effects of biosurfactant adsorption, creating elongation variations (Rasheed et al., 2024). Meanwhile, the uniformity of biosurfactant application substantially impacted the correlation between biosurfactant treatment and the isolate-hardening capacity of the steel across the specimens. Varying deformation characteristics could be exhibited in several localised areas due to inconsistencies in surface preparation or treatment protocols, while R_m and R_e remained unchanged (Sivakumar et al., 2024).

The lowest average R_m of 452 N/mm^2 and an average R_e of 315 N/mm^2 were recorded for the bars treated with 0.9% NaCl solution containing 5% Tween 80. Although the bars demonstrated the lowest R_m and R_e, they exhibited consistent elongation across the various concentrations. Consequently, the R_m and R_e of the reinforcements could be improved using biosurfactants on mild steel bars with biosurfactant. Increased ductility and mechanical properties of the material based on the R_e /R_m ratio could be indicated when biosurfactants were employed (Morales, 1998). These mechanical enhancements also aligned closely with the corrosion inhibition performance documented in previous experiments. The enhanced R_m and R_e resulted from the capacity of the biosurfactant to create a protective organic film (indicated by EDX), which reduced surface oxidation and corrosive damage. This process could then maintain the mechanical integrity of the bars. Likewise, previous studies revealed that the mechanical properties of mild steel (R_m) markedly decreased with advancing corrosion (Anthony et al., 2016; Sohail et al., 2020; Pham Van et al., 2024). The primary cause was the pitting and uniform thinning of the metal, which produced stress concentration and diminished load-bearing capacity. Al-Moubaraki and Obot (2021). indicated that the formation of corrosion products generated non-uniform stress distribution along the steel bar, leading to localised weakening. This phenomenon could compute lower R_m and reduced ductility.

Table 4.26
Summary Of The Mechanical Properties Of Plain Mild Steel After Immersion In 0.9%NaCl Solution With Various Inhibitors Concentrations For 28 Days

Inhibitor	Sample	R_m (N/mm2)	R_e (N/mm^2)	Elongation at maximum force (%)	Maximum Load at maximum Force (kN)	(R_m/R_e)	Ductility (R_e/R_m)
Tween 80 (5%)	1	449	314	18	35	1.43	0.70
	2	456	320	18	36	1.43	0.70
	3	451	311	18	35	1.45	0.69
	Average	452.00	315.00	18.00	35.33	1.44	0.70
5.0%	1	515	359	15	40	1.43	0.70
	2	501	340	15	39	1.47	0.68
	3	501	347	14	39	1.44	0.69
	Average	505.67	348.67	14.67	39.33	1.45	0.69
10.0%	1	505	347	13	40	1.46	0.69
	2	506	349	11	40	1.45	0.69
	3	508	349	15	40	1.46	0.69
	Average	506.33	348.33	13.00	40.00	1.45	0.69
15.0%	1	574	396	14	45	1.45	0.69
	2	506	351	11	40	1.44	0.69
	3	519	363	14	41	1.43	0.70
	Average	533.00	370.00	13.00	42.00	1.44	0.69
20.0%	1	576	405	15	45	1.42	0.70
	2	572	394	13	45	1.45	0.69
	3	571	395	15	45	1.45	0.69
	Average	573.00	398.00	14.33	45.00	1.44	0.69

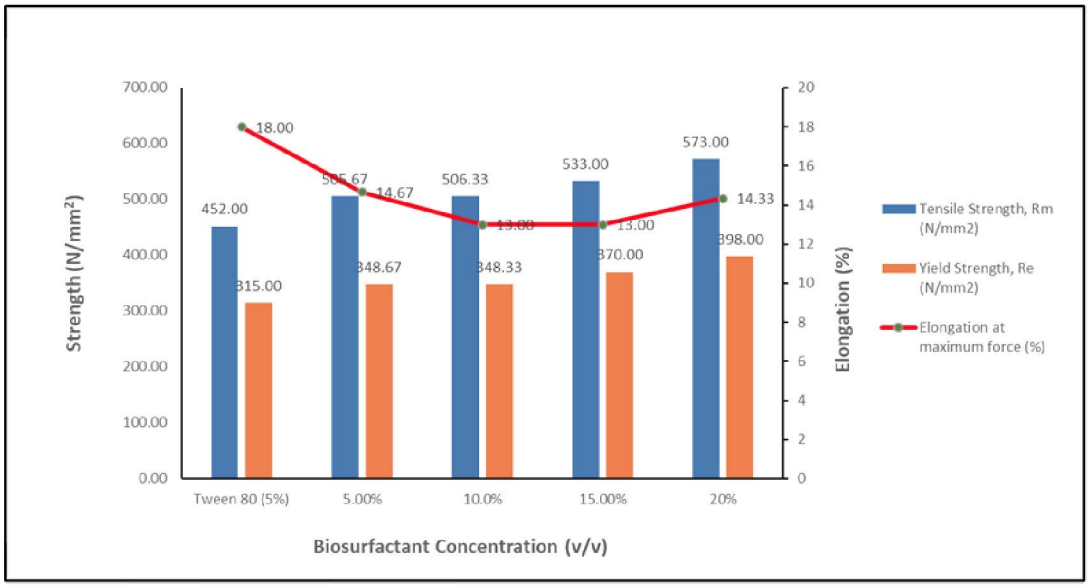

Figure 4.42 The Impact Of Inhibitors Concentration On Mechanical Properties Of Steel Reinforcement

4.8 Fresh Concrete Flowability Tests

The result collected assessed the influence of phospholipid-based biosurfactants and Tween 80 on the flowability of fresh concrete through measurements of vertical slump, slump flow, and T500 at different dosages. Table 4.27 and Figure 4.43 elucidate the impact of these admixtures on the workability, consistency, and fluidity of the concrete mix. The flowability test results were analysed according to the European Federation of National Associations Representing for Concrete (EFNARC) and JKR standard specifications for building works.

Table 4.27
Summary Of The Slump Variation (Vertical and Horizontal) With Different Inhibitor Concentrations

Mix ID	Admixture Type	Water Replacement (%)	Vertical Slump (mm)	Slump Flow (mm)	T500 (Seconds)	Shape of Slump
Control	None	0.0	90	300	8	True
B-1	Biosurfactant	5.0	160	620	5	Collapsed
B-2	Biosurfactant	7.5	180	675	4.5	Collapsed
B-3	Biosurfactant	10.0	200	690	4	Collapsed
B-4	Biosurfactant	12.5	220	700	3.5	Collapsed
B-5	Biosurfactant	15.0	240	715	3	Collapsed
B-6	Biosurfactant	17.5	260	730	2.8	Collapsed
B-7	Biosurfactant	20.0	280	745	2.5	Collapsed
T-1	Tween 80	5.0	140	600	4.5	True
T-2	Tween 80	7.5	160	620	4	Collapsed
T-3	Tween 80	10.0	210	700	3	Collapsed
T-4	Tween 80	12.5	230	750	2.8	Collapsed
T-5	Tween 80	15.0	250	770	2.5	Collapsed
T-6	Tween 80	17.5	270	790	2.3	Collapsed
T-7	Tween 80	20.0	290	810	2	Collapsed

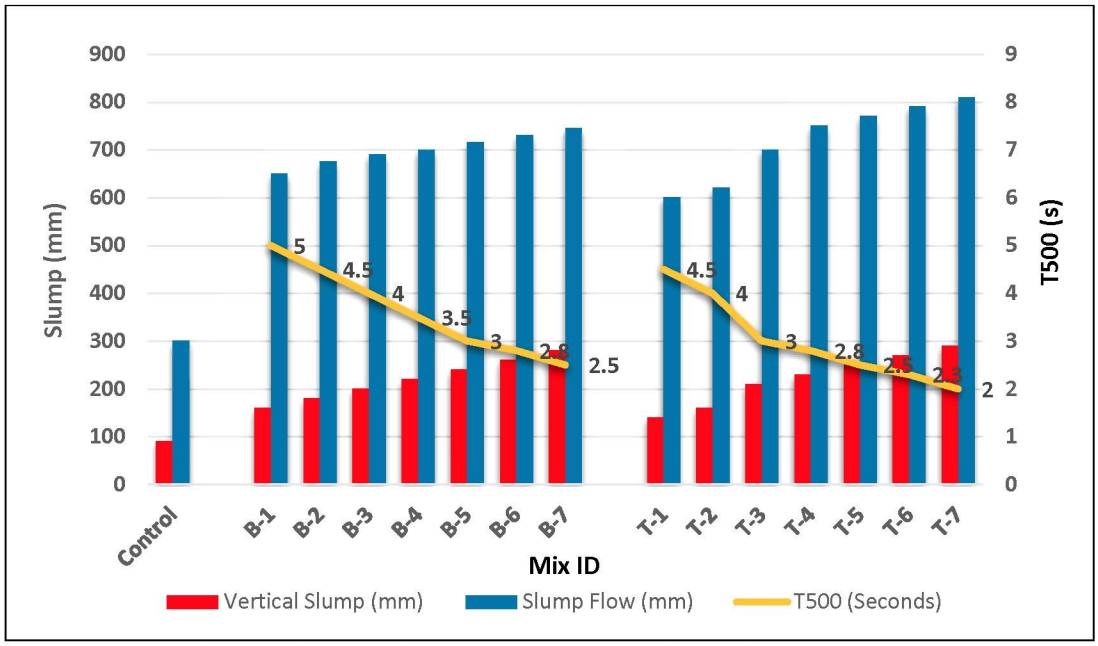

Figure 4.43 The Vertical And Horizontal Slump Flow Values Of Fresh Concretes With T500 Time Analysis

4.8.1 Effect of Admixture Dosage on Vertical Slump and Slump Flow

The control mix (0% admixture) demonstrated the lowest vertical slump (90 mm) and a slump flow of 300 mm, signifying a stiff mix with reduced workability. This vertical slump increased progressively with higher biosurfactant dosage, ranging from 160 mm (5% biosurfactant) to 280 mm (20% biosurfactant). Conversely, slump flow increased from 650 mm to 745 mm. At 5% Tween 80, the vertical slump (140 mm) was lower than the biosurfactant at the same dosage (160 mm). This outcome implied that Tween 80 exerted a marginally less aggressive effect on workability at lower concentrations. The vertical slump reached 290 mm when the Tween 80 concentration increased to 20%, while the slump flow rose 810 mm (marginally higher than that of the biosurfactant at the equivalent dosage). Despite the mix maintaining a true slump at 5%, it collapsed at increased dosages (similar to the biosurfactant). Overall, the slump flow test results demonstrated a notable enhancement in flowability corresponding to increased water replacement percentages for both biosurfactant and Tween 80 admixtures.

4.8.2 Effect of Admixture Dosage on T500 (Flow Time)

The T500 test quantified the duration needed for concrete to achieve a slump flow of 500 mm, provides an important indicator of the viscosity and filling ability of fresh concrete and is widely used in the assessment of self-compacting concrete (SCC) performance. According to EFNARC guidelines, lower T500 values correspond to reduced yield stress and improved flowability, reflecting a concrete mix capable of rapid and uniform spreading without external compaction.

Notably, the control mix exhibited the longest T500 time (8 s), indicating inadequate flowability. With an increase in biosurfactant dosage, T500 consistently decreased from 5 s (5% biosurfactant) to 2.5 s (20% biosurfactant), suggesting that a higher admixture content enhanced flowability. Tween 80 also exhibited a T500 of 4.5 s at 5%, which was marginally lower than that of the biosurfactant at the equivalent dosage. At 20% Tween 80, T500 decreased to 2 s. This value was lower observed for the biosurfactant at the same concentration.

In this study, the progressive reduction in T500 time with increasing biosurfactant dosage indicates enhanced flow dynamics consistent with SCC behaviour. The observed T500 trends suggest that the biosurfactant-modified mixes approach the viscosity characteristics required for SCC applications, while excessive reductions in T500 may indicate overly fluid behaviour with an increased risk of segregation. Therefore, T500 results not only confirm the plasticising effect of the biosurfactant but also provide a framework for evaluating its suitability within SCC performance classifications.

4.8.3 Results Analysis of Flowability Tests

The SCC is categorised into three slump flow classifications defined by EFNARC as follows (BIBM, CEMBUREAU, ERMCO, EFCA, 2005):

i) Slump flow class 1 (SF1, 550–650 mm) is suitable for non-RC or slightly RC structures that are cast from the top with free displacement from the delivery point (housing slabs). This concrete is also applicable for casting via a pump injection system (tunnel linings) and sections small enough to prevent long horizontal flow (piles and some deep foundations).

ii) Slump flow class 2 (SF2, 660–750 mm) is suitable for various standard applications (walls and columns).
iii) Slump flow class 3 (SF3, 760–850 mm) is characterised by a small maximum aggregate size (less than 16 mm) and is utilised for vertical applications in highly congested structures, complex-shaped structures, and for filling beneath formwork.

Concrete is classified as SCC under the JKR standard if it exhibits a slump flow exceeding 630 mm and a vertical slump greater than 160 mm, ensuring adequate self-compaction and cohesion (JKR, 2021). Conversely, the JKR standard does not specify T500 time, it instead emphasises slump flow and vertical slump measurements to define SCC performance. The EFNARC also classifies SCC according to its T500 flow time, which quantifies the time taken for the concrete to expand to a 500 mm diameter. This EFNARC classifies viscosity into two categories as follows:

i) VS1 (≤ 2 s T500): Exhibits low viscosity, heightening the risk of segregation
ii) VS2 (> 2 s T500): Higher viscosity, which enhances stability

Concrete mixtures with biosurfactant concentrations ranging from 7.5% to 20% were classified as SF2 according to EFNARC standards and satisfied the JKR requirement (> 630 mm) for SCC (see Table 4.28). On the contrary, T-5 to T-7 (Tween 80 at 15% – 20%) surpassed SF2 limits, resulting in heightened segregation risks. The B-1 (5%), T-1 (5%), and T-2 (7.5%) also exhibited reduced flowability, restricting their applicability for SCC purposes. Furthermore, the substitution of water content with an optimal dosage from 7.5% to 17.5% biosurfactant improved the filling ability of fresh concrete and preserved segregation resistance, rendering it appropriate for general-purpose SCC (Kamaruddin et al., 2021). These properties also make these mixtures suitable for SCC applications in structural elements (Dinakar & Manu, 2014). Nevertheless, exceeding 20% biosurfactant content was inadvisable, as the flowability was near the SF3 range. This selection could lead to diminished mix cohesion and heightened segregation risk due to excessive workability.

The results demonstrated a significant relationship between admixture dosage and the flowability of fresh concrete. Concrete mixtures with biosurfactant improved

workability relative to the control mix. Increased admixture content led to higher slump and flow values, indicating enhanced workability.

The reduction in surface tension induced by the biosurfactant directly influenced the measured slump flow and T500 parameters. The observed trend was corroborated by a reduction in T500 time as admixture content increased. A lower interfacial tension enhanced the dispersion of cement particles, minimising flocculation and reducing interparticle friction within the fresh mix. This improved dispersion allowed the concrete to spread more freely, resulting in increased slump flow diameters (Freitas Silva et al., 2012; Jahan et al., 2020; Milagre et al., 2018). Concurrently, the reduced internal resistance facilitated faster flow initiation and propagation, as reflected by the progressive decrease in T500 time with increasing admixture dosage. These results confirm that the observed improvements in fresh concrete workability arise from a physicochemical plasticising mechanism rather than an increase in free water content.

Even though the biosurfactant notably enhanced workability, excessive dosages resulted in increased fluidity. This process could heighten the risk of segregation and diminish the cohesion among concrete components.

Table 4.28
Summary Of The Tabulated Results According To EFNARC And JKR Standards

Mixture	Slump Flow (mm)	EFNARC Classification	JKR Requirement	SCC Viscosity (T500 Time)	EFNARC Viscosity Class	Suitability for SCC
Control	300	Not SCC	Does not meet	-	-	Not suitable
B-1 (5% Biosurfactant)	620	Not SCC	Below JKR limit	> 2 sec	VS2	Limited SCC use
B-2 to B-7 (7.5%–20% Biosurfactant)	660–745	SF2	Meets SCC (> 630 mm)	> 2 sec	VS2	Optimal for SCC
T-1, T-2 (5%–7.5% Tween 80)	580–630	Not SCC	Meets SCC	≤ 2 sec	VS1	Limited SCC use
T-3 to T-4 (10%–12.5% Tween 80)	700–750	SF2	Meets SCC (> 630 mm)	> 2 sec	VS2	Optimal for SCC
T-5 to T-7 (15%–20% Tween 80)	770–810	SF3	Exceeds SCC	> 2 sec	VS2	Risk of segregation

** SF1 (550–650 mm) – Suitable for precast applications
** SF2 (660–750 mm) – Ideal for reinforced elements (walls, columns, slabs)
** SF3 (760–850 mm) – High flowability but increased segregation risk

4.9 Mechanical Properties of RC

The f_c, f_s, and τ tests were performed to assess the impact of biosurfactant treatment on the performance of RC. This section presents and analyses the experimental results with particular emphasis on the underlying mechanisms governing strength development. The incorporation of biosurfactant is hypothesised to enhance strength performance by improving cement particle dispersion and hydration efficiency, which may contribute to reduced pore connectivity and a denser cementitious matrix. Consequently, these microstructural modifications are expected to translate into improved mechanical properties of RC elements (Hamada et al., 2018; Kim et al., 2020).

4.9.1 f_c and Density of Concrete with Admixtures

The influence of phospholipid biosurfactant and Tween 80 as water replacement admixtures on the compressive strength, density, and water absorption of concrete was analysed at dosages ranging from 5% to 20% and compared to the control mix. The compressive strength trends are presented in Figure 4.44 and Table 4.29, highlighting the performance of these admixtures at 7 and 28 days. The control mix, prepared without any admixtures, achieved compressive strengths of 23.06 N/mm^2 at 7 days and 35.20 N/mm^2 at 28 days, with corresponding densities of 2470.23 kg/m^3 and 2490.54 kg/m^3. The water absorption at 28 days for the control specimen was 3%. These values serve as a benchmark for evaluating the impact of biosurfactant and Tween 80 on concrete properties.

The increase in compressive strength and density observed at the 10% biosurfactant dosage can be attributed to enhanced cement hydration and more efficient formation of hydration products. At this optimal dosage, the biosurfactant improves cement particle dispersion, facilitating greater contact between cement grains and water, which promotes the formation of calcium silicate hydrate (C–S–H) gel. The increased development of C–S–H contributes to pore refinement and matrix densification, resulting in higher density and improved load-bearing capacity (Kamaruddin et al., 2021; Prasad et al., 2019). In contrast, higher dosages may disrupt the balance between dispersion and cohesion, limiting further strength gains. These findings suggest that the

10% biosurfactant dosage provides an optimal condition for hydration-driven strength development in reinforced concrete.

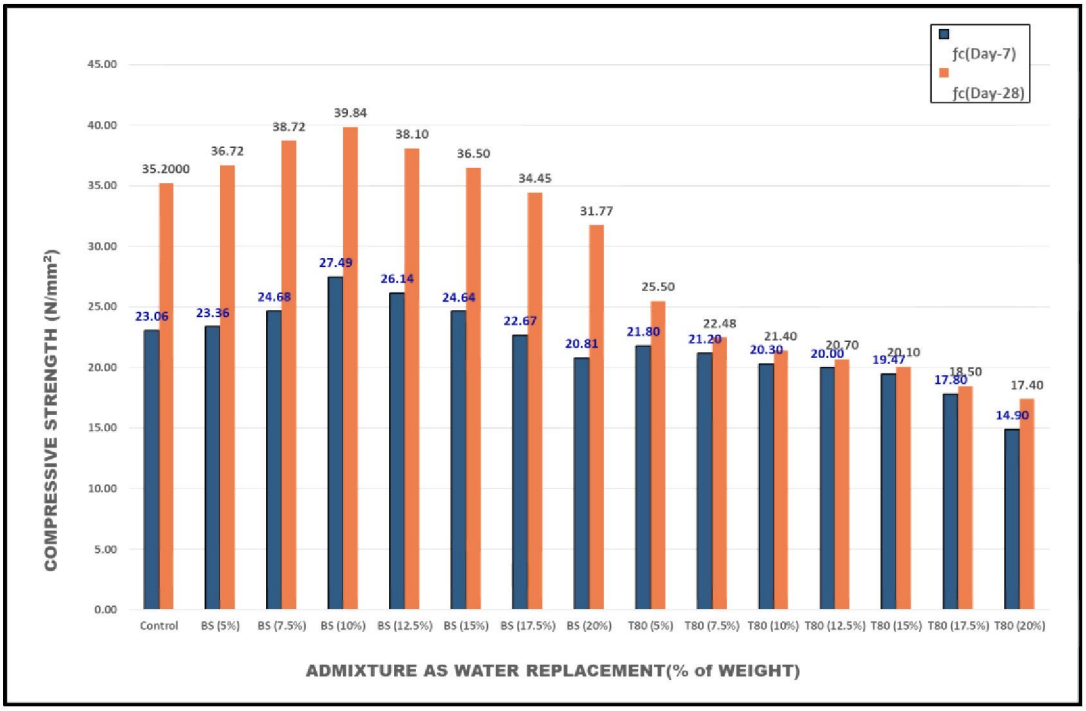

Figure 4.44 The Effect Of Admixture On The f_c Of Concrete

Table 4.29
Summary Of f_c For Concrete Cubes After 7 And 28 Days Of Curing

Mix ID	Admixture Type	% of Water Replacement	Initial Weight (kg)	7 Days					28 Days				
				Weight (kg)	Water Absorption (%)	Density (kg/m³)	Failure Load (kN)	Compressive Strength (N/mm²)	Weight (kg)	Water Absorption (%)	Density (kg/m³)	Failure Load (KN)	Compressive Strength (N/mm²)
Control	None	0.0	8.16	8.34	2.16	2470.23	518.76	23.06	8.41	3.00	2490.54	792.00	35.20
B-1	BS	5.0	8.32	8.42	1.30	2496.16	525.69	23.36	8.47	1.80	2508.58	826.20	36.72
B-2	BS	7.5	8.37	8.45	1.01	2503.65	555.21	24.68	8.48	1.40	2513.37	871.20	38.72
B-3	BS	10.0	8.39	8.46	0.94	2507.70	618.52	27.49	8.49	1.30	2516.74	896.40	39.84
B-4	BS	12.5	8.37	8.45	0.95	2503.17	588.07	26.14	8.48	1.32	2512.33	857.25	38.10
B-5	BS	15.0	8.30	8.39	1.08	2484.48	554.34	24.64	8.42	1.50	2494.81	821.25	36.50
B-6	BS	17.5	8.27	8.39	1.40	2485.34	510.03	22.67	8.43	1.95	2498.73	775.13	34.45
B-7	BS	20.0	8.20	8.35	1.79	2473.91	468.21	20.81	8.41	2.48	2490.79	714.83	31.77
T-1	Tween 80	5.0	7.96	8.19	2.88	2425.46	490.56	21.80	8.28	4.00	2451.87	573.75	25.50
T-2	Tween 80	7.5	7.95	8.21	3.25	2431.28	476.95	21.20	8.31	4.52	2461.08	505.80	22.48
T-3	Tween 80	10.0	7.95	8.21	3.31	2433.54	456.68	20.30	8.32	4.60	2463.88	481.50	21.40
T-4	Tween 80	12.5	7.91	8.19	3.49	2425.55	450.00	20.00	8.29	4.85	2457.37	465.75	20.70
T-5	Tween 80	15.0	7.88	8.15	3.53	2416.20	438.01	19.47	8.26	4.90	2448.22	452.25	20.10
T-6	Tween 80	17.5	7.84	8.14	3.78	2411.86	400.50	17.80	8.26	5.25	2446.02	416.25	18.50
T-7	Tween 80	20.0	7.83	8.13	3.87	2409.49	335.25	14.90	8.25	5.38	2444.43	391.50	17.40

4.9.1.1 Performance of Biosurfactant-Admixed Concrete

Concrete specimens incorporating biosurfactant exhibited notable improvements in compressive strength and density while reducing water absorption. The highest performance was observed at a 10% biosurfactant dosage (B-3), where the compressive strength reached 27.49 N/mm² at 7 days (19.2% higher) and 39.84 N/mm² at 28 days (13.2% higher) compared to the control mix. The density of the concrete at this dosage was recorded at 2507.70 kg/m³ at 7 days and 2516.74 kg/m³ at 28 days, reflecting a 2.75% increase. Water absorption was lowest at 10% biosurfactant, measuring 0.94% at 7 days and 1.30% at 28 days.

Beyond the 10% dosage, a gradual decline in strength was observed, though concrete with 15% biosurfactant (B-5) still outperformed the control specimens, achieving a 28-day compressive strength of 36.59 N/mm² (4% higher). However, at 17.5% biosurfactant dosage (B-6), the compressive strength exhibited a significant reduction, measuring 22.67 N/mm² at 7 days and 34.45 N/mm² at 28 days (2% lower than the control). Water absorption at 20% biosurfactant was observed to increase slightly to 1.79% at 7 days and 2.48% at 28 days, correlating with a decline in compressive strength to 31.77 N/mm² at 28 days. The increase in f_c and density observed within the 5% to 17.5% biosurfactant range was due to the aerobic activity promoted by biosurfactants, which allowed microbial use of internal air. This process could lower the overall air voids in the matrix (Turlapati, 2019). The plasticising effect of biosurfactants also enhanced the flowability of fresh concrete, generating denser and more compact microstructure. Alternatively, the water absorption of biosurfactant-based specimens (across all water replacement percentages) was lower than the control and Tween 80 specimens. This feature promoted a denser and stronger concrete, which was in agreement with findings reported by Nibudey et al. (2014), Ayob et al. (2016), and Shunmuga Vembu and Ammasi (2023).

The biosurfactants enhanced the fluidity of cementitious particles, improving particle distribution while reducing interparticle friction (Uysal & Yilmaz, 2011). This behaviour was consistent with previous studies indicating that biosurfactants facilitated cement hydration and decreased porosity, enhanced fluidity, and improved mechanical strength (He et al., 2020; Kim et al., 2020). In contrast, exceeding 17.5% biosurfactant resulted in increased air entrapment and hydration interference, compromising strength. This pattern aligned with the outcomes recorded by Monika et al. (2019) concerning

chemical surfactants in cementitious materials. (Monika et al., 2019). Figure 4.5(a–h) presents the visual observations of the tested concrete cube specimens. No evidence of explosive cracking or sudden brittle failure was observed in the cubes incorporating phospholipid biosurfactant as a bio-admixture, indicating a stable failure mode under compressive loading.

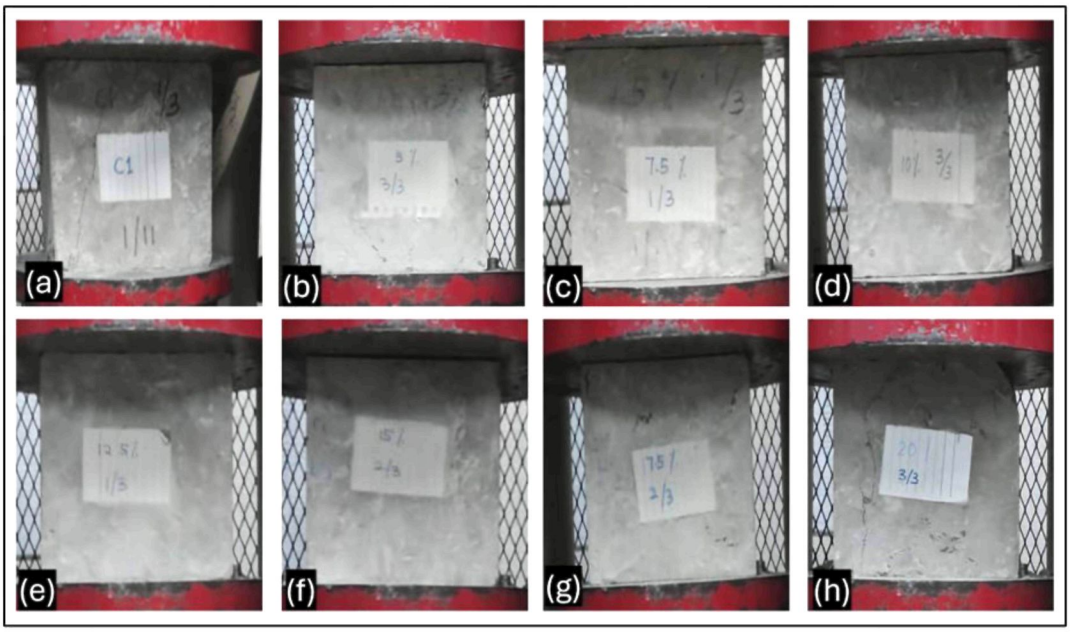

Figure 4.45 Post-Compression Failure Patterns Of Concrete Cube Specimens (a) Control Specimen Without Admixture And Specimens With Biosurfactant Dosages Of (b) 5%, (c) 7.5%, (d) 10%, (e) 12.5%, (f) 15%, (g) 17.5%, And (h) 20%

Despite reduced water absorption at elevated biosurfactant dosages, the observed decrease in f_c is attributed to numerous factors as follows:

i) Hydration Disruption and Reduced Bonding Efficiency - At elevated dosages (exceeding 17.5% biosurfactant), biosurfactants could disrupt cement hydration by encapsulating cement particles in micelles. This process could lower the efficacy of hydration reactions. Consequently, diminished interparticle bonding occurred, even if the overall porosity appeared lower due to decreased water absorption (Patel & Shah, 2015).

ii) Entrapped Air and Microstructural Changes - Biosurfactants typically diminish large air voids. Nonetheless, excessive application could encourage the stabilisation of micro-air bubbles within the cement paste, producing localised weak zones in the matrix. This procedure could lower the strength, even with a reduction in capillary water absorption (Amin et al., 2022; Rawat & Khan, 2022).

iii) Altered Pore Structure and Curing Conditions - A reduced water absorption rate did not inherently signify a denser or more compact concrete matrix. Instead, the alteration of pore structure by biosurfactants could create smaller and more isolated pores, decreasing permeability and compromising the overall cohesion of the hardened paste (He et al., 2020). The pores within and surrounding the cementitious materials were also generated during the hydration of cement, with porosity being closely linked to strength. Hence, biosurfactant admixtures in concrete could alter the type and proportion of hydration products and hydration degree, affecting porosity and strength (H. Kim et al., 2020).

iv) Hydrophilic-Lipophilic Balance (HLB) Effect - The HLB effect could lower the f_c. Notably, the amphiphilic characteristics of biosurfactants affected their interactions with cement particles. Excessive dosages of biosurfactants could impede effective particle-to-particle contact, weakening the bonding within the matrix. Despite lower water absorption, this process could reduce the f_c (Abdallah et al., 2014).

4.9.1.2 Performance of Tween 80-Admixed Concrete

A gradual decline in f_c and density as dosages increased was observed for the specimen containing Tween 80. This observation presented the negative effect of this process on concrete properties. Generally, improved flowability can be produced by utilising Tween 80. Nevertheless, this study noted that Tween 80 generated the lowest density and f_c among all tested specimens. This specimen presented water absorption peaked at 3.87% (7 days) and 5.38% (28 days) at a 20% dosage (T-7). The f_c recorded was also 14.90 N/mm^2 (7 days) and 17.40 N/mm^2 (28 days). This study concluded that

the observation was attributed to the surfactant characteristics of Tween 80 in reducing the strength and density.

Cement hydration was interfered by these properties while inhibiting the development of a dense cementitious matrix. The chemical interactions between Tween 80 and cement were thought to be the primary cause of this outcome, causing hydration incompatibilities. Unosson et al. (2016) published similar outcomes, in which reduced f_c was caused by the increasing macroporosity in concrete when Tween 80 was employed. The microbubbles within the fresh concrete matrix can also be stabilised owing to the improved air-entraining properties caused by Tween 80. Therefore, this process diminished the overall mechanical integrity of the hardened concrete lower based on the higher total porosity with interconnected air voids (Algaifi et al., 2024).

The breakdown of cement particle agglomerates was facilitated by Tween 80, which improved due to the HLB effect improving the dispersing properties. Concurrently, a more uniform mixture was produced. Although workability could be enhanced through these processes, reduced f_c could occur owing to excessive air entrapment and insufficient particle-to-particle bonding (He et al., 2020). Figure 4.46 portrays the failure observed in a concrete cube specimen containing 10% Tween 80. A sudden disintegration under compressive loading was observed due to the brittle characteristics of the specimen. This outcome implied diminished ductility, weakened bonding among concrete components, and incompatibility between cement and Tween 80.

Figure 4.46 Explosive Failure Of Concrete Cubes Specimens Containing 10% Tween 80 Due To Brittle Behaviour

4.9.1.3 Relationship Between Water Absorption and Compressive Strength

The analysis of water absorption and f_c demonstrated an inverse correlation, indicating that reduced water absorption was associated with increased f_c concerning the biosurfactant-admixed concretes (See Figure 4.47). Optimal biosurfactant dosages (up to 10%) decreased water absorption, increasing strength and density attributed to improved cement hydration and reduced voids. On the contrary, concrete mixed with Tween 80 exhibited higher water absorption, which was linked with lower f_c. This finding was attributed to an increase in air voids and inadequate cement bonding (Alsayed & Amjad, 1996; Hassan et al., 2000).

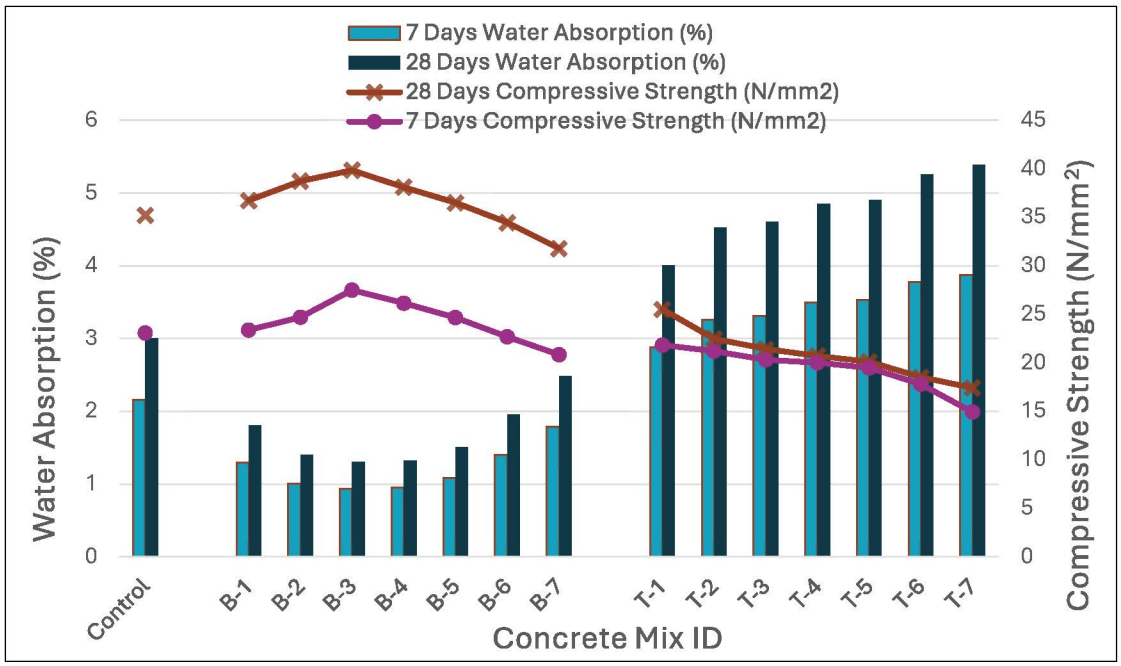

Figure 4.47 The Effect Of Water Absorption On The f_c of Concrete Specimens

4.9.1.4 Conclusion

The results demonstrated that biosurfactant as a water replacement admixture significantly improved f_c and density within an optimal dosage range of 5% to 15%. Particularly, the 10% biosurfactant was identified as the most effective concentration. The introduction of biosurfactant exceeding this threshold then disrupted hydration kinetics and increased air void content, resulting in a deterioration of mechanical properties. Conversely, Tween 80 demonstrated a consistent negative influence on f_c and density, although it positively affected flowability. The surfactant behaviour

resulted in excessive air entrainment, heightened macroporosity, and diminished interparticle bonding, undermining the structural integrity of the concrete. Overall, these findings corroborated earlier studies indicating that the advantageous effects of surfactants in cementitious materials were contingent upon dosage, with excess amounts resulting in performance decline (Monika et al., 2019).

4.9.2 f_s of Non-RC Beams

The f_s (MR) was assessed for RC and non-RC Grade 30 beams at 7 and 28 days. This study investigated the effects of fungal-based biosurfactants and Tween 80 on the tensile performance of concrete beams under central point bending loads when utilised as partial water replacement admixtures. All specimens were prepared and tested following with MS EN 12390-5:2012 - *Testing hardened concrete - Part 5: Flexural strength of test specimens (Second revision).* The flexural properties of the non-RC beams were also examined through the f_s test based on a simple beam test with central point loading. Tables 4.30 and 4.31 tabulate the density and strength development at 7 and 28 days of curing to assess the impact of admixture on flexural behaviour characteristics. Figure 4.48 illustrates that phospholipid-based biosurfactant as a water replacement admixture markedly affected the f_s and density of concrete.

The control specimen (benchmark) achieved a density of 2470.6 kg/m^3 and a f_s of 4.15 MPa at 28 days. Concrete specimens containing 5% to 15% biosurfactants then demonstrated significant improvements in density and f_s. The B-3 mix (10% biosurfactant) revealed the highest density (2492.6 kg/m^3) and f_s (4.51 MPa) at 28 days, indicating an 8.67% enhancement in strength relative to the control specimen. At dosages exceeding 10% biosurfactant (12.5% - 20%), there was a gradual decline in density and f_s. Significant reductions were then noted in B-6 (17.5% biosurfactant) and B-7 (20% biosurfactant), with density and f_s falling below the levels of the control. This decline was attributable to excessive air entrainment resulting from elevated surfactant concentrations, which increased porosity and undermined mechanical performance.

Concrete incorporating Tween 80 demonstrated a consistent reduction in f_s and density at all evaluated dosages. The density was measured at 2434.5 kg/m^3 at a 5% Tween 80 replacement level (T-1), and f_s was recorded at 3.53 MPa, both of which were lower than those of the control specimen. The deterioration then increased with a higher dosage, with T-7 (20% Tween 80) exhibiting the smallest density (2430.2 kg/m^3) and

the f_s (2.92 MPa) at 28 days. The results indicate that the incorporation of Tween 80 as corrosion inhibition concrete admixture led to a progressive reduction in the flexural performance and density of non-reinforced concrete beams.

The positive correlation between f_s and density reflects fundamental concrete behavior, where reduced porosity and enhanced particle bonding lead to improved mechanical performance. Furthermore, f_s was influenced by several factors, including the w/c ratio, microbial aerobic activities, biosurfactant texture, and its interaction with other concrete constituents (Turlapati, 2019). Due to its plasticity and fluidity, the biosurfactant enhanced the flowability of fresh concrete, promoting better cement dispersion and a denser matrix. This densification improved f_s, consistent with the known relationship between lower w/c ratios and enhanced concrete strength and durability (Anggraini et al., 2017). Biosurfactant interactions also contributed to a more uniform aggregate coating, reinforcing the matrix–aggregate interface and increasing both τ and f_s (Yehia et al., 2015).

The optimal dosage of the phospholipid-based biosurfactant for partial water replacement in G30 concrete was determined to be 10%. Dosages above this threshold reduced density and strength, as excess surfactant interfered with cement hydration, increased porosity, and weakened particle bonding. This finding is consistent with previous research conducted by Eloget et al. (2021).

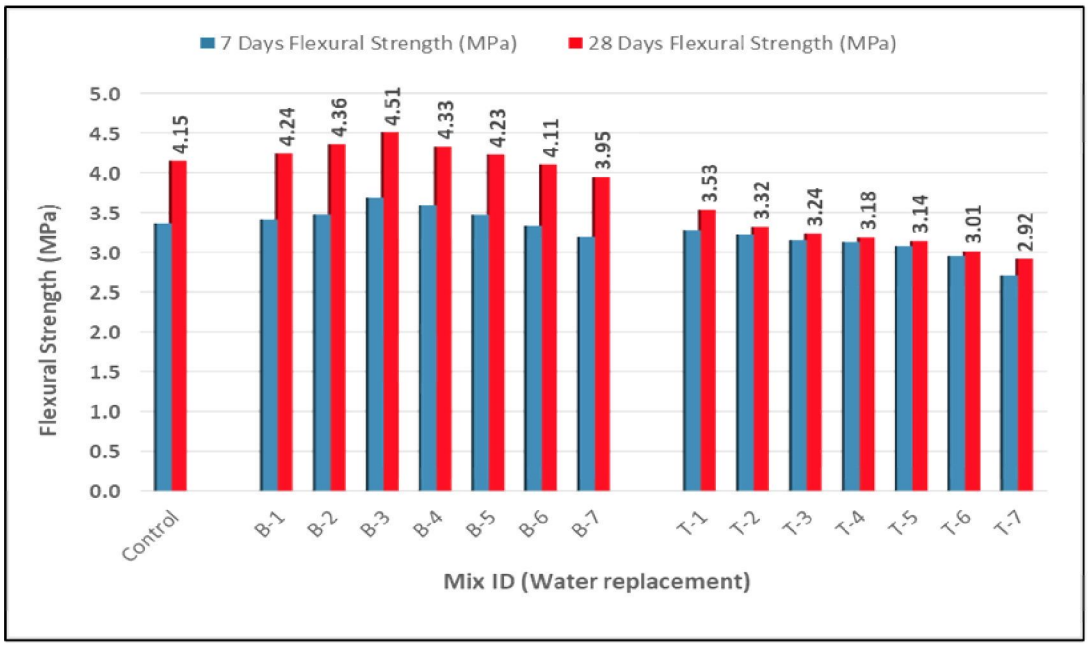

Figure 4.48 The Relationship Of Phospholipid Biosurfactant And Tween 80 Dosage With f_s Of Concrete Over Time

Table 4.30
Summary Of The f_s Of Non-RC Beams Tested On Day 7 With Biosurfactant And Tween 80 As Water Replacement Admixtures

Mix ID	Admixture Type	% of Admixture	Initial Weight (kg)	7 Days					
				Weight (kg)	Water absorption (%)	Density (kg/m³)	Load at Failure (N)	Failure Point Depth (mm)	Flexural Strength (f_s /MPa)
Control	None	0.0	11.96	12.24	2.38	2448.52	8,402.92	100	3.36
B-1	Biosurfactant	5.0	12.19	12.36	1.43	2472.16	8,525.00	100	3.41
B-2	Biosurfactant	7.5	12.26	12.39	1.11	2478.88	8,693.09	100	3.48
B-3	Biosurfactant	10.0	12.29	12.41	1.03	2482.71	9,225.00	100	3.69
B-4	Biosurfactant	12.5	12.26	12.39	1.05	2478.26	8,975.00	100	3.59
B-5	Biosurfactant	15.0	12.16	12.30	1.19	2460.08	8,686.33	100	3.47
B-6	Biosurfactant	17.5	12.12	12.31	1.54	2461.71	8,331.93	100	3.33
B-7	Biosurfactant	20.0	12.02	12.26	1.96	2451.28	7,983.02	100	3.19
T-1	Tween 80	5.0	11.66	12.03	3.17	2405.79	8,200.00	100	3.28
T-2	Tween 80	7.5	11.65	12.06	3.58	2412.40	8,057.21	100	3.22
T-3	Tween 80	10.0	11.65	12.07	3.64	2414.78	7,884.13	100	3.15
T-4	Tween 80	12.5	11.59	12.04	3.84	2407.25	7,826.24	100	3.13
T-5	Tween 80	15.0	11.54	11.99	3.88	2398.05	7,700.00	100	3.08
T-6	Tween 80	17.5	11.49	11.97	4.16	2394.30	7,383.26	100	2.95
T-7	Tween 80	20.0	11.47	11.96	4.26	2392.16	6,775.00	100	2.71

Table 4.31
Summary Of The f_s Of Non-RC Beams Tested On Day 28 With Biosurfactant And Tween 80 As Water Replacement Admixtures

Mix ID	Admixture Type	% of Admixture	Initial Weight (kg)	28 Days					
				Weight (kg)	Water absorption (%)	Density (kg/m³)	Load at Failure (N)	Failure point depth (mm)	Flexural Strength (MPa)
Control	None	0.0	11.96	12.35	3.30	2470.62	10,382.68	100	4.15
B-1	Biosurfactant	5.0	12.19	12.43	1.98	2485.67	10,604.48	100	4.24
B-2	Biosurfactant	7.5	12.26	12.45	1.54	2489.45	10,900.00	100	4.36
B-3	Biosurfactant	10.0	12.29	12.46	1.43	2492.55	11,275.00	100	4.51
B-4	Biosurfactant	12.5	12.26	12.44	1.45	2488.23	10,825.00	100	4.33
B-5	Biosurfactant	15.0	12.16	12.36	1.65	2471.31	10,572.67	100	4.23
B-6	Biosurfactant	17.5	12.12	12.38	2.15	2476.27	10,271.47	100	4.11
B-7	Biosurfactant	20.0	12.02	12.35	2.73	2469.65	9,863.85	100	3.95
T-1	Tween 80	5.0	11.66	12.17	4.40	2434.52	8,837.07	100	3.53
T-2	Tween 80	7.5	11.65	12.22	4.97	2444.83	8,297.29	100	3.32
T-3	Tween 80	10.0	11.65	12.24	5.06	2447.79	8,095.52	100	3.24
T-4	Tween 80	12.5	11.59	12.21	5.34	2441.88	7,962.02	100	3.18
T-5	Tween 80	15.0	11.54	12.16	5.39	2432.89	7,850.00	100	3.14
T-6	Tween 80	17.5	11.49	12.16	5.78	2431.48	7,527.03	100	3.01
T-7	Tween 80	20.0	11.47	12.15	5.92	2430.18	7,299.83	100	2.92

4.9.3 f_s Test of Single RC Beams

Prior experimental investigations determined that a 10% biosurfactant was optimal for enhancing the f_c and f_s of non-RC, with an effective range between 5% and 17.5%. Similarly, corrosion inhibition analysis suggested a 10% biosurfactant was most effective in the treatment of mild steel reinforcement prior to casting. This study then investigated the f_s of singly RC beams that utilised biosurfactant as a water-replacement admixture and a corrosion inhibitor. For uniform corrosion protection, the reinforcing steel bars were treated with a solution containing 10% crude biosurfactant in distilled water. The f_s of the beams was evaluated after 28 days of curing. Table 4.32 and Figure 4.49 present the results.

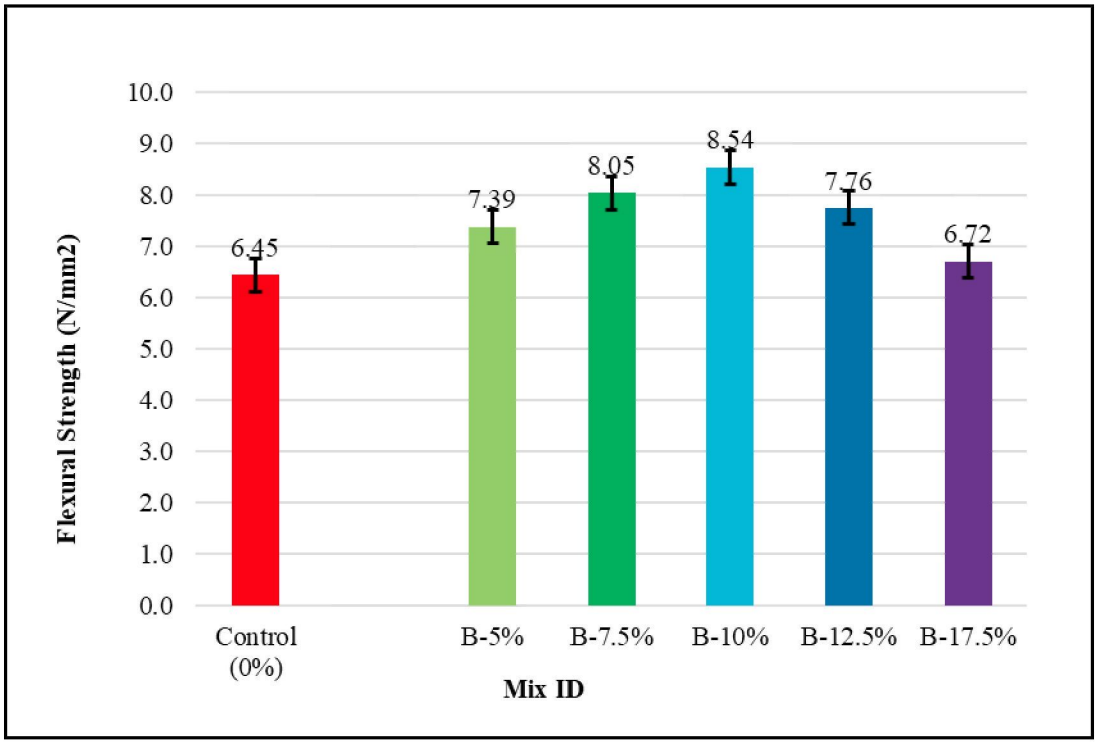

Figure 4.49 The f_s Of RC Beam Specimens With Biosurfactant As Admixture After 28 Days Of Curing

Table 4.32
Summary Of f_s And Physical Properties Of Single RC Beams With Varying Admixture Percentages

Mix ID	Corrosion inhibitor for MS (%)	% of Admixture	Initial Weight (kg)	Final Weight (kg)	Water Absorption (%)	Density (kg/m³)	Mean Density (kg/m³)	Load at Failure (N)	Mean Load at Failure (N)	f_s (N/mm²)	Mean f_s (N/mm²)
Control	0	0	14.75	15.05	2.03	3010	3002.67	16,290	16,120	6.52	6.45
			14.66	14.98	2.18	2996		15,890		6.36	
			14.72	15.01	1.97	3002		16,180		6.47	
B-1	10	5	14.89	15.09	1.34	3018	3013.33	18,620	18,470	7.45	7.39
			14.82	15.04	1.48	3008		18,290		7.32	
			14.85	15.07	1.48	3014		18,500		7.40	
B-2	10	7.5	14.96	15.12	1.07	3024	3018.67	20,310	20,120	8.12	8.05
			14.91	15.07	1.07	3014		19,870		7.95	
			14.94	15.09	1.00	3018		20,180		8.07	
B-3	10	10	15.02	15.15	0.87	3030	3026.00	21,580	21,350	8.63	8.54
			14.97	15.12	1.00	3022		21,120		8.45	
			14.99	15.13	0.93	3026		21,350		8.54	
B-4	10	12.5	14.98	15.11	0.87	3022	3019.33	19,500	19,400	7.80	7.76
			14.91	15.08	1.14	3016		19,270		7.71	
			14.95	15.1	1.00	3020		19,430		7.77	
B-5	10	15	14.90	15.06	1.07	3012	3008.00	16,920	16,783	6.77	6.72
			14.84	15.02	1.21	3004		16,640		6.66	
			14.86	15.04	1.21	3008		16,790		6.72	

The experimental findings indicated the effect of different fungal-based biosurfactant concentrations on concrete density, load-bearing capacity, and f_s. The control specimen demonstrated an average density of 3002.67 kg/m^3, while specimens with a 10% biosurfactant admixture achieved 3026.00 kg/m^3, suggesting improved compaction and decreased porosity. The load-bearing capacity also exhibited a comparable trend, in which the control specimen failed at a load of 16.12kN, whereas specimens containing 5% and 10% biosurfactant sustained loads of 18.47kN and 21.35kN, respectively. The maximum failure load (10% biosurfactant) then demonstrated a 32.44% enhancement compared to the control. Conversely, the load-bearing capacity declined to 16.785 kN at 15% biosurfactant, indicating that an excessive amount of biosurfactant negatively affected structural integrity.

The trends in f_s corresponded with the load-bearing outcomes. Notably, the control beam demonstrated a f_s of 6.45 N/mm^2, while beams incorporating 5% and 10% biosurfactants reached strengths of 7.39 N/mm^2 and 8.54 N/mm^2, respectively. A 10% biosurfactant also led to a 32.40% increase in f_s, demonstrating its efficacy in improving mechanical performance. Nonetheless, the f_s decreased to 6.72 N/mm^2 at 15% biosurfactant, representing a mere 4.19% increase over the control. This outcome suggested a threshold beyond which further addition of biosurfactants negatively impacted structural performance.

In addition to strength enhancement, the observed flexural behaviour provides important implications for beam ductility. Visual examination of the failed specimens (Figure 4.50) revealed a dominant flexural failure mode characterised by the formation of a principal vertical crack at the mid-span, corresponding to the region of maximum bending moment.

The steel reinforcement remained fully embedded within the concrete after failure, indicating adequate bond strength (τ) between the steel and concrete. No significant evidence of debonding or bar slippage was observed, demonstrating that the incorporation of the biosurfactant admixture did not adversely affect the steel–concrete bond. Furthermore, the concrete surrounding the reinforcement exhibited no longitudinal splitting cracks, confirming effective stress transfer across the steel–concrete interface and satisfactory bond performance. In addition, the reinforcement bar presented in Figure 4.51 showed minimal corrosion, suggesting that the concrete matrix provided adequate protection. This observation was probably due to the impact of the biosurfactant on pore structure and permeability.

Overall, these findings corroborated previous studies on the f_c and f_s in non-RC, substantiating the hypothesis that biosurfactants improved hydration and cementitious bonding. The enhanced density in optimised mixtures demonstrated enhanced particle packing, lowering porosity while improving strength. In contrast, exceeding the optimal dosage could produce inefficiencies, as an excessive biosurfactant concentration could disrupt the microstructure, increase air voids, and weaken the interfacial bond between aggregate and cement paste. Furthermore, the data suggested that a 10% biosurfactant solution for treating mild steel corrosion treatment did not impair the bond between steel and concrete or load transfer. Instead, the selection offered corrosion protection while preserving f_s, positioning biosurfactants as a suitable dual-purpose additive for RC applications.

Figure 4.50 Biosurfactant Flexural Failure Pattern Of Singly Reinforced Concrete Beams With 10% Biosurfactant.

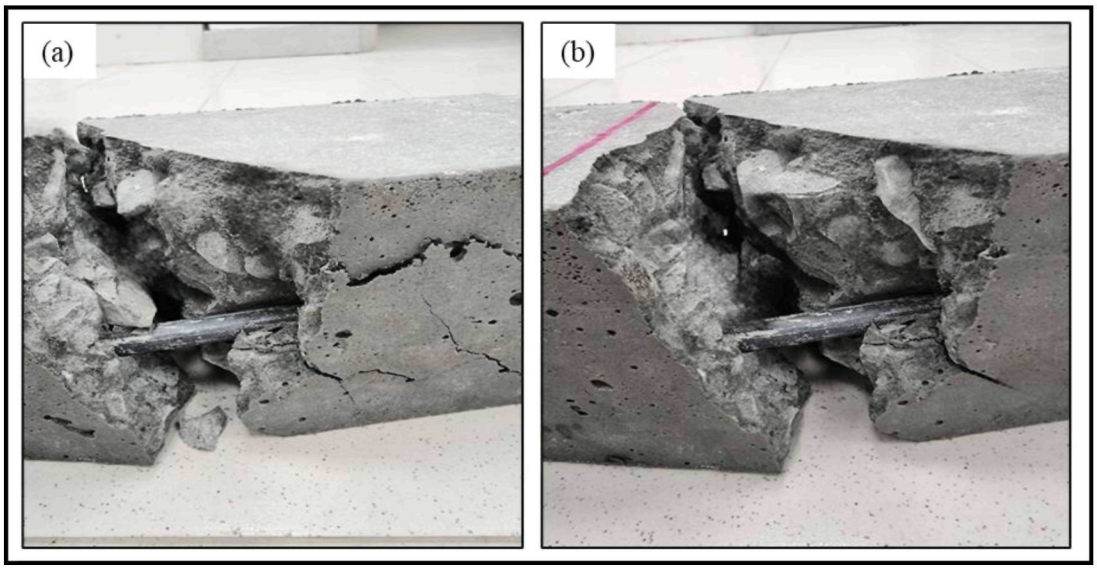

Figure 4.51 The Flexural Failure Modes Of (a) Control Specimen And (b) Beam Incorporating 10% Biosurfactant As A Corrosion Inhibitor And As An Admixture (10% Water Replacement By Weight)

4.9.4 Pull-out Test of Reinforcement Bars Embedded in Concrete

Table 4.33 and Figure 4.52 present data that elucidate the impact of corrosion on τ over 120 days. Even though the results indicated that the control group demonstrated lower τ on days 14 and 28, a significant increase on days 60 and 100 was observed. This phenomenon suggested improved adhesion between the reinforcement and concrete as a result of early-stage corrosion. At 120 days, the τ reached a near plateau. This value could attain a point at which additional corrosion ceased to improve adhesion as corrosion advanced. The B-10% group also consistently demonstrated smaller CRs and higher τ compared to the control group at all time points (albeit there was only a slight increase in τ at day 120). Therefore, this study observed that initial corrosion for control specimens commenced on day 60, whereas corrosion initiation only occurred on day 120 for treated specimens (B-10%).

The initiation of corrosion produced higher τ, as the expansive corrosion products generated radial pressure at the interface. This pressure was caused between the components, enhancing the mechanical interlocking between the reinforcement and surrounding concrete. In cases of slight corrosion of the reinforcing steel bar, the friction increase is dominant over the reduction of mechanical interaction, and thus the overall τ is increased (Y. Te Lin et al., 2017). Consequently, this stage marked the initiation of CO_2 or chloride ingress through the cover to the steel reinforcement, leading to

depassivation and increased roughness of the steel bar surface. The phenomenon enhanced the friction component, explaining the initial increase in τ. This stage also marked the onset of rebar corrosion and the formation of rust products (Ayop & Cairns, 2013). Almusallam et al. (1996) performed bond tests on cubes featuring open stirrups. The study concluded a 17% increase in τ at 4% weight loss, which was attributed to enhanced rebar roughness and its confinement by concrete.

Extended exposure of specimens to saline solutions led to a reduction in τ in all specimens. The decline in τ over time resulted from ongoing progressive corrosion, causing expansion of the steel bar, microcracking within the concrete matrix, and a loss of adhesion. This phenomenon aligned with the trend observed in Zhao et al.'s (2013) study, indicating that extended corrosion exposure diminished bond performance through internal cracking and mechanical interlock loss. With an increase in corrosion percentage, there was a rapid decrease in the maximum bond stress.

Overall, a higher τ was observed from day 14 to day 120 in specimens incorporating biosurfactant. This dosage enhanced the concrete-reinforcement interface by improving concrete porosity, resulting in denser concrete and more negligible permeability. Hence, O_2 and water were prevented from penetrating the concrete surface and reaching the reinforcement. The higher τ at this concentration was also due to the capacity of the biosurfactant to create a protective layer on the steel surface, minimising corrosion and maintaining surface roughness. This layer was pivotal for mechanical interlocking. Furthermore, this observation was consistent with previous studies suggesting that moderate corrosion improved τ through enhanced surface roughness (Almusallam et al., 1996; Zhang et al., 2016).

Meanwhile, the outcomes of this study were similar to other studies examining the impact of corrosion on τ. Almusallam et al. (1996) indicated that mild corrosion could improve τ through enhanced surface roughness. Nevertheless, the study noticed that extended exposure led to bond weakening as a result of reinforcement degradation and concrete cracking. Zhang et al. (2016) reported that protective coatings on reinforcement could delay bond deterioration but not under prolonged exposure to aggressive environments. Overall, the findings demonstrated that employing a 10% biosurfactant solution as a pretreatment for steel reinforcement and as a concrete admixture could improve τ over time.

Table 4.33
Comparison Summary Of The Corrosion Resistance And Mechanical Performance Between The Control And Biosurfactant-Treated Groups

Day	Control			B-10%		
	CR (mm/year)	Maximum Pull-Out Load (N)	τ (N/mm^2)	CR (mm/year)	Maximum Pull-Out Load (N)	τ (N/mm^2)
14	0.0032	1499.98	0.9548	0.0016	1702.10	1.0835
28	0.0070	2023.74	1.2882	0.0044	2468.05	1.5710
60	0.0357	2556.17	1.6271	0.0186	2714.85	1.7281
100	0.0716	2688.66	1.7114	0.0363	2742.00	1.7454
120	0.0896	2690.98	1.7129	0.0451	2933.94	1.8676

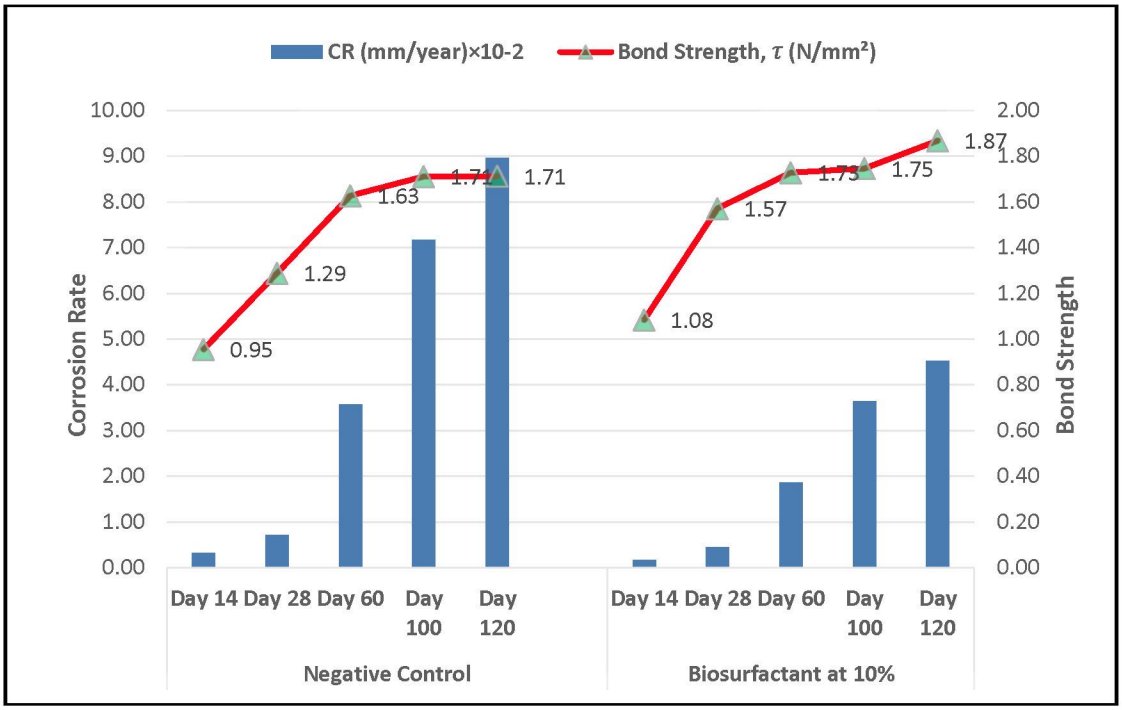

Figure 4.52 The Relationship Of CR And the τ of Control Specimens and Specimens Incorporating 10% Biosurfactant As A Corrosion Inhibitor And Water Replacement Admixture

CHAPTER 5
CONCLUSION AND RECOMMENDATIONS

5.1 Introduction

Corrosion of steel reinforcement in reinforced concrete structures remains a critical global durability challenge, particularly under aggressive tropical exposure, leading to premature deterioration, increased maintenance costs, and reduced infrastructure service life. To address this issue, this study investigated the application of fungal-derived phospholipid biosurfactants as an environmentally sustainable corrosion inhibitor and water-replacement admixture for reinforced concrete. This chapter synthesises the key findings of the study, encompassing soil fungal isolation, biosurfactant production, and the evaluation of fresh and hardened concrete properties using biosurfactants as eco-admixtures, as well as their effectiveness in enhancing steel reinforcement protection against corrosion.

5.2 Summary of Major Findings

This study demonstrates, for the first time, that a *Rhizopus*-derived phospholipid biosurfactant produced from waste frying oil can function as a dual-action corrosion inhibitor and eco-admixture for reinforced concrete applications. Unlike conventional surfactants, the biosurfactant exhibited stable performance across biological, electrochemical, and structural domains, supporting its suitability for integrated corrosion mitigation strategies. Notably, this is the first study to establish that *Rhizopus*-derived phospholipids act as both anodic and cathodic inhibitors, achieving a corrosion inhibition efficiency approximately 30% higher than Tween 80 at an optimal concentration of 10% (v/v).

5.2.1 Biosurfactant Production, Characterisation and Analysis of Stability

This study successfully isolated biosurfactant-producing fungi from contaminated soils in Kota Samarahan and Kuching, Sarawak, demonstrating the ecological diversity and resilience of fungal species in polluted environments. The

physicochemical characteristics of the soil samples (pH and temperature) significantly influenced fungal diversity and biosurfactant activity. Various screening tests (drop collapse, oil displacement, and E_{24}) also confirmed the surface activity of the biosurfactants. These findings are as follows:

i) The optimisation of biosurfactant production was conducted through submerged-batch fermentation utilising MSM as the nitrogen source and WFO at 5% of MSM as the carbon source at a controlled temperature of 30°C.

ii) The fungal isolates responsible for biosurfactant production were identified through microscopic examination and comparative analysis with established microbial databases and reported studies. Based on this screening, *Fusarium sp.*, *Trichoderma sp.*, *Rhizopus sp.*, and *Penicillium sp.* were confirmed as biosurfactant-producing strains. Among these isolates, *Rhizopus* sp. exhibited the highest biosurfactant yield and the most effective corrosion inhibition performance and was therefore selected for further investigation. In the present study, the *Rhizopus*-derived biosurfactant produced using waste frying oil (WFO) as the sole carbon source achieved a yield of 0.8509 g L^{-1}. This yield is comparable to values reported for fungal biosurfactant production under submerged fermentation using alternative waste-based substrates. For instance, Pele et al. (2019) reported a biosurfactant yield of 1.74 g L^{-1} from *Rhizopus oryzae* cultivated using 3% crude glycerol supplemented with 5% corn-steep liquor. Although the yield obtained in this study is lower in absolute terms, the comparison remains meaningful given that the present work utilised WFO as a single carbon source without additional nutrient-rich supplements, resulting in a simpler and more sustainable fermentation system. These findings demonstrate that competitive biosurfactant production can be achieved using a low-cost and locally abundant waste substrate, thereby supporting the economic and environmental viability of the proposed production approach.

iii) The biosurfactant exhibiting the highest corrosion IE was characterised using LC-QTOF-MS. This process then validated the classification of this examined biosurfactant as a phospholipid-based biosurfactant.

iv) This study indicated that heating the phospholipid-based biosurfactant at 60°C did not substantially impact its emulsification activity, suggesting a high degree of thermal stability. A 60-day time-based assessment demonstrated that the biosurfactant preserved significant emulsification capacity and sustained fungal growth based on continuous mycelium development. Conversely, exposure to high salinity conditions (30% NaCl) led to a 13% decrease in E_{24}, implying that high salt concentrations adversely affected biosurfactant efficacy. Despite these findings presenting the resilience of the biosurfactant against temperature and temporal degradation, salinity fluctuations in practical applications must be considered.

v) The biosurfactant revealed low minimal toxicity to the aquatic model, with only 10% mortality (1 out of 10 fish). The surviving fish exhibited normal gill movement, fin condition, and feeding behaviour. Nonetheless, a slight decrease in swimming activity was denoted. The water pH was also maintained at a safe range (6.3), while dissolved O_2 levels decreased to 6.3 mg/L. This outcome was presumably a result of microbial O_2 consumption. Although this O_2 depletion resulted in mild physiological stress, fish survival rates were not substantially affected. Likewise, the plant models exhibited no observable stress (leaf wilting or chlorosis) and sustained normal growth during the study period. These results indicated that the *Rhizopus sp.*-based biosurfactant was biocompatible and did not significantly adversely affect aquatic organisms or plants under the tested conditions.

5.2.2 Efficiency of Phospholipid-Based Biosurfactants as a Green Corrosion Inhibitor

The corrosion inhibition performance of the biosurfactant was comprehensively evaluated using weight loss analysis, electrical resistivity (ER) measurements, and surface morphological examination, complemented by electrochemical impedance spectroscopy (EIS) and SEM–EDX characterisation to quantify inhibition efficiency and surface interactions. The findings indicate that at an optimum biosurfactant concentration of 10% (v/v), the phospholipid-based biosurfactant achieved an inhibition efficiency of 49.32% at 28 days of exposure period, signifying a substantial

enhancement in corrosion protection. Under identical experimental conditions, this inhibition efficiency was approximately 30% higher than that obtained using Tween 80, demonstrating the superior protective performance of the *Rhizopus*-derived phospholipid biosurfactant. Furthermore, the observed level of corrosion mitigation is comparable to the performance range reported for commercial corrosion inhibitors such as Sika® FerroGard®-903 and Sika® FerroGard®-903+, which are documented to delay corrosion initiation and reduce overall corrosion activity by up to 65% relative to untreated control specimens over extended exposure periods. Collectively, these results substantiate the effectiveness of the phospholipid-based biosurfactant as a green corrosion inhibitor, offering protection comparable to conventional synthetic systems while providing additional advantages associated with renewable sourcing and reduced environmental impact. The CI findings are re summarised as follows:

i) The weight loss measurement demonstrates that phospholipid-based biosurfactants significantly decreased the weight loss of mild steel at all examined concentrations (5–20% biosurfactant). Notably, the IE rose from 30.15% (5% biosurfactant) to 69.22% (20% biosurfactant). A gradual decrease in enhancement beyond 15% biosurfactant was then observed, culminating at 75.08% (20% biosurfactant). Meanwhile, a significant positive correlation existed between biosurfactant concentration and corrosion IE. This outcome was due to the adsorption of biosurfactant molecules onto the metal surface, creating a protective barrier against corrosive agents in reducing the corrosion resistance. Despite higher biosurfactant concentrations improving corrosion resistance, this efficiency improvement rate diminished beyond 15% biosurfactant.

ii) The ER test indicated that biosurfactant concentration possessed a substantial impact on the electrical conductivity of mild steel specimens, in which higher concentrations produced increased conductivity while lowering resistivity. Consequently, phospholipid-based biosurfactants exhibited the highest IE, attaining the lowest resistance value of 0.73 Ω at 20% biosurfactant.

iii) The EIS analysis demonstrated the efficacy of phospholipid-based biosurfactants in inhibiting corrosion of mild steel. Initially, the IE was 18.82% at 5% biosurfactant. Raising the biosurfactant concentration to 10% then improved the transfer charge resistance, R_{ct} to 621 Ω cm^2 and 625 Ω cm^2, resulting in increased IEs of 30.19% and 30.64%, respectively. A higher heterogeneity factor, n also suggested that the phospholipid-based biosurfactants enhanced the development of a more uniform and smoother protective film on the steel surface.

iv) The SEM analysis presented that specimens treated with phospholipid-based biosurfactants demonstrated markedly improved surface morphology than the negative control and those subjected to higher synthetic inhibitor concentrations. The surface quality enhancement was also associated with elevated biosurfactant concentration. Furthermore, the enhanced corrosion IE of phospholipid-based biosurfactants could be ascribed to their distinctive molecular architecture and adsorption characteristics.

v) The tensile test data denoted that phospholipid-based biosurfactants enhanced both R_e and R_m, resulting in stronger specimens. Conversely, this process resulted in a slight reduction in elongation, indicating a decrease in the ductility of the bars. Although the observed enhancements in strength were recorded, elongation exhibited inconsistent variation (11–15%), which was likely attributable to microstructural modifications and localised effects resulting from biosurfactant adsorption. Differences in biosurfactant application and surface preparation could also lead to variations in localised deformation.

5.2.3 Phospholipid-Based Biosurfactants as Bio-Admixtures for Corrosion Inhibition in RC

The potential use of phospholipid-based biosurfactants as bio-admixtures for corrosion inhibition in RC was assessed through a series of performance tests. The flowability of concrete containing phospholipid-based biosurfactants was assessed using slump (vertical and flow) and T500 tests. The f_c, f_s, and pull-out tests were also

performed to determine the impact of biosurfactant treatment on the performance of RC. The results of these tests are summarised as follows:

i) Concrete mixtures with biosurfactant improved workability relative to the control mix. Increased admixture content led to higher slump and flow values, indicating enhanced workability. The observed trend was corroborated by a reduction in T500 time as admixture content increased. This behaviour is attributed to the ability of phospholipid molecules to reduce surface tension within the mixing water, promoting improved wetting of cement particles and aggregates. The reduced interparticle friction facilitates better particle dispersion and lubrication, thereby enhancing flowability without excessive water demand.

ii) The f_c test result demonstrated that biosurfactant utilised as a water replacement admixture significantly improves f_c and density within an optimal dosage range of 5% biosurfactant to 15% biosurfactant, with 10% biosurfactant identified as the most effective concentration. Specifically, the f_c of concrete cubes with 10% biosurfactant as water replacement admixture was 13.2% greater than that of standard concrete Grade 30. Nonetheless, the efficacy of biosurfactants in f_c of concrete was contingent upon dosage, with levels surpassing optimal thresholds resulting in structural deterioration. This improvement is attributed to enhanced hydration kinetics arising from improved water distribution and cement particle dispersion, leading to a denser microstructure. However, biosurfactant dosages exceeding the optimal threshold resulted in strength deterioration, likely due to disruption of cementitious bonding.

iii) Concrete specimens containing 5% biosurfactant to 15% biosurfactant exhibited notable improvements in density and f_s. A concrete beam incorporating biosurfactant as a water replacement admixture at a 10% biosurfactant produced an 8.67% enhancement in f_s at 28 days relative to the control specimen. On the contrary, reductions were noted in B-6 (17.5% biosurfactant) and B-7 (20% biosurfactant), with both density and f_s felling below the levels of the control specimen. The f_s test of single RC beams indicated that a 10% biosurfactant

solution for mild steel corrosion treatment did not impede the steel-concrete bond or load transfer. Instead, corrosion protection was offered while preserving f_s, positioning biosurfactants as a viable dual-purpose additive for RC applications. The improved flexural performance is associated with enhanced cement paste–aggregate bonding facilitated by the amphiphilic nature of phospholipids, which promotes stronger interfacial transition zones (ITZ).

iv) The bond strength (τ) results demonstrated a significant correlation between corrosion IE and reinforcement-concrete adhesion. Specimens subjected to a 10% biosurfactant demonstrated reduced corrosion rates, enhancing bond retention. Previous studies also reported that τ in RC initially rose during the early stages of corrosion but started to decrease once corrosion exceeded 1%. Nevertheless, this trend was not evident in this study, as the induced corrosion did not attain the specified threshold. The addition of biosurfactant as an admixture at 10% water replacement also improved concrete density and f_c, forming a protective barrier on steel surfaces and reducing chloride-induced degradation.

5.3 Conclusion

This study conclusively demonstrated the effectiveness of fungal phospholipid-based biosurfactants derived from *Rhizopus sp.* as multifunctional materials for corrosion inhibition in RC. The biosurfactant was successfully produced via batch submerged fermentation using waste frying oil as the sole carbon source, achieving a DCW yield of 0.8509 g L^{-1}, and exhibited good thermal stability and sustained emulsification activity. However, reduced performance under high-salinity conditions indicates the need for formulation optimisation for marine or highly saline exposure environments.

Corrosion inhibition assessment revealed that at an optimum concentration of 10% (v/v), the phospholipid-based biosurfactant achieved a corrosion inhibition efficiency of 49.32%, representing a 30% improvement compared to Tween 80 under identical conditions. Electrochemical analyses and surface characterisation confirmed the formation of a stable protective film on steel surfaces, effectively suppressing both anodic and cathodic corrosion reactions. Based on its electrochemical behaviour, the

biosurfactant was classified as a dual-action (mixed-type) corrosion inhibitor. While tensile properties showed slight increases in R_e and R_m, a reduction in ductility was observed, highlighting a trade-off that warrants consideration in structural applications.

When applied as a bio-admixture in RC, the phospholipid-based biosurfactant significantly enhanced fresh and hardened concrete properties within an optimal dosage range. At 10% water replacement, f_c increased by 13.2% relative to Grade 30 control concrete, while f_s improved by 8.67% at 28 days. These improvements were attributed to reduced surface tension, enhanced cement hydration, and improved cement paste–aggregate bonding. Importantly, pull-out test results demonstrated that the biosurfactant preserved reinforcement–concrete bond strength (τ) while simultaneously reducing corrosion activity, confirming its suitability as a dual-function additive. Exceeding the optimal dosage threshold resulted in deterioration of mechanical performance, emphasising the importance of precise dosage control.

Overall, this research establishes that *Rhizopus*-derived phospholipid biosurfactants function effectively as both migrating corrosion inhibitors and water-replacement bio-admixtures, delivering quantifiable improvements in corrosion resistance, mechanical performance, and workability of reinforced concrete. These findings provide a robust scientific basis for the development of biosurfactant-based technologies in sustainable construction and corrosion protection, particularly for applications prioritising renewable materials and environmental compatibility.

5.4 Future Recommendations

While this study has demonstrated the effectiveness of *Rhizopus sp.* phospholipid-based biosurfactants as corrosion inhibitors and bio-admixtures for RC, further targeted investigations are recommended to strengthen their applicability under real service conditions and advance their technical readiness. The following future research directions are proposed:

i) Future studies should evaluate the long-term effects of biosurfactant incorporation on RC strength development and reinforcement corrosion resistance through extended curing and exposure durations, such as 365 days or longer. The prolonged testing phase can enable researchers to assess the impact of the biosurfactant on concrete durability over time, which is crucial for

evaluating its efficacy in practical, long-term construction applications.

ii) Study the potential application of *Rhizopus*-derived phospholipid biosurfactants as eco-friendly cleaning agents for the removal of corrosion products from contaminated water systems. This may include controlled laboratory-scale experiments assessing flocculation and coagulation efficiency in water containing suspended iron corrosion products. During the weight loss measurement, all the biosurfactants tested demonstrated the ability to promote the aggregation and removal of metal corrosion products from contaminated water. Key performance indicators in future study should include turbidity reduction, sedimentation rate, residual metal concentration, and sludge volume, with comparative evaluation against conventional chemical coagulants. Such investigations would extend the functionality of the biosurfactant beyond corrosion inhibition, supporting its potential use in integrated corrosion control and water remediation applications.

iii) Feasibility examination of integrating phospholipid-based biosurfactants with other commonly used synthetic admixtures to quantify synergistic or antagonistic effects on workability, hydration kinetics, strength development, and corrosion resistance.

Addressing these research areas can enhance the development of phospholipid-based biosurfactants as eco-friendly, cost-effective, and efficient alternatives for various industrial applications, facilitating the transition to greener construction technology.

REFERENCES

Abate, G. G. (2025). Soil sampling and sample p reparation. Agricultural and Biological Research, 41(2), 1–5. https://doi.org/10.37532/0970-1907.25.41.2.1-5

Abdallah, M., Benoliel, C., Drider, D., Dhulster, P., & Chihib, N. E. (2014). Biofilm formation and persistence on abiotic surfaces in the context of food and medical environments. Archives of Microbiology, 196(7), 453–472. https://doi.org/10.1007/ s00203-014-0983-1

Abe, A., Oda, Y., Asano, K., & Sone, T. (2006). The molecular phylogeny of the genus *Rhizopus* based on rDNA sequences. *Bioscience, Biotechnology and Biochemistry, 70*(10), 2387–2393. https://doi.org/10.1271/bbb.60101

Abe, A., Sone, T., Sujaya, N., Saito, K., Oda, Y., Asano, K., & Tomita, F. (2003). rDNA ITS Sequence of *Rhizopus* oryzae: Its application to classification and identification of lactic acid producers. *Bioscience, Biotechnology and Biochemistry, 67*(8), 1725–1731. https://doi.org/10.1271/bbb.67.1725

Abosrra, L. R. (2010). Corrosion of steel reinforcement in concrete. Corrosion of mild steel bars in concrete and its effect on steel-concrete bond strength. University of Bradford, UK.

Adnan, M., Alshammari, E., Ashraf, S. A., Patel, K., Lad, K., & Patel, M. (2018). Physiological and Molecular Characterization of Biosurfactant Producing Endophytic Fungi Xylaria regalis from the Cones of Thuja plicata as a Potent Plant Growth Promoter with Its Potential Application. *BioMed Research International, 2018*. https://doi.org/10.1155/2018/7362148

Ai, Z., Jiang, J., Sun, W., Song, D., Ma, H., Zhang, J., & Wang, D. (2016). Passive behaviour of alloy corrosion-resistant steel Cr10Mo1 in simulating concrete pore solutions with different pH. *Applied Surface Science, 389*, 1126–1136. https://doi.org/10.1016/j.apsusc.2016.07.142

Al-Amier, A. A., Nik, W. M. N. W., Ghazali, M. S. M., Yousif, E. M. E. D., Isahak, W. N. R. W., AL-Azzawi, W. K., Zulkifli, M. F. R., Daoudi, W., Vincent, I. O., & Dhande, D. Y. (2024). Recent Innovations in Organic Inhibitors for Mild Steel in Corrosive Solutions: a Mini Review. *Journal of Sustainability Science and Management*, *19*(5), 146–173. https://doi.org/10.46754/jssm.2024.05.009

Al-Badran, A. S., & Mechler, A. (2019). Corrosion inhibition of iron surfaces with phosphatidic acid. *Eurobiotech Journal, 3*(3), 128–134. https://doi.org/10.2478/ebtj-2019-0015

Al-Kashef, A., Shaban, S., Nooman, M., & Rashad, M. (2018). Effect of fungal glycolipids produced by a mixture of sunflower oil cake and pineapple waste as green corrosion inhibitors. *Journal of Environmental Science and Technology*, *11*(3), 119–131. https://doi.org/10.3923/jest.2018.119.131

Al-Moubaraki, A. H., & Obot, I. B. (2021). Corrosion challenges in petroleum refinery operations: Sources, mechanisms, mitigation, and future outlook. *Journal of Saudi Chemical Society*, *25*(12), 101370. https://doi.org/10.1016/j.jscs.2021.101370

Algaifi, H. A., Syamsir, A., Baharom, S., Alrshoudi, F., Qaid, A., Al-Fakih, A. M., Mhaya, A. M., & Salah, H. A. (2024). Assessment of acoustic and mechanical properties in modified rubberized concrete. *Case Studies in Construction Materials*, *20*(March), e03063. https://doi.org/10.1016/j.cscm.2024.e03063

Almusallam, A. A., Al-Gahtani, A. S., Aziz, A. R., & Rasheeduzzafar. (1996). Effect of reinforcement corrosion on bond strength. *Construction and Building Materials*, *10*(2), 123–129. https://doi.org/10.1016/0950-0618(95)00077-1

Alsayed, S. H., & Amjad, M. A. (1996). Strength, Water Absorption and Porosity of Concrete Incorporating Natural and Crushed Aggregate. *Journal of King Saud University - Engineering Sciences*, *8*(1), 109–119. https://doi.org/10.1016/S1018-3639(18)30642-1

Alyamaç, K. E., & İnce, R. (2010). The Effect of Powder Admixture Type and Maximum Aggregate Size on Self-Compacting Concrete Characteristics. *Construction*, *September*, 27–30.

Amin, J., Acharjee, R., Hossain, M., Tahmid, A., & Chowdhury, S. R. (2022). Factors Affecting Mix Design of Concrete. *Malaysian Journal of Civil Engineering*, *34*(2), 19–28. https://doi.org/10.11113/mjce.v34.18311

Andalib, R., Abd Majid, M. Z., Hussin, M. W., Ponraj, M., Keyvanfar, A., Mirza, J., & Lee, H. S. (2016). Optimum concentration of Bacillus megaterium for strengthening structural concrete. *Construction and Building Materials*, *118*, 180–193. https://doi.org/10.1016/j.conbuildmat.2016.04.142

Andrade, C., & Alonso, C. (2001). On-site measurements of corrosion rate of reinforcements. *Construction and Building Materials*, *15*(2–3), 141–145. https://doi.org/10.1016/S0950-0618(00)00063-5

Andrade, C. J. de, Andrade, L. M. de, Rocco, S. A., Sforça, M. L., Pastore, G. M., & Jauregi, P. (2017). A novel approach for the production and purification of mannosylerythritol lipids (MEL) by Pseudozyma tsukubaensis using cassava wastewater as substrate. *Separation and Purification Technology*, *180*, 157–167. https://doi.org/10.1016/ j.seppur.2017.02.045

Anggraini, V., Asadi, A., Syamsir, A., & Huat, B. B. K. (2017). Three point bending flexural strength of cement treated tropical marine soil reinforced by lime treated natural fiber. *Measurement: Journal of the International Measurement Confederation*, *111*(February 2016), 158–166. https://doi.org/10.1016/j.measurement.2017.07.045

Angst, U., Elsener, B., Larsen, C. K., & Vennesland, Ø. (2009). Critical chloride content in reinforced concrete - A review. *Cement and Concrete Research*, *39*(12), 1122–1138. https://doi.org/10.1016/j.cemconres.2009.08.006

Anthony, U., Ikenna, M., Ufuma, O. B., & Ezemuo, D. T. (2016). Corrosion Rates and its Impact on Mild Steel in Some Selected Environments. *Journal of Scientific and Engineering Research*, *3*(1), 34–43. http://jsaer.com/download/vol-3-iss-1-2016/JSAER2016-03-01-34-43.pdf

Antoniou, E., Fodelianakis, S., Korkakaki, E., & Kalogerakis, N. (2015). Biosurfactant production from marine hydrocarbon-degrading consortia and pure bacterial strains using crude oil as carbon source. *Frontiers in Microbiology*, *6*(APR), 1–14. https://doi.org/10.3389/fmicb.2015.00274

Asgher, M., Arshad, S., Qamar, S. A., & Khalid, N. (2020). Improved biosurfactant production from Aspergillus niger through chemical mutagenesis: characterization and RSM optimization. *SN Applied Sciences*, *2*(5), 1–11. https://doi.org/10.1007/s42452-020-2783-3

Asri, R. I. M., Harun, W. S. W., Samykano, M., Lah, N. A. C., Ghani, S. A. C., Tarlochan, F., & Raza, M. R. (2017). Corrosion and surface modification on biocompatible metals: A review. *Materials Science and Engineering C*, *77*(September), 1261–1274. https://doi.org/10.1016/j.msec.2017.04.102

Ayob, A., Razali, M. E., Alias, S., Ahmad, A. G., & Ali, D. S. H. (2016). Engineering Behavior of Concrete with Recycled Aggregate. *MATEC Web of Conferences*, *87*. https://doi.org/10.1051/matecconf/20178701002

Ayop, S. S., & Cairns, J. J. (2013). Critical Study of Corrosion Damaged Concrete Structures. *International Journal of Integrated Engineering*, *5*(2), 43–50.

B. A. Abd-El-Nabey, S. El-Housseiny, H. M. El-Kshlan, M. A. A.-E.-F. (2017). Effect of Tween-80 Surfactant on the Corrosion Resistance of Zn-Phosphated Steel. *Physical Chemistry*, *7*(1), 17–26. https://doi.org/10.5923/j.pc.20170701.03

Ban, C., Kang, W., Wei, C., & Heng, K. (2020). The influence of type and combination of polycarboxylate ether superplasticizer on the mechanical properties and microstructure of slag-silica fume ternary blended self-consolidating concrete. *Journal of Building Engineering*, *31*(March), 101412. https://doi.org/10.1016/j.jobe.2020.101412

Barnita Ghosh, & Ray, R. R. (2011). Current commercial perspective of *Rhizopus oryzae*. In *Journal of Applied Sciences* (Vol. 11, Issue 14, pp. 2470-2486.).

Bertolini, L., Elsener, B., Pedeferri, P., Redaelli, E., & Polder, R. B. (2013). Degradation of Concrete. *Corrosion of Steel in Concrete*, 49–69. https://doi.org/10.1002/9783527651696.ch3

Bhardwaj, G. (2013). Biosurfactants from Fungi: A Review. *Journal of Petroleum & Environmental Biotechnology*, *04*(06), 1–6. https://doi.org/10.4172/2157-7463.1000160

BIBM, CEMBUREAU, ERMCO, EFCA, E. (2005). The European Guidelines for Self-Compacting Concrete. In *The European Guidelines for Self Compacting Concrete* (Issue May). http://www.efnarc.org/pdf/SCCGuidelinesMay2005.pdf

Binns, T. (2003). Pumped concrete. In *Advanced Concrete Technology* (Issue 1687). Woodhead Publishing Limited. https://doi.org/10.1016/B978-075065686-3/50301-3

Bodour, A. A., & Miller-Maier, R. M. (1998). Application of a modified drop-collapse technique for surfactant quantitation and screening of biosurfactant-producing microorganisms. *Journal of Microbiological Methods*, *32*(3), 273–280. https://doi.org/10.1016/S0167-7012(98)00031-1

Bogumił Eugeniusz Brycki, I. H. K., & Adrianna Szulc, O. K. and M. P. (2018). *Organic corrosion inhibitors*. https://doi.org/10.5772/intechopen.72943

Brodňan, M., Koteš, P., Vaněrek, J., & Drochytka, R. (2017). Corrosion determination of reinforcement using the electrical resistance method. *Materiali in Tehnologije*, *51*(1), 85–93. https://doi.org/10.17222/mit.2015.217

Bruyako, M., Grigor'Eva, A., Stepina, I., Golotenko, D., & Podsevalova, A. (2021). Biomodified building materials on the base of mineral binders. *IOP Conference Series: Materials Science and Engineering*, *1030*(1). https://doi.org/10.1088/1757-899X/1030/1/012005

Çelik, A., Manga, E. B., Çabuk, A., & Banat, I. M. (2021). Biosurfactants' potential role in combating covid-19 and similar future microbial threats pınar. *Applied Sciences (Switzerland)*, *11*(1), 1–16. https://doi.org/10.3390/app11010334

Chahardehi, A. M., Arsad, H., & Lim, V. (2020). Zebrafish as a successful animal model for screening toxicity of medicinal plants. *Plants*, *9*(10), 1–35. https://doi.org/10.3390/plants9101345

Chakrabarti, S. (2013). *Bacterial Biosurfactant : Characterization , Antimicrobial and Metal Remediation Properties*. National Institute of Technology, Rourkela.

Cheah, Y. K., Abdul Adzis, A., Abu Bakar, J., & Applanaidu, S. D. (2021). Factors associated with household expenditure on oil and fat products in malaysia: Application of quantile regression. *Food Research*, *5*(3), 112–120. https://doi.org/10.26656/fr.2017.5(3).650

Chen, G. Q., & Liu, X. (2021). On the future fermentation. *Microbial Biotechnology*, *14*(1), 18–21. https://doi.org/10.1111/1751-7915.13674

Chen, X., Yang, X., Shen, Y., Hou, J., & Bao, X. (2017). Increasing Malonyl-CoA Derived Product through Controlling the Transcription Regulators of Phospholipid Synthesis in Saccharomyces cerevisiae. *ACS Synthetic Biology*, *6*(5), 905–912. https://doi.org/10.1021/acssynbio.6b00346

Choi, H. B., & Kang, K. I. (2008). Bond behaviour of deformed bars embedded in RAC. *Magazine of Concrete Research*, *60*(6), 399–410. https://doi.org/10.1680/macr.2008.60.6.399

Chooklin, C. S., Petmeaun, S., Maneerat, S., & Saimmai, A. (2014). Isolation and characterization of a biosurfactant from Deinococcus caeni PO5 using jackfruit seed powder as a substrate. *Annals of Microbiology*, *64*(3), 1007–1020. https://doi.org/10.1007/s13213-013-0738-2

Chooklin, C. S., Phertmean, S., Cheirsilp, B., Maneerat, S., & Saimmai, A. (2013). Utilization of palm oil mill effluent as a novel and promising substrate for

biosurfactant production by Nevskia ramosa NA3. *Songklanakarin Journal of Science and Technology*, *35*(2), 167–176.

Chu, S. H., & Kwan, A. K. H. (2018). A new method for pull out test of reinforcing bars in plain and fibre reinforced concrete. *Engineering Structures*, *164*(November 2017), 82–91. https://doi.org/10.1016/j.engstruct.2018.02.080

Cicek, V. (2017). Corrosion in Engineering Materials. *Corrosion Engineering and Cathodic Protection Handbook*, 503–549. https://doi.org/10.1002/9781119284338.ch53

Classen, A. T., Sundqvist, M. K., Henning, J. A., Newman, G. S., Moore, J. A. M., Cregger, M. A., Moorhead, L. C., & Patterson, C. M. (2015). Direct and indirect effects of climate change on soil microbial and soil microbial-plant interactions: What lies ahead? *Ecosphere*, *6*(8). https://doi.org/10.1890/ES15-00217.1

Cooper, D. G., & Goldenberg, B. G. (1987). Surface-active agents from two Bacillus species. *Applied and Environmental Microbiology*, *53*(2), 224–229. https://doi.org/10.1128/aem.53.2.224-229.1987

da Silva, A. F., Banat, I. M., Giachini, A. J., & Robl, D. (2021). Fungal biosurfactants, from nature to biotechnological product: bioprospection, production and potential applications. In *Bioprocess and Biosystems Engineering* (Vol. 44, Issue 10). Springer Berlin Heidelberg. https://doi.org/10.1007/s00449-021-02597-5

Das, A. J., & Kumar, R. (2018). Bioslurry phase remediation of petroleum-contaminated soil using potato peels powder through biosurfactant producing Bacillus licheniformis J1. *International Journal of Environmental Science and Technology*, *15*(3), 525–532. https://doi.org/10.1007/s13762-017-1410-3

Deepalaxmi, R.K, & Gayathri, C. (2018). Screening for the corrosion inhibition of mild steel metal using biofilm forming halophilic bacteria isolated from the saltpans of Thoothukudi district. *Journal of Bacteriology & Mycology: Open Access*, *6*(5), 280–282. https://doi.org/10.15406/jbmoa.2018.06.00218

Dhiman, R. (2016). Biosurfactants and their Screening Methods ds Polymeric biosurfactants. Research Journal of Recent Sciences, 5(10), 1–6.

Dinakar, P., & Manu, S. N. (2014). Concrete mix design for high strength self-compacting concrete using metakaolin. *Materials and Design*, *60*(March 2014), 661–668. https://doi.org/10.1016/j.matdes.2014.03.053

Dinakarkumar, Y., Ramakrishnan, G., Gujjula, K. R., Vasu, V., Balamurugan, P., & Murali, G. (2024). Fungal bioremediation: An overview of the mechanisms, applications and future perspectives. *Environmental Chemistry and Ecotoxicology*, *6*(July), 293–302. https://doi.org/10.1016/j.enceco.2024.07.002

dos Santos, B. F., Simiqueli, A. P. R., Ponezi, A. N., Pastore, G. M., & Fileti, A. M. F. (2018). Monitoring of biosurfactant production by bacillus subtilis using beet peel as culture medium via the development of a neural soft-sensor in an electronic spreadsheet. *Brazilian Journal of Chemical Engineering*, *35*(4), 1355–1367. https://doi.org/10.1590/0104-6632.20180354s20160664

Elsener, B., Büchler, M., Stalder, F., & Böhni, H. (1999). Migrating corrosion inhibitor blend for reinforced concrete: Part 1 - Prevention of corrosion. *Corrosion*, *55*(12), 1155–1163. https://doi.org/10.5006/1.3283953

Ermolenko, E. V., Sikorskaya, T. V., & Grigorchuk, V. P. (2022). The Phospholipid Molecular Species Profile of Apostichopus japonicus Tissues Modifies through Exposure to n-3 Polyunsaturated Fatty Acid-Deficient Diet. *Marine Drugs*, *20*(9). https://doi.org/10.3390/md20090578

Faqe, H., Dabaghh, H., & Mohammed, A. (2020). Natural Admixture As An Alternative for Chemical Admixture in Concrete Technology: A Review. *The Journal of the University of Duhok*, *2*, 301–308. https://doi.org/10.26682/csjuod.2020.23.2.24

Faria, M., Ziv, T., Gómez-Canela, C., Ben-Lulu, S., Prats, E., Novoa-Luna, K. A., Admon, A., Piña, B., Tauler, R., Gómez-Oliván, L. M., & Raldúa, D. (2018). Acrylamide acute neurotoxicity in adult zebrafish. *Scientific Reports*, *8*(1), 1–14. https://doi.org/10.1038/s41598-018-26343-2

Fourie, G., Steenkamp, E. T., Ploetz, R. C., Gordon, T. R., & Viljoen, A. (2011). Current status of the taxonomic position of Fusarium oxysporum formae specialis cubense within the Fusarium oxysporum complex. *Infection, Genetics and Evolution*, *11*(3), 533–542. https://doi.org/10.1016/j.meegid.2011.01.012

Freitas Silva, M. C., Souza, P. M., Antunes, A. A., Cardoso, A., Lins, C. I., Batista, A. C. L., Stamford, T. C. M., & Campos-Takaki, G. M. (2012). Biosurfactant production by *Rhizopu*s arrhizus using agro industrials substrates as alternative medium. Microbes in Applied Research: Current Advances and Challenges, Malaga, Spain, 14 - 16 September 2011, 353–357. https://doi.org/10.1142/9789814405041_0071

G, K. S., & Yagnik, B. N. (2013). Current Trend and Potential for Microbial Biosurfactants. *Asian Journal of Experimental Biologcal Sciences*, *4*(1), 1–8.

Gana, M. L., Kebbouche-Gana, S., Touzi, A., Zorgani, M. A., Pauss, A., Lounici, H., & Mameri, N. (2011). Antagonistic activity of Bacillus sp. obtained from an Algerian oilfield and chemical biocide THPS against sulfate-reducing bacteria consortium inducing corrosion in the oil industry. *Journal of Industrial Microbiology and Biotechnology*, *38*(3), 391–404. https://doi.org/10.1007/s10295-010-0887-2

Gandage, A. (2023). Admixtures in Concrete -A Review. *International Conference on Construction Real Estate Infrastructure and Projects 2018*, *016*, 66–67. https://doi.org/10.3989/mc.1950.i016.3159

Ganjoo, R., Sharma, S., Sharma, P. K., Dagdag, O., Berisha, A., Ebenso, E. E., Kumar, A., & Verma, C. (2023). Coco Monoethanolamide Surfactant as a Sustainable Corrosion Inhibitor for Mild Steel: Theoretical and Experimental Investigations. *Molecules*, *28*(4). https://doi.org/10.3390/molecules28041581

Gope, A., & Mauro, C. (2025). Palmitate. *Trends in Endocrinology and Metabolism*, 1–2. https://doi.org/10.1016/j.tem.2025.01.001

Gryganskyi, A. P., Golan, J., Dolatabadi, S., Mondo, S., Robb, S., Idnurm, A., Muszewska, A., Steczkiewicz, K., Masonjones, S., Liao, H. L., Gajdeczka, M. T., Anike, F., Vuek, A., Anishchenko, I. M., Voigt, K., de Hoog, G. S., Smith, M. E., Heitman, J., Vilgalys, R., & Stajich, J. E. (2018). Phylogenetic and phylogenomic definition of *Rhizopus* species. *G3: Genes, Genomes, Genetics*, *8*(6), 2007–2018. https://doi.org/10.1534/g3.118.200235

Gutiérrez-Méndez, N., Chavez-Garay, D. R., & Leal-Ramos, M. Y. (2022). Lecithins: A comprehensive review of their properties and their use in formulating microemulsions. *Journal of Food Biochemistry*, *46*(7). https://doi.org/10.1111/jfbc.14157

Hanisah, K., Kumar, S., & Tajul, A. (2013). The Management of Waste Cooking Oil: A Preliminary Survey. *Health and the Environment Journal*, *4*(1), 76–81. http://hej.kk.usm.my/pdf/HEJVol.4No.1/Article08.pdf

Hartanti, A. T., Rahayu, G., & Hidayat, I. (2015). *Rhizopus* Species from Fresh Tempeh Collected from Several Regions in Indonesia. *HAYATI Journal of Biosciences*, *22*(3), 136–142. https://doi.org/10.1016/j.hjb.2015.10.004

Hassan, K. E., Cabrera, J. G., & Maliehe, R. S. (2000). Effect of mineral admixtures on the properties of high-performance concrete. *Cement and Concrete Composites*, *22*(4), 267–271. https://doi.org/10.1016/S0958-9465(00)00031-7

Herrera Hernández, H., M. Ruiz Reynoso, A., C. Trinidad González, J., O. González Morán, C., G. Miranda Hernández, J., Mandujano Ruiz, A., Morales Hernández, J., & Orozco Cruz, R. (2020). Electrochemical Impedance Spectroscopy (EIS): A Review Study of Basic Aspects of the Corrosion Mechanism Applied to Steels. Electrochemical Impedance Spectroscopy, 1–35. https://doi.org/10.5772/intechopen.94470

He, H., Serres, N., Meylheuc, T., Wynns, J. T., & Feugeas, F. (2020). Modifying Mechanical Strength and Capillary Porosity of Portland Cement-Based Mortar Using a Biosurfactant from Pseudomonas fluorescens. *Advances in Materials Science and Engineering*, *2020*(1). https://doi.org/10.1155/2020/2948731

Hisham, A. (2015). *Microbiologically Influenced Corrosion of Mild Steel and Stainless Steel by Pseudomonas Aeruginosa In Enriched Artificial Sea Water* (Issue November). University Technology Mara.

Honarvar Nazari, M., Shihab, M. S., Havens, E. A., & Shi, X. (2020). Mechanism of corrosion protection in chloride solution by an apple-based green inhibitor: experimental and theoretical studies. *Journal of Infrastructure Preservation and Resilience*, *1*(1), 1–19. https://doi.org/10.1186/s43065-020-00007-w

Houbraken, J. A. M. P., Frisvad, J. C., & Samson, R. A. (2010). Taxonomy of Penicillium citrinum and related species. *Fungal Diversity*, *44*, 117–133. https://doi.org/10.1007/s13225-010-0047-z

Hugo Le ´on-Santiesteban, Rosa Bernal, F. J. F. ´andez and A. T. (2008). Wastewater treatment forproductionofH2S-free biogas. *Journal of Chemical Technology & Biotechnology*, *83*(May), 1394–1400. https://doi.org/10.1002/jctb

Hussin, M. H., & Kassim, M. J. (2010). *Electrochemical Studies of Mild Steel Corrosion Inhibition in Aqueous Solution by Uncaria gambir Extract*. *21*(1), 1–13.

Hussin, M. H., & Kassim, M. J. (2011). Electrochemical, thermodynamic and adsorption studies of (+)-catechin hydrate as natural mild steel corrosion inhibitor in 1 M HCl. *International Journal of Electrochemical Science*, *6*(5), 1396–1414. https://doi.org/10.1016/s1452-3981(23)15082-6

Hussin, M. H., Rahim, A. A., Mohamad Ibrahim, M. N., & Brosse, N. (2015). Improved corrosion inhibition of mild steel by chemically modified lignin polymers from

Elaeis guineensis agricultural waste. *Materials Chemistry and Physics*, *163*, 201–212. https://doi.org/10.1016/j.matchemphys.2015.07.030

Ibrahim, H., & Kutty, A. A. (2013). Recreational stream assessment using Malaysia water quality index. *AIP Conference Proceedings*, *1571*(December), 620–624. https://doi.org/10.1063/1.4858723

Ishaq, U., Akram, M. S., Iqbal, Z., Rafiq, M., Akrem, A., Nadeem, M., Shafi, F., Shafiq, Z., Mahmood, S., & Baig, M. A. (2015). Production and characterization of novel self-assembling biosurfactants from Aspergillus flavus. *Journal of Applied Microbiology*, *119*(4), 1035–1045. https://doi.org/10.1111/jam.12929

Jahan, R., Bodratti, A. M., Tsianou, M., & Alexandridis, P. (2020). Biosurfactants, natural alternatives to synthetic surfactants: Physicochemical properties and applications. *Advances in Colloid and Interface Science*, *275*, 102061. https://doi.org/10.1016/j.cis.2019.102061

Jain Kassim, M., Jian Ming, W., Hazwan Hussin, M., & Kang Wei, T. (2010). Corrosion inhibition of mild steel in acidic solution by ethanol extract of Uncaria gambir. *Journal of Corrosion Science and Engineering*, *13*(May).

Jambhulkar, P. P., Singh, B., Raja, M., Ismaiel, A., Lakshman, D. K., Tomar, M., & Sharma, P. (2024). Genetic diversity and antagonistic properties of Trichoderma strains from the crop rhizospheres in southern Rajasthan, India. *Scientific Reports*, *14*(1), 1–21. https://doi.org/10.1038/s41598-024-58302-5

JKR. (2021). Standard Specifications for Building Works 2014. *Angewandte Chemie International Edition, 6(11), 951–952.*, 2013–2015.

Kamaruddin, S., Goh, W. I., Abdul Mutalib, N. A. N., Jhatial, A. A., Mohamad, N., & Rahman, A. F. (2021). Effect of Combined Supplementary Cementitious Materials on the Fresh and Mechanical Properties of Eco-Efficient Self-Compacting Concrete. *Arabian Journal for Science and Engineering*, *46*(11), 10953–10973. https://doi.org/10.1007/s13369-021-05656-x

Kaur, G., Wang, H., To, M. H., Roelants, S. L. K. W., Soetaert, W., & Lin, C. S. K. (2019). Efficient sophorolipids production using food waste. *Journal of Cleaner Production*, *232*, 1–11. https://doi.org/10.1016/j.jclepro.2019.05.326

Khan, M. S., Yang, C., Zhao, Y., Pan, H., Zhao, J., Shahzad, M. B., Kolawole, S. K., Ullah, I., & Yang, K. (2020). An induced corrosion inhibition of X80 steel by using marine bacterium Marinobacter salsuginis. *Colloids and Surfaces B:*

Biointerfaces, *189*(February), 110858. https://doi.org/10.1016/j.colsurfb.2020.110858

Kim, H., Son, H. M., Park, S., & Lee, H. K. (2020). Effects of biological admixtures on hydration and mechanical properties of Portland cement paste. *Construction and Building Materials*, *235*, 117461. https://doi.org/10.1016/j.conbuildmat.2019.117461

Kim, Y., Sim, J., & Park, C. (2012). Mechanical properties of recycled aggregate concrete with deformed steel re-bar. *Journal of Marine Science and Technology (Taiwan)*, *20*(3), 274–280. https://doi.org/10.51400/2709-6998.1804

Kondratova, I. L., Montes, P., & Bremner, T. W. (2003). Natural marine exposure results for reinforced concrete slabs with corrosion inhibitors. *Cement and Concrete Composites*, *25*(4-5 SPEC), 483–490. https://doi.org/10.1016/S0958-9465(02)00088-4

Kristen, U. (1997). <Use of Higher Plants As Screens.Pdf>. *Toxicology in Vitro*, *2333*(11), 181–191.

Kumar, A. P., Janardhan, A., Viswanath, B., Monika, K., Jung, J. Y., & Narasimha, G. (2016). Evaluation of orange peel for biosurfactant production by Bacillus licheniformis and their ability to degrade naphthalene and crude oil. *3 Biotech*, *6*(1), 1–10. https://doi.org/10.1007/s13205-015-0362-x

Kwon, J. H., Kim, J., & Kim, W. Il. (2011). First report of *rhizopus* oryzae as a postharvest pathogen of apple in Korea. *Mycobiology*, *39*(2), 140–142. https://doi.org/10.4489/MYCO.2011.39.2.140

Lammer, E., Carr, G. J., Wendler, K., Rawlings, J. M., Belanger, S. E., & Braunbeck, T. (2009). Is the fish embryo toxicity test (FET) with the zebrafish (Danio rerio) a potential alternative for the fish acute toxicity test? *Comparative Biochemistry and Physiology - C Toxicology and Pharmacology*, *149*(2), 196–209. https://doi.org/10.1016/ j.cbpc.2008.11.006

Lee, H. S., Noguchi, T., & Tomosawa, F. (2002). Evaluation of the bond properties between concrete and reinforcement as a function of the degree of reinforcement corrosion. *Cement and Concrete Research*, *32*(8), 1313–1318. https://doi.org/10.1016/S0008-8846(02)00783-4

Lee Taylor, D., & Sinsabaugh, R. L. (2015). The Soil Fungi. In *Soil Microbiology, Ecology and Biochemistry* (Issue December 2015). https://doi.org/10.1016/b978-0-12-415955-6.00004-9

Lennartsson, P. R., Taherzadeh, M. J., & Edebo, L. (2014). *Rhizopus. Encyclopedia of Food Microbiology: Second Edition*, *3*, 284–290. https://doi.org/10.1016/B978-0-12-384730-0.00391-8

Lesik, E. I., Buryukin, F. A., & Vaganov, R. A. (2021). Phospholipids from plant materials as a corrosion inhibitor in oil production. *Journal of Physics: Conference Series*, *2094*(5). https://doi.org/10.1088/1742-6596/2094/5/052044

Li, X. H., Deng, S. D., Fu, H., & Mu, G. N. (2009). Inhibition action of tween-80 on the corrosion of cold rolled steel in sulfuric acid. *Materials and Corrosion*, *60*(12), 969–976. https://doi.org/10.1002/maco.200905217

Liepins, J., Balina, K., Soloha, R., Berzina, I., & Lukasa, L. K. (2021). *Glycolipid Biosurfactant Production from Waste Cooking Oils by Yeast: Review of Substrates, Producers and Products.* https://doi.org/10.3390/fermentation7030136

Lin, H., Zhao, Y., Feng, P., Ye, H., Ozbolt, J., Jiang, C., & Yang, J. Q. (2019). State-of-the-art review on the bond properties of corroded reinforcing steel bar. *Construction and Building Materials*, *213*, 216–233. https://doi.org/10.1016/j.conbuildmat.2019.04.077

Lin, Y. Te, Jia, Z., Wang, D., & Chiu, C. Y. (2017). Effects of temperature on the composition and diversity of bacterial communities in bamboo soils at different elevations. *Biogeosciences*, *14*(21), 4879–4889. https://doi.org/10.5194/bg-14-4879-2017

Little, B. J., Blackwood, D. J., Hinks, J., Lauro, F. M., Marsili, E., Okamoto, A., Rice, S. A., Wade, S. A., & Flemming, H. C. (2020). Microbially influenced corrosion—Any progress? *Corrosion Science*, *170* (March), 108641. https://doi.org/10.1016/ j.corsci.2020.108641

Liu, J. F., Mbadinga, S. M., Yang, S. Z., Gu, J. D., & Mu, B. Z. (2015). Chemical structure, property and potential applications of biosurfactants produced by Bacillus subtilis in petroleum recovery and spill mitigation. *International Journal of Molecular Sciences*, *16*(3), 4814–4837. https://doi.org/10.3390/ijms16034814

Lopes, V. dos S., Fischer, J., Pinheiro, T. M. A., Cabral, B. V., Cardoso, V. L., & Coutinho Filho, U. (2017). Biosurfactant and ethanol co-production using Pseudomonas aeruginosa and Saccharomyces cerevisiae co-cultures and

exploded sugarcane bagasse. *Renewable Energy*, *109*, 305–310. https://doi.org/10.1016/j.renene.2017.03.047

Mansfeld, F., & Little, B. (1991). A Technical Review Of Electrochemical Techniques Applied To Microbiologically Influenced Corrosion. *Corrosion Science, 32*(3), 247–272.

Marajan C. (2020). *Application of BS in Enhancing Bioremediation.pdf*. Universiti Teknologi Mara.

Marajan, C., Alias, S., Ramasamy, K., & Abdul-Talib, S. (2018). The effect of incubation time, temperature and pH variations on the surface tension of biosurfactant produced by Bacillus spp. *AIP Conference Proceedings*, *2020*(January). https://doi.org/10.1063/1.5062673

Marcelino, P. R. F., Peres, G. F. D., Terán-Hilares, R., Pagnocca, F. C., Rosa, C. A., Lacerda, T. M., dos Santos, J. C., & da Silva, S. S. (2019). Biosurfactants production by yeasts using sugarcane bagasse hemicellulosic hydrolysate as new sustainable alternative for lignocellulosic biorefineries. *Industrial Crops and Products*, *129*(November 2018), 212–223. https://doi.org/10.1016/j.indcrop.2018.12.001

Marchant, R., & Banat, I. M. (2012). Biosurfactants: A sustainable replacement for chemical surfactants? *Biotechnology Letters*, *34*(9), 1597–1605. https://doi.org/10.1007/s10529-012-0956-x

Menna Barreto, M. F. F., Timm, J. F. G., Passuello, A., Dal Molin, D. C. C., & Masuero, J. R. (2021). Life cycle costs and impacts of massive slabs with varying concrete cover. *Cleaner Engineering and Technology*, *5*, 100256. https://doi.org/10.1016/ j.clet.2021.100256

Milagre, A. P., Dayana, M.-R., Daylin, R.-R., Adriana, F. S., Marcos, A. C. L., Michele, F. S., Rosileide, F. S. A., Thayse, A. L. e S., André, L. C. M. A. S., & Galba, M. C.-T. (2018). Development and improved selected markers to biosurfactant and bioemulsifier production by *Rhizopus* strains isolated from Caatinga soil. African Journal of Biotechnology, 17(6), 150–157. https://doi.org/10.5897/ajb2017.16230

Monika, F., Prayuda, H., Zega, B. C., & Cahyati, M. D. (2019). Flexural and compressive strength on no-fines concrete slab using variations of fly ash and superplasticizer. *International Journal of Integrated Engineering*, *11*(9 Special Issue), 275–284.

Morales, E. M. (1998). Significance of the Ratio of Tensile Strength To Yield Stress (Ts/Ys) of Reinforcing Bars. *CAST '98 Conference on Concrete Art, Science & Technology*. internal-pdf://131.89.193.131/Morales.PDF

Morikawa, M., Hirata, Y., & Imanaka, T. (2000). A study on the structure-function relationship of lipopeptide biosurfactants. *Biochimica et Biophysica Acta - Molecular and Cell Biology of Lipids*, *1488*(3), 211–218. https://doi.org/10.1016/S1388-1981(00)00124-4

Mukherjee, A. K. (2007). Potential application of cyclic lipopeptide biosurfactants produced by Bacillus subtilis strains in laundry detergent formulations. *Letters in Applied Microbiology*, *45*(3), 330–335. https://doi.org/10.1111/j.1472-765X.2007.02197.x

Murlidhar, B. R., Mohamad, E. T., Alel, M. N. A. Bin, & Armaghani, D. J. (2016). Geological study and mining plan importance for mitigating alkali silica reaction in aggregate quarry operation. *Jurnal Teknologi*, *78*(7–3), 71–79. https://doi.org/10.11113/ jt.v78.9486

Myrdal, R. (2007). Accelerating admixtures for concrete. In *Accelerating admixtures for concrete* (Issue May). https://www.researchgate.net/publication/288883755

Ni'matuzahroh, Sari, S. K., Trikurniadewi, N., Ibrahim, S. N. M. M., Khiftiyah, A. M., Abidin, A. Z., Nurhariyati, T., & Fatimah. (2020). Bioconversion of agricultural waste hydrolysate from lignocellulolytic mold into biosurfactant by Achromobacter sp. BP(1)5. *Biocatalysis and Agricultural Biotechnology*, *24*(October 2019), 101534. https://doi.org/10.1016/j.bcab.2020.101534

Nibudey, R. N., Nagarnaik, P. B., Parbat, D. K., Pande, A. M., & Polytechnic, G. (2014). *C Ompressive S Trength and S Orptivity P Roperties of. 7*(4), 1206–1216.

Nur Afini Binti Wan Adlin, W., Jong Yi Mian, V., Chung Huap, A., & Lee, W.-C. (2020). Characterization of Biosurfactants Produced by Bacillus Subtilis using Fresh and Waste Cooking Oil Enriched Medium. *Journal of Asian Scientific Research*, *10*(3), 156–164. https://doi.org/10.18488/journal.2.2020.103.156.164

Nurul Fatihah Khairudin. (2016). *Optimization of Biosurfactant Production Condition By Thermophilic Bacteria Using Waste Frying Oil* (Issue April). Universiti Teknologi Mara.

OECD. (2013). Test No. 236: Fish Embryo Acute Toxicity (FET) Test. *OECD Guidelines for the Testing of Chemicals, Section 2, OECD Publishing*, *July*, 1–22

Olivia, R., Ang, C. H., Clotilda, P., Caroline, M., Rudy, T., & Joe, N. (2023). Corrosion inhibition of mild steel bars by biosurfactant produced by Penicillium citrinum. *IOP Conference Series: Earth and Environmental Science*, *1135*(1). https://doi.org/10.1088/1755-1315/1135/1/012057

Örnek, D., Wood, T. K., Hsu, C. H., Sun, Z., & Mansfeld, F. (2002). Pitting corrosion control of aluminum 2024 using protective biofilms that secrete corrosion inhibitors. *Corrosion*, *58*(9), 761–767. https://doi.org/10.5006/1.3277659

Osouli, A., Chaulagai, R., Tutumluer, E., & Shoup, H. (2019). Strength characteristics of crushed gravel and limestone aggregates with up to 12% plastic fines evaluated for pavement base/subbase applications. *Transportation Geotechnics*, *18*, 25–38. https://doi.org/10.1016/j.trgeo.2018.10.004

Palanisamy, M. (2023). *Mechanical Behaviour of concrete incorporating Sea Shell Powder and Residue of Wood ash*. *October*.

Panjiar, N., Mattam, A. J., Jose, S., Gandham, S., & Velankar, H. R. (2020). Valorization of xylose-rich hydrolysate from rice straw, an agroresidue, through biosurfactant production by the soil bacterium Serratia nematodiphila. *Science of the Total Environment*, *729*. https://doi.org/10.1016/j.scitotenv.2020.138933

Paraszkiewicz, K., Bernat, P., Kuśmierska, A., Chojniak, J., & Płaza, G. (2018). Structural identification of lipopeptide biosurfactants produced by Bacillus subtilis strains grown on the media obtained from renewable natural resources. *Journal of Environmental Management*, *209*, 65–70. https://doi.org/10.1016/j.jenvman.2017.12.033

Parthipan, P., Sabarinathan, D., Angaiah, S., & Rajasekar, A. (2018). Glycolipid biosurfactant as an eco-friendly microbial inhibitor for the corrosion of carbon steel in vulnerable corrosive bacterial strains. *Journal of Molecular Liquids*, *261*(2017), 473–479. https://doi.org/10.1016/j.molliq.2018.04.045

Patel, V., & Shah, N. (2015). Durability properties of porcelain waste based high-performance concrete. *Magazine of Concrete Research*, *67*(4), 187–196. https://doi.org/10.1680/macr.14.00189

Pele, M. A., Ribeaux, D. R., Vieira, E. R., Souza, A. F., Luna, M. A. C., Rodríguez, D. M., Andrade, R. F. S., Alviano, D. S., Alviano, C. S., Barreto-Bergter, E.,

Santiago, A. L. C. M. A., & Campos-Takaki, G. M. (2019). Conversion of renewable substrates for biosurfactant production by *Rhizopus* arrhizus UCP 1607 and enhancing the removal of diesel oil from marine soil. *Electronic Journal of Biotechnology*, *38*, 40–48. https://doi.org/10.1016/j.ejbt.2018.12.003

Pham Van, N., Hoang, N. C. T., Manh, T. D., Dung, L. T., Hoai Vu, N. S., Prabhakar Vattikuti, S. V., Panaitescu, C., Pham, T. T., & Nguyen Dang, N. (2024). Enhancing corrosion resistance of mild steel in hydrochloric acid with Chiquita banana sap extract. *RSC Advances*, *14*(20), 14263–14277. https://doi.org/10.1039/d4ra00132j

Płaza, G. A., Zjawiony, I., & Banat, I. M. (2006). Use of different methods for detection of thermophilic biosurfactant-producing bacteria from hydrocarbon-contaminated and bioremediated soils. *Journal of Petroleum Science and Engineering*, *50*(1), 71–77. https://doi.org/10.1016/j.petrol.2005.10.005

Płaza, G., & Achal, V. (2020). Biosurfactants: Eco-friendly and innovative biocides against biocorrosion. *International Journal of Molecular Sciences*, *21*(6). https://doi.org/10.3390/ijms21062152

Prado, A. A. O. S., Santos, B. L. P., Vieira, I. M. M., Ramos, L. C., de Souza, R. R., Silva, D. P., & Ruzene, D. S. (2019). Evaluation of a new strategy in the elaboration of culture media to produce surfactin from hemicellulosic corncob liquor. *Biotechnology Reports*, *24*, e00364. https://doi.org/10.1016/j.btre.2019.e00364

Prasad, D. D., Kiran, T., Vinay, M., & Ravande, K. (2019). Strength and Durability Studies on Concrete made using Treated Recycled Coarse and Fine Aggregate. *International Research Journal of Engineering and Technology (IRJET)*, *06*(11/Nov 2019), 2300–2309.

Radzuan, M. N. (2018). *Biosurfactant Production by Fermentation of Palm Oil Agricultural Refinery Waste* [University of Manchester]

Rahim, N. L., Ibrahim, N. M., Salehuddin, S., Mohammed, S. A., & Othman, M. Z. (2020). Investigation of bamboo as concrete reinforcement in the construction for low-cost housing industry. *IOP Conference Series: Earth and Environmental Science*, *476*(1). https://doi.org/10.1088/1755-1315/476/1/012058

Randhawa, K. K. S., & Rahman, P. K. S. M. (2014). Rhamnolipid biosurfactants-past, present, and future scenario of global market. *Frontiers in Microbiology*, *5*(SEP), 1–7. https://doi.org/10.3389/fmicb.2014.00454

Rao, P., & Mulky, L. (2023). Microbially Influenced Corrosion and its Control Measures: A Critical Review. *Journal of Bio- and Tribo-Corrosion*, *9*(3), 1–13. https://doi.org/10.1007/s40735-023-00772-7

Rasheed, S., Khushnood, R. A., Raza, A., Ahmed, S., & Kanwal, M. (2024). Development of biological techniques to prevent corrosion of reinforcing steel bars. *Heliyon*, *10*(18), e37966. https://doi.org/10.1016/j.heliyon.2024.e37966

Rawat, V. S., & Khan, Z. (2022). SELF-COMPACTING CONCRETE. *IJCRT21X0038 International Journal of Creative Research Thoughts (IJCRT)*, *10*(6), 721–772.

Roberge, P. R. (2015). Corrosion Engineering; Principles and practice. In *Decentralization and Infrastructure in the Global Economy: From Gaps to Solutions*. The McGraw-Hill Companies. https://doi.org/10.4324/9781315694108

Sa'adi, Z., Shahid, S., Ismail, T., Chung, E., & Wang, X. (2017). Distributional Changes in Rainfall and River Flow in Sarawak , Malaysia. *ASIA-PACIFIC JOURNAL OF ATMOSPHERIC SCIENCES*, *53*(4), 489–500. https://doi.org/10.1007/s13143-017-0051-2

Sabri, M. A. M., Sulong, A. B., Chin, F. K., & Sahari, J. (2012). Effect of corrossion on the electrical conductivity of metals and polymer composite. *Jurnal Teknologi (Sciences and Engineering)*, *59*(SUPPL.2), 81–85. https://doi.org/10.11113/jt.v59.2566

Samson, R. A., Seifert, K. A., Kuijpers, A. F. A., Houbraken, J. A. M. P., & Frisvad, J. C. (2004). Phylogenetic analysis of Penicillium subgenus Penicillium using partial β-tubulin sequences. *Studies in Mycology*, *2004*(49), 175–200.

Samsu, Z. A., Jeffry, F. N., & Azizan, W. N. A. N. W. A. R. (2020). Isolation and screening of potential biosurfactant-producing bacteria from used engine oil-contaminated soil. Materials Today: Proceedings, 31, A67–A71. https://doi.org/10.1016/j.matpr. 2020.12.43

Sandle, T. (2014). Trichoderma. *Encyclopedia of Food Microbiology: Second Edition*, *3*, 644–646. https://doi.org/10.1016/B978-0-12-384730-0.00337-2

Sani, M. S. H. M., & Osman, A. R. (2010). Basic Principles and Requirements of Self Compacting Concrete. *Jurnal Gading*, 107–123.

Sari, I. P., Basyiruddin, M. I., & Hertadi, R. (2018). Bioconversion of palm oil into biosurfactant by halomonas meridiana BK-AB4 for the application of corrosion inhibitor. *Indonesian Journal of Chemistry*, *18*(4), 718–723. https://doi.org/10.22146/ijc.27040

Sarma, H., Bustamante, K. L. T., & Prasad, M. N. V. (2019). Biosurfactants for oil recovery from refinery sludge: Magnetic nanoparticles assisted purification. In *Industrial and Municipal Sludge: Emerging Concerns and Scope for Resource Recovery*. Elsevier Inc. https://doi.org/10.1016/B978-0-12-815907-1.00006-4

Sena, H. H., Sanches, M. A., Rocha, D. F. S., Segundo, W. O. P. F., De Souza, É. S., & De Souza, J. V. B. (2018). Production of Biosurfactants by Soil Fungi Isolated from the Amazon Forest. *International Journal of Microbiology*, *2018*. https://doi.org/10.1155/2018/5684261

Shaffer, J. (2015). Steel reinforcement bar: A tensile testing guide. *Advanced Materials and Processes*, *173*(6), 23–27.

Sharma, A., Soni, J., Kaur, G., & Kaur, J. (2014). A Study on biosurfactant production in Lactobacillus and Bacillus sp. *International Journal of Current Microbiology and Applied Sciences*, *3*(11), 723–733.

Shunmuga Vembu, P. R., & Ammasi, A. K. (2023). A Comprehensive Review on the Factors Affecting Bond Strength in Concrete. *Buildings*, *13*(3). https://doi.org/10.3390/buildings13030577

Sivakumar, D., Ramasamy, R., Thiagarajan, Y. R., Thirumalairaj, B., Krishnamoorthy, U., Haque Siddiqui, M. I., Lakshmaiya, N., Kumar, A., & Shah, M. A. (2024). Biosurfactants in biocorrosion and corrosion mitigation of metals: An overview. *Open Chemistry*, *22*(1), 1–16. https://doi.org/10.1515/chem-2024-0036

Sobrinho, H. B. S., Luna, J. M., Rufino, R. D., Porto, A., & Sarubbo, L. A. (2014). Biosurfactants: classification, properties and environmental applications. *Recent Developments in Biotechnology*, *11*(14), 1–29. https://www.researchgate.net/profile/Leonie-Sarubbo/publication/280841136_Biosurfactants_Classification_Properties_and_Environmental_Applications/links/55c90f1008aebc967df90aea/Biosurfactants-Classification-Properties-and-Environmental-Applications.pdf

Sohail, M. G., Al Nuaimi, N., Alnahhal, W., & Kahraman, R. (2023). Performance of Mild Steel and Corrosion-Resistant Steel Rebars in Chloride-Contaminated Concrete. *Proceedings of the 2nd International Conference on Civil*

Infrastructure and Construction (CIC 2023), *Cic*, 792–797. https://doi.org/10.29117/cic.2023.0103

Sohail, M. G., Kahraman, R., Alnuaimi, N. A., Gencturk, B., Alnahhal, W., Dawood, M., & Belarbi, A. (2020). Electrochemical behavior of mild and corrosion resistant concrete reinforcing steels. *Construction and Building Materials*, *232*, 117205. https://doi.org/10.1016/j.conbuildmat.2019.117205

Speight, J. G. (2014). Corrosion Monitoring and Control. *Oil and Gas Corrosion Prevention*, 109–149. https://doi.org/10.1016/b978-0-12-800346-6.00006-5

Srivastava, V. K., Srivastava, A., & Kumar, V. (2023). Effect of Substrate Concentration and pH on Biosurfactant Production from Pineapple Peel. *Journal of Energy Research and Environmental Technology (JERET)*, *6*(1), 56–60. http://www.krishisanskriti.org

Sudantha, I. M., & Suwardji, S. (2021). Biodiversity of Trichoderma antagonist saprophytic fungi and its use for biocontrol of Fusarium wilt disease on shallots at Lombok Island, West Nusa Tenggara, Indonesia. *IOP Conference Series: Earth and Environmental Science*, *886*(1). https://doi.org/10.1088/1755-1315/886/1/012123

Sundaram, T., Govindarajan, R. K., Vinayagam, S., Krishnan, V., Nagarajan, S., Gnanasekaran, G. R., Baek, K.-H., & Rajamani Sekar, S. K. (2024). Advancements in biosurfactant production using agro-industrial waste for industrial and environmental applications. *Frontiers in Microbiology*, *15*(February). https://doi.org/10.3389/fmicb.2024.1357302

Tahershamsi, M. (2016). *THESIS FOR THE DEGREE OF DOCTOR OF PHILOSOPHY Structural Effects of Reinforcement Corrosion in Concrete Structures*. Chalmers University of Technology.

Taiji, I., & Yoshito, T. (1964). Taxonomical Studies on Genus *Rhizopus*. *Bulletin of the Japan Institute of Metals*, *3*(5), 249–258. http://joi.jlc.jst.go.jp/JST.Journalarchive/materia 1962/3.249

Tan, S. T., Ramesh, T., Toh, X. R., & Nguyen, L. N. (2020). Emerging roles of lysophospholipids in health and disease. *Progress in Lipid Research*, *80*(August), 101068. https://doi.org/10.1016/j.plipres.2020.101068

Tang, M., Zhou, W., Liu, Y., Yan, J., & Gong, Z. (2018). A two-stage process facilitating microbial lipid production from N-acetylglucosamine by Cryptococcus curvatus cultured under non-sterile conditions. *Bioresource*

Technology, *258*(March), 255–262. https://doi.org/10.1016/j.biortech.2018.03.015

Thrane, U. (2014). Fusarium. *Encyclopedia of Food Microbiology: Second Edition*, *2*, 76–81. https://doi.org/10.1016/B978-0-12-384730-0.00141-5

Turlapati, V. V. (2019). a Comparitive Study on Compressive and Flexural Strength of Fiber Reinforced Concrete (Steel and Polypropylene) and Ordinary Concrete. *Journal of Emerging Technologies and Innovative Research (JETIR)*, *6*(4), 485–506.

Unosson, J., Montufar, E. B., Engqvist, H., Ginebra, M. P., & Persson, C. (2016). Brushite foams - The effect of Tween® 80 and Pluronic® F-127 on foam porosity and mechanical properties. *Journal of Biomedical Materials Research - Part B Applied Biomaterials*, *104*(1), 67–77. https://doi.org/10.1002/jbm.b.33355

Uysal, M., & Yilmaz, K. (2011). Effect of mineral admixtures on properties of self-compacting concrete. *Cement and Concrete Composites*, *33*(7), 771–776. https://doi.org/10.1016/j.cemconcomp.2011.04.005

Uzoigwe, C., Burgess, J. G., Ennis, C. J., & Rahman, P. K. S. M. (2015). Bioemulsifiers are not biosurfactants and require different screening approaches. *Frontiers in Microbiology*, *6*(APR), 1–6. https://doi.org/10.3389/fmicb.2015.00245

Vieira, I. M. M., Santos, B. L. P., Silva, L. S., Ramos, L. C., de Souza, R. R., Ruzene, D. S., & Silva, D. P. (2021). Potential of pineapple peel in the alternative composition of culture media for biosurfactant production. *Environmental Science and Pollution Research*, *28*(48), 68957–68971. https://doi.org/10.1007/s11356-021-15393-1

Wahyuni, L., Wirjosentono, B., & Tamrin, T. (2020). JCNaR Journal of Chemical Natural Resources Effect of Surfactant Tween 80 (Polyoxyethylene Sorbitan Mono Oleate) Addition on Viscosity and Activation Energy on Making Asphalt Emulsion. *Journal of Chemical Natural Resources*, *02*(02), 2020–2113. https://talenta.usu.ac.id/JCNaR/article/view/9324

Wang, D. Y., Nie, B. L., Li, H. J., Zhang, W. W., & Wu, Y. C. (2021). Anticorrosion performance of grape seed proanthocyanidins extract and Tween-80 for mild steel in hydrochloric acid medium. *Journal of Molecular Liquids*, *331*, 115799. https://doi.org/10.1016/j.molliq.2021.115799

Yehia, S., Helal, K., Abusharkh, A., Zaher, A., & Istaitiyeh, H. (2015). Strength and Durability Evaluation of Recycled Aggregate Concrete. *International Journal of Concrete Structures and Materials*, *9*(2), 219–239. https://doi.org/10.1007/s40069-015-0100-0

Youssef, N. H., Duncan, K. E., Nagle, D. P., Savage, K. N., Knapp, R. M., & McInerney, M. J. (2004). Comparison of methods to detect biosurfactant production by diverse microorganisms. *Journal of Microbiological Methods*, *56*(3), 339–347. https://doi.org/10.1016/j.mimet.2003.11.001

Zhang, X., Wu, Z., Zheng, J., Dong, W., & Bouchair, A. (2016). Ultimate bond strength of plain round bars embedded in concrete subjected to uniform lateral tension. *Construction and Building Materials*, *117*, 163–170. https://doi.org/10.1016/j.conbuildmat.2016.05.029

Zhang, X. Y., Li, B., Huang, B. C., Wang, F. B., Zhang, Y. Q., Zhao, S. G., Li, M., Wang, H. Y., Yu, X. J., Liu, X. Y., Jiang, J., & Wang, Z. P. (2022). Production, Biosynthesis, and Commercial Applications of Fatty Acids From Oleaginous Fungi. *Frontiers in Nutrition*, *9*(May), 1–15. https://doi.org/10.3389/fnut.2022.873657

Zhao, Y., Lin, H., Wu, K., & Jin, W. (2013). Bond behaviour of normal/recycled concrete and corroded steel bars. *Construction and Building Materials*, *48*, 348–359. https://doi.org/10.1016/j.conbuildmat.2013.06.091

Zin, I. M., Pokhmurskii, V. I., Korniy, S. A., Karpenko, O. V., Lyon, S. B., Khlopyk, O. P., & Tymus, M. B. (2018). Corrosion inhibition of aluminium alloy by rhamnolipid biosurfactant derived from pseudomonas sp. PS-17. *Anti-Corrosion Methods and Materials*, *65*(6), 517–527. https://doi.org/10.1108/ACMM-03-2017-1775

Zulfareen, N., Kannan, K., Venugopal, T., & Gnanavel, S. (2016). Synthesis, characterization and corrosion inhibition efficiency of N-(4-(Morpholinomethyl Carbamoyl Phenyl) Furan-2-Carboxamide for brass in HCl medium. *Arabian Journal of Chemistry,* *9*(1), 121–135. https://doi.org/10.1016/j.arabjc.2015.08.023

APPENDICES

APPENDIX 1

Laboratory Testing

Figure A.1 The Fresh Concrete Flowability Test

Figure A.2 Separation Process of Crude Biosurfactant from Liquid to Crystalline State

Figure A.3 Corrosion Analysis With EIS

Figure A.4 Samples Preparation for the R_m Test

Sample Reference	Nominal Size	Length	Yield Strength, Re	Maximum Load at Maximum Force	Tensile Strength, Rm	Elongation at Maximum Force, Agt	Tensile/Yield Strength Ratio, Rm/Re
	mm	mm	N/mm²	kN	N/mm²	%	%
BS 20 % - 1/3	10	601	405	45	576	15.0	-

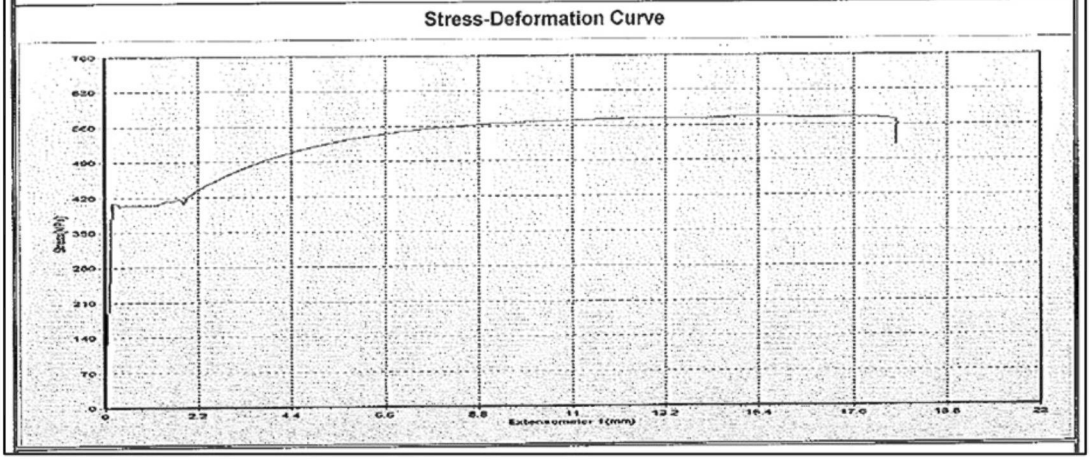

Figure A.5 The Stress Deformation Curve of Steel Bar treated with 0.9%NaCl and 20% Biosurfactant

Sample Reference	Nominal Size	Length	Yield Strength, Re	Maximum Load at Maximum Force	Tensile Strength, Rm	Elongation at Maximum Force, Agt	Tensile/Yield Strength Ratio, Rm/Re
	mm	mm	N/mm²	kN	N/mm²	%	%
BS 15 % - 1/3	10	600	396	45	574	14.0	-

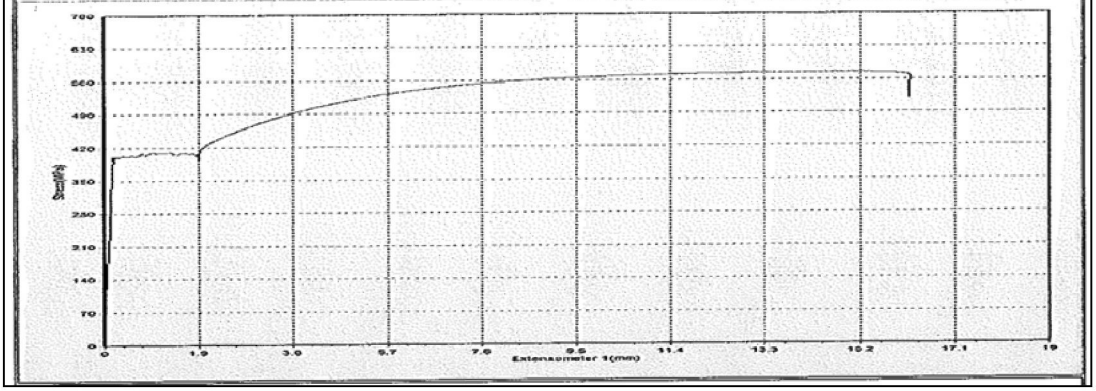

Figure A.6 The Stress Deformation Curve of Steel Bar treated with 0.9%NaCl and 15% Biosurfactant

Sample Reference	Nominal Size	Length	Yield Strength, Re	Maximum Load at Maximum Force	Tensile Strength, Rm	Elongation at Maximum Force, Agt	Tensile/Yield Strength Ratio, Rm/Re
	mm	mm	N/mm²	kN	N/mm²	%	%
BS 10 % - 3/3	10	601	349	40	508	15.0	-

Stress-Deformation Curve

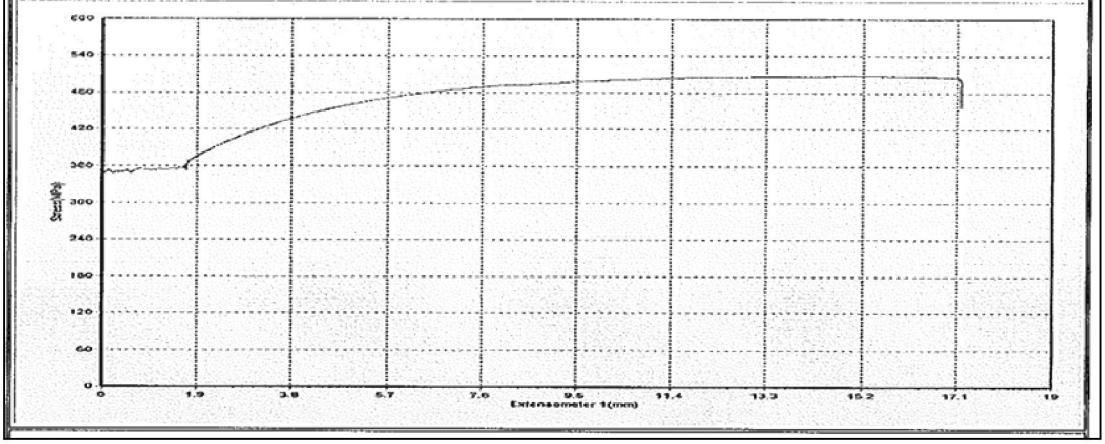

Figure A.7 The Stress Deformation Curve of Steel Bar treated with 0.9%NaCl and 10% Biosurfactant

Sample Reference	Nominal Size	Length	Yield Strength, Re	Maximum Load at Maximum Force	Tensile Strength, Rm	Elongation at Maximum Force, Agt	Tensile/Yield Strength Ratio, Rm/Re
	mm	mm	N/mm²	kN	N/mm²	%	%
BS 5 % - 1/3	10	600	359	40	515	15.0	-

Stress-Deformation Curve

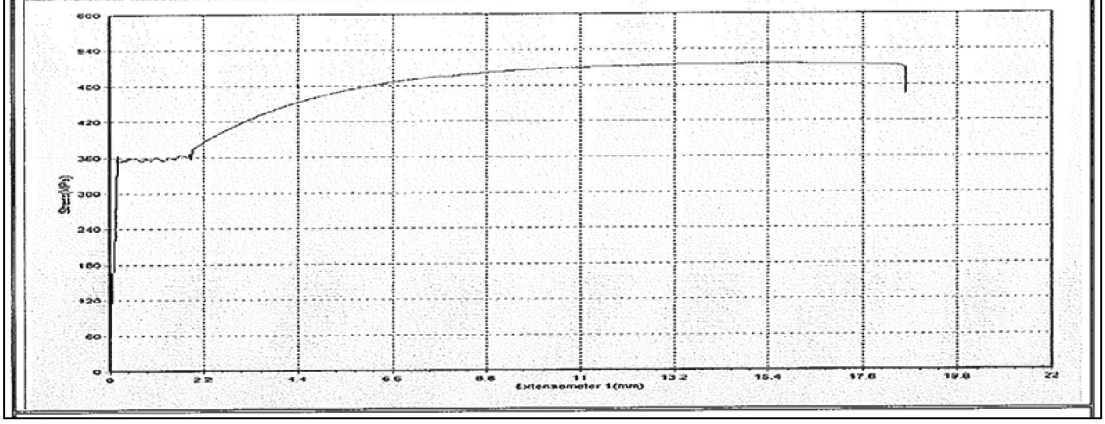

Figure A.8 The Stress Deformation Curve of Steel Bar treated with 0.9%NaCl and 5% Biosurfactant

Sample Reference	Nominal Size	Length	Yield Strength, Re	Maximum Load at Maximum Force	Tensile Strength, Rm	Elongation at Maximum Force, Agt	Tensile/Yield Strength Ratio, Rm/Re
	mm	mm	N/mm²	kN	N/mm²	%	%
Tween 80- 2/3	10	600	320	36	456	18.0	-

Stress-Deformation Curve

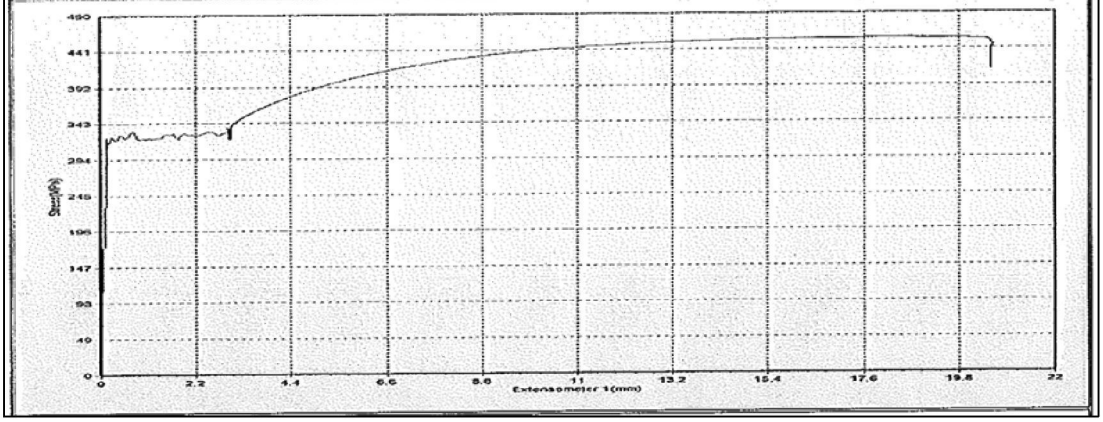

Figure A.9 The Stress Deformation Curve of Steel Bar treated with 0.9%NaCl and 10% of Tween 80

Figure A.10 Sample Preparation for the f_c Test

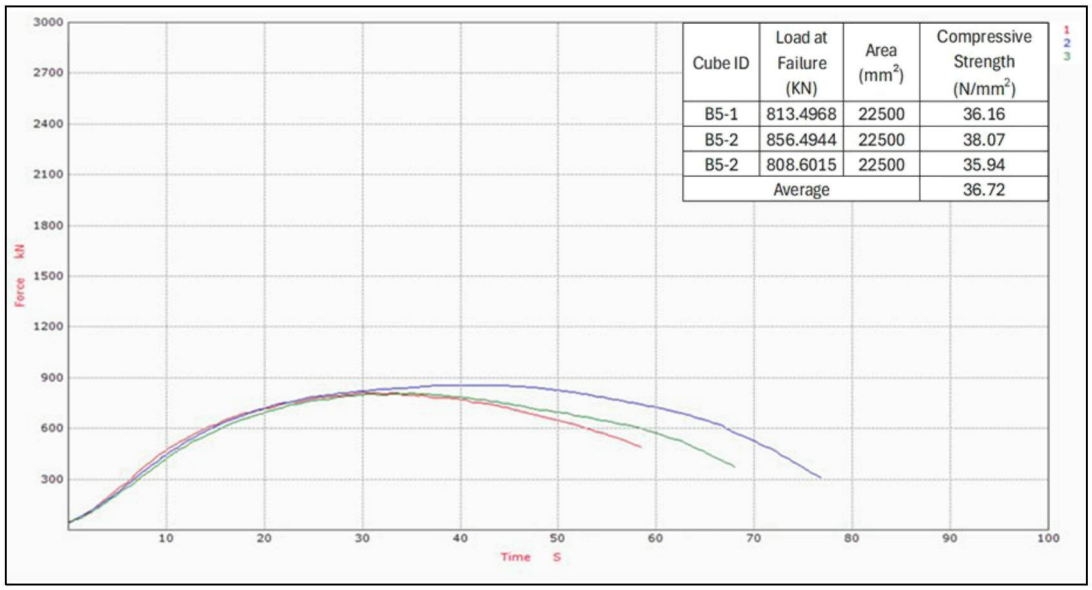

Cube ID	Load at Failure (KN)	Area (mm^2)	Compressive Strength (N/mm^2)
B5-1	813.4968	22500	36.16
B5-2	856.4944	22500	38.07
B5-2	808.6015	22500	35.94
Average			36.72

Figure A.11 Load-Time Curve Analysis for Concrete Specimens with 5% Biosurfactant as Water Replacement Admixture

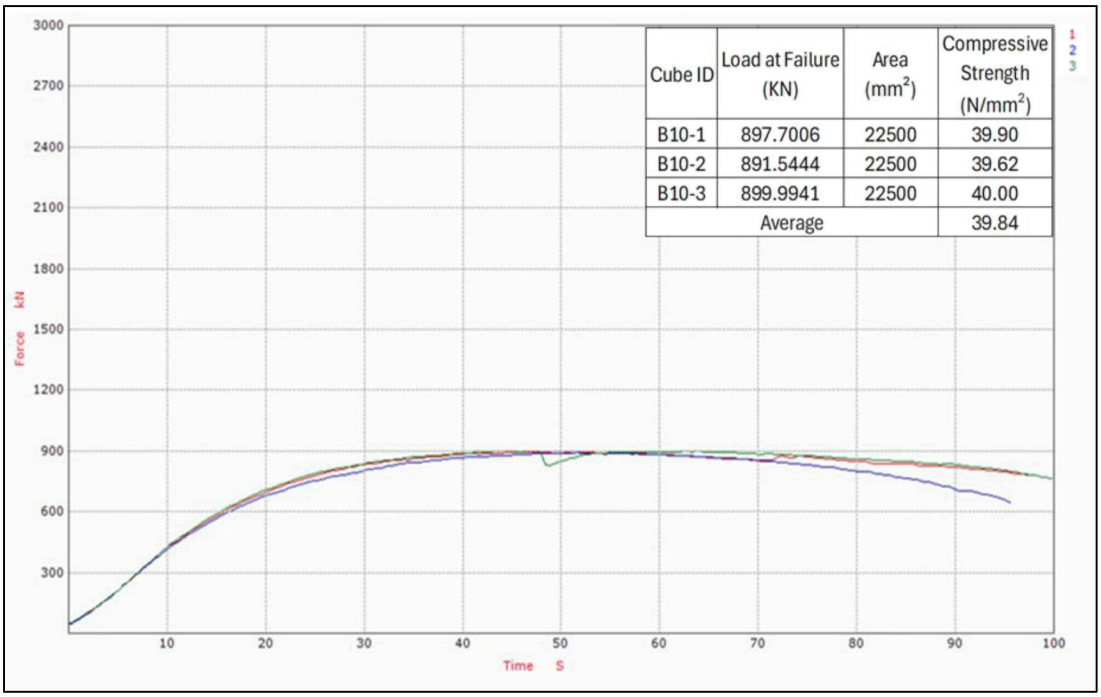

Cube ID	Load at Failure (KN)	Area (mm^2)	Compressive Strength (N/mm^2)
B10-1	897.7006	22500	39.90
B10-2	891.5444	22500	39.62
B10-3	899.9941	22500	40.00
Average			39.84

Figure A.12 Load-Time Curve Analysis for Concrete Specimens with 10% Biosurfactant as Water Replacement Admixture

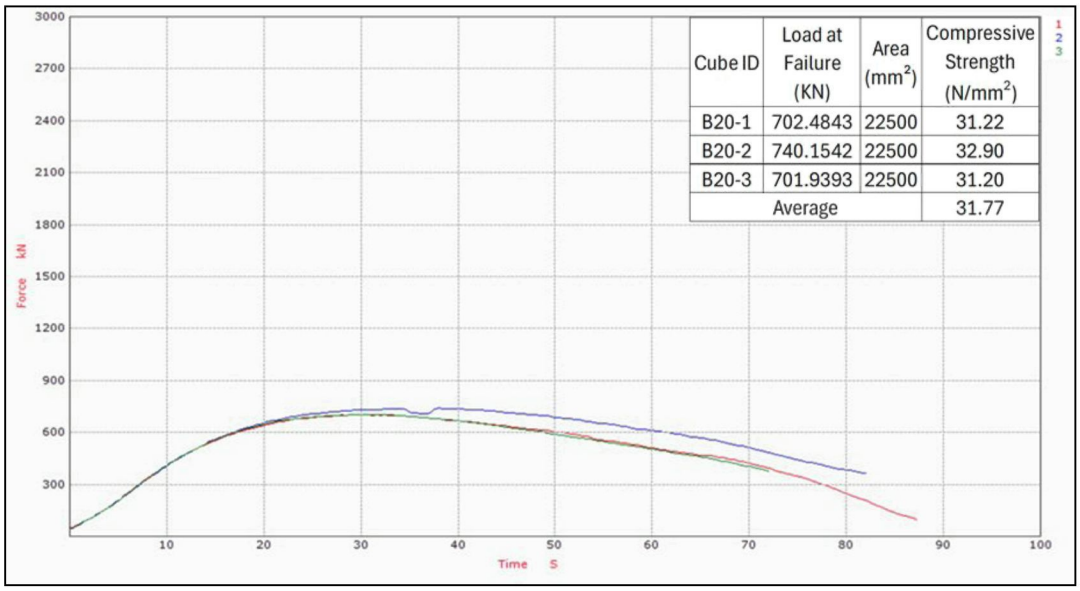

Figure A.13 Load-Time Curve Analysis for Concrete Specimens with 20% Biosurfactant as Water Replacement Admixture

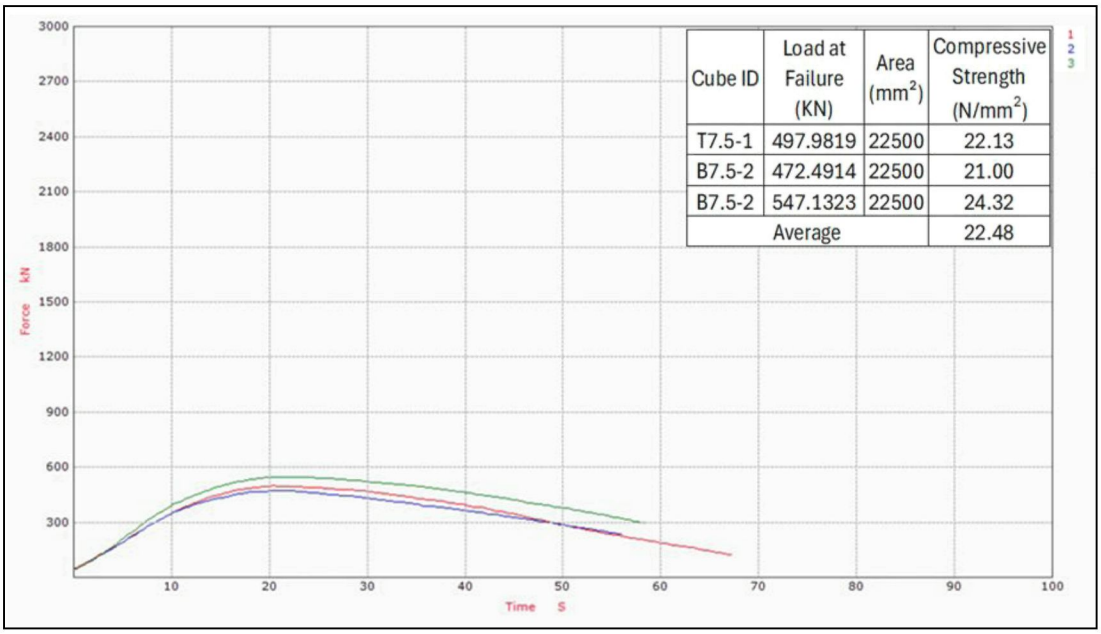

Figure A.14 Load-Time Curve Analysis for Concrete Specimens with 7.5% Tween 80 as Water Replacement Admixture

APPENDIX 2

Design Mix

CONCRETE MIX DESIGN FORM

Job Title : Concrete Grade 30 (Trial mix 1)

Stage	Item		Ref.	Values
1	1.1	Characteristic strength		30 N/mm² at 28 days
	1.2	Standard deviation		Proportion Defectives 5 % N/mm² or no data 8 N/mm² (k = 1.64)
	1.3	Margin		8 x 1.64 = 13.12 N/mm²
	1.4	Target mean strength		30 + 13 = 43 N/mm²
	1.5	Cement type		OPC/SRPC/RHPC
	1.6	Aggregate type: Coarse Aggregate type: Fine		Crushed/Uncrushed Crushed/Uncrushed
	1.7	Free water/cement ratio		0.50 } Use the lower value 0.5
	1.8	Maximum free water/cement ratio		0.60 }
2	2.1	Slump or Vebe time		Slump 75 mm or Vebe time s
	2.2	Maximum aggregate size		20 mm
	2.3	Free-water content		205 kg/m³
3	3.1	Cement content		205 / 0.5 = 410.00 kg/m³
	3.2	Maximum cement content		kg/m³
	3.3	Minimum cement content		kg/m³ Use cement content Use 3.1, if < 3. Use 3.3, if ≥ 3.1
	3.4	Modified free-water/cement ratio		0.5
4	4.1	Relative density of aggregate (SSD)		2.7 known/~~assumed~~
	4.2	Concrete density		2420 kg/m³
	4.3	Total aggregate content		2420 -410 - 205 = 1805 kg/m³
5	5.1	Grading of fine aggregate		Percentage passing 600µm 65 %
	5.2	Proportion of fine aggregate		33 to 39.5 (36.25) %
	5.3	Fine aggregate content		1805 x 0.3625 = 654.31 kg/m³
	5.4	Coarse aggregate content		1805 – 654.31 = 1150.69 kg/m³

Quantities	Water (kg)	Cement (kg)	Fine Aggregate (kg)	Coarse Aggregate (kg)		
				10 mm	20 mm	40 mm
1m³ (To nearest 5kg)	205	410	654		1151	
Per trial mix of ____ m³						

Figure B.1 The Composition of Concrete Trial Mix 1

CONCRETE MIX DESIGN FORM

Job Title : Concrete Grade 30 (Trial mix 2)

Stage		Item	Ref.	Values
1	1.1	Characteristic strength		30 N/mm² at 28 days
	1.2	Standard deviation		Proportion Defectives 5 % N/mm² or no data 8 N/mm² (k = 1.64)
	1.3	Margin		8 x 1.64 = 13.12 N/mm²
	1.4	Target mean strength		30 + 13 = 43 N/mm²
	1.5	Cement type		OPC/SRPC/RHPC
	1.6	Aggregate type: Coarse Aggregate type: Fine		Crushed/Uncrushed Crushed/Uncrushed
	1.7	Free water/cement ratio		0.50 } Used value 0.55
	1.8	Maximum free water/cement ratio		0.60 }
2	2.1	Slump or Vebe time		Slump 75 mm or Vebe time s
	2.2	Maximum aggregate size		20 mm
	2.3	Free-water content		205 kg/m³
3	3.1	Cement content		205 / 0.55 = 372.73 kg/m³
	3.2	Maximum cement content		kg/m³
	3.3	Minimum cement content		kg/m³ Use cement content Use 3.1, if < 3. Use 3.3, if ≥ 3.1
	3.4	Modified free-water/cement ratio		0.55
4	4.1	Relative density of aggregate (SSD)		2.7 known/~~assumed~~
	4.2	Concrete density		2420 kg/m³
	4.3	Total aggregate content		2420-372.73-205 = 1842.27 kg/m³
5	5.1	Grading of fine aggregate		Percentage passing 600µm 65 %
	5.2	Proportion of fine aggregate		33 to 39.5 (36.25) %
	5.3	Fine aggregate content		1842.27 x 0.3625 = 667.82 kg/m³
	5.4	Coarse aggregate content		1842.27 – 667.82 = 1174.45 kg/m³

Quantities	Water (kg)	Cement (kg)	Fine Aggregate (kg)	Coarse Aggregate (kg)		
				10 mm	20 mm	40 mm
1m³ (To nearest 5kg)	205	373	668		1174	
Per trial mix of _____ m³						

Figure B.2 The Composition of Concrete Trial Mix 2

CONCRETE MIX DESIGN FORM

Job Title : Concrete Grade 30 (Trial mix 3)

Stage		Item	Ref.	Values
1	1.1	Characteristic strength		30 N/mm² at 28 days
	1.2	Standard deviation		Proportion Defectives 5 % N/mm² or no data 8 N/mm² (k = 1.64)
	1.3	Margin		8 x 1.64 = 13.12 N/mm²
	1.4	Target mean strength		30 + 13 = 43 N/mm²
	1.5	Cement type		OPC/SRPC/RHPC
	1.6	Aggregate type: Coarse Aggregate type: Fine		Crushed/Uncrushed Crushed/Uncrushed
	1.7	Free water/cement ratio		0.50 } Use the lower value 0.60
	1.8	Maximum free water/cement ratio		0.60 }
2	2.1	Slump or Vebe time		Slump 75 mm or Vebe time s
	2.2	Maximum aggregate size		20 mm
	2.3	Free-water content		205 kg/m³
3	3.1	Cement content		205 / 0.6 = 341.67 kg/m³
	3.2	Maximum cement content		- kg/m³
	3.3	Minimum cement content		- kg/m³ Use cement content Use 3.1, if < 3. Use 3.3, if ≥ 3.1
	3.4	Modified free-water/cement ratio		0.60
4	4.1	Relative density of aggregate (SSD)		2.7 known/assumed
	4.2	Concrete density		2420 kg/m³
	4.3	Total aggregate content		2420 - 341.67 - 205 = 1873.33 kg/m³
5	5.1	Grading of fine aggregate		Percentage passing 600µm 65 %
	5.2	Proportion of fine aggregate		33 to 39.5 (36.25) %
	5.3	Fine aggregate content		1873.33 x 0.3625 = 679.10 kg/m³
	5.4	Coarse aggregate content		1873.33 – 679.10 = 1194.20 kg/m³

Quantities	Water (kg)	Cement (kg)	Fine Aggregate (kg)	Coarse Aggregate (kg)		
				10 mm	20 mm	40 mm
1m³ (To nearest 5kg)	205	342	679		1194	
Per trial mix of m³						

Figure B.3 The Composition of Concrete Trial Mix 3

CONCRETE MIX DESIGN FORM

Job Title : Concrete Grade 30 (Trial mix 4)

Stage	Item		Ref.	Values
1	1.1	Characteristic strength		30 N/mm² at 28 days
	1.2	Standard deviation		Proportion Defectives 5 % N/mm² or no data 8 N/mm² (k = 1.64)
	1.3	Margin		8 x 1.64 = 13.12 N/mm²
	1.4	Target mean strength		30 + 13 = 43 N/mm²
	1.5	Cement type		OPC/SRPC/RHPC
	1.6	Aggregate type: Coarse Aggregate type: Fine		Crushed/Uncrushed Crushed/Uncrushed
	1.7	Free water/cement ratio		0.50 } Used value 0.55
	1.8	Maximum free water/cement ratio		0.60 }
2	2.1	Slump or Vebe time		Slump 75 mm or Vebe time s
	2.2	Maximum aggregate size		20 mm
	2.3	Free-water content		225 kg/m³
3	3.1	Cement content		225 / 0.55 = 409 kg/m³
	3.2	Maximum cement content		- kg/m³
	3.3	Minimum cement content		- kg/m³ Use cement content Use 3.1, if < 3. Use 3.3, if ≥ 3.1
	3.4	Modified free-water/cement ratio		0.55
4	4.1	Relative density of aggregate (SSD)		2.7 known/~~assumed~~
	4.2	Concrete density (F3)		2380 kg/m³
	4.3	Total aggregate content		2374 – 409 - 225 = 1740 kg/m³
5	5.1	Grading of fine aggregate		Percentage passing 600µm 65 %
	5.2	Proportion of fine aggregate		33 to 39.5 (36.25) %
	5.3	Fine aggregate content		1740 x 0.3625 = 631 kg/m³
	5.4	Coarse aggregate content		1740 – 631 = 1110 kg/m³

Quantities	Water (kg)	Cement (kg)	Fine Aggregate (kg)	Coarse Aggregate (kg)		
				10 mm	20 mm	40 mm
1m³ (To nearest 5kg)	225	409	631		1110	
Per trial mix of ____ m³						

Figure B.4 The Composition of Concrete Trial Mix 4

AUTHOR'S PROFILE

Ts. Olivia Anak Rayeg obtained a Bachelor of Engineering (Hons.) in Civil Engineering from Universiti Teknologi MARA, Shah Alam in 2004, and a Master of Science in Construction Contract Management from Universiti Teknologi Malaysia in 2010. She began her career as a Project Engineer with Guobena Sdn. Bhd., Sinarsara Sdn. Bhd., and Wekajaya Sdn. Bhd., before joining the Ministry of Human Resources, Malaysia. Throughout her career, she has overseen several notable projects, including the construction of Mutiara Plaza in Jalan Ipoh, Kuala Lumpur; the Ulu Layar–Nanga Tiga rural road; Sekolah Kebangsaan Upper Lanang in Sibu; Sekolah Kebangsaan Balingian; and the Police Headquarters in Mukah. While at the Ministry of Human Resources, she supervised the construction of the Industrial Training Institute (ILP) in Miri, Advanced Technology Training Centre (ADTEC) in Bintulu and the Advanced Technology Training Centre (ADTEC) in Serian, Sarawak.

LIST OF PUBLICATIONS:

Olivia, R., Ang, C. H., Clotilda, P., Caroline, M., Rudy, T., & Joe, N. (2023). Corrosion inhibition of mild steel bars by biosurfactant produced by Penicillium citrinum. *IOP Conference Series: Earth and Environmental Science*, *1135*(1). https://doi.org/10.1088/1755-1315/1135/1/012057

Olivia, R., Clotilda, P., Ang, C. H., Caroline, M., Rudy, T., & Joe, N. (2023). *Corrodeshield, An Eco-Friendly Fungal Biosurfactant Corrosion Inhibitor Produced By Penicillium Citrinum.* (pp. 45–47). Penerbit UTem Press,

Universiti Teknikal Malaysia Melaka. https://iconbee.uitm.edu.my/wp-content/uploads/2023/02/IConBEE2022-Proceedings.pdf

Rayeg, O. A., Nyuin, J. D., Petrus, C., & Ascotia, A. R. (2025). Fungal Biosurfactant : A Catalyst for Improved Fresh and Hardened Concrete Characteristics. *Journal of Advance Research in Applied Mechanics, 1*(1), 148–160.

Rayeg, O. A., Petrus, C., Huap, A. C., Nyuin, J., Marajan, C., & Tawie, R. (2024). Exploring the Green Potential of Rhizopus-Derived Biosurfactant for Corrosion Inhibition in Mild Steel. *Journal of Engineering Science and Technology*, *19*(3), 1074–1089. https://jestec.taylors.edu.my/Vol 19 Issue 3 June 2024/19_3_23.pdf

Rayeg, O. A., Petrus, C., Marajan, C., Tawie, R., Na, W. S., Huap, A. C., Nyuin, J., Huap, C., & Nyuin, J. (2021). A Review on the Application and Morphology of Organic Corrosion I